الجمهورية الجزائرية الديمقراطية الشعبية
People's Democratic Republic of Algeria
وزارة التعليم العالي والبحث العلمي
Ministry of Higher Education and Scientific Research

جامعة زيان عاشور بالجلفة
Ziane Achour University of Djelfa

كلية العلوم و التكنولوجيا
Faculty of Science and Technology

Department: Electrical Engineering

Order N° : . …. / 2024

Defense authorization N° ……/2024

DOCTORAL THESIS

3rd Cycle Doctoral (D-LMD)

Presented by

Djaloul KARBOUA

With a view to obtaining the doctoral diploma in 3rd Cycle Doctoral (D-LMD)

Branch: Electrotechnics

Specialty: Electrical control

Topic

Contribution to the control of three-phase Permanent Magnet Synchronous based on advanced technique

Supported, on 15/05/2024, before the jury composed of:

Last and first name	Grade	Institution of affiliation	Designation
Mr Lakhdar MAZOUZ	Professor	Ziane Achour University of Djelfa	President
Mr Belgacem TOUAL	MCA	Ziane Achour University of Djelfa	Supervisor
Mr Abdellah KOUZOU	Professor	Ziane Achour University of Djelfa	Co-Supervisor
Mr Abdechafik HADJADJ	Professor	University of Laghouat	Examiner
Mr Aissa AMEUR	Professor	University of Laghouat	Examiner
Mr Mohamed BOUDIAF	Professor	Ziane Achour University of Djelfa	Examiner

Acknowledgements

In the name of Allah, the Most Gracious, the Most Merciful.

I begin by expressing my deepest gratitude to Allah for granting me the strength, guidance, and perseverance throughout my academic journey.

I extend my sincere appreciation to my supervisor, Dr. Belgacem Toual, for his unwavering support, invaluable guidance, and profound insights. Your mentorship has been instrumental in shaping the trajectory of this research, and I am grateful for the knowledge and wisdom you shared.

I would like to extend my heartfelt thanks to my esteemed examiners, Pr. Mazouz Lakhdar, Pr. Hadjaj Abdechafik, Pr. Ameur Aissa, and Pr. Boudiaf Mohamed. Your meticulous examination, constructive feedback, and scholarly contributions have immensely enriched this thesis.

To my collaboration authors your collaborative spirit and dedication have significantly enhanced the depth and breadth of this research. I appreciate the synergy and shared commitment to advancing our collective understanding in the field.

I am deeply thankful to my family, especially my parents and siblings, for their unconditional love, encouragement, and understanding. Your support has been my source of strength, and I am blessed to have you by my side.

To my friends and colleagues, your camaraderie and encouragement have lightened the academic load and added joy to the journey. Your belief in my abilities has been a constant motivator.

I express gratitude to my teachers and mentors who have played pivotal roles in shaping my academic foundation. Your dedication to education has inspired me to strive for excellence.

Last but not least, I thank everyone who, directly or indirectly, contributed to this academic endeavor. Your collective influence has left an indelible mark on this thesis.

As I submit this work, I am mindful of the support and collaboration that have shaped its development. May this contribution be a source of benefit to the academic community and beyond.

Djaloul Karboua

Dedicates

I dedicate this thesis to the dear's individuals who have been the pillars of support and inspiration throughout my academic journey:

To My Parents: Your unwavering love and encouragement have been my guiding light. Thank you for instilling in me the values of resilience and determination.

To My Siblings, Abderahman , Bilal, Djamal eddine, Ali, Ahmed, Adel and Hisham: Your camaraderie and shared laughter have made this journey memorable. Your belief in my abilities has been a constant source of motivation.

To My Sisters: Your strength and camaraderie have added warmth and joy to my life. Thank you for being my confidantes and cheerleaders.

To My Teachers and Enseignements, especially B.boulanouar, B.Ibrahim, T. Belgacem : Your guidance and knowledge have shaped my academic path. I am indebted to your dedication and passion for imparting wisdom.

To My Maternal kin: Your wisdom and encouragement have been a guiding force. I am grateful for the lessons in perseverance and determination.

To My Friends and Colleagues, Especially D.Ben ouadeh, C.Yousef, M.Toufik, B.A Abdelkader and B.N.Ali: Your camaraderie and shared experiences have made the academic challenges more enjoyable. Thank you for the collaborative spirit and enduring friendships.

To Mentors, Especially Z.Mauro, L. Chouaib, Z.H. Khan, M.I.mosaad and B.I Farouk: Your guidance and the stories you've shared have truly enhanced my academic journey. I deeply appreciate your collaborative approach and the lasting friendships we've formed. Thank you.

This thesis stands as a testament to the collective influence of these remarkable individuals. Your belief in me has fueled my aspirations, and for that, I am eternally grateful.

Djaloul Karboua

Abstract

Nowadays, the three-phase Permanent Magnet Synchronous Motor (PMSM) becomes a very competitive motor to the conventional AC induction motor, which is more commonly found in motor-driven industrial applications systems, and they are often larger in size and less efficient than PMSM solutions. Indeed, PMSM solutions tend to have a higher initial cost, but they may offer a smaller size for more compact mechanical packages (permanent magnet motors can be as much easier), have the ability to maintain full torque at low speed (which makes their application for precise motion more efficient), and more importantly, have higher efficiencies. The expected work of the thesis aims at the application of new control techniques to three-phase PMSM. The main objective is to improve the dynamics of this kind of machine, which is intended to be used in several sensitive and precise industrial applications where maintenance is difficult and the speed range variation is very large. Whereas the main aim is to improve control performance and reduce computational complexity under a variety of different operating conditions, which can occur in practical cases.

Keywords: Permanent Magnet Synchronous Motor (PMSM), Advanced control Technique, Sensorless control, Three phase motor, Model Reference Adaptive System (MRAS).

Résumé

De nos jours, le moteur synchrone à aimant permanent triphasé (MSAP) devient très compétitif par rapport au moteur asynchrone conventionnel, largement utilisé dans les systèmes industriels entraînés par moteur, souvent plus volumineux et moins efficaces que les solutions MSAP. En effet, bien que les solutions MSAP aient tendance à avoir un coût initial plus élevé, elles offrent généralement une taille réduite pour des ensembles mécaniques plus compacts (les moteurs à aimants permanents étant souvent plus faciles à intégrer), la capacité de maintenir un couple complet à basse vitesse (ce qui rend leur application pour des mouvements précis plus efficace), et surtout, des rendements plus élevés. Le travail envisagé dans cette thèse vise à appliquer de nouvelles techniques de contrôle aux MSAP triphasés. L'objectif principal est d'améliorer la dynamique de ce type de machine, destinée à être utilisée dans diverses applications industrielles exigeantes et précises où la maintenance est complexe et la plage de variation de vitesse est très étendue. L'objectif principal est d'améliorer les performances de contrôle et de réduire la complexité computationnelle dans une variété de conditions de fonctionnement, telles qu'elles peuvent se présenter dans des cas pratiques.

.

Mots clés: Moteur synchrone à aimant permanent (MSAP), technique de contrôle avancée, contrôle sans capteur, moteur triphasé, système adaptatif de référence de modèle (MRAS).

ملخص

في الوقت الحاضر، أصبح المحرك المتزامن ذو المغناطيس الدائم ثلاثي الطور (PMSM) محركًا تنافسيًا للغاية مقارنة بالمحرك المتناوب AC التقليدي، والذي يوجد بشكل أكثر شيوعًا في أنظمة التطبيقات الصناعية التي تعمل بمحرك، وغالبًا ما يكون أكبر حجمًا وأقل كفاءة من نوع ال PMSM . في الواقع، تميلPMSM إلى أن تكون ذات تكلفة أولية أعلى، ولكنها قد توفر حجمًا أصغر للحزم الميكانيكية الأكثر إحكاما (يمكن أن تكون المحركات ذات المغناطيس الدائم أسهل بكثير)، ولديها القدرة على الحفاظ على عزم الدوران الكامل بسرعة منخفضة (مما يجعل تطبيقها للحصول على حركة دقيقة أكثر كفاءة)، والأهم من ذلك، أن تتمتع بكفاءة أعلى. يهدف العمل المتوقع للأطروحة إلى تطبيق تقنيات التحكم الجديدة على PMSM ثلاثي المراحل. كذلك من أجل تحسين ديناميكيات هذا النوع من الآلات، والتي تم تصميمها للاستخدام في العديد من التطبيقات الصناعية الحساسة والدقيقة حيث تكون الصيانة صعبة ويكون تباين نطاق السرعة كبيرًا جدًا. علاوة على ذلك تحسين أداء التحكم وتقليل التعقيد الحسابي في ظل مجموعة متنوعة من ظروف التشغيل المختلفة، والتي يمكن أن تحدث في الحالات العملية.

الكلمات المفتاحية : محرك متزامن ذو مغناطيس دائم (PMSM)، تقنية تحكم متقدمة، تحكم بدون مستشعر، محرك ثلاثي الطور، نظام التكيف المرجعي للنموذج (MRAS).

NOMENCLATURE

Symbols		Unit
R_s	Stator resistance	Ω
v_a	Stator voltage	*V*
v_b	Stator voltage	*V*
v_c	Stator voltage	*V*
i_a	Stator current	*A*
i_b	Stator current	*A*
i_c	Stator current	*A*
φ_a	Stator fluxe	*Wb*
φ_b	Stator fluxe	*Wb*
φ_c	Stator fluxe	*Wb*
ψ_r	Permanent-magnet flux linkage	*Wb*
$\psi_{f.a}$	is rotor magnetic flux linking the stator	*Wb*
$\psi_{f.b}$	is rotor magnetic flux linking the stator	*Wb*
$\psi_{f.c}$	is rotor magnetic flux linking the stator	*Wb*
θ	Mechanical angular position	*Rad*
Ω	Mechanical speed	*Rad/second*
F	Coefficient of viscous friction	*constant*
p	Number of poles	*constant*
ω_e	Electrical speed	*Tr/min*
T_l	Load torque	*N.m*
T_e	Electromagnetic torque	*N.m*
j	Momentum Inertia	*Kg.m^2*
L_q	is d axe induction stator	*H*
L_d	Is q axe induction stator	*H*
i_d	Is d axe equivalent stator current	*A*
i_q	Is q axe equivalent stator current	*A*
E_d	Is d axe back-EMF	*V*
E_q	Is q axe back-EMF	*V*
v_d	Is d axe equivalent stator voltage	*V*
v_q	Is q axe equivalent stator voltage	*V*
v_{dc}	DC-linkage voltage	*V*

ABBREVIATIONS

Abbreviations	
PMSM	Permanent Magnet Synchronous Motor
SISO	Single Input Single Output
SIMO	Single Input Multi Output
MIMO	Multi Input Multi Output
FOC	Filed Oriented Control
DTC	Direct Torque Control
FBLC	Feedback linearization control
BSC	Backstepping control
IBSC	Integral Backstepping control
SMC	Sliding mode control
I-SMC	Integral sliding mode control
T-SMC	Terminal sliding mode control
NT-SMC	Non-singular terminal sliding mode controller
FS-SMC	Fast terminal sliding mode control
NFTSM	Non-singular fast terminal sliding mode
FLC	Fuzzy logic control
NNAC	Neural Network Artificial control
FNNC	Fuzzy Neural Network control
STA	Super Twisting Algorithm
HO-STA	High Order Super Twisting Algorithm
LQR	Linear Quadratic Regulator control
SSE-LQR	steady-state error for the LQR
MPC	Model predictive control
SQP	Sequential Quadratic Programming
PSO	Particle Swarm Optimization
FEM	Finite Element Method
MILP	Mixed-Integer Linear Programming
FCS-MPC	Finite-Control-Set Model Predictive Control
ERL	Exponential reaching low

TABLE DES FIGURES

CHAPTER I

CHAPTER II

CHAPTER III

CHAPTER IV

CHAPTER V

LIST OF TABLES

CHAPTER II

CHAPTER III

CHAPTER IV

CHAPTER V

Publications

My thesis represents a culmination of rigorous research and scholarly contributions, as evidenced by the publication of four articles in reputable indexed journals and numerous presentations at esteemed international conferences, including those indexed by IEEE. Delving into diverse topics, my work not only underscores a depth of understanding but also a commitment to advancing knowledge in my field. Through these publications and conference contributions, my thesis stands as a testament to my dedication to academic excellence and the pursuit of innovative solutions within my discipline:

- **Conferences:**

D. Ben ouadeh , K. Abdellah, C. Youcef, K. Djaloul, M. Toufik"A Robust Control for Wind Energy Conversion System Based on Five Phases Permanent Magnet Synchronous Generator", II. INTERNATIONAL ENERGY DAYS Sivas Cumhuriyet University, September 27th, 2023

C. Youcef, Beladel Abdelkader, K. Abdellah, D. Ben ouadeh, K. Djaloul, M. Toufik, "Solar pumping system based on an induction motor" II. INTERNATIONAL ENERGY DAYS Sivas Cumhuriyet University, September 27th, 2023

K.Djaloul, T.Belgacem, I.Atif, C.Youcef, M.Toufik, D.Ben ouadeh, ”High Order Sliding Mode Control based on a New Terminal Strategy Applied on the Speed Permanent Magnet Synchronous Machine ,” XIX International Scientific Technical Conference «ALTERNATING CURRENT ELECTRIC DRIVES» – ACED 2023, Ural Federal University, Ekaterinburg, Russia, 23 - 25 May 2023.

K.Djaloul, T.Belgacem, B.Mohamed Lamine, ”A Super-twisting Algorithm based the Sliding Mode Control Applied on the Speed Permanent Magnet Synchronous Machine ,” in 20th IEEE International Multi-Conference on Systems, Signals & Devices (SSD'23), Mahdia, Tunisia, 2023.

M.Toufik, G.Amar, B.Mohamed Lamine, K.Djaloul, D.Ben ouadeh, C.Youcef,”Control of wind system based on DFIG using a Supper Twisting Algorithm”International Conference on Global Practice of Multidisciplinary Scientific Studies Dedicated to the 100th Anniversary of GEORGIAN TECHNICAL UNIVERSITY - GTU at Tbilisi, Georgia.

K.Djaloul, T.Belgacem, D.Ben ouadeh, M.Toufik, B.Mohamed Lamine, C.Youcef,”Expansion Switching Law Based Sliding Mode Applied on a Three-Phase Permanent Magnet Synchronous Machine ,” in 2st International Conference on Advanced Electrical Engineering(ICAEE's 2022), Constantine University , Algeria, 2022.

M.Toufik, G.Amar, B.Rabia, K.Djaloul, C.Youcef,"ACTIVE AND REACTIVE POWER CONTROL WITH SLIDING MODE APPLIED ON THE WIND TURBINE BASED ON DFIG"International Conference on Global Practice of Multidisciplinary Scientific Studies Dedicated to the 100th Anniversary of GEORGIAN TECHNICAL UNIVERSITY - GTU at Tbilisi, Georgia.

D.Ben ouadeh, K.Abdellah, H.Ahmed, K.Djaloul, M.Toufik, B.Mohamed Lamine,”Sliding Mode Control based on Exponential Reaching Law applied on a Five-phase Permanent Magnet Synchronous Generator based Wind System ,” in 5th International Conference on

Electrical Engineering and control Applications (ICEECA'2022), Khenchela University , Algeria, 2022.

K.Djaloul, T.Belgacem, M.Toufik, C.Youcef, D.Ben ouadeh, B.Mohamed Lamine, ”Sliding mode control with chattering minimize based on Continuous Approximation Method applied on a Permanent Magnet Synchronous Machine,” in 3th International Cappadocia Scientific Research Congress (ICSRCE'2022), Cappadocia-Nevsehir, Turkey, December 11-12, 2022

K.Djaloul, T.Belgacem, B.Mohamed Lamine, C.Youcef, M.Toufik, D.Ben ouadeh, ”Vector control based on a nonlinear technique applied to the Permanent Magnet Synchronous Machine,” in 6th International Icontech Conferance on Innovative Surveys in Positive Sciences (ICONTECH'2022), Rijeka, Croatia, December 4-5, 2022

K.Djaloul, T.BelgacemT , K.Abdellah, B.Nacreddine Bendenidina ,E.Ahmed ,K.Cherif and B.Mohamed LAMINE "CONTROL OF THREE-PHASE PERMANENT MAGNET SYNCHRONOUS MACHINE BASED ON SLIDING MODE CONTROL"6th INTERNATIONAL CONGRESS ON INNOVATIVE SCIENTIFIC APPROACHESAt, Samsun, Turkey.

K.Djaloul, K.Cherif"Methodology for the structure of the scientific article for the experimental article"1st NATIONAL conference ON Foundations and Methods of Scientific Research at Mohamed Boudiaf University of M'sila.

K. Djaloul, K.Cherif, T . Belgacem and K. Abdellah, "Application of the linear quadratic regulator control on mechanical subsystem of wind turbine," in 1st International Conference on Electrical-Electronics and ComputerEngineering(ICEECE 2021), Avrasya University , Trabzon, Turkey , 2021.

K.Djaloul, T.BelgacemT , D.Zohair and K.Abdellah, "Control of Three-phase Permanent Magnet Synchronous Machine Based on Integral Backstepping Control T echnique," INTERNATIONAL HAZAR SCIENTIFIC RESEARCHES CONFERANCE-II, Hazar University , Baku, Azerbaijan, 2021.

- **Journals articles:**

Mebkhouta, T., Golea, A., Boumaraf, R., Benchouia, T. M., Karboua, D. “A High Robust Optimal Nonlinear Control with MPPT Speed for Wind Energy Conversion System (WECS) Based on Doubly Fed Induction Generator (DFIG)”, Periodica Polytechnica Electrical Engineering and Computer Science, 2023. https://doi.org/10.3311/PPee.22595

Karboua D, Belgacem T, Khan ZH, Labiod C, Ibraheem IK. Toward an optimal twisting-sliding mode control of a three-phase PMSM for electric vehicles. Advances in Mechanical Engineering. 2023;15(9). https://doi:10.1177/16878132231198664

K. Djaloul, Belgacem T, Khan ZH, Kellal C(2023) Robust performance comparison of PMSM for flight control applications in more electric aircraft. PLoS ONE 18(7): e0283541. https://doi.org/10.1371/journal.pone.0283541

K. Djaloul, T . Belgacem and K. Abdellah, D.Ben ouadeh, M.Toufik, B.Nacreddine Bendenidina "High-order Supper-twisting Based Terminal Sliding Mode Control Applied on Three Phases

Permanent Synchronous Machine," Periodica Polytechnica Electrical Engineering and Computer Science, 67(1), pp. 40–50, 2023. https://doi.org/10.3311/PPee.21026

TABLE OF CONTENTS

General Introduction

Electric motors are ubiquitous devices that are vital to modern life; they run everything from home appliances to industrial machinery and transportation systems. Electrical energy is converted into mechanical energy and vice versa via electromechanical machines, also referred to as electric machines. AC machines fall into three broad categories: synchronous, electrically commutated, and asynchronous. Since the stator windings are connected to the AC supply and the rotor is not connected to the stator or any other power source, asynchronous machines are also known as single excited machines. For this reason, asynchronous motors with squirrel cage rotors or a field-wrapped circuit are called induction machines. Only mutual induction can transfer power from the stator to the rotor. For the stator windings of the synchronous motors, an AC supply is needed, and for the rotor windings, a DC supply. The rotor rotates at the speed of the stator's spinning field at synchronous speed, which is constant. The number of poles in a synchronous motor and the frequency of the AC supply determine the motor's speed. Changes in the mechanical load within the machine's rating will not affect the motor's synchronous speed. They fall into three primary categories: rotor-excited types, synchronous reluctance types, and permanent magnets. Electronically commutated machines, which replace mechanical commutations with inverter-based commutations, are modelled after DC machines. Brushless DC motors and switching reluctance motors are the two main kinds of motors that fall under this category. Other variations of these fundamental designs of electric machines used for specific purposes include stepper motors, hysteresis motors, permanent magnet-assisted synchronous reluctance motors, hysteresis-reluctance motors, universal motors, claw pole motors, frictionless active bearing-based motors, linear induction motors, etc [4,5,6]. Permanent Magnet Synchronous Motors (PMSMs) are a type of electric motor that have gained widespread recognition and are utilized in a wide range of sectors due to their unique features and capacities. These motors function by using permanent magnets to create an internal rotating magnetic field. Mechanical motion is produced by the interaction between this magnetic field and the stator windings. PMSMs are an excellent choice for applications needing accurate speed control, energy efficiency, and performance due to their high power density, tremendous efficiency, and exact control. One of the main features of PMSMs is its permanent magnet rotor, which eliminates the need for rotor current excitation, reducing losses and increasing efficiency compared to other motor types. This design reduces maintenance requirements while simultaneously increasing the motor's overall dependability and efficiency. PMSMs are widely employed in a wide range of applications, including industrial machinery, robotics, electric cars, and renewable energy sources. PMSMs are crucial to the advancement of technology and the switch to greener, more energy-efficient solutions in each of these applications. Despite this, PMSMs are extensively utilized in the several sectors mentioned above because of their advantages and characteristics. Control strategies are therefore used on them to both stabilize and enhance their performance. Vector control and scalar control are the two general categories into which PMSM control design approaches fall. Scalar control has slower dynamics but is easier to operate and results in a mostly steady-state response. As a result, in order to achieve both good dynamic and steady-steady response and increased precision, the closed-loop vector control

technique is usually chosen. The vector control is the largest control group, incorporating both conventional and advanced techniques. Conventional techniques, such direct torque control (DTC) and field oriented control (FOC). Advanced techniques include nonlinear, optimum, adaptive, and intelligent techniques. Each technique has a different purpose, set of features, and control architecture; some can be used straight to a nonlinear model, while others call for the application of decoupling or linearization techniques. Nonlinear techniques like backstepping (BSC), sliding mode control (SMC), feedback linearization control (FBLC), and passivity-based control (PBC) are commonly used in PMSM. The best control strategies are linear quadratic regulator control (LQR), model predictive control (MPC), and others. The Model Reference Adaptive Control (MRAC) is used to classify direct, indirect, and matching orders in terms of adaptive control. In order to improve data-based systems or the aforementioned approaches, artificial neural networks (ANNC), genetic algorithms (GAC), fuzzy logic (FLC), and other intelligence techniques have recently been developed.

Motivation for research

In recent years, Permanent Magnet Synchronous Motors (PMSMs) have emerged as a cornerstone in the field of electric propulsion systems, owing to their high efficiency, compact size, and superior dynamic performance. The efficient control of PMSMs plays a pivotal role in optimizing their operation and ensuring optimal energy utilization across various applications such as electric vehicles, renewable energy systems, and industrial automation. The need for more precision, improved efficiency, and increased reliability in PMSM systems is progressively surpassing the effectiveness of conventional control strategies. The incorporation of advanced control techniques presents an exceptional chance to push PMSM performance limits to new heights as we lead the way in technical innovation. This research endeavors to explore and harness the potential of cutting-edge control techniques, including but not limited to nonlinear control approaches, optimal and advanced optimization strategies. And hybridization designs between the different techniques. By delving into these innovative methodologies, we aim to address the inherent challenges in conventional PMSM control, such as torque ripple, speed fluctuations, and response time, thereby unlocking new levels of efficiency and performance. Furthermore, the integration of these advanced control techniques is expected to contribute significantly to the broader goals of sustainable energy and environmental conservation. Achieving tighter control over PMSMs will lead to increased energy efficiency and a more sustainable future.

Problem Description

The dynamic performance of the PMSM is crucial in many industrial applications, particularly when abrupt speed changes are needed. This means the speed performance may be changed between different levels, such as low, medium, and high speeds. Over time, some internal and external operating conditions may cause the uncertainty phenomenon to occur during the operation mode of the PMSM. This uncertainty represents the variation parameters such as the stator resistance, the stator inductance, and the inertia value. This phenomenon, the variation of the load torque and the speed variation will cause a deterioration in the PMSM's performance, reducing its efficiency and characteristics. In addition, performance characteristics such as rise time, steady-

state error, stability, and other characteristics are extremely important in order to improve the performance of PMSM for its application in numerous fields. Furthermore, simplicity, smoothing, and flexibility are some of the biggest obsessions before applying any control or observation techniques during PMSM operation. There are several challenges in PMSM control; we can arrange some of them as follows:

- The dynamic response and transient behavior of PMSMs are challenged by abrupt disruptions and rapid changes in load circumstances. The inability of conventional control algorithms to achieve the necessary responsiveness has led to the exploration of advanced control techniques as a means of improving the stability and flexibility of the system;
- There are questions regarding real-time viability and computing complexity when implementing advanced control systems. The effective implementation of advanced PMSM control techniques requires a unique challenge: balancing the complexity of control algorithms with the realistic requirements of real-time applications;
- When in operation, PMSMs are vulnerable to harmonic distortions and torque ripple, which can cause unwanted mechanical vibrations and lower system efficiency. Conventional control approaches find it difficult to fully resolve these problems, so it is necessary to investigate more sophisticated strategies that can reduce torque anomalies;
- It is critical to achieve high levels of energy efficiency in PMSM control due to the growing emphasis on energy conservation. To reduce energy losses and increase overall system efficiency, control parameters can be fine-tuned with the use of advanced optimization algorithms;
- Because PMSM systems are inherently nonlinear, control algorithms have substantial hurdles when dealing with variations in parameters brought on by elements like ageing and temperature fluctuations. Nonlinear, optimal, and adaptive techniques are examples of advanced control systems that have the capacity to address these nonlinearities and adjust in real-time to parameter alterations.

Objectives of thesis

The principal aim of this thesis is to examine and suggest remedies for the previously mentioned difficulties in PMSM control by employing sophisticated methodologies. Through an exploration of the complexities surrounding torque ripple reduction, dynamic response enhancement, nonlinearity compensation, energy optimization, and the viability of real-time implementation, this study hopes to offer novel solutions that will open up new avenues for PMSM control system development. This research aims to not only address the existing limitations in PMSM control but also to foster advancements that will redefine the standards for efficiency, reliability, and adaptability in electric propulsion systems through a thorough understanding of these challenges and the development of advanced control methodologies. The following is a summary of the thesis's main research goals:

a) State of the art on the three phase PMSM and three phase inverter;
b) State of the art of the control use previously for driving the PMSM;
c) Studying different conventional vector control for the PMSM;

d) Studying different nonlinear vector control for the PMSM;
e) Proposed new techniques to overcome the drawbacks found in the conventional control;
f) Hybridization, or a combination of advanced techniques, to overcome the challenges mentioned above;
g) Verify the efficacy of estimators and control strategies with comprehensive simulations under various conditions.

A substantial amount of new knowledge has been created by accomplishing the aforementioned goals. The research articles that the thesis has already led to being published serve as some evidence for this. The articles are the primary contributions of this thesis since they include the unique findings from the contribution.

Thesis organization

This thesis work is arranged into six chapters, which are organized as follows:

In Chapter I, we will delve into the comprehensive description and generalities of the permanent magnet synchronous machine (PMSM), where we'll start with the historical background of the electrical machines, their classifications, and some similarities between these classifications. After that, we will present a general overview of PMSMs, subgroups, definitions, advantages, disadvantages, and characteristics. The construction, properties, and standards of the PMSM for industrial applications, factors for choosing permanent magnets, and principles of how the PMSM operates will be explained in the next section. In addition, the structure of the PMSM will be described in detail, including the various topologies, categories, 3D designs, and configurations of the PMSMs, as well as the comparative study between them. Moreover, some applications that used the PMSM (rail transport, elevator doors, aeronautics, EVs, WECS, EAs, and photovoltaic pumping systems) will be explained with an overall description, and their schemes will be presented too.

In Chapter II, we will include a full explanation of the mathematical formulas as well as a model of the PMSM and inverter. The two frame references (d-q and d-q) have been achieved by starting with the conventional equations for the machine in the ABC frame reference and using the conversion coordinate transformation (Clark and Park). Furthermore, the various techniques for PMSM modeling transfer function, state space approach, and nonlinear method have been examined. A detailed explanation of its PWM-based control techniques has been provided, along with a model of the three-phase, two-level voltage inverter. Lastly, MATLAB Simulink has been used to validate the PMSM model.

In Chapter III, we will cover the PMSM drive design and the application of traditional controls to the PMSM. By simplifying the PMSM model, the control design will aid in our understanding of the PMSM. The stability of the PMSM will next be shown using a pole-zero map technique, and the controllability will be shown by applying Kalman's theorem as well. Subsequently, the FOC and DTC applications to the PMSM model will be examined, and the control law will be calculated accordingly. A comparative analysis will be carried out comparing the two methods according to robustness, performance attributes, and additional standards. Lastly, MATLAB Simulink will be used to validate each control's efficacy. The specific requirements of the application determine

which option DTC or FOC to choose, taking into consideration factors like torque ripple, dynamic response, simplicity, and sensor requirements. Each control strategy has advantages and disadvantages, and the optimal strategy will depend on the goals of the motor control application.

In Chapter IV, the nonlinear controls and strategies for the PMSM drive will be applied, along with an explanation of the FBLC, BSC, and SMC. Each technique's definition, goal, control design, employed procedures, guiding principles, benefits, and downsides will all be covered in detail. The SMC will also involve a thorough analysis of numerous algorithms, approaches, and strategies, including the super-twisting algorithm (STA), high-order design (HO), terminal sliding mode control (SMC), approach laws, and estimated continuation for enhancing the traditional SMC difficulties. Moreover, a novel hybrid design for the PMSM speed loop that combines the HO-STA and T-SMC will be demonstrated. Finally, MATLAB Simulink will be used to validate each of the aforementioned controls, and a comparative study based on a few scenarios will be added.

In Chapter V, We shall examine the optimal controls for the PMSM drive. The PMSM current loop will be addressed using MPC and LQR, while the speed loop will be addressed using the sliding mode technique. Furthermore, by using a unique design based on steady state as new state variables (SS-LQR), we will enhance the conventional LQR and create the conventional finite-control-set model predictive control (FCS-MPC).The key motivations for applying both approaches to the motor current loop are their robust performance, ease of implementation, and ideal properties. Additionally, the MATLAB Simulink simulation results will confirm that both approaches improved performance characteristics and performed exceptionally well during speed variations between different levels and in the robustness feature under disturbances and uncertainties.

Lastly, a general conclusion of the thesis will discussed. Additionally, a few aspirations for this work are presented.

CHAPITRE I

STATE OF THE ART: PMSM GENERALITIES

I.1 Introduction

Electric motors are ubiquitous devices crucial to modern life, driving everything from industrial machinery and transportation systems to household appliances. Known for their reliability and efficiency, these electromechanical machines convert electrical energy into mechanical motion. There are various types of electric motors, each tailored for specific applications, including DC motors, AC induction motors, and Permanent Magnet Synchronous Motors (PMSMs).

Because of their special qualities and capacities, Permanent Magnet Synchronous Motors (PMSMs) are a type of electric motor that have become widely known and used in many different industries. These motors work by generating a revolving magnetic field inside the motor through the use of permanent magnets. This magnetic field interacts with the stator windings to generate mechanical motion. Because of their great efficiency, high power density, and precise control, PMSMs are a great option for applications requiring precise speed control, energy efficiency, and performance.

A fundamental feature of Permanent Magnet Synchronous Motors (PMSMs) is that their rotors operate without requiring an excitation current, resulting in the absence of rotor losses. This design improves the motor's overall dependability and efficiency while also lowering maintenance needs. PMSMs are widely used in many different applications, such as robotics, electric vehicles, industrial machinery, and renewable energy systems. In all of these applications, PMSMs are essential to the growth of technology and the transition to cleaner, more energy-efficient solutions.

In this chapter, we will delve into the state-of-the-art of the PMSM generalities, where we'll start with the historical background of the electrical machines and their classifications, exploring the overview of PMSMs, their construction, their structure, and their applications.

I.2 Research background of the electrical machines

Since Michael Faraday introduced the initial idea of electrical motors in 1821, there have been ongoing advancements in the field of electric drives. William Sturgeon had the idea for the first electric device, which was actually a DC device, in 1832. After Nikola Tesla took into account the rotating attractive field in 1882 and used it to create the first AC machine, which led to his obtaining the first induction machine patent (US Patent 381968) in 1888, the world underwent a significant change [1]. The first focus of study was on machine design with the goal of lowering weight per unit power and raising motor efficiency. Researchers' ongoing work has resulted in the creation of machines with energy-efficient industrial motors that have smaller volumes. Since there are so many motors on the market that are nearly 95–96% efficient, there are no longer any serious consumer complaints [2]. Electromechanical machines, often known as electric machines, are utilized to transform electrical energy into mechanical energy and vice versa. Three general categories can be used to describe AC machines: synchronous, electronically commutated, and asynchronous. Because only mutual induction can transport power from the stator to the rotor, asynchronous motors with squirrel cage rotors or a field-wrapped circuit are referred to as induction machines [3, 4].

The synchronous motors require an AC supply for the stator windings and a DC supply for the rotor windings. The number of poles in a synchronous motor and the frequency of the AC supply define the motor's speed; at synchronous speed, which is constant, the rotor revolves at the speed of the stator's rotating field. The synchronous speed of the motor will not be impacted by changes in mechanical load within the machine's rating [5]. They are divided into three main categories: permanent magnets, synchronous reluctance types, and rotor-excited kinds. The concept of DC machines is applied to electronic commutated machines, which substitute inverter-based commutations for the mechanical commutations. This category includes two primary types of motors: switching reluctance motors and brushless DC motors. Stepper motors, hysteresis motors, permanent magnet-assisted synchronous reluctance motors, hysteresis-reluctance motors, universal motors, claw pole motors, frictionless active bearing-based motors, linear induction motors, etc. are some other variations of these basic configurations of electric machines used for particular applications [4]. Figure. I.1 is represents the classifications of the electrical motors.

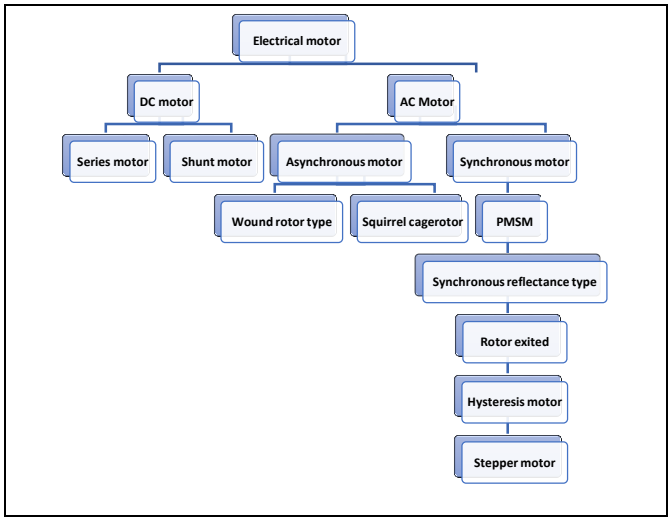

Figure I.1: Classifications of the Electric Motor

I.3 General overview on the PMSM

PMSMs were first employed in history at the start of the 19th century. Over the course of a century, advancements in technology have led to the development of magnet machines, which started out with extremely low performance. Nowadays, permanent magnets can be utilized as inductors in synchronous machines thanks to advancements in their design, which can be attributed to either metallic or rare earth alloys (such as manico, samarium cobalt, neodymium iron boron, etc.). As a result, it provides numerous benefits over other kinds of machines, including high saturation induction, minimal demagnetization, high specific power density, and a larger maximum stored energy. By substituting magnets for the inductor in the PMSM permanent magnet machine, brushes and rotor losses can be avoided while simultaneously creating an excitation field [6, 7].

I.3.1 Subgroups of the permanent synchronous machine

The mechanical structure of Permanent Magnet Synchronous Motors (PMSMs) varies due to distinct production methods and application requirements, resulting in diverse control principles. The classification of Permanent Magnet Synchronous Motors (PMSMs) is typically based on the shape of their back-electromotive force (back-EMF), which can be categorized as either trapezoidal or sinusoidal, as seen in Figures. I.2(a) and I.2(b). In a similar vein, the control method can be categorized as either brushless DC (BLDC), characterized by rectangular or trapezoidal phase current waveforms, or brushless AC (BLAC), characterized by sinusoidal phase current waveforms. When making a decision regarding the appropriate motor for a certain application, it is imperative to consider the individual strengths and disadvantages associated with each motor option. In addition, the number of phases, stator windings, and magnetic poles might vary depending on the specific needs and intended use of the motor. In order to enhance the performance of motors for high-performance applications, it is imperative to consider design requirements, including stator stack skewing and rotor type. In the context of brushless DC (BLDC) motors, the commutation of phase currents is limited to the activation and deactivation of certain phases. This characteristic allows for the implementation of straightforward control strategies, such as the 6-step method or hysteresis control [8,9].

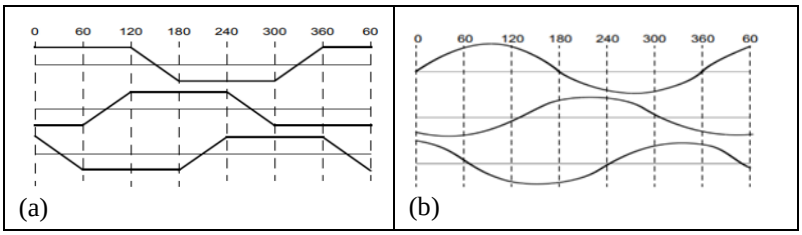

Figure I.2 : Back-EMF shape of (a) BLDC motor, (b) BLAC motor

The BLDC motor is characterised by a stator winding that is concentrated, nonoverlapping, and fractional-slot in nature (see Figure. I.3(a)). The presence of a greater torque ripple can be attributed to the challenges associated with obtaining an optimum trapezoidal phase current. Primarily, it finds extensive application in traction systems, particularly in the context of electric vehicles (EVs) or unmanned aerial vehicles (UAVs). Hall sensors of low cost are frequently employed for the purpose of detecting the position of the rotor. However, the implementation of BLAC necessitates the use of a resolver or encoder with a somewhat higher cost, which enables the precise control of phase current waveforms. While there may be several rotor topologies and stator winding dispositions, the primary mechanical distinction lies in the configuration of the stator winding (see Figure. I.3(b)). In the case of BLAC, it is customary to employ a distributed, overlapping stator winding. This technology finds application in high-speed or high-precision contexts, such as robotics and machine tools [10, 11, 12]. The distinction between the two types of PMSM lies in their winding distribution, rendering the cost of the motor itself inconsequential in the comparative analysis. Nevertheless, it is worth noting that the BLAC is typically controlled using vector control techniques, while the BLDC is commonly controlled by phase commutation. This discrepancy in control complexity is evident in the hardware requirements for operating these two types of permanent magnet motors. The progress in microcontroller technologies has rendered the cost of computing power negligible [13].

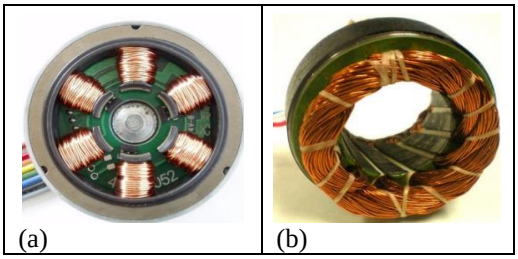

(a) (b)

Figure I.3 : Different stator coils configuration of a PMSM

I.3.2 Description of the PMSM

Magnets possess inherent excitability in their natural form, although we can also impart this magnetic feature to specific substances primarily consisting of iron, nickel, and cobalt, which are commonly referred to as artificial magnets. The region encompassing the poles of a magnet is characterized by the presence of a magnetic field, which is comprised of lines of flux or lines of force. The lines exhibit a loop-like pattern, originating at the geographic North Pole and extending towards the geographic South Pole. The majority of these lines of force comprise the magnetic spectrum [14].

I.3.3 Characteristics of the PMSM

In this part, we highlight the characteristics that distinguish the PMSM, mentioning the differences that distinguish it from other machines, such as induction and DC machines [10, 15, 16, 17]:

- High torque-current ratio and high flux density:

The recent advancements in neodymium-iron-boron (NdFeB) magnets have opened up the potential to achieve significantly high levels of flux density. The presence of high flux density allows for the attainment of equivalent torque with less current, as described by Ampère's Force Law. Consequently, this outcome leads to diminished copper losses within the stator coil and an overall increase in efficiency. In contrast, a permanent magnet synchronous motor (PMSM) has the capability to generate significantly greater torque compared to an induction motor (IM), even when their respective volumes are equivalent. This particular attribute renders numerous direct-drive systems viable. However, a downside is also evident in situations involving high speeds, as observed in Faraday's law of induction. The implementation of flux weakening control is necessary in order to expand the operational speed range of the system. However, it should be noted that this control method is associated with a decrease in efficiency. Given the aforementioned factors, it is noteworthy that synchronous excitation machines have resurfaced in applications characterized by high-speed dynamics, such as the electric vehicle Renault.

- High reliability and lower maintenance:

In comparison to a DC motor, a permanent magnet synchronous motor (PMSM) addresses inherent limitations by substituting the mechanical commutation with an electronic counterpart.

Therefore, PMSM has the advantages of a DC motor, like good speed regulation performance, as well as the advantages of an AC motor, such as a simple structure, no spark, dependable operation, and easy maintenance.

- High-resolution Feedback:

To achieve precise speed control, PMSMs rely on high-resolution feedback devices such as encoders or resolvers. These devices provide real-time feedback on the motor's rotor position and speed, allowing the control system to adjust the motor's operation accordingly. The high resolution of these feedback devices enables the control system to detect even small deviations from the desired speed and quickly correct them.

- Dynamic Response:

PMSMs exhibit excellent dynamic response characteristics, meaning they can quickly respond to changes in speed commands or external disturbances. This is due to their low rotor inertia and high torque-to-inertia ratio, which allow them to accelerate and decelerate rapidly. As a result, PMSMs are well-suited for applications where rapid changes in speed are required, such as in servo systems and robotics.

- Power-weight ratio and high efficiency:

Currently, the most widely utilized electric machines in electrical propulsion systems are the induction motor (IM) and the permanent magnet synchronous motor (PMSM). In comparison to induction motors (IM), permanent magnet synchronous motors (PMSM) typically exhibit little rotor loss due to the absence of current flow in the rotor. In the context of a conventional synchronous motor, permanent magnet synchronous motors (PMSMs) employ a permanent magnet instead of a rotor excitation circuit to provide a consistent magnetic field in the rotor. Consequently, the copper losses in the excitation circuit are eliminated. The utilization of a permanent magnet synchronous motor (PMSM) results in superior operational efficiency when compared to alternative motor types. For instance, the efficiency maps and speed-torque curves of the used induction motor (IM) and permanent magnet synchronous motor (PMSM) with respective rated powers of 40 kW and 22.8 kW are illustrated in Figures I.4(a) and I.4(b). The Permanent Magnet Synchronous Motor (PMSM) exhibits superior average efficiency compared to the Induction Motor (IM) throughout their respective ranges of operation speeds. Finally, it should be noted that the Permanent Magnet Synchronous Motor (PMSM) exhibits a higher operational efficiency, exceeding 90%, compared to the Induction Motor (IM). One additional benefit is that the stator coil of a PMSM is responsible for generating all of the heat, facilitating the cooling process. The possession of this characteristic is crucial in applications requiring high levels of power.

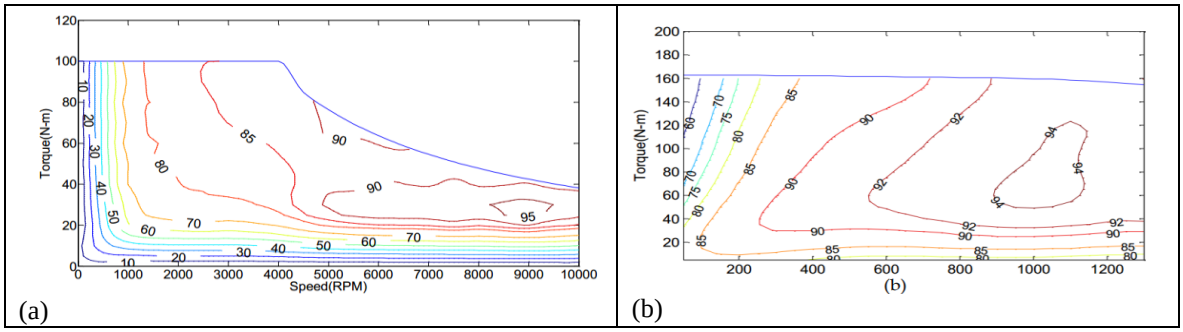

Figure I.4 : Efficiency map of (a) the IM, (b) the PMSM [16]

I.4 Construction of the PMSM

A PMSM is a brushless electric motor that is rotating because of an induced magnetic field. The three main components of a permanent magnet synchronous motor are the stator, which houses the windings that make up the armature, and the rotor, which is a mobile component that makes up the inductor. An "air gap" is the thin space that exists between these two components [18].

I.4.1 The stator

The non-moving component that holds the electromagnets is called the stator. Three identical windings spaced 120 degrees apart and inserted into the fixed magnetic circuit's slots make up the stator of a three-phase PMSM. The latter is laminated to minimize iron losses and minimize eddy currents. Typically, it is made of sheet metal made of an iron-silicon alloy, which enables high induction [18, 19].

I.4.2 The rotor

The rotating component that contains the permanent magnets is called the rotor. Permanent magnets with alternating north and south poles take the role of the windings that, in the case of a wound rotor machine, carried a direct current at the rotor. The inductor flux sweeps the stator windings and induces alternating electromotive forces (e.m.f.). The motor rotates at synchronous speed due to torque generated on the motor shaft by the interaction of the stator and rotor fields. The type of outrunner under investigation has the rotor rotating outside the stator [18, 19, 20].

I.4.3 The different materials types of permanent magnets

Due to the fact that the permanent magnet (PM) is mounted in or on the rotor, there are several natural materials for manufacturing the PM, whose properties and applications are diverse. Under that, we'll describe the most commonly used in Figure. I.5 below [15, 21]:

(d) (e) (f)

Figure I.5 : Materials types of the PM: (a) Alnicos, (b) Ferrites, (c) Neodymium-Iron-Boron (Nd-Fe-B), (d) Rare earth alloys, (e) Samarium cobalt

- Alnicos:

Alnico magnets exhibit a notably elevated remanent field, but concurrently display a much diminished coercive field, hence presenting significant challenges in terms of demagnetization. The magnets in question are incapable of being detached from their magnetic circuit without undergoing demagnetization; this material type is presented in Figure. I.5(a).

- Ferrites:

Ferrites are chemical compounds composed of iron oxide, together with barium and strontium. The aforementioned materials are acquired through the process of sintering and possess the ability to exhibit either isotropic or anisotropic properties. These magnets exhibit modest performance characteristics; nevertheless, they have gained widespread acceptance in numerous applications owing to their affordability and strong magnetic properties, enabling their utilization in various machinery. Ferrites are commonly employed in magnet machines that operate at low power and are cost-effective, mostly due to their relatively low remanent magnetization values, typically around 0.4 T. These material types are presented in Figure. I.5(b).

- Neodymium-Iron-Boron (Nd-Fe-B):

The latest variety of magnets is known as neodymium-iron-Boron. The initial utilization of this can be traced back to the year 1985. Over a brief period of time, it experienced an increase in momentum with regards to its production. It possesses characteristics that make it highly suitable for the generation of electrical machine excitations. The induction generated in the air gap is of considerable magnitude, exhibiting a high coactive field. The composition of these entities primarily consists of Nd2Fe14B. The aforementioned materials exhibit enhanced magnetic characteristics and are more cost-effective in comparison to samarium-cobalt. The volume energy product (BH)max attains a value of 400 KJ/m3 at standard room temperature. One primary drawback associated with this particular magnet variant is its limited use at temperatures beyond 100°C, coupled with its heightened susceptibility to air oxidation. This material type is presented in Figure. I.5(c).

- Rare earth:

Rare earth elements exhibit superior magnetic properties, making them the most effective materials for magnetization. These devices exhibit a high degree of compatibility with electrical

machinery. The continued high cost associated with their implementation tends to impede the widespread adoption and growth of their utilization. Nevertheless, there have been emerging intermediate solutions, including the utilization of Plasto-Neodymium. The substance in question is a composite material consisting of neodymium-iron-Boron particles combined with a plastic binder. This material enables the production of moulded components, hence streamlining assembly processes and minimizing the quantity of mechanical parts required. These material types are presented in Figures. I.5(d) and I.5(e).

- Samarium cobalt (SmCo5, Sm2Co17):

Samarium cobalt magnets exhibit superior energy volume density compared to other magnet types, with values ranging from 140 to 200 kJ/m3 for SmCo5 and 180 to 240 kJ/m3 for Sm2Co17. These magnets also possess the advantage of being capable of operating at high temperatures, up to 350°C. However, their high cost is primarily attributed to the inclusion of cobalt in their composition; this material type is presented in Figure. I.5(f).

I.4.4 Properties and standards of the PMSM for industrial applications

While it is crucial to possess knowledge regarding the mechanical and physicochemical characteristics, as well as the price and Curie point (the temperature at which a magnet ceases to exhibit magnetic qualities), this discussion will mostly focus on the magnetic properties. The materials utilized for their magnetic properties are categorized based on the breadth of their hysteresis cycle, as depicted in Figure. I.6(a), and can be divided into two major groups. One category pertains to hard magnetic materials, often referred to as "permanent magnets" due to their consistent magnetization even when subjected to an external magnetic field. The second category pertains to materials sometimes referred to as "soft" magnetic materials, which exhibit magnetic properties just when subjected to external excitation. In addition, the magnet's operational condition is situated within the second quadrant of its hysteresis cycle, as depicted in Figure. I.6(b). Furthermore, permanent magnets possess many standards that play a crucial role in their utilization in industrial applications. The standards under consideration among others are as follows [15, 21]:

- The remanence, denoted as B_r, is a measure of the magnet's potential power and is used to establish the required cross-sectional area for the passage of useful flux to sustain the air gap flux;
- The coercivity, denoted as H_{CB}, refers to the magnetizing field that has the ability to neutralize the remanence. The magnitude of H_{CB} increases as the stability of the magnet increases;
- When the coercive polarization field, denoted as H_{CJ}, is applied, it effectively nullifies the intrinsic magnetization of the material. As a result, the demagnetization process becomes complete and irreversible;
- The energy product, denoted as $(B.H)_{max}$, represents the energy value of a magnet per unit volume.

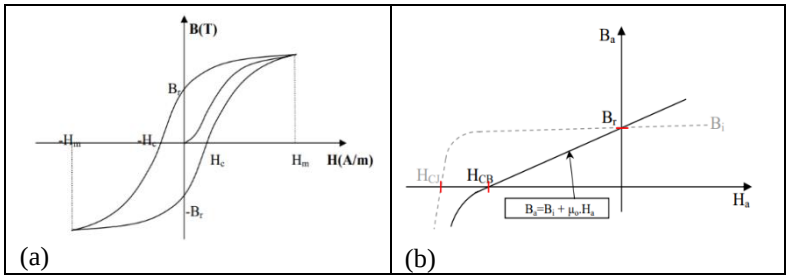

Figure I.6 : PMSM Properties, (a): Hysteresis cycle, (b): Demagnetization curve

I.4.5 Factors for choosing permanent magnets

In order to choose the type of permanent magnet, we must take the following factors into consideration:

- Machine performance, efficiency and mechanical strength;
- A machine size, shape and weight;
- Magnetic properties, magnetization direction and demagnetization resistance;
- Temperature Stability of the machine;
- An economic factor, environmental Impact and availability.

I.4.6 Operating Principles of the Permanent Magnet Synchronous Motor (PMSM)

The operational mechanism of the motor involves the transmission of an electric current through an electromagnetic coil. When the coil is magnetized, a permanent magnet on the rotor, possessing opposite polarity, will endeavor to align itself with the coil, while a magnet exhibiting the same polarity will experience repulsion from the electromagnet. Moreover, an additional coil is energized, resulting in the continuous rotation of the rotor, thereby perpetuating the process. This phenomenon is depicted in Figure. I.7(a). When a three-phase current with a specific frequency is applied, the motor will exhibit rotational motion at a speed equivalent to the frequency divided by the number of pole pairs. In a Δ-connection, the phases are connected individually, as depicted in Figure. I.7(b). The Δ-connection is not as widely utilized as the Y-connected configuration, primarily because it possesses a significant drawback. The aforementioned losses can be attributed to the ohmic motor, specifically 2R. The utilization of Δ-connected motors is predominantly observed in motors with lower power output, as this configuration allows for a reduction in material costs that can offset the losses incurred [19, 22].

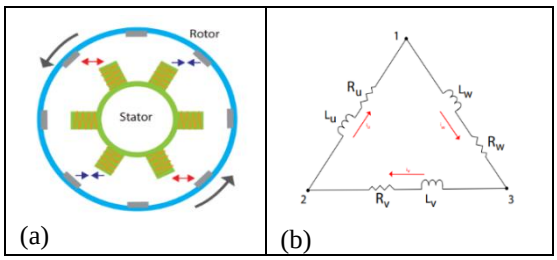

Figure I.7 : Principle of the PMSM operating, (a): PMSM working, (b): PMSM based on delta connection

I.5 Structure of the PMSM

The Initially, the primary aim of early Permanent Magnet Synchronous Motors (PMSMs) was to leverage permanent magnet excitation to enhance the efficiency of traditional electric motors. However, initial attempts to enter the market faced challenges as clients did not perceive the efficiency boost as significant enough. Despite these setbacks, recent years have seen a notable shift in the landscape, with several companies successfully introducing permanent magnet devices. Over the past decade, the situation has evolved dramatically. According to [34], ABB pioneered the production of permanent magnet machines with power ratings up to 5 MW around the turn of the millennium. These machines found applications in areas such as ship propulsion drives and windmill generators, marking the onset of the permanent magnet machine era for large-scale industrial uses. Concurrently, a new family of permanent magnet machines emerged, specifically designed for low-speed applications in the lower power range. In recent years, companies like Baumüller, Yaskawa, Siemens, and Rotatek have demonstrated significant activity and innovation in the PMSM field. Moreover, there is a growing interest in research focused on low-speed permanent magnet machines with concentrated windings. In this section, we will delve into the various aspects of PMSMs, including their topologies, categories, configurations, and types, providing a comprehensive understanding of these increasingly vital components in modern industrial applications. [23-26].

I.5.1 Categories of the PMSM structure

It is difficult to list every category, configuration, and type of permanent magnet synchronous machine and compare how effective they are. However, we will provide the comparative studies that have been carried out in this regard, taking into account the compatibility of the topologies considered [3,20]. In contrast, the three PMSM topologies are described as follows in this section:

a) Transverse Flux PMSM:

The stator winding of each phase in this topology is surrounded by magnetic circuits that are placed in a regular horseshoe pattern, as shown in Figure. I.8(a). Several single-phase machines (magnetic circuits) installed on the same shaft and offset by a geometric angle of $2\pi/q$ will then make up a phased q transverse flux motor, as shown in Figures. I.8(b) and I.8(c). It is especially well-suited for applications requiring high torque densities, but they are still in the development stage due to their mechanical complexity and production costs. Due to the three-dimensional nature of the field, we also emphasize strong pulsate couplings, vibrations, and excessive iron losses. The volume torque associated with a rather low saturation induction level of this kind of material could be negatively impacted by the use of compact powder composite magnetic materials in an attempt to minimize these losses. Furthermore, the limited successes have demonstrated that achieving a large volume of torque leads to an oversizing of the converter component [20, 27-30].

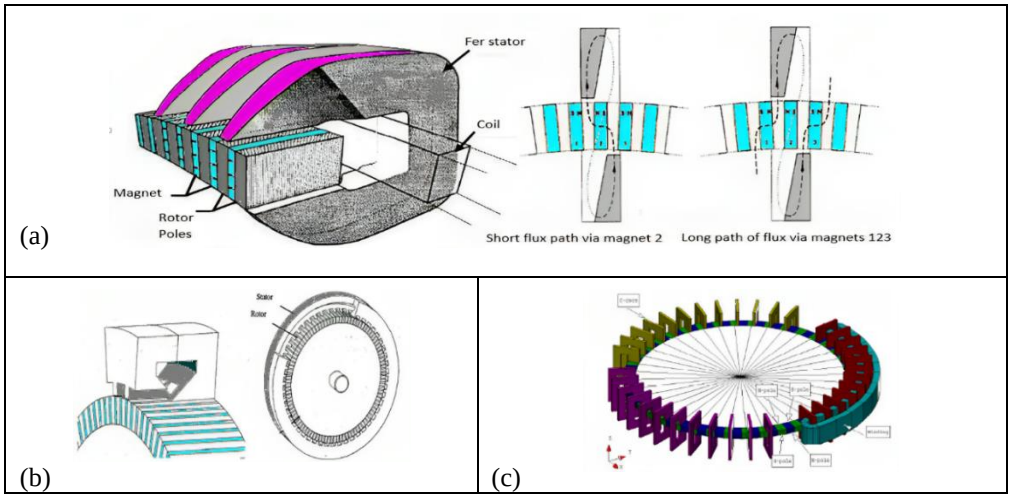

Figure I.8 : Topology of Transverse Flux PMSM, (a): Principle of Transverse Flux PMSM, (b): View of Transverse Flux PMSM, (c): View of a three-phase Transverse Flux PMSM

b) Radial Field Permanent Magnet (RFPM):

Radial Radial-field permanent magnets, or RFPMs for short, are the first permanent magnet machines used in the industry. They have been extensively employed in fractional horsepower applications for a number of decades, but not in large-scale industrial applications. Radial-field permanent magnet devices (see Figure. I.11) have since seen some significant developments, though. Furthermore, one of the key requirements in integrated systems is to choose the best electrical equipment for a certain application. [34] It provides a thorough analysis of the evolution and design of the radial-field PM machines as of the present day. Within a radial field, the flux direction runs along the machine's radius. It has the same stator as a traditional induction machine. These arrangements can have an externally mounted or internally located rotor. The primary drawback of this device is the permanent magnets' surface placement, which makes high-speed applications challenging. For this reason, an external placement of the machine's rotor can lower the likelihood of the magnets breaking. Centrifugal force is responsible for the placement of the surface magnets on the rotor. As a result of improvements in permanent magnet technology and power electronics, it is also starting to replace asynchronous machines. The structure of the RFPM is presented as follows [3, 35]:

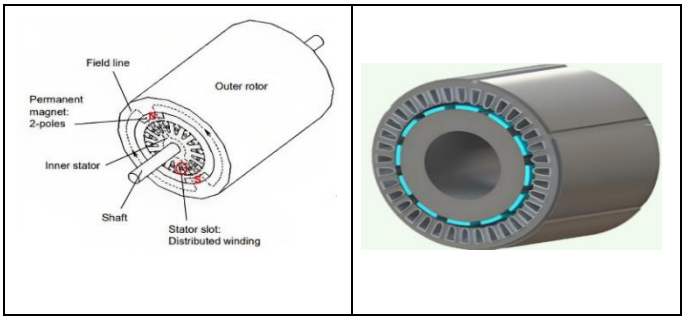

Figure I.9 : Structure of RFPMs categories

c) Axial Field Permanent Magnet (AFPM) :

Axial field permanent magnets, or so-called AFPMs, are made up of one or more movable discs that hold the permanent magnets in place and one or more stationary wound discs, where the rotor shaft and the flux direction are parallel in an axial field (see Figure. I.12) [7]. The 1990s saw a rise in interest in axial flux permanent magnet (AFPM) synchronous machines, primarily because of their performance and structure, which so closely match the needs of low-speed, high-torque. Furthermore, AFPM motor applications, such as various types of ship propulsion drives, electrical vehicles' wheels, and other industrial applications, are currently being researched [36-39].

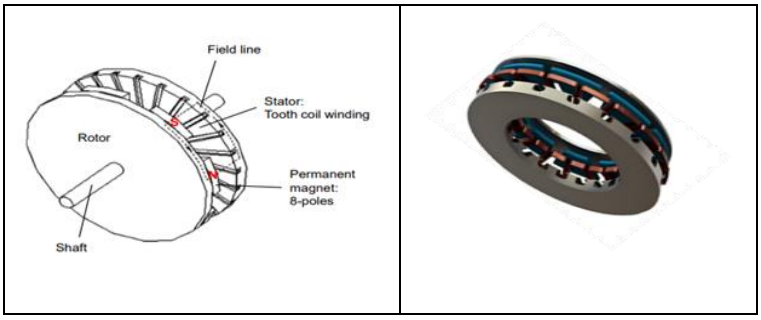

Figure I.10 : Structure of AFPMs categories

I.5.2 Configurations of the PMSMs

The diversity and development of the PMSM configuration, which came successively, as well as the research that contributed to that, is what distinguishes the PMSM and keeps it up to date with modern research, so that each configuration meets the requirements of every system of industrial applications and other systems in which this machine resonated greatly compared to the rest of AC machines. The number of stator and rotor, their respective positions, and the type of magnet construction are the most significant factors that contributed to the diversity of motor configurations. Furthermore, these configurations have a close relationship with the types of PMSM mentioned above, as half of them take the structure of RFPM and the other half take the structure of AFPM. We'll highlight each configuration of the PMSM's structures in this section.

A. Configurations of the PMSM based RFPM type

These configurations belong to the category of RFPM, where most of them are classified according to the position of the rotor and the stator. They are considered popular in the wind energy system due to the simplicity of their category construction as well as the fact that they are commonly used for direct drive; their stator is identical to that of a classic induction machine. Furthermore, a few configurations for permanent magnet machines were introduced; these may be regarded as novel [41, 42]. These configurations are designed as follows [23]:

- External Stator and Internal Rotor (ES-IR)

The configuration of an external stator-internal rotor motor, or ES-IR, is a traditional electric motor configuration, where it is considered the most commonly used machine in manufacturing. In addition, this configuration is classified into two types: the first is internal rotor structures

with surface-mounted magnets, or what is called SM-PMSM, and the second is buried magnets. Figure. I.15 provides a more thorough explanation of each of these two types [23].

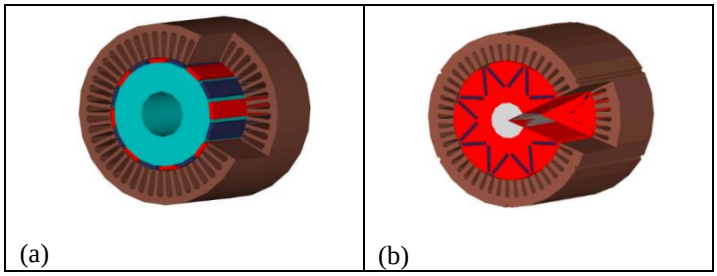

Figure I.11 : Structure of External Stator and Internal Rotor (ES-IR), (a): to internal rotor structures with surface mounted magnets, (b): buried magnets

- Drum motor: Toroidally Wound Internal Stator and Two Rotors (TWIS-TR)

The drum motor is the second configuration of the RFPM category, which is constructed from an internal stator and an external rotor. When the rotor can be integrated directly into the machine being used, this motor layout is appropriate. Examples of such applications are driving rolls, convey belts, and wheel motors in electrical vehicles. It is an alternative configuration, and it is designed as shown in the below figure [23].

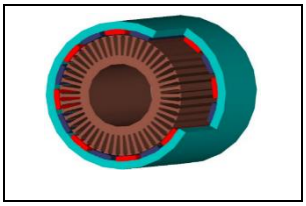

Figure I.12 : Configuration of the drum motor

- Toroidally Wound Internal Stator and Two Rotors (TWIS-TR):

The last configuration that will be presented in this section is a machine structure with a toroidally wound internal stator and two rotors, which was introduced recently by [41]. Given the more complex mechanical structure and the need for effective internal air circulation to remove heat from the stator, the latter design does not appear to be very practicable. Nonetheless, the structure essentially increases the machine's torque density and might be helpful in some situations where the machine's total volume is constrained. Figure. I.17 is presents this configuration [23].

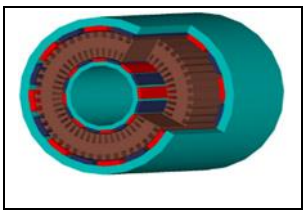

Figure I.13 : Configuration of a double rotor configuration with internal toroidally wound stator

B. The configuration of the permanent magnets in the rotor

There are various feasible and reasonable configurations to assemble the magnets into the rotor of an RFPM. In the same context, the difference in the inductance values of the direct and quadrature axes, which is detailed below, is a significant effect of the permanent magnet attachment method on the rotor. The direct axis is the main flux channel via the permanent magnet rotor. When the stator winding is lined with permanent magnets, the stator inductance measured at their position is referred to as the direct axis inductance. The measurement of the quadrature axis inductance involves turning the magnets from their pre-aligned (direct axis) configuration by 90°. In this orientation, the rotor's iron (inter-polar region) is exposed to the stator flux. The permanent magnets in the rotor can be categorized into two main configuration types. The first one is called the surface PMSM because the magnet of its configurations exists on the surface, while the second one is called the buried PMSM because the magnet of its configurations exists inside the PMSM. Furthermore, each configuration is characterized by different features, layouts, and structures compared to the other configurations. In order to identify these differences, we'll provide a description of the structures (layout) and features of each configuration as follows [3,23, 42]:

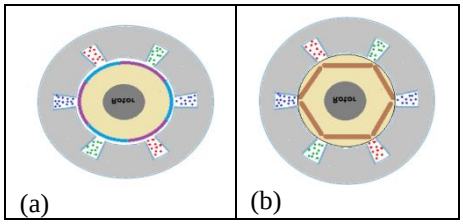

Figure I.14 : The PMSM's rotor configurations, (a): surface PMSM (SPMSM), (b): Buried PMSM (BPMSM)

1. Surface PMSM (SPMSM)

In types of this configuration, the magnet is situated on the surface of the rotor, which is classified into three types: surface-mounted, surface-mounted magnets with pole shoes, and inset PMSM. While rotor lamination or solid rotor core construction can be used to build these configurations, laminated rotors are typically required for other sorts of machines. Losses should be taken into account if solid components are handled with caution. The synchronous machines are typically noticed in relation to the d- and q-axes since they are inherently magnetically unsymmetrical. Strong effects on the Ld and Lq inductances are caused by the rotor's geometrical structure [23]. In order to become acquainted with the layout of these configurations, Figure. I.9 is presented below:

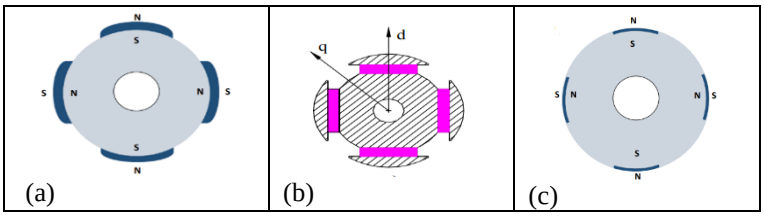

Figure I.15 : Layouts of SPMSM, (a): surface mounted PMSM, (b): surface mounted with pole shoes PMSM, (c): Inset PMSM

- Surface-mounted PMSM

The fabrication and assembly of surface-mounted structures are comparatively easy, which makes them the most commonly used. The magnets in this motor are in contact with a demagnetizing field since they are surface-mounted. Moreover, because the effective length of the air gap is large, the machine's inductance is low due to permanent magnets' relative permeability being similar to that of air. The surface permanent magnet machine's beginning torque is minimal because the air gap reluctance is theoretically constant for all rotor orientations. Furthermore, the machine's rotation speed needs to be restricted if permanent magnets are adhered to the rotor's surface to prevent centrifugal forces from rupturing the glue joint. A reinforcing belt around the rotor can increase the mechanical rigidity of the rotor construction. A stainless steel cylinder or a band of carbon fibre or fibreglass could serve as the reinforcement. However, the previously mentioned are thermal insulators, which further complicate the rotor cooling process. Because stainless steel is conductive, there is an issue with eddy currents when employing it to create a reinforcement cylinder. Due to slotting and, particularly when an inverter is used, the supply current's harmonic content, eddy currents are created inside the cylinder [23, 42, 43]. Figure. I.20 represents the layout and structure of this configuration:

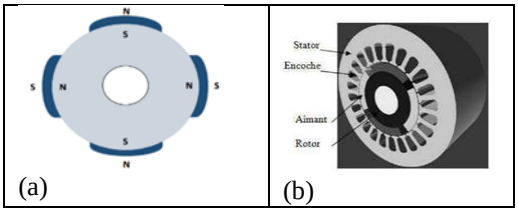

Figure I.16 : Layout and structure of the surface-mounted PMSM

- Surface mounted with pole shoes PMSM:

Aside from the previously described configuration of the surface-mounted PMSM, other configurations, such as the ones shown in Figure. I.19(b), are called surface-mounted PMSM with pole shoes. This configuration structure can be employed to achieve both mechanical protection for the magnets and a sinusoidal air-gap flux density waveform.

- Inset PMSM:

As seen in Figure. I.21, this kind of motor has magnets placed on the rotor's surface to aid in mechanical assembly. Its d-axis inductance differs somewhat from its q-axis inductance. Interpolar gaps exist between the iron components of the permanent magnets, which increase saliency. The height of the magnets in relation to the iron and their aperture determine the salience value. Still, this structure's properties are essentially similar to those of the surface-mounted PMSM [35, 42].

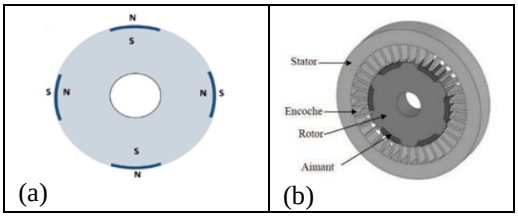

Figure I.17: Layout and structure of the surface-mounted PMSM

2. The buried PMSM (BPMSM)

This configuration is characterized by the presence of the magnet inside the rotor, and it has three types: interior PMSM, circumferential orientation PMSM, and buried PMSM with a shaped air-gap outline. Their layouts are illustrated in Figure. I.22. The rotor construction has a few advantages over the surface-mounted structure, albeit being somewhat more complicated to manufacture [23].

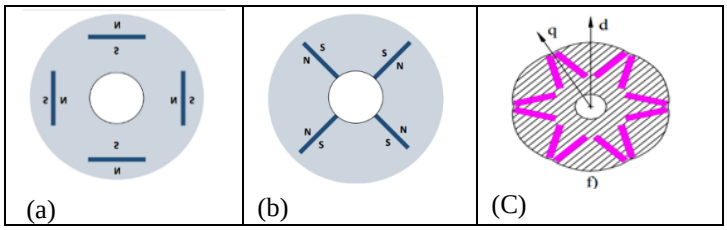

Figure I.18 : Layouts of BPMSM, (a) interior PMSM, (b): circumferential orientation PMSM, (c): buried PMSM with a shaped air-gap outline

- Interior PMSM:

Interior magnet machines have complex inductors due to magnets that are embedded into the rotor, as shown in Figure. I.23, and that are magnetically radially. Nonetheless, this structural arrangement is required to enhance mechanical resistance and safeguard the permanent magnets in force deflux mode or in the event of a short circuit. The inside magnet machine is appropriate for applications requiring continuous power across a broad speed range, as previously noted. Additionally, the IPMSM inductance values exhibit a geometric saliency that is crucial for low-speed management and vary in accordance with the rotor position. The active air gap space is smaller in this configuration than it is in the corresponding machine that uses surface magnets. The IPMSM has distinct d- and q-axis inductances, with Ld < Lq. As a result, a reluctance torque exists, and compared to a comparable surface permanent magnet machine, the torque density may be greater [3, 35, 42].

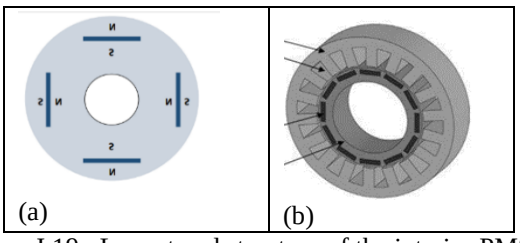

Figure I.19 : Layout and structure of the interior PMSM

- Circumferential orientation PMSM :

The magnets in this configuration of motor are housed inside the rotor, as Figure. I.24 illustrates. Buried deep within the rotor, the magnets are positioned radially into it. The magnets are oriented in the circumference directions in this design. Next, by focusing the flux from the permanent magnets, the magnetic poles are generated at the level of the ferromagnetic portions of the rotor. The concentration of the flux produced by the magnets and the increased inductance that is gained are two of this type of PMSM's primary advantages. The magnets in this machine are similarly well shielded from mechanical stress and demagnetization as those in internal magnet machines. In comparison to the d axis, the synchronous reactance is larger on the q axis [29, 42, 44].

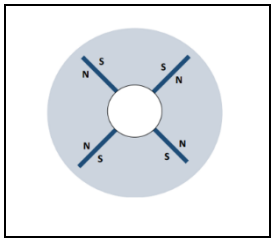

Figure I.20 : Layout of the circumferential PMSM

- Buried PMSM with a shaped air-gap outline:

Buried PMSM with a shaped air-gap outline is one of the novel configurations for the PMSM, like Figure. I.25, which characterizes the radial nature as well as represents the third architecture of the buried PMSM. It is also called flux concentration. Furthermore, this configuration has a nearly sinusoidal air-gap flux density waveform and low cogging torque, which thus improves the torque quality. The demagnetization risk of the permanent magnets is reduced since they are surrounded by ferromagnetic iron and fixed relatively far from the air gap [23].

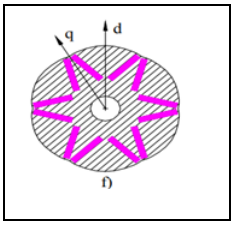

Figure I.21 : Layout of buried PMSM with a shaped air-gap outline PMSM

C. Configurations of the PMSM based AFPM type

These configurations fall under the AFPM category, most of which are categorized based on the number of rotors and stators. They also comprise the winding arrangements and the stator(s) position with respect to the rotor(s) locations. They offer flexibility in selecting the ideal machine construction for the application at hand and are readily available. Among the possible setups are: [23, 36].

- Structure with one rotor and one stator:

This configuration is considered to be the most basic for an axial-flux permanent magnet machine. However, compared to configurations in which the axial forces are balanced, this structure suffers from an uneven axial force between the rotor and the stator, necessitating more intricate bearing arrangements and a larger rotor disc. The structure of this configuration is shown in Figure. I.26 [23,45,46].

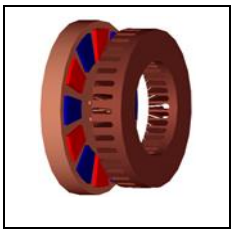

Figure I.22 : Structure with one rotor and one stator

- Structure, in which the stator is located between two rotors:

The axial-flux machine construction of this configuration is a "TORUS" type, with phase coils wound around either a slotted or non-slotted stator. The first permanent-magnet machine of the "TORUS" type with a nonslotted stator was released in the late 1980s. Short end-windings on the toroidally wound phase winding increase machine efficiency and power density. The more intricate connection of the stator to the frame is a disadvantage. Additionally, there is less room for the winding in this arrangement than in the alternative, known as the axial flux interior rotor permanent-magnet machine, or AFIPM, where the rotor is positioned between the stators [23,47-52].

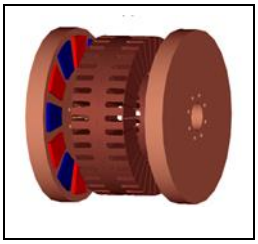

Figure I.23 : Structure, in which the stator is located between two rotors

- Structure, in which the rotor is located between two stators:

This structure is designed as follows:

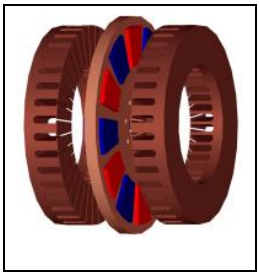

Figure I.24 : Structure, in which the rotor is located between two stators

- Multistage structure including several rotors and stators :

As seen in Figure. I.29, more intricate configurations can be achieved by stacking multiple machines parallel to one shaft and creating a multistage axial-flux machine [23]. These devices could be taken into consideration for research [53], high-speed permanent-magnet generator applications [54], ship propulsion drive use [41], and pump applications [55].

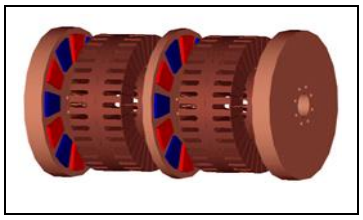

Figure I.25 : Structure with multistage including several rotors and stators

I.6 Application field of the PMSM

With the rapid evolution of technology and the onset of the Fourth Industrial Revolution, electric motors have continually proven their effectiveness and adapted to meet the evolving needs of industries. Researchers have made significant progress in enhancing the performance of industrial motors while reducing energy consumption. Various types of electrical machines have found application in a diverse range of sophisticated tasks. Among these, Permanent Magnet Synchronous Machines (PMSMs) have gained widespread acceptance across industries due to their exceptional power density, high torque-to-inertia ratio, superior efficiency, minimal losses, precise control, simple structure, and notable durability. The multitude of advantages offered by PMSMs has made them indispensable in critical applications such as CNC machine tools, industrial robots, space exploration technology, computer drives, electric vehicles, and servo precise position control systems. Moreover, PMSMs are utilized in both single and multiple configurations across different applications. This section will highlight some of the most prominent applications reliant on PMSMs, starting with several notable or ambitious uses in multi-machine systems. [10]:

I.6.1 Rail transport

A distributed traction system (Figure. I.30(a)) is typically utilized in the traction system of a railway car due to space limitations caused by mechanical constraints (track width, wheel diameter, ground clearance, etc.). Then, every wheel on the bogie is fitted with a device that satisfies the overall traction power specifications. This makes it the perfect application for a shared workspace. The concept of employing PMSM as the foundation of a traction system has recently been developed for applications in metro, commuter trains, and high-speed trains. Such a gearless traction drive system can be constructed because of the high mass torque of a PMSM (Figure. I.30(b)). It is expected that the PMSM-based shared architecture will provide significant railroad traction.

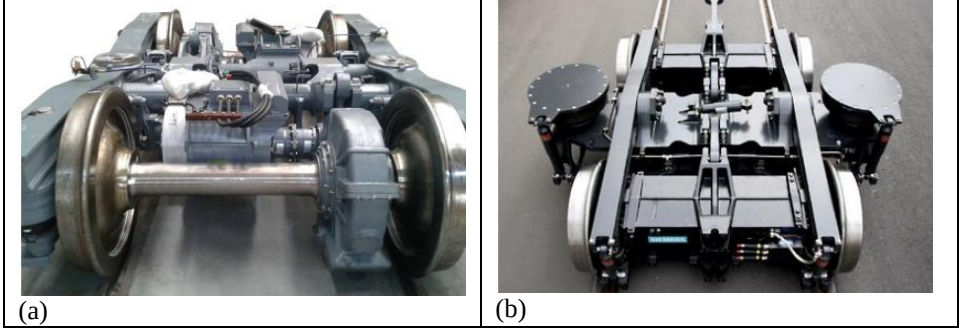

(a) (b)

Figure I.26 : Bogie structure (a) with reduction; (b) direct drive (Syntegra from Siemens) [10].

1.6.2 Elevator doors

The two doors of a traditional elevator door system are powered by an intricate mechanical link. This mechanical mechanism is driven by a machine, which causes the two doors to open and close simultaneously. It is clear that this mechanical connection system is intricate and prone to malfunction. Since an PMSM's speed is always synchronous with power frequency, we can think of pooling the inverter over multiple machines in order to do away with the intricate mechanical connection system. The command law's definition will serve as the basis for the synchronization of actions.

I.6.3 Aeronautics

Aeronautics is interested in substituting electrical energy for mechanical or hydraulic power on board, spurred by the idea of "more electric aircraft." In this sense, the shared architecture plays a key role in the system's electrification, especially for the flying controls. First and foremost, hardware redundancy is typically used to achieve fault tolerance in aeronautical applications. As such, every actuator has many redundant drive systems installed. Because of this, the entire control system is complicated and laborious. Redundancy is only required for this inverter in the shared design that uses it to control several actuators. Second, it's common for multiple actuators to be in charge of the same system, such as an elevator, a spoiler, or a flap (Figure. I.31). This increases the effective aerodynamic force and decreases the structure's weight by uniformly distributing the driving force over a long, thin control surface. Since these actuators are entirely synchronous, it makes sense to link the PMSMs in parallel in this case.

Figure I.27 : Spoiler system for a commercial aircraft [10].

After the applications that use the multi-PMSM form mentioned above, we will mention some important applications that depend on the single-PMSM form as follows:

I.6.4 Electric vehicles (EVs)

Reducing environmental consequences is a significant concern for the automotive and transportation industries, especially with regard to CO2 emissions, sulphur oxides, and nitrogen oxides. As part of the ecological and energy transition, policies seek to achieve carbon neutrality in this sector by 2050. Battery electric cars (BEVs), hybrid electric vehicles (HEVs), and fuel cell electric vehicles (FCEVs) are regarded as important answers to the present environmental issues. BEVs are fully electric cars that run exclusively on batteries. They have several benefits, including no emissions, top performance, no need for oil, and a smooth, noiseless ride with minimal disturbance to the surrounding area. Both the scientific community and the automotive industry place a high value on the development of electric vehicles (EVs), paying close attention to crucial aspects of their performance. Improved EV energy sources, structures, and electrical drive systems are the focus of ongoing research, which is of great interest to automakers and academics. The core components of an electric motor, controller, battery stack, and power converters make up an EV's propulsion system. A variety of electric motor types, including permanent magnet synchronous motors (PMSM), variable reluctance motors (VRM), induction motors (IM), and direct current (DC) motors, are used to ensure the propulsion of electric vehicles. In order to improve the performance of EVs and achieve the above-mentioned goals, PMSM is considered the best choice for driving electric vehicles (EVs). Due to the features mentioned above, the EV drive based on PMSM has been configured in Figure. I.32 [58-63].

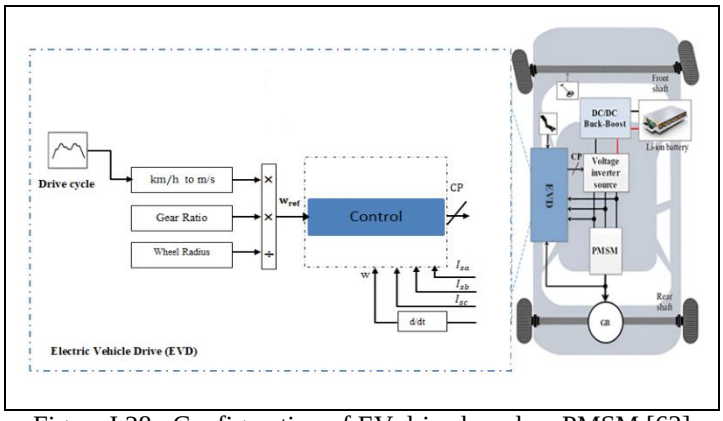

Figure I.28 : Configuration of EV drive based on PMSM [63]

I.6.5 Wind energy conversion system (WECS)

Decentralized electricity production made possible by renewable energy sources can help address the issue of electrifying remote locations where a large number of people lack access to energy, making it difficult for them to meet their basic needs and improve their quality of life. On a human scale, renewable energy is defined as a source of energy that renews itself swiftly enough to be seen as limitless. One benefit of renewable energy sources is that their supply is limitless. By using them, we can meet our energy needs while protecting the environment [64].

Wind energy is one renewable energy source that has drawn a lot of interest. It is extensively utilized and, in recent decades, has gained the ability to compete with traditional energy sources. Consequently, the installed wind turbine capacity globally is increasing at an accelerated rate. By the end of 2030, the World Wind Association predicts that installed wind capacity could reach 1600 GW [65]. Among other renewable energy sources, wind energy is prioritized due to a number of factors, including its cost-effectiveness, ease of installation, reliability, and efficiency. Furthermore, offshore or onshore wind farms are possible [66]. Numerous buildings have been engineered to include wind energy conversion systems (WECS); some of them include squirrel cage induction generators (SCIGs) and doubly fed induction generators (DFIGs). The sole drawback to these devices is that they need both an excitation and a multistage gearbox. Because of this, PMSG has drawn attention from researchers recently due to its improved performance, increased economy and dependability, and capacity to run at low speed, which does away with the requirement for a gearbox. Additionally, this control system requires less maintenance [66,67]. The machine is electrically connected to the constant frequency three-phase grid network via a power electronic interface (back-to-back converter), as seen in Figure. I.33, and mechanically coupled to the blades. The latter is made up of a grid-side converter (GSC) and a machine-side converter (MSC) coupled by an intermediary capacitor and a shared DC link. This arrangement enables the generator to function in variable wind conditions while regulating and adapting its power to the grid code [68,69].

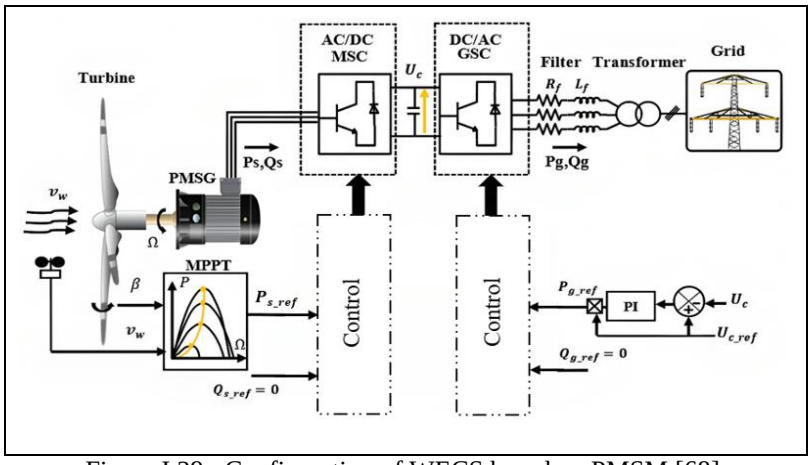

Figure I.29 : Configuration of WECS based on PMSM [68].

I.6.6 Electric aircrafts (EAs)

All non-propulsive systems in conventional commercial aircraft technology are powered by a mix of secondary power sources, including electric, pneumatic, hydraulic, and mechanical systems. This leads to higher costs, heavier aircraft, and decreased reliability [70]. Reliable actuators for flight controls are displacing the traditional architecture with the introduction of recent innovation in electrical machine design and power electronics, leading to an increase in electric aircraft (MEA), such as the Boeing 787, Airbus 380, and Lockheed F-35 [71]. The goal of the technology is to create an all-electric aircraft (AEA) in the future. The biggest benefit of this technological revolution is that, in comparison to conventional technology, it uses less fuel, emits fewer emissions, makes less noise, and has a reduced failure rate [72]. But in contrast to

previous designs that used only a quarter of the power, this alteration has increased the power requirement onboard the aircraft, reaching 1 MW (Boeing-777) [73]. When the two architectures are compared in Figure. I.34, it is readily apparent that the MEA technology retains the Ram air turbine (RAT) and environmental control system (ECS), but the anti-icing system is electrically powered by a modified auxiliary power unit (APU) design. Although they are electrically operated, the distributed flight control surfaces are hydraulic.

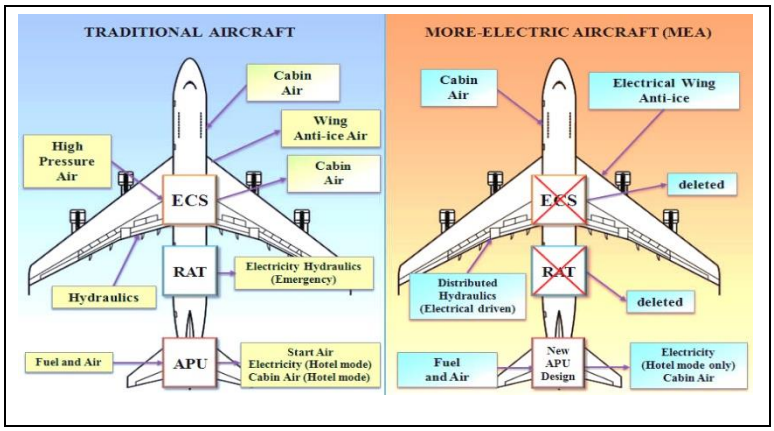

Figure I.30 : Comparison of conventional vs. more electric aircraft (MEA) technology [73]

One of the most popular devices in aerospace electromechanical or electrohydrostatic actuators (EMA/EHA) for MEA flight control applications is the permanent magnet synchronous motor (PMSM) [74]. Three key benefits of the permanent magnet synchronous motor account for its dominance: cheap maintenance costs, a high torque-to-current ratio, and compact design. Figure. I.35 compares the two actuation technologies. Moreover, PMSM-based electrical actuators are a well-liked option because of their better performance, which is demonstrated by a higher steady-state torque in comparison to induction machines, a simpler PM motor controller, and other previously mentioned characteristics [72,75].

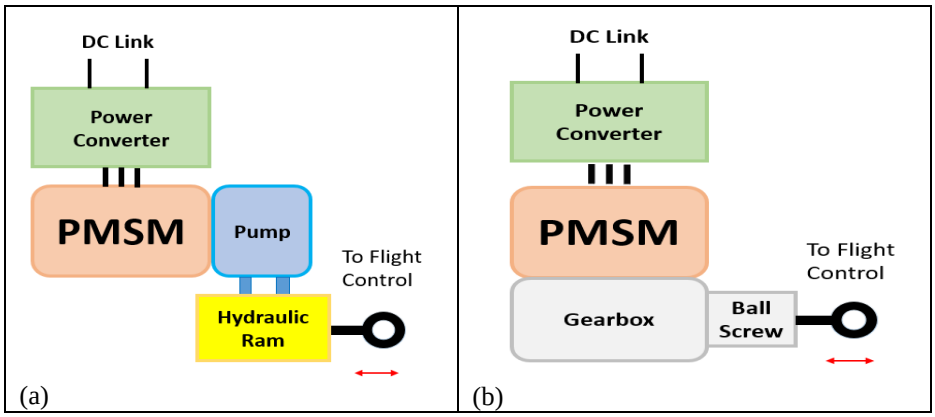

Figure I.31 : Flight control actuators in MEA. (a) Electrohydrostatic (EHA) ,(b) Electromechanical Actuator (EMA)

I.6.7 Photovoltaic pumping system

A photovoltaic pumping system based on permanent magnet synchronous motors (PMSMs) represents a compelling synergy between renewable energy and efficient water pumping technology. The researchers explore the innovative combination of photovoltaic panels and PMSM-driven water pumps, highlighting their numerous advantages and significant contributions to sustainability and resource management. By utilizing solar energy through photovoltaic panels, these systems provide a clean, sustainable, and economically viable means of powering water pumps. PMSMs, with their high efficiency, precise control, and ability to adapt to varying environmental conditions, enhance the overall performance of such systems. Their permanent magnets in the rotor ensure synchronous operation, optimizing energy conversion and water delivery. Key benefits of this integrated approach include reduced dependence on fossil fuels, minimized greenhouse gas emissions, and decreased operational costs. Furthermore, the adaptability of PMSMs to different water pumping requirements, coupled with the abundance of sunlight in many regions, makes photovoltaic PMSM pumping systems an ideal solution for remote and off-grid areas.

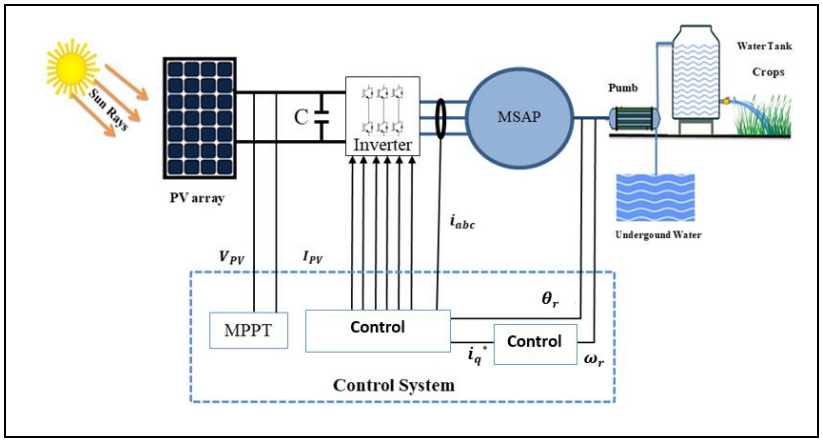

Figure I.32 : Configuration of the Photovoltaic pumping system

I.7 Conclusion

In recent years, significant advancements have occurred in the state of the art for Permanent Magnet Synchronous Motors (PMSMs) owing to the escalating demand for precise and efficient electric machines across various applications. The inclusion of permanent magnets in the rotor of PMSM electric machines has led to remarkable power-to-weight ratios, eliminating the need for field windings. Another distinguishing feature is their efficient conversion of electrical energy into mechanical work. Recent developments in magnet materials and production processes have greatly enhanced the performance of PMSMs, facilitating their widespread adoption. To mitigate risks associated with rare-earth element supply chains, researchers continue to explore alternative magnet materials.

PMSMs have evolved into a pivotal technology offering outstanding efficiency and precise control for diverse applications. Their ongoing refinement and adaptation to meet the specific demands of various industries underscore their critical role in fulfilling the energy and

performance requirements of modern engineering and technology. Moreover, their compact size, lightweight design, high efficiency, excellent power factor, rapid response, broad speed range, and accuracy make permanent magnet synchronous machines (PMSMs) highly sought after across a wide spectrum of applications. These include wind power generation, electric vehicles, aerospace, numerical control systems, and photovoltaic pumping systems.

CHAPITRE II

COMPREHENSIVE MODELING AND PWM TECHNIQUES FOR PMSM DRIVE SYSTEMS

II.1 Introduction

Understanding the behavior of PMSMs, designing effective control systems, and optimizing performance all necessitate thorough modeling of them. Equations that explain the electromagnetic, mechanical, and control characteristics of the motor are usually included in the mathematical model of a PMSM. Capturing the electrical properties, switching dynamics, and control schemes used in PMSMs are all part of the modeling process. The creation of mathematical formulas that explain the link between input and output voltages, currents, and power flows is at the core of this modeling project. This involves taking into account the effects of PMSM features on system performance as a whole, such as rising time, steady-state error…etc. In order to conduct an in-depth theoretical analysis of the PMSM drive, an appropriate mathematical model of the device must be created and put into use, one that will enable a satisfactory level of precision in characterizing its behavior and quantities. Because the PMSM and the traditional synchronous motor are so similar in terms of construction, the dynamic model of the PMSM may be obtained using the well-known formulas for the classical synchronous machine. The resultant equations are usually non-linear, which means they are relatively complex, and the variables are time-variant when the three phase frame is applied to the PMSM. The equations that are derived are substantially simpler if the machine is described using a coordinate transformation using Clark or Park. This makes it possible to speed up the numerical calculations needed for the computational simulations. Moreover, the resulting variables do not change over time under steady-state operation, which facilitates further computations and streamlines the control system's implementation. When these limitations are taken into consideration, the resulting equations become extremely straightforward and may reasonably accurately anticipate the behavior of the machine. The inverter and PMSM form a closely integrated system where the inverter controls the electrical power supplied to the motor, influencing its speed, torque, and overall performance. The design and implementation of the inverter are critical factors in achieving efficient and reliable operation of PMSM-based systems. In this chapter, we'll get to know the modeling of the PMSM in the abc, α-β and d-q frames, the different methods of its modeling based on the d-q frame, as well as the modeling of the three-phase voltage inverter and its control approaches. In addition, Modeling of the machine based on the open loop was also simulated using MATLAB Simulink.

II.2 Mathematical Modeling of three-phase PMSM Systems

The permanent magnet (PM) rotor and three-phase stator make up the PMSM. The three-phase windings are positioned 120 degrees electrically apart in the stator slots created by the ferromagnetic lamination stacks, like the architecture of an induction machine. The design of the rotor, particularly the location of the permanent magnet therein, determines the properties of PMSM, Figure. II.1 explains this description [76].

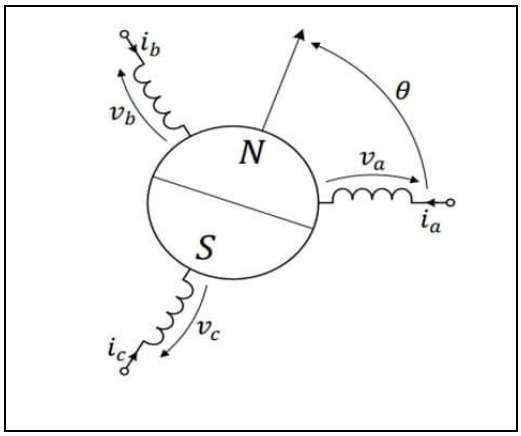

Figure II.1: A PMSM's three-phase representation

II.2.1 Electrical equations of the PMSM

The equations for the three-phase stator voltage, as seen in the three-phase stationary frame (abc − axis), can be written as follows [76]:

$$v_{abc} = R_s . i_{abc} + \frac{d\varphi_{abc}}{dt} \tag{II.1}$$

Where: $v_{abc} = [v_a \quad v_b \quad v_c]^{\mathrm{T}}$ represents stator voltages, R_s is stator resistance, $i_{abc} = [i_a \quad i_b \quad i_c]^{\mathrm{T}}$ represents stator currents and $\varphi_{abc} = [\varphi_a \quad \varphi_b \quad \varphi_c]^{\mathrm{T}}$ represents stator fluxes. Furthermore to, φ_{abc} is described as follows:

$$\varphi_{abc} = L_{ss} . i_{abc} + \psi_{f.abc} \tag{II.2}$$

Where: $\psi_{f.abc} = [\,\psi_{f.a} \quad \psi_{f.b} \quad \psi_{f.c}]^T = \psi_r . \left[\cos(p\theta) \quad \cos(p\theta - \frac{2\pi}{3}) \quad \cos(p\theta + \frac{2\pi}{3})\right]^T$

With ψ_r is the permanent-magnet flux linkage, θ is the mechanical angular position, p is the number of poles, and L_{ss} is given as follows:

$$L_{ss} = L_{so} + L_{sv} \tag{II.3}$$

Where;

$$L_{so} = \begin{bmatrix} l_{so} & M_{so} & M_{so} \\ M_{so} & l_{so} & M_{so} \\ M_{so} & M_{so} & l_{so} \end{bmatrix} \quad , \quad L_{sv} = l_{sv} \begin{bmatrix} \cos(2p\theta) & \cos(2p\theta - \frac{2\pi}{3}) & \cos(2p\theta + \frac{2\pi}{3}) \\ \cos(2p\theta - \frac{2\pi}{3}) & \cos(2p\theta + \frac{2\pi}{3}) & \cos(2p\theta) \\ \cos(2p\theta + \frac{2\pi}{3}) & \cos(2p\theta) & \cos(2p\theta - \frac{2\pi}{3}) \end{bmatrix}$$

Given that $M_{so} = -\,0.5.\, l_{so}$, define M_{so}, l_{so}, and l_{sv} as the mutual and own inductances, respectively. In addition, depending on the machine, l_{so} and l_{sv} are positive values. Through the equations mentioned above, the PMSM-based three phases of equation (II.1) can be written as follows:

$$\begin{bmatrix} v_a \\ v_b \\ v_c \end{bmatrix} = R_s . \begin{bmatrix} i_a \\ i_b \\ i_c \end{bmatrix} + \frac{d}{dt} \left\{ [L_{ss}] \begin{bmatrix} i_a \\ i_b \\ i_c \end{bmatrix} + \begin{bmatrix} \psi_{f.a} \\ \psi_{f.b} \\ \psi_{f.c} \end{bmatrix} \right\} \tag{II.4}$$

II.2.2 Mechanical equations of the PMSM

The following equation can be obtained by treating the rotor according to the fundamental principle of dynamics [76]:

$$j.\frac{d\Omega}{dt} = T_e - T_l - F\Omega \quad \text{(II.5)}$$

With;

$$\begin{cases} \omega_e = p.\Omega \\ \frac{d\theta}{dt} = \Omega \end{cases} \quad \text{(II.6)}$$

Ω, ω_e are mechanical(rotor) and electrical(stator) speed respectively; p is number of pole pairs ; T_e, T_l are electromagnetic and load torques respectivelly; j is moment of inertia of the rotor ; F is friction constant of the rotor and θ is angular speed of rotor.

II.3 Coordinate transformations

Coordinate transformations refer to the process of converting coordinates from one reference frame to another. This is often done to simplify the analysis or representation of data in a particular context. There are various types of coordinate transformations, depending on the nature of the coordinate systems involved. Two common types include linear transformations and nonlinear transformations. Due to the fact that the PMSM belongs to the physics and engineering fields, coordinate transformations are often used to simplify the analysis of the PMSM. These transformations are applied to convert the three-phase quantities (typically represented in the abc coordinate system) into two components. Among these coordinate transformations are Park and Clark's popular ones used in power systems engineering. Figures. II.2 shows the quadrupole schematic depiction of a three-phase system. The voltages of the input terminals (sometimes referred to as the phase voltages) are expressed as $u_a(t)$, $u_b(t)$ and $u_c(t)$ accordingly the three input terminals are designated as a, b, and c. The three input currents in the system, sometimes referred to as the phase currents, are denoted by the symbols $i_a(t)$, $i_b(t)$, and $i_c(t)$. The neutral point is represented by the fourth terminal, N. Phase-to-phase voltage is the voltage between any two input terminals; for instance, the voltage between terminals a and b is expressed as $u_{ba}(t) = u_b(t) - u_a(t)$. Similarly, $u_{bc}(t) = u_b(t) - u_c(t)$ and $u_{ca}(t) = u_c(t) - u_a(t)$, where the sum of these quantities is zero according to the Kirchhoff's voltage law. Furthermore, since the neutral point N is typically unavailable, the phase currents' sum equals zero according to Kirchhoff's current law: $i_a(t) + i_b(t) + i_c(t) = 0$ [77].

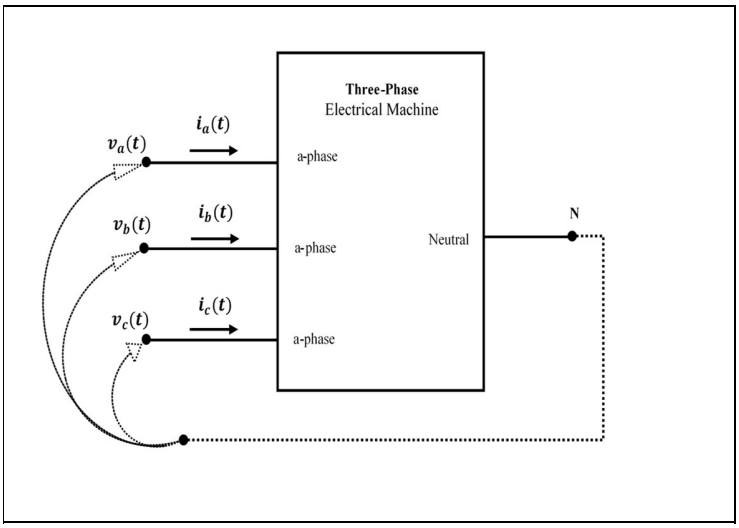

Figure II.2 : Schematic illustration of a three-phase system

II.3.1 Transformation of Clark

Firstly, the Clark transformation is used to transform the three-phase quantities $f_{abc}(t)$ into a two-axis frame (α, β) that is connected to the stator, where the balanced three-phase quantities are three-phase currents or voltages. As shown in Figures. II.3, the Clark transform reduces the 120◦ evenly spaced frame system to a two axis stationary reference frame attached to the stator by taking use of the symmetry of the three phase system. The bright red arrow in Figures. II.3, designated $\bar{f}(t)$, represents the vector formed by the sum of the abc-axis, which is the same as the sum of (α, β) vectors times 2/3 but with just two coordinate axes instead of three. Here, we investigate the balanced three-phase quantities denoted as $f_a(t)$, $f_b(t)$ and $f_c(t)$ with a zero homopolar component $f_o(t)$, where $f_o(t)$ can be described as follows [77-79].

$$f_o(t) = \frac{f_a(t)+f_b(t)+f_c(t)}{3} \tag{II.7}$$

The space vector $\bar{f}(t)$ cab be defined by considering the three-phase quantities as,

$$\bar{f}(t) = \frac{2}{3}\left[f_a(t) + f_b(t)e^{\frac{j2\pi}{3}} + f_c(t)e^{\frac{j4\pi}{3}}\right] = f_\alpha(t) + jf_\beta(t) \tag{II.8}$$

Where $f_\alpha(t)$ represent the real component and $f_\beta(t)$ represents the imaginary component of the space vector$\bar{f}(t)$. Considering equation (II.7) the real and imaginary component of the space vector can be calculated as,

$$\begin{cases} f_\alpha(t) = R_e\{\bar{f}(t)\} = \frac{2}{3}[f_a(t) - \frac{1}{2}f_b(t) - \frac{1}{2}f_c(t) = f_a(t) \\ f_\beta(t) = Im\{\bar{f}(t)\} = \frac{2}{3}\left[\frac{\sqrt{3}}{2}f_b(t) - \frac{\sqrt{3}}{2}f_c(t)\right] = \frac{1}{\sqrt{3}}[f_b(t) - f_c(t) \end{cases} \tag{II.9}$$

Figures. II.3 shows the graphical representation of the space vector $\bar{f}(t)$ corresponding to the three-phase quantities $f_a(t)$, $f_b(t)$and $f_c(t)$ and its real and imaginary components.

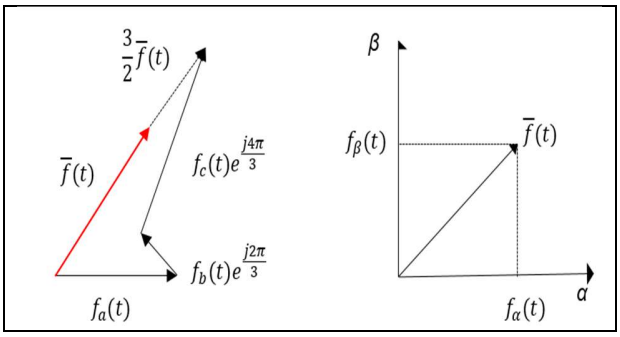

Figure II.3 : Space vector representation

As per equation (II.10), $f_a(t)$ directly correlates to $f_\alpha(t)$. On the other hand, $f_b(t)$ and $f_c(t)$ can be obtained by taking the real and imaginary components of the space vector $\bar{f}(t)$ and rotating it clockwise by $2/3\pi$ and $4/3\pi$, respectively. $f_a(t)$, $f_b(t)$ and $f_c(t)$ are obtained by inversely transforming $f_\alpha(t)$ and $f_\beta(t)$, as shown in equation (II.11).

$$\begin{cases} f_a(t) = R_e\{\bar{f}(t)\} = f_\alpha(t) \\ f_b(t) = R_e\left\{\bar{f}(t)e^{\frac{-j2\pi}{3}}\right\} = -\frac{1}{2}f_\alpha(t) + \frac{\sqrt{3}}{2}f_\beta(t) \\ f_c(t) = R_e\left\{\bar{f}(t)e^{\frac{-j4\pi}{3}}\right\} = -\frac{1}{2}f_\alpha(t) - \frac{\sqrt{3}}{2}f_\beta(t) \end{cases} \quad \text{(II.10)}$$

The transformation equations can be written in a compact form using the transformation matrices as below

$$\underline{f}_{\alpha\beta o} = \underline{T}_{abc\to\alpha\beta o} \cdot \underline{f}_{abc} \quad \text{(II.11)}$$

Where $f_{\alpha\beta o} = [f_\alpha(t) f_\beta(t) f_o(t)]^{\mathrm{T}}$, $f_{abc} = [f_a(t) f_b(t) f_c(t)]^{\mathrm{T}}$ and $\underline{T}_{abc \to \alpha\beta o}$ is the transformation from $abc \to \alpha\beta o$ given as below:

$$\underline{T}_{abc\to\alpha\beta o} = \sqrt{\frac{2}{3}}\begin{bmatrix} 1 & 0 & \frac{1}{\sqrt{2}} \\ -\frac{1}{2} & \frac{\sqrt{3}}{2} & \frac{1}{\sqrt{2}} \\ -\frac{1}{2} & -\frac{\sqrt{3}}{2} & \frac{1}{\sqrt{2}} \end{bmatrix} \quad \text{(II.12)}$$

In the same way, the inverse Clarke's transformation matrix for the transformation $\alpha\beta o \to abc$ is

$$\underline{T}_{\alpha\beta o\to abc} = \sqrt{\frac{2}{3}}\begin{bmatrix} 1 & -\frac{1}{2} & -\frac{1}{2} \\ 0 & \frac{\sqrt{3}}{2} & -\frac{\sqrt{3}}{2} \\ \frac{1}{\sqrt{2}} & \frac{1}{\sqrt{2}} & \frac{1}{\sqrt{2}} \end{bmatrix} \quad \text{(II.13)}$$

Depending on the Clark transformation, we can transform the electrical equations of the PMSM-based three-phase frame (abc − axis) that are presented in equation (II.4) into the model-based

two-phase frame ($\alpha\beta$ − axis) using the matrix transformation $\underline{T}_{abc\rightarrow\alpha\beta o}$ represented in equation (II.12) as follows [80]:

$$\begin{cases} v_\alpha = R_s.i_\alpha + L_\alpha \frac{di_\alpha}{dt} + E_\alpha \\ v_\beta = R_s.i_\beta + L_\alpha \frac{di_\beta}{dt} + E_\beta \end{cases} \quad \text{(II.14)}$$

The expression of the electromagnetic torque will be as follows:

$$T_{em} = \frac{3}{2} \cdot p \cdot \left(-\emptyset_\beta \cdot I_\alpha + \emptyset_\alpha \cdot I_\beta\right) \quad \text{(II.15)}$$

Where, $\boldsymbol{i_\alpha, i_\beta}$ are **α-β** axis equivalent stator currents; $\boldsymbol{v_\alpha, v_\beta}$ are **α-β** axis equivalent stator voltages; $\mathbf{R_s}$ is per phase stator resistance ; $\boldsymbol{L_\alpha, L_\beta}$ are α-β axis equivalent stator and $\boldsymbol{E_\alpha, E_\beta}$ are **α-β** axis back-EMFs. The $\boldsymbol{E_\alpha}$ and $\boldsymbol{E_\beta}$ are presented as follow:

$$\begin{cases} E_\alpha = -\omega_e.\psi_f.\sin\theta_e \\ E_\beta = \omega_e.\psi_f.\cos\theta_e \end{cases} \quad \text{(II.16)}$$

Where $\boldsymbol{\omega_e}$ is an electrical (stator) speed; $\boldsymbol{\psi_f}$ is rotor magnetic flux linking the stator, $\boldsymbol{\theta_e}$ is angular speed of rotor.

II.3.2 Transformation of Park

The rotating reference frame dq, which rotates with respect to the two-phase stationary reference $\alpha\beta$ frame introduced by Clarke's transformation, can represent the space vector $\bar{f}(t)$ corresponding to the three phase system quantities $f_a(t)$, $f_b(t)$and $f_c(t)$. Its angular speed is $\omega_{dq}(t)$. The stationary reference frame ($\alpha\beta$) and revolving reference frame (dq), along with the associated notations, are schematically represented in Figures. II.4 The angle between the two-phase rotating reference frame (dq) and the two-phase stationary reference frame ($\alpha\beta$) is represented in Figures. II.4 by $\vartheta_{dq}(t)$, the angle between the dq reference frame and the space vector $\bar{f}(t)$ is represented by $\gamma_{dq}(t)$, and the angle between the $\alpha\beta$ reference frame and the space vector $\bar{f}(t)$ is represented by $\gamma_{\alpha\beta}$(t). The space vector in the dq reference frame is denoted by $\overline{f}_{dq}(t)$, which has the following definition [78,79]:

$$\begin{aligned} \bar{f}_{dq}(t) &= \left|\bar{f}(t)\right| e^{j\gamma_{dq}(t)} \\ &= \left|\bar{f}(t)\right| e^{j(\gamma_{\alpha\beta}(t)-\vartheta_{dq}(t))} \\ &= \left(\left|\bar{f}(t)\right| e^{j\gamma_{\alpha\beta}(t)}\right) e^{-j\vartheta_{dq}(t)} \\ &= \bar{f}_{\alpha\beta}(t) e^{-j\vartheta_{dq}(t)} \\ &= f_d(t) + jf_q(t) \end{aligned} \quad \text{(II.17)}$$

The following formulas can be used to represent the real and imaginary components, $f_d(t)$ and $f_q(t)$, of the space vector $\bar{f}_{dq}(t)$ in the two-phase rotating reference frame:

$$\begin{cases} f_d(t) = f_\alpha(t)\cos(\vartheta_{dq}) - f_\beta(t)\sin(\vartheta_{dq}) \\ f_q(t) = -f_\alpha(t)\sin(\vartheta_{dq}) + f_\beta(t)\cos(\vartheta_{dq}) \end{cases} \quad \text{(II.18)}$$

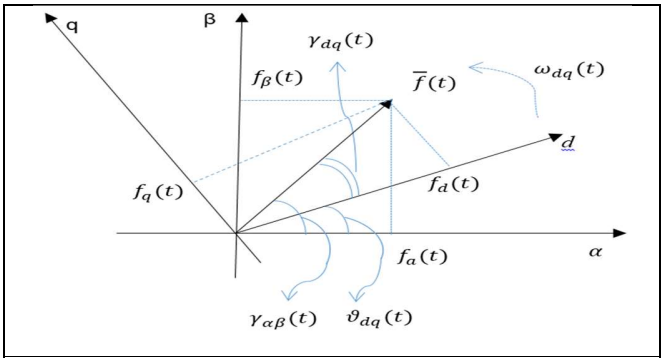

Figure II.4 : Representation of stationary reference frame ($\alpha\beta$) and rotating reference frame (dq)

In the $\alpha\beta$ reference frame, the real and imaginary components of the space vector are obtained by inversely transforming equation (II.18).

$$\begin{cases} f_\alpha(t) = f_d(\vartheta_{dq})\cos(\vartheta_{dq}) - f_q(t)\sin(\vartheta_{dq}) \\ f_\beta(t) = f_d(t)\sin(\vartheta_{dq}) + f_q(t)\cos(\vartheta_{dq}) \end{cases} \quad \text{(II.19)}$$

With the use of the transformation matrices, the transformation equations can be expressed compactly as shown below.

$$\underline{f}_{dqo} = \underline{T}_{\alpha\beta o \to dqo} \cdot \underline{f}_{\alpha\beta o} \quad \text{(II.20)}$$

Where $\underline{f}_{\alpha\beta o} = [f_\alpha(t) f_\beta(t) f_o(t)]$, $\underline{f}_{dqo} = [f_d(t) f_q(t) f_o(t)]$ and $\underline{T}_{\alpha\beta o \to dqo}$ is the transformation from $\alpha\beta o \to dqo$ given as below:

$$\underline{T}_{\alpha\beta o \to dqo} = \begin{bmatrix} \cos(\vartheta_{dq}(t)) & -sin(\vartheta_{dq}(t)) & 0 \\ sin(\vartheta_{dq}(t)) & cos(\vartheta_{dq}(t)) & 0 \\ 0 & 0 & 1 \end{bmatrix} \quad \text{(II.21)}$$

Likewise, for the $dqo \to \alpha\beta o$ transformation, the inverse Park's transformation matrix is:

$$\underline{T}_{dqo \to \alpha\beta o} = \begin{bmatrix} \cos(\vartheta_{dq}(t)) & sin(\vartheta_{dq}(t)) & 0 \\ -sin(\vartheta_{dq}(t)) & cos(\vartheta_{dq}(t)) & 0 \\ 0 & 0 & 1 \end{bmatrix} \quad \text{(II.22)}$$

The following represents the direct inverse transformation from the abc frame to the two-phase rotating reference dqo frame and the matching direct transformation from the three-phase abc frame to the dqo frame:

$$\underline{T}_{abc \to dqo} = \begin{bmatrix} cos(\vartheta_{dq}(t)) & cos(\vartheta_{dq}(t) - \frac{2}{3}\pi) & cos(\vartheta_{dq}(t) - \frac{4}{3}\pi) \\ -sin(\vartheta_{dq}(t)) & -sin(\vartheta_{dq}(t) - \frac{2}{3}\pi) & -sin(\vartheta_{dq}(t) - \frac{4}{3}\pi) \\ \frac{1}{2} & \frac{1}{2} & \frac{1}{2} \end{bmatrix} \quad \text{(II.23)}$$

$$\underline{T}_{dqo\to abc} = \begin{bmatrix} cos\,(\vartheta_{dq}(t)) & -sin(\vartheta_{dq}(t)) & 1 \\ cos(\vartheta_{dq}(t)-\frac{2}{3}\pi) & -sin(\vartheta_{dq}(t)-\frac{2}{3}\pi) & 1 \\ cos(\vartheta_{dq}(t)-\frac{4}{3}\pi) & -sin(\vartheta_{dq}(t)-\frac{4}{3}\pi) & 1 \end{bmatrix} \quad \text{(II.24)}$$

The electrical equations of the PMSM-based three-phase frame (abc − axis) can be transformed, depending on the Park transformation, using the matrix transformation $\underline{T}_{abc\to dqo}$ given in equation (II.22) into the model-based two-phase frame (dq − axis) as follows [81]:

$$\begin{cases} v_d = R_s.i_d + L_d\frac{di_d}{dt} + E_d \\ v_q = R_s.i_q + L_q\frac{di_q}{dt} + E_q \end{cases} \quad \text{(II.25)}$$

The expression of the electromagnetic become as follows:

$$T_e = (3.\tfrac{p}{2})((L_d - L_q)i_d.i_q + \psi_f.i_q) \quad \text{(II.26)}$$

Where, $\boldsymbol{i_d, i_q}$ are d-q axis equivalent stator currents; $\boldsymbol{v_d, v_q}$ are d-q axis equivalent stator voltages; $\mathbf{R_s}$ is per phase stator resistance; $\boldsymbol{L_d, L_q}$ are d-q axis equivalent stator and $\boldsymbol{E_d, E_q}$ are d-q axis back-EMFs. The $\boldsymbol{E_d}$ and $\boldsymbol{E_q}$ are presented as follow:

$$\begin{cases} E_d = -L_q.\omega_e.i_q \\ E_q = L_d.\omega_e.i_d + \omega_e.\psi_f \end{cases} \quad \text{(II.27)}$$

Where $\boldsymbol{\omega_e}$ is an electrical (stator) speed; $\boldsymbol{\psi_f}$ is rotor magnetic flux linking the stator, $\boldsymbol{\theta_e}$ is angular speed of rotor.

II.4 Regions where PMSM operates

The electrical and mechanical operating limits of the PMSM define its characteristics. Electrical operating limitations are related to voltage and current, while mechanical operating limits are related to torque and rotor speed.

II.4.1 Electrical operating limits

The highest voltage that can be applied and the drive's output current capabilities set boundaries for the operating zones of electric machines. The following assumptions are taken into account while calculating the operational limitations. Therefore, the voltages (u_{d} and u_{q}) and currents ($i_{\mathrm{d}}(t)$ and $i_{\mathrm{q}}(t)$) will have constant amplitudes in the rotor reference frame. The maximum voltage, or phase-to-phase nominal voltage, is represented by the symbol u_{nom}. The nominal current, or i_{nom}, corresponds to the thermal limit under steady state operating conditions [77].

- At each operational point, the limits of electric machines, which are the demagnetization of the permanent magnet, the temperature limits, and the insulation limits, must be equal to the drive limits (the voltage and current limits).
- Constant electrical speed (ω_e)

- Constant amplitude and frequency of the sinusoidal voltages and currents
- The operation of the drive's steady-state.

The rotor reference frame describes the machine's current limits as follows.

$$I_d^2 + I_q^2 \leq I_N^2 \tag{II.28}$$

In the case where $I_N = \sqrt{2}\, I_{nom}$, the nominal phase current peak value

In a similar vein, the voltage limit can be shown as:

$$U_d^2 + U_q^2 \leq U_N^2 \tag{II.29}$$

Where $U_N = \sqrt{\frac{2}{3}}\, U_{nom}$, the peak value of nominal phase voltage.

II.4.2 Mechanical operating limits

With the use of the speed vs. torque plan, as demonstrated in Figures. II.5, the mechanical operating limits of a PMSM can be demonstrated. Regarding torque and power, the two primary operating regions are:

- Constant torque zone: here, the voltage should be less than or equal to the highest voltage that is allowed, and the operation is restricted by a constant current locus. In this case, the PMSM can provide the maximum amount of torque at any speed lower than the base speed;
- Constant power area: in this region, the PMSM can deliver its maximum power at any speed above the rate speed, with the torque output decreasing as speed increases.

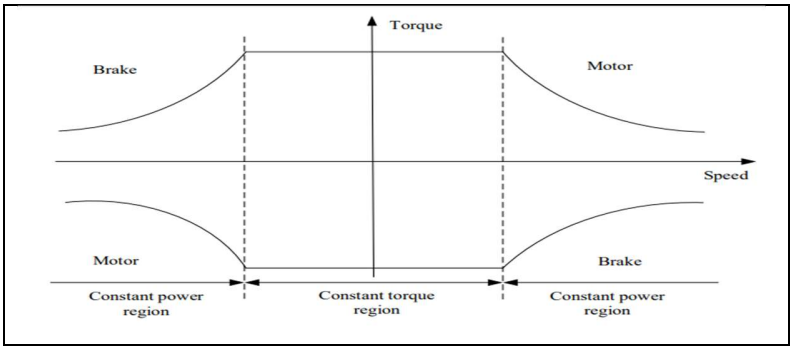

Figure II.5 : The mechanical operating limits of the PMSM

The PMSM's operating limits as stated above pertain to continuous steady state operation; nevertheless, overloading the drive within the thermal limits is conceivable for brief periods of time.

II.5 Modeling of the PMSM system using deferent strategy

The derived equations are substantially simpler if the machine is characterized using a d-q rotor reference frame, which speeds up the numerical calculations needed for the computational simulations. Additionally, the resulting variables do not change over time under steady-state

operation, which facilitates subsequent computations and streamlines the design of the control system. Furthermore, The d-q model in the rotor reference frame is the most widely used and well-liked model in the literature. It is assumed that the rotor is cage-free, that the back-EMF is sinusoidal, that the saturation is unimportant, and that the eddy currents and hysteresis losses are negligible [82-90]. For this, we will use PMSM modeling in this reference, There are various methods available for modeling a PMSM, including state-space model, transfer function, and a nonlinear model.

II.5.1 PMSM model based on the state space model

In this method, the decoupling or linearization strategy is applied between the linear model of the PMSM on the d-q axis and its disturbances because the PMSM is designed as a nonlinear system, where the disturbances are the d-q axis back-EMFs (E_d and E_q) that represent in the equation (II.27) and the load torque (T_l) that represent in the equation (II.5). The state space expression based the linear model of the PMSM is presented as follows:

$$\begin{cases} \frac{d}{dt}\boldsymbol{x(t)} = \boldsymbol{A}.\boldsymbol{x(t)} + \boldsymbol{Bu(t)} \\ y(t) = \boldsymbol{C}.\boldsymbol{x(t)} + \boldsymbol{D}.\boldsymbol{u(t)} \end{cases} \tag{II.30}$$

Where; x(t) is the state variable vector, u(t) is the input vector, y(t) is the output vector, A is the state matrix, B is input matrix, C is output matrix, and D is a matrix of direct transmission as per standard state space notation.

Through the expression of the state space method based the linear model of the PMSM mentioned above can be written as follows:

$$\begin{cases} \frac{d}{dt}\begin{bmatrix} i_d \\ i_q \\ \omega_e \end{bmatrix} = \begin{bmatrix} -\frac{R_s}{L_d} & 0 & 0 \\ 0 & -\frac{R_s}{L_q} & 0 \\ 0 & 0 & -\frac{F}{j} \end{bmatrix}.\begin{bmatrix} i_d \\ i_q \\ \omega_e \end{bmatrix} + \begin{bmatrix} \frac{1}{L_d} & 0 & 0 \\ 0 & \frac{1}{L_q} & 0 \\ 0 & 0 & \frac{p}{j} \end{bmatrix}\begin{bmatrix} u_d \\ u_q \\ T_e \end{bmatrix} \\ \begin{bmatrix} i_d \\ i_q \\ \Omega \end{bmatrix} = \begin{bmatrix} 1 & 0 & 0 \\ 0 & 1 & 0 \\ 0 & 0 & p \end{bmatrix}.\begin{bmatrix} i_d \\ i_q \\ \omega_e \end{bmatrix} \end{cases} \tag{II.31}$$

Where D=0 and $[v_d \quad v_d]^T = [u_d + E_d \quad u_q + E_q]^T$. Furthermore, the scheme of the PMSM based on this method can be designed as follows:

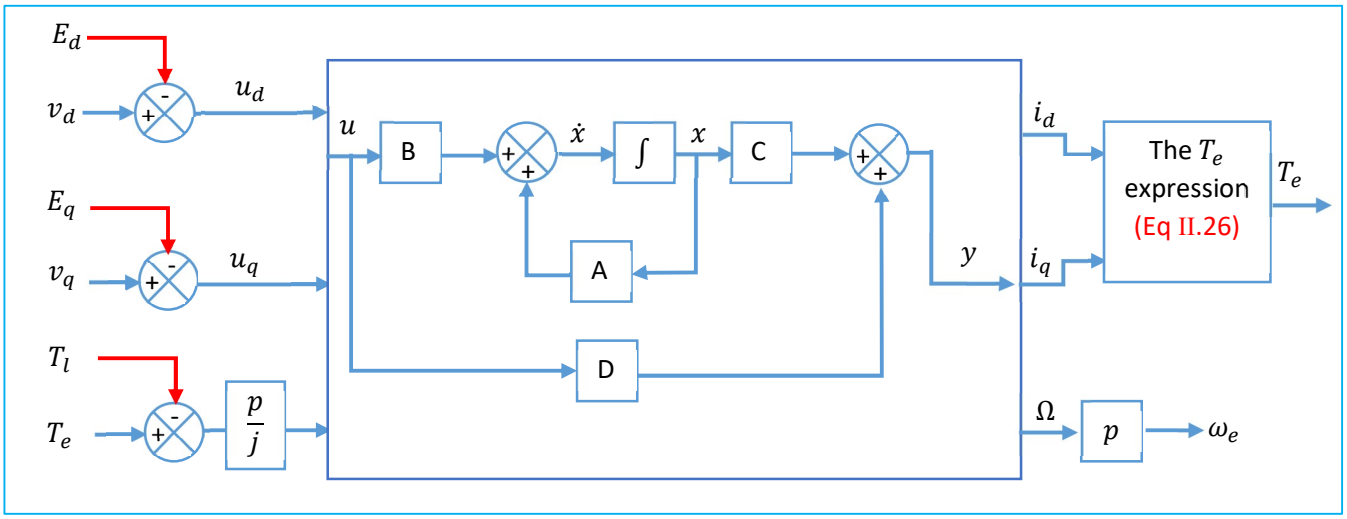

Figure II.6 : The design of the PMSM model using state space model

II.5.2 PMSM model based on the transfer function

The transfer function, or filter, is considered one of the most common methods for modeling a linear system. Therefore, the PMSM needs the linearization strategy in order to use this method. It is also possible to use the decoupling strategy with the PMSM model in this method. Furthermore, the system will change based on the time into a system based on frequency, and the disturbances will be decoupled from the linear model of the system, where the disturbances are the back-EMFs and the load torque. The filter expression is presented as follows:

$$FT(s) = \frac{Y(s)}{U(s)} = \frac{k}{1+\tau.s} \tag{II.32}$$

Where; $FT(s)$ is the transfer function based on the first order, $U(s)$ is the input of the system based on the frequency variable, $Y(s)$ is the output of the based on the frequency variable, τ the time constant and k is the system amplitude.

In light of this method, the PMSM model can be written as follows:

$$\begin{cases} FT_d(s) = \frac{i_d(s)}{v_d(s)-E_d(s)} = \frac{1}{R_s+L_d.s} \\ FT_q(s) = \frac{i_q(s)}{v_q(s)-E_q(s)} = \frac{1}{R_s+L_q.s} \\ FT_\omega(s) = \frac{\Omega(s)}{T_e(s)-T_l(s)} = \frac{1}{F+j.s} \end{cases} \tag{II.33}$$

Where $[v_d \quad v_d]^T = [u_d + E_d \quad u_q + E_q]^T$. Furthermore, the scheme of the PMSM based on this method can be designed as follows:

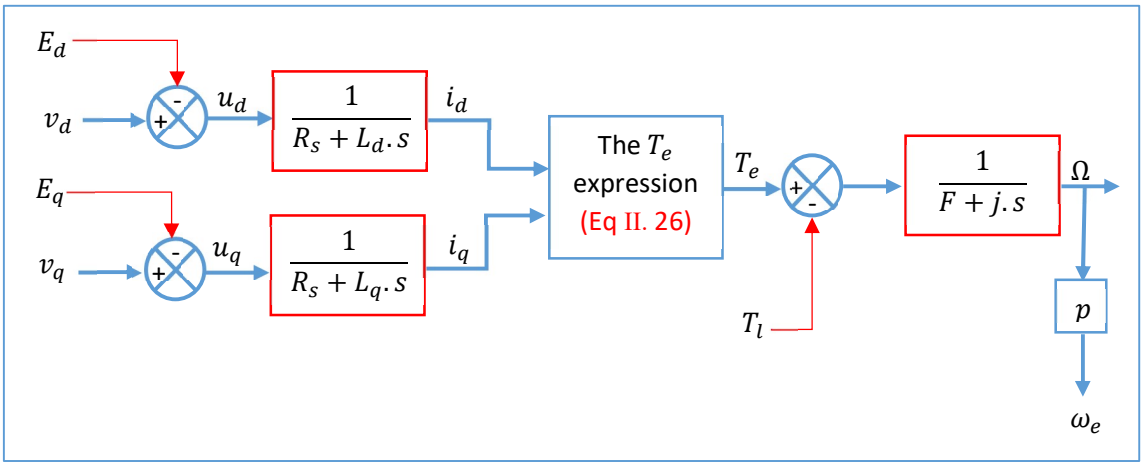

Figure II.7 : The design of the PMSM model using filters

II.5.3 PMSM model based on the nonlinear system

Due to the fact that PMSM is a nonlinear system, the nonlinear method is more comprehensive for modeling it; in addition, this method is suitable for selecting a control law when applying nonlinear techniques. Furthermore, it doesn't need to decouple or linearize the system, whereas it models the system directly under disturbances through the nonlinear function. The PMSM based on the nonlinear model is presented as follows:

$$\begin{cases} \frac{\mathrm{d}}{\mathrm{dt}} x(t) = f(x(t), t) + \mathrm{g}(x).u(\mathrm{t}) \\ y(t) = h(x(t)) \end{cases} \tag{II.34}$$

Where, the $x(\mathrm{t})$ are the state variable, $f(x(t)\ , t)$ is the nonlinear function, $u(\mathrm{t})$ is the system input and $y(t)$ is the system output and $\mathrm{g}(x)$ is the input matrix.

The inputs, state space variables and the output for the PMSM model is designed as follows:

$$\begin{cases} u(t) = [v_d \quad v_q]^T \\ x(\mathrm{t}) = [i_d \quad i_q \quad \omega_e]^T \\ y(t) = h(x) = \omega_e \end{cases} \tag{II.35}$$

The terms of the nonlinear mentioned above for the PMSM model is identified as follow:

$$\begin{cases} f(x(t), t) = \begin{bmatrix} \mathrm{f}_1(x) \\ \mathrm{f}_2(x) \\ \mathrm{f}_3(x) \end{bmatrix} = \begin{bmatrix} -\frac{\mathrm{R_s}}{\mathrm{L_d}}.\mathrm{i_d} + \frac{\mathrm{L_q}}{\mathrm{L_d}}.\mathrm{i_q}.\omega_\mathrm{e} \\ -\frac{\mathrm{R_s}}{\mathrm{L_q}}.\mathrm{i_q} - \frac{\mathrm{L_d}}{\mathrm{L_q}}.\mathrm{i_d}.\omega_\mathrm{e} - \frac{\psi_f}{\mathrm{L_q}}.\omega_\mathrm{e} \\ -\frac{F}{j}.\omega_\mathrm{e} + \frac{3.p^2}{2}.\frac{\mathrm{L_d}-\mathrm{L_q}}{j}.\mathrm{i_d}.\mathrm{i_q} + \frac{3.p^2}{2}.\frac{\psi_f}{j}.\mathrm{i_q} - \frac{p}{j}.T_l \end{bmatrix} \\ \mathrm{g}(x) = \begin{bmatrix} \frac{1}{\mathrm{Ld}} & 0 \\ 0 & \frac{1}{\mathrm{Lq}} \\ 0 & 0 \end{bmatrix} \end{cases} \tag{II.36}$$

II.6 Explanation of the PMSM source supply

In the context of electric drive systems, the interaction between the inverter and the Permanent Magnet Synchronous Motor (PMSM) is essential. The inverter acts as a bridge connecting the PMSM and the electrical power supply, which is usually a DC bus. Its main job is to change the DC power into the three-phase AC power needed to run the PMSM. The following are the main facets of the inverter and PMSM relationship:

- **Power Conversion:** A power source, such as a battery or rectifier, supplies DC power which the inverter converts into AC power suitable for the Permanent Magnet Synchronous Motor (PMSM). Since PMSMs operate on AC power, this conversion process is essential for their operation;
- **Voltage and Frequency Control:** The inverter adjusts the voltage and frequency of the output AC waveform in addition to controlling the speed and torque of the PMSM. There are numerous ways to achieve accurate control. Pulse Width Modulation (PWM) is one such technique that controls the effective voltage and frequency supplied to the motor by varying the pulse width;
- **Dynamic Response:** The inverter plays a crucial role in providing a rapid and accurate response to changes in the motor's operating conditions. This is important for maintaining stable and efficient operation, especially in applications where rapid changes in speed or torque are required;
- **Regenerative Braking:** The inverter can facilitate regenerative braking in certain systems, allowing the PMSM to act as a generator and feed energy back into the DC bus when decelerating;
- **Efficiency and Losses:** The inverter's efficiency has an impact on the system's overall efficiency. Optimizing the energy efficiency of the PMSM-driven system requires minimizing losses in the inverter, including switching and conduction losses.

II.6.1 Modeling of the Inverter

In a three-phase, two-level voltage source inverter, each arm features two switches. These switches stand out for their exceptional capability to operate bidirectional, affording precise control over both opening and closing actions in both directions. For low powers and very high frequencies, they can be MOSFETs; for high powers and high frequencies, they can be IGBTs; and for extremely high powers and low frequencies, they can be GTOs. To ensure current flow in both directions, the switch must be positioned in antiparallel with a diode. Figure. II.8 illustrates the overall design of a two-level voltage inverter.

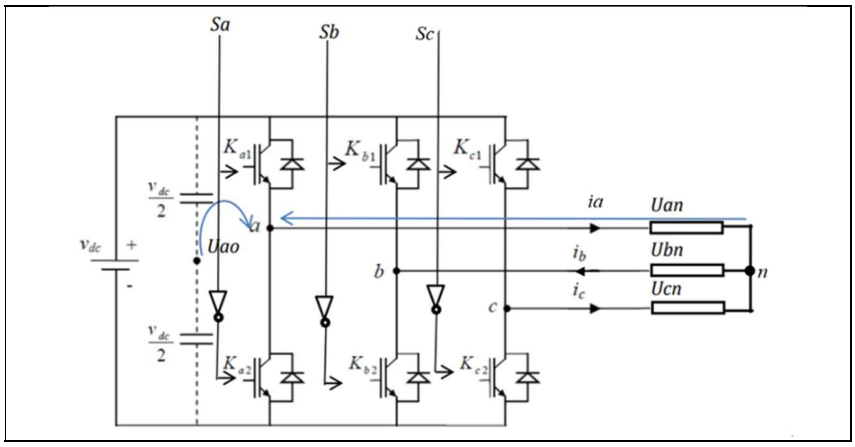

Figure II.8 : Schematic diagram of the three-phase voltage inverter

The reference voltages are the desired simple voltages U_{an}; U_{bn}; U_{cn} referenced to the neutral point. The state of the switches, assuming perfection, can be defined by three Boolean control variables denoted as S_i (i= a, b, c):

- $S_i = 1$ the case where the upper switch is closed and the lower one is open.
- $S_i = 0$ the case where the upper switch is open and the lower one is closed.

Under these conditions we can write the phase voltages U_{ao}, U_{bo} and U_{co} as a function of the control signals S_i:

$$U_{ao} = \begin{cases} \frac{V_{dc}}{2}, & S_a = 1 \\ -\frac{V_{dc}}{2}, & S_a = 0 \end{cases} \rightarrow U_{ao} = K_a * \frac{V_{dc}}{2} \quad \text{(II.37)}$$

$$U_{bo} = \begin{cases} \frac{V_{dc}}{2}, & S_b = 1 \\ -\frac{V_{dc}}{2}, & S_b = 0 \end{cases} \rightarrow U_{bo} = K_b * \frac{V_{dc}}{2} \quad \text{(II.38)}$$

$$U_{co} = \begin{cases} \frac{V_{dc}}{2}, & S_c = 1 \\ -\frac{V_{dc}}{2}, & S_c = 0 \end{cases} \rightarrow U_{co} = K_c * \frac{V_{dc}}{2} \quad \text{(II.39)}$$

According to the definition of the equations U_{ao}, U_{bo} and U_{co}, we have K_a, K_b and K_c presents the situation 1 or -1 depends on Si. The load is considered to be balanced, the result is:

$$U_{an} + U_{bn} + U_{cn} = 0 \quad \text{(II.40)}$$

$$\begin{cases} U_{ao} + U_{on} = U_{an} \\ U_{bo} + U_{on} = U_{bn} \\ U_{co} + U_{on} = U_{cn} \end{cases} \quad \text{(II.41)}$$

According to the sum of equations (II.41), we have

$$(U_{ao} + U_{bo} + U_{co}) + 3\,U_{on} = U_{an} + U_{bn} + U_{cn} \quad \text{(II.42)}$$

Substituting equation (II.40) into equation (II.42) gives us:

$$U_{on} = -\frac{1}{3}\,(U_{ao} + U_{bo} + U_{co}) \quad \text{(II.43)}$$

Replacing equation (II.43) in equation (II.41) we obtain:

$$\begin{cases} U_{an} = \frac{2}{3} U_{ao} - \frac{1}{3} U_{bo} - \frac{1}{3} U_{co} \\ U_{bn} = -\frac{1}{3} U_{ao} + \frac{2}{3} U_{bo} - \frac{1}{3} U_{co} \\ U_{cn} = -\frac{1}{3} U_{ao} - \frac{1}{3} U_{bo} + \frac{2}{3} U_{co} \end{cases} \quad \text{(II.44)}$$

Substituting equation (II.37), equation (II.38) and equation (II.39) in equation (II.44):

$$\begin{cases} U_{an} = \frac{2}{3} Ka * \frac{V_{dc}}{2} - \frac{1}{3} Kb * \frac{V_{dc}}{2} - \frac{1}{3} Kc * \frac{V_{dc}}{2} \\ U_{bn} = -\frac{1}{3} Ka * \frac{V_{dc}}{2} + \frac{2}{3} Kb * \frac{V_{dc}}{2} - \frac{1}{3} Kc * \frac{V_{dc}}{2} \\ U_{cn} = -\frac{1}{3} Ka * \frac{V_{dc}}{2} - \frac{1}{3} Kb * \frac{V_{dc}}{2} + \frac{2}{3} Kc * \frac{V_{dc}}{2} \end{cases} \quad \text{(II.45)}$$

The different combinations of the three quantities (K_a, K_b, K_c) make it possible to generate eight voltage vectors, two of which correspond to the zero vector. With simple voltages as a function of control quantities:

$$\begin{bmatrix} U_{an} \\ U_{bn} \\ U_{cn} \end{bmatrix} = \frac{V_{dc}}{2} \begin{bmatrix} \frac{2}{3} & -\frac{1}{3} & -\frac{1}{3} \\ -\frac{1}{3} & \frac{2}{3} & -\frac{1}{3} \\ -\frac{1}{3} & -\frac{1}{3} & \frac{2}{3} \end{bmatrix} \begin{bmatrix} Ka \\ Kb \\ Kc \end{bmatrix} \quad \text{(II.46)}$$

Thus, the model presented in equation (II.46) expresses the three-phase inverter as well as its simulation using MATLAB Simulink is presented as follows:

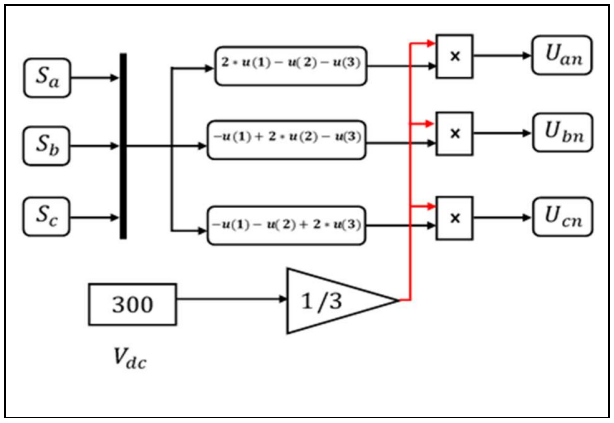

Figure II.9 : Simulation of the three-phase voltage inverter

II.6.2 Types of the PWM technique

The Pulse Width Modulation (PWM) technique generates an output signal through a series of slots characterized by varying widths and amplitudes, mirroring the supply voltage. The selection of a specific strategy dictates how a triangular signal (known as the carrier) intersects with a reference signal, thereby governing the activation and deactivation sequences of switches. Various PWM strategies exist, among them are the following distinguished methods:

- **PWM with a single pulse:**

In the simple PWM approach, the width of a single pulse determines the variation in voltage amplitude at the inverter's output every half-cycle. This method involves comparing a triangular carrier wave signal, having an amplitude of , with a reference signal of A. The control and output signals of a single-phase full-bridge inverter, utilizing basic PWM modulation, are depicted in Figures II.10 below. The fundamental frequency of the output voltage aligns with that of the reference signal. The pulse width δ can range from 0 to 180° by adjusting A_r, which varies between 0 and A_P . The control variable, often termed the "voltage adjustment coefficient (r)" of the output voltage, is defined by the relationship A_r / A_P.

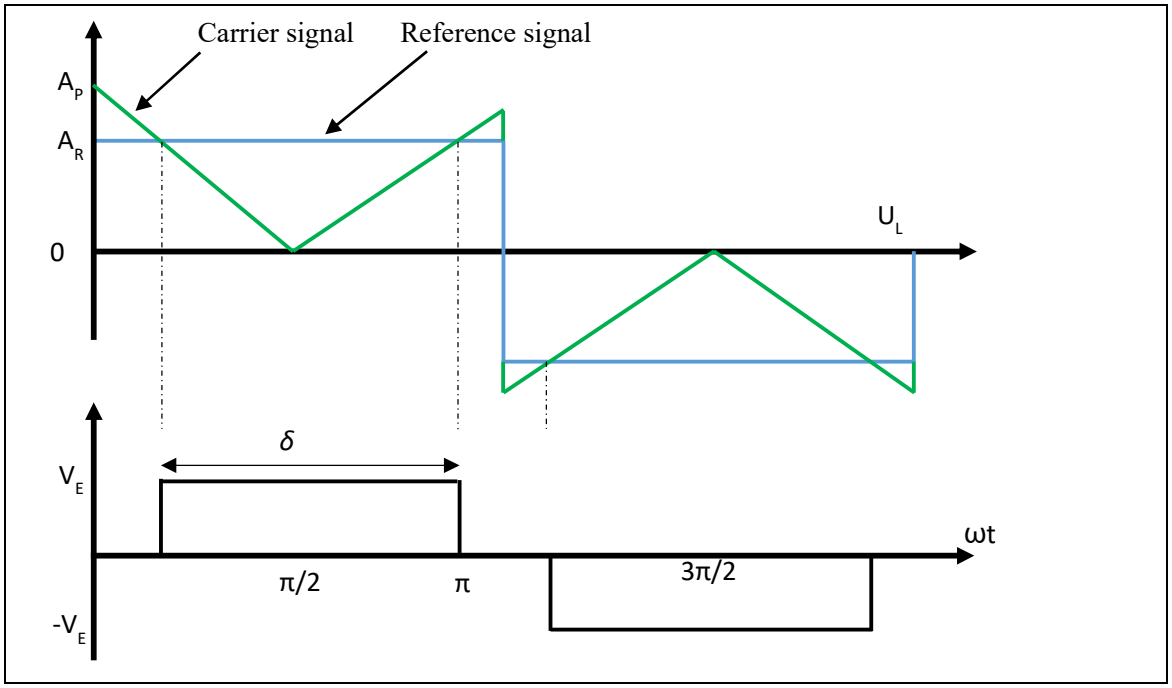

Figure II.10 : PWM with a single pulse

- **PWM with multiple pulses:**

With this method, multiple pulses are added to each half-wave of the output voltage, so reducing harmonics. The intersections of a triangular carrier signal and a reference signal yield the switch control pulses. The carrier frequency (f_p) of the signal determines the number of pulses during the half-wave, while the frequency of the reference signal sets the output frequency (f_r). The number of pulses per half cycle is determined by:

$$N_{impulsion} = \frac{f_p}{2.f_r} \quad \text{(II.47)}$$

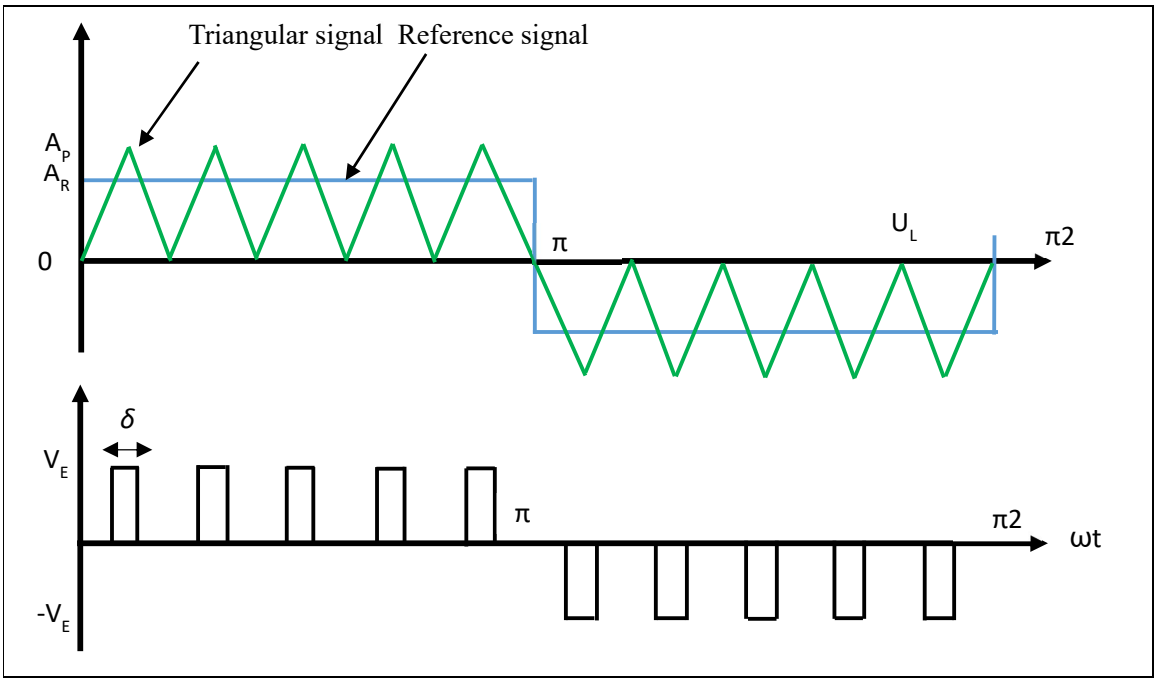

Figure II.11: PWM with a multiple pulse

- **Sine-Triangle PWM control technique:**

The number of pulses sent back to the inverter switches increases through this method. Consequently, both the frequency and amplitude of the output voltage's fundamental component can vary. The PWM technique is employed to determine the timing for switching operations of the switches. This process entails identifying the intersections between three sinusoidal reference voltages (modulations) and a triangular carrier signal to establish the switching times. The fundamental principle of the triangular-sinusoidal control strategy involves comparing a high-frequency triangular signal (carrier) with the reference signal (modulator) to regulate each arm. The source of the reference signals is:

$$V_{ref}(t)=\begin{cases} v_{aref} = v_m.\sin(2.\pi.f_s) \\ v_{bref} = v_m.\sin\left(2.\pi.f_s - \frac{2\pi}{3}\right) \\ v_{Cref} = v_m.\sin\left(2.\pi.f_s + \frac{2\pi}{3}\right) \end{cases} \quad \text{(II.48)}$$

The carrier equation over a period is given by:

$$V_p(t) = \begin{cases} V_{pm}\left(\frac{4t}{T_p} - 1\right) \ \ if\ t \in \left[0, \frac{T_p}{2}\right] \\ V_{pm}\left(3 - \frac{4t}{T_p}\right) \ \ if\ t \in \left[\frac{T_p}{2}, T_p\right] \end{cases} \quad \text{(II.49)}$$

Where $T_p = \frac{1}{f_p}$ and $f_p = m \cdot f_s$, with m the modulation index: equal to the ratio of the carrier frequency to the reference frequency.

The voltage adjustment coefficient (r) equal to the ratio of the amplitude of the reference voltage (V_m) to the peak value of the modulation wave (V_{pm}). The way this technique works is:

- If $V_{ref}(t)>V_p(t)$ the upper transistor of the bridge arm conducts.
- If $V_{ref}(t)<V_p(t)$ the lower transistor of the bridge arm conducts.

The adjustment is made by the opening and closing times of the switches and by the operating sequences.

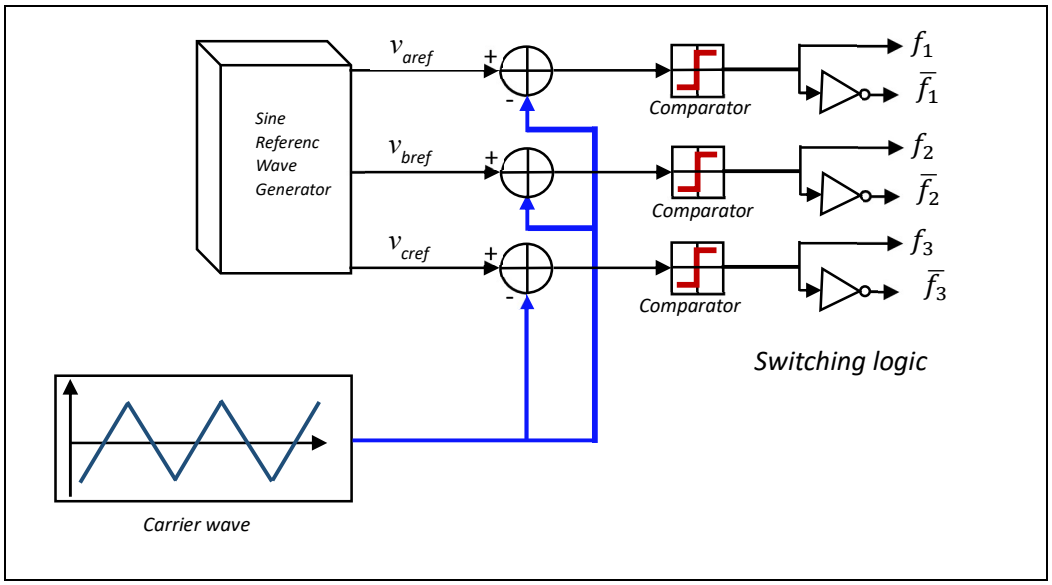

Figure II.12 : Principle of the PWM control based on sinus triangular control strategy

The PWM results show the classic signals of this method:

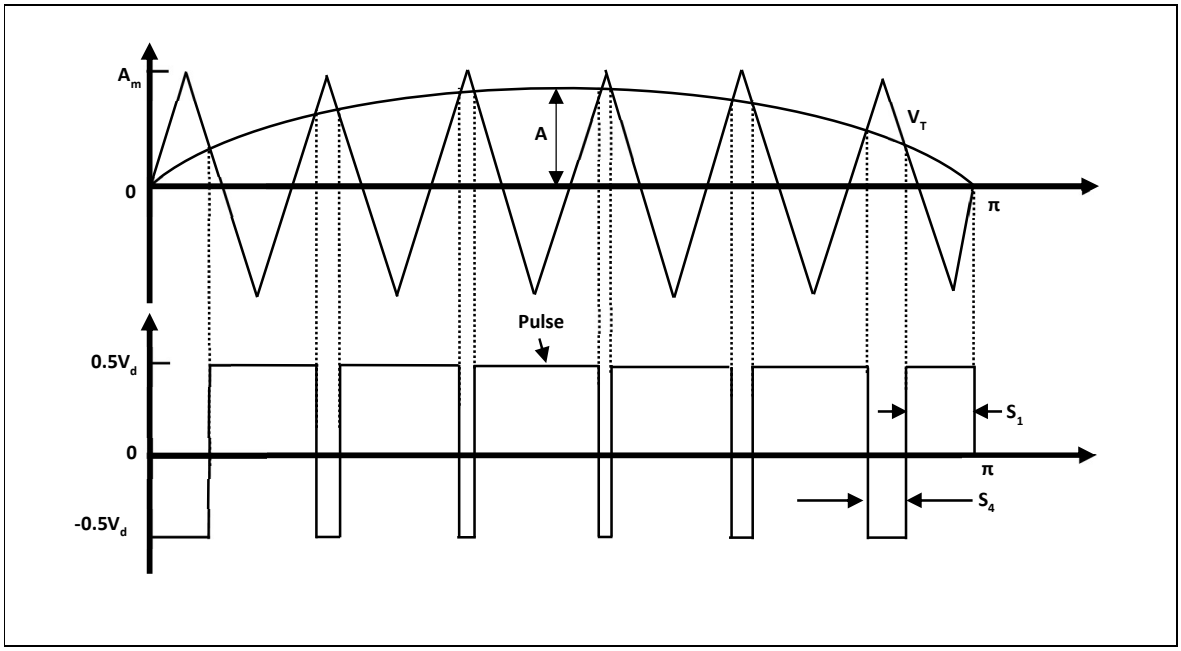

Figure II.13 : The carrier and the modulator

- **Hysteresis current control**

This type of comparator does not require prior process analysis. The choice of hysteresis band width determines the precision on the currents as well as the switching frequency. Figures. II.14 represents the hysteresis comparator.

$$\begin{cases} \text{Si} : \left|I_{ref} - I\right| < \frac{h}{2} & ,So: \quad K_i = 1 \quad \text{and} \quad \bar{s} = 0 \\ \text{Si} : \left|I_{ref} - I\right| > \frac{h}{2} & ,\text{So: } K_j = 0 \quad \text{and} \quad \bar{s} = 1 \\ \text{Si} : \left|I_{ref} - I\right| = \frac{h}{2} & ,\text{So: } K_j = -1 \quad \text{and} \quad \bar{s} = 0 \end{cases} \tag{II.50}$$

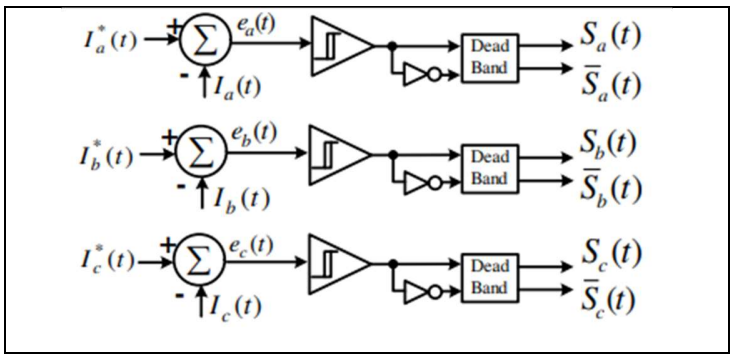

Figure II.14 : Two-state comparator with electric current hysteresis

Through the PWM technique, Figures. II.15 is a summarized functional diagram of the hysteresis current control.

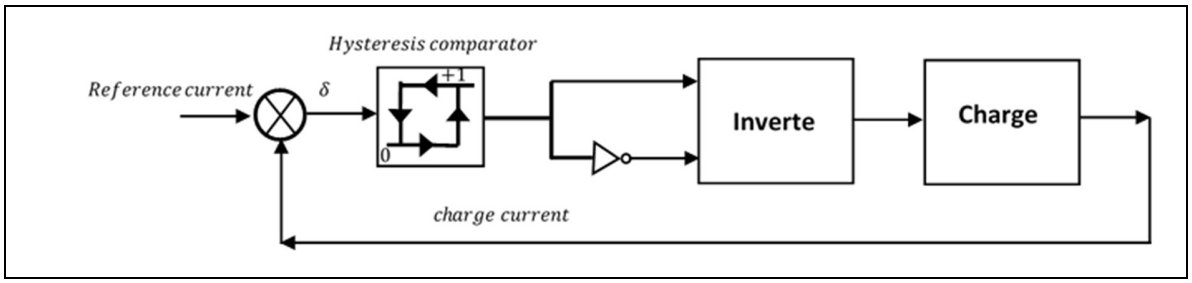

Figure II.15 : Functional diagram of hysteresis current control

Figure II.16 illustrates the operational concept of a control unit employing this technique. Hysteresis state imposition is achieved by monitoring the disparity between the reference current and the actual current, referred to as the upper limit (δ) or lower limit (δ). Hysteresis control operates asynchronously, allowing for variable switching frequencies. However, in three-phase systems featuring an isolated neutral or delta connection, this method may introduce phase interference and filtering challenges.

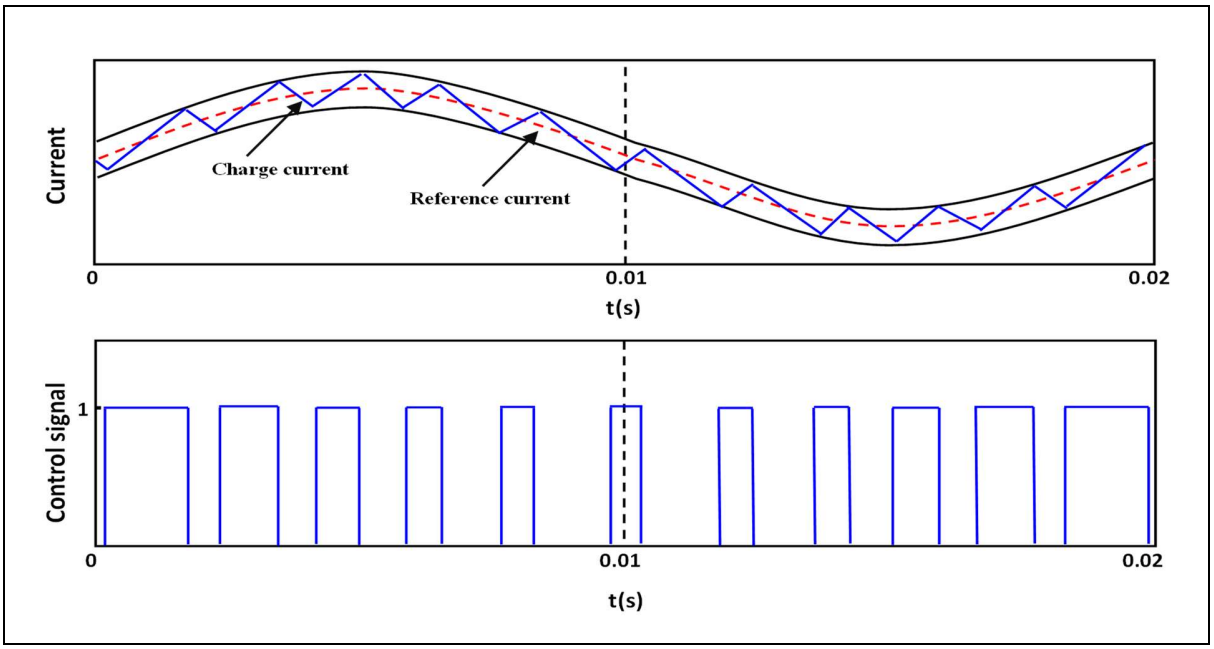

Figure II.16 : Principle of current control by hysteresis

- **Space vector PWM (SVPWM) technique :** When controlling three-phase voltage source inverters in power electronics applications, especially motor drives and renewable energy systems, one of the most widely utilized modulation techniques is Space Vector Pulse Width Modulation (SVPWM). Creating the right switching signals for the inverter is the aim of space vector PWM, which regulates the voltage provided to the three-phase load (such a motor). Listed below are space vector PWM's primary goals:
- **Improved Voltage Utilization:** SVPWM seeks to provide the intended output voltage in the three-phase system by making the most use of the available DC bus voltage. Higher efficiency and improved power supply utilization are made possible by this.
- **Reduced Total Harmonic Distortion (THD):** SVPWM is a modulation technique that is intended to yield output waveforms with a lower Total Harmonic Distortion than other methods. For many applications, this produces an output voltage that is cleaner and more sinusoidal.
- **Precise Voltage Control:** Precise control over the output voltage magnitude and phase angle is possible with SVPWM. This is essential for applications like motor control, where precise and effective torque and speed control of the motor is needed.
- **Optimal Use of Inverter Switching States:** The method ensures smooth and effective transitions between various voltage vectors by making the best use of the inverter's available switching states. This enhances overall performance and better utilizes the inverter's potential.

- **Reduction of Common Mode Voltage:** SVPWM contributes to the reduction of common mode voltage, which is critical for lowering motor bearing currents and guaranteeing the dependability of the associated machinery.
- **Dynamic Response:** For applications requiring precise and quick control, SVPWM's quick and dynamic response to reference signal changes makes it a good choice.
  Through the inverter work, it is obvious that switching two switches on the same arm in the same period of time causes a short circuit, in order to avoid this situation, only one switch per arm must be switched per period of time. Hence, there are eight switching states for the switches T1 to T6. From V_0 to V_7, these eight vectors are programmed (Figures. II.17). The "SV" modulation technique involves progressively shifting the PWM switches from one state to the next. The three phases of the motor are supplied by the three outputs (a, b, and c) of the inverter, as shown in Figure. II.8, creating magnetic fields that are phase shifted by 120°. The magnetic field orientation for each of the eight states can then be shown. The voltage vectors V_0 to V_7 in table.1 are then created from these states.

Table II.1.Voltage vectors V_0 *to* V_7

Vector space	S_1	S_2	S_3	V_{as}	V_{bs}	V_{cs}
V_0	0	0	0	0	0	0
V_1	1	0	0	$\frac{2}{3}V_{dc}$	$-\frac{1}{3}V_{dc}$	$-\frac{1}{3}V_{dc}$
V_2	1	1	0	$\frac{1}{3}V_{dc}$	$\frac{1}{3}V_{dc}$	$-\frac{2}{3}V_{dc}$
V_3	0	1	0	$-\frac{1}{3}V_{dc}$	$\frac{2}{3}V_{dc}$	$-\frac{1}{3}V_{dc}$
V_4	0	1	1	$-\frac{2}{3}V_{dc}$	$\frac{1}{3}V_{dc}$	$\frac{1}{3}V_{dc}$
V_5	0	0	1	$-\frac{1}{3}V_{dc}$	$-\frac{1}{3}V_{dc}$	$\frac{2}{3}V_{dc}$
V_6	1	0	1	$\frac{1}{3}V_{dc}$	$-\frac{2}{3}V_{dc}$	$\frac{1}{3}V_{dc}$
V_7	1	1	1	0	0	0

Since there is no magnetic field created by the states S_0 and S_7, the vectors $V_0$and V_7 have zero length. The remaining vectors respect the following relationships and have a length of 1:

$$\begin{cases} \overrightarrow{V_1} = -\overrightarrow{V_4} \\ \overrightarrow{V_2} = -\overrightarrow{V_5} \\ \overrightarrow{V_3} = -\overrightarrow{V_6} \\ \overrightarrow{V_1} + \overrightarrow{V_3} + \overrightarrow{V_5} = 0 \end{cases} \quad \text{(II.51)}$$

Figure II.17 illustrates the six active vectors alongside the two zero vectors. To generate sinusoidal voltages on phases A, B, and C, it's typically necessary to rotate the vector $\vec{V}$ throughout the entire hexagon. However, in the context of Space Vector Pulse Width Modulation (SVPWM), a vector $\vec{V}$ can be positioned within the hexagon by combining the two reference vectors that define the sector where $\vec{V}$ is located. Unlike conventional modulation

methods where $\vec{V}$ must lie within the circle, SVPWM allows for vector placement inside the hexagon

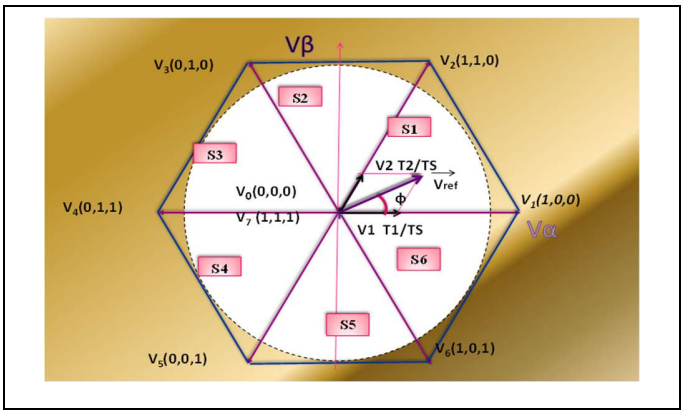

Figure II.17 : The seven positions of the space vector of the output voltage in the plane (α, β)

Where; $\vec{V}$ and $\vec{V}_2$ respectively components of vectors $\vec{V}_{001}$ and $\vec{V}_{011}$ they are generated by the respective application of vector $\vec{V}_{001}$ and $\vec{V}_{011}$ during fixed percentages of a period Ts. So by the definition of these percentages of T_s as:

T_1= Portion of the period T_s during which the vector $\vec{V}_{001}$ is applied.

T_2= Portion of the period T_s during which the vector $\vec{V}_{011}$ is applied.

T_0= Portion of the period T_s during which the vector $\vec{V}_{011}$ or $\vec{V}_{011}$ is applied.

To optimize control and minimize the number of switch activations per component, which is a distinct advantage of Space Vector Pulse Width Modulation (SVPWM), each sector (1 to 6) dictates a specific sequence for the inverter switches' conduction. It's essential to ensure a single pulse centered within an interval that minimizes deviation from the reference circle defined by the succession of vectors V_i. This approach reduces non-linearity resulting from pulse shape and minimizes harmonic distortion rates. For efficient switching and to mitigate losses, it's preferable that the transition from one state to the next occurs with a single switch change, such as from $V_{1(100)}$ to $V_{2(110)}$. This necessitates positioning the null state 111 after one of the states 110, 101, or 011, and the null state 000 after one of the states 100, 001, or 010. Table 2 displays two possible combinations for pulse centering when the control vector is located in sectors 1 to 6, respectively.

Table II.2. SVPWM control signals depending on sectors

1sr Sector 0≤φ ≤π/3	Switch	Times	$T_0/2$	T_1	T_2	$T_0/2$	$T_0/2$	T_2	T_1	$T_0/2$
			V_0	V_1	V_2	V_7	V_7	V_2	V_1	V_0
	S1	$T_1+T_2+T_0/2$								
	S2	$T_2+T_0/2$								
	S3	$T_0/2$								
2nd Sector π/3≤φ ≤2π/3	Switch	Times	$T_0/2$	T_2	T_1	$T_0/2$	$T_0/2$	T_1	T_2	$T_0/2$
			V_0	V_3	V_2	V_7	V_7	V_2	V_3	V_0

	S1	$T_1+T_0/2$								
	S2	$T_2+T_1+T_0/2$								
	S3	$T_0/2$								
3rd Sector $2\pi/3\leq\varphi\leq\pi$	Switch	Times	$T_0/2$	T_1	T_2	$T_0/2$	$T_0/2$	T_2	T_1	$T_0/2$
			V_0	V_3	V_4	V_7	V_7	V_4	V_3	V_0
	S1	$T_0/2$								
	S2	$T_2+T_1+T_0/2$								
	S3	$T_2+T_0/2$								
4th Sector $\pi\leq\varphi\leq4\pi/3$	Switch	Times	$T_0/2$	T_2	T_1	$T_0/2$	$T_0/2$	T_1	T_2	$T_0/2$
			V_0	V_5	V_4	V_7	V_7	V_4	V_5	V_0
	S1	$T_0/2$								
	S2	$T_1+T_0/2$								
	S3	$T_2+T_1+T_0/2$								
5th Sector $4\pi/3\leq\varphi\leq5\pi/3$	Switch	Times	$T_0/2$	T_1	T_2	$T_0/2$	$T_0/2$	T_2	T_1	$T_0/2$
			V_0	V_5	V_6	V_7	V_7	V_6	V_5	V_0
	S1	$T_2+T_0/2$								
	S2	$T_0/2$								
	S3	$T_2+T_1+T_0/2$								
6th Sector $5\pi/3\leq\varphi\leq2\pi$	Switch	Times	$T_0/2$	T_2	T_1	$T_0/2$	$T_0/2$	T_1	T_2	$T_0/2$
			V_0	V_1	V_6	V_7	V_7	V_6	V_1	V_0
	S1	$T_2+T_1+T_0/2$								
	S2	$T_0/2$								
	S3	$T_1+T_0/2$								

The amplitude and phase shift of the reference voltage in α-β frame are presented as follows:

$$\begin{cases} V_{ref} = \sqrt{(V_\alpha)^2 + (V_\beta)^2} \\ \varphi = \operatorname{atan}\left(\frac{V_\beta}{V_\alpha}\right) \end{cases} \quad \text{(II.52)}$$

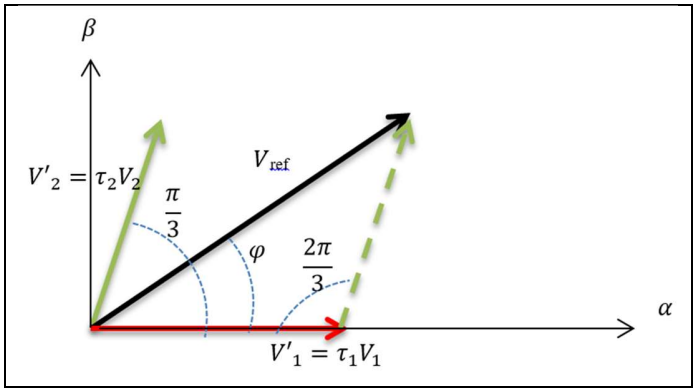

Figure II.18 : Application time of vectors V1 and V2 for sector 1

Depending on the Figures. II.18, we can identify V_1', V_2' and their duration as follows:

$$\begin{cases} V'_1 = \tau_1 V_1 = \frac{T_1}{T_s} V_{dc} \rightarrow T_1 = T_s \frac{V'_1}{V_{dc}} \\ V'_2 = \tau_2 V_2 = \frac{T_2}{T_s} V_{dc} \rightarrow T_2 = T_s \frac{V'_2}{V_{dc}} \end{cases} \quad \text{(II.53)}$$

According to Figures. II.12, the law of sines tells us that:

$$\frac{V_{ref}}{\sin(\frac{2\pi}{3})} = \frac{V'_1}{\sin(\frac{\pi}{3}-\varphi)} = \frac{V'_2}{\sin(\varphi)} \quad \text{(II.54)}$$

For $\varphi < \frac{\pi}{3}$, V_1', V_2' have been estimated as follow:

$$\begin{cases} V'_1 = \frac{\sin(\varphi)}{\sin(\frac{2\pi}{3})} V_{ref} \rightarrow V'_1 = \frac{2}{\sqrt{3}} V_{ref} \sin(\frac{\pi}{3} - \varphi) \\ V'_2 = \frac{T_2}{T_s} V_{ref} \rightarrow V'_2 = \frac{2}{\sqrt{3}} V_{ref} \sin(\varphi) \end{cases} \quad \text{(II.55)}$$

Replaces equation (II.55) in equation (II.53) to have the application time for the first sector

$$\begin{cases} T_1 = \frac{2T_s}{\sqrt{3}V_{dc}} V_{ref} \sin(\frac{\pi}{3} - \varphi) \\ T_2 = \frac{2T_s}{\sqrt{3}V_{dc}} V_{ref} \sin(\varphi) \end{cases} \quad \text{(II.56)}$$

For the section number K, the equation (II.56) becomes as follows:

$$\begin{cases} T_1 = \frac{2T_s}{\sqrt{3}V_{dc}} V_{ref} \sin(\frac{K.\pi}{3} - \varphi) \\ T_2 = \frac{2T_s}{\sqrt{3}V_{dc}} V_{ref} \sin(\varphi - \frac{(K-1).\pi}{3}) \end{cases} \quad \text{(II.57)}$$

Where; $T_0 = T_s - T_1 - T_2$

II.7 Simulation of the PMSM based on the open loop

In order to give a very simple example of a PMSM power by a healthy three phase voltages system, MATLAB Simulink has been used, where the PMSM model based on the transfer function mentioned above has been simulated. The inputs are three phases' voltages; they have been given through three sine waves, each of which is shifted to 2π/3. They are distinguishable by having the same amplitude (300 v) and frequency (50 Hz). Using the Clark and Park matrixes, the α-β frame and d-q frame of the current and the voltages have been given, as shown in Figures. II.19, Figures. II.22-b, and Figures. II.22-c respectively. About the three phases of the current, they have been given using inverse Park transformation, as shown in Figures. II.22-c. The mechanical equations of the PMSM, shown in equation (II.6), were used to find the mechanical speed, the electrical speed, and the electromagnetic torque as shown the Figures. II.20 and Figures. II.21 respectively. The PMSM was operated in the no load state, with $T_l = 0$ N.m. Through these results, the PMSM suffers from initial overshoots, big chattering and a slow response time. The motor parameters that used in the simulation are represented in the table.3.

Table II.3. Parameters of PMSM [81]

R_s=0.6 ohm	L_d =1.4e-3 h	L_q=2.8e-3 h	ω=314 rad/s
F =0.0014 M.m.s^{-1}	ψ_f =0.12 Wb	j =0.0011 kg.m^2	p = 4

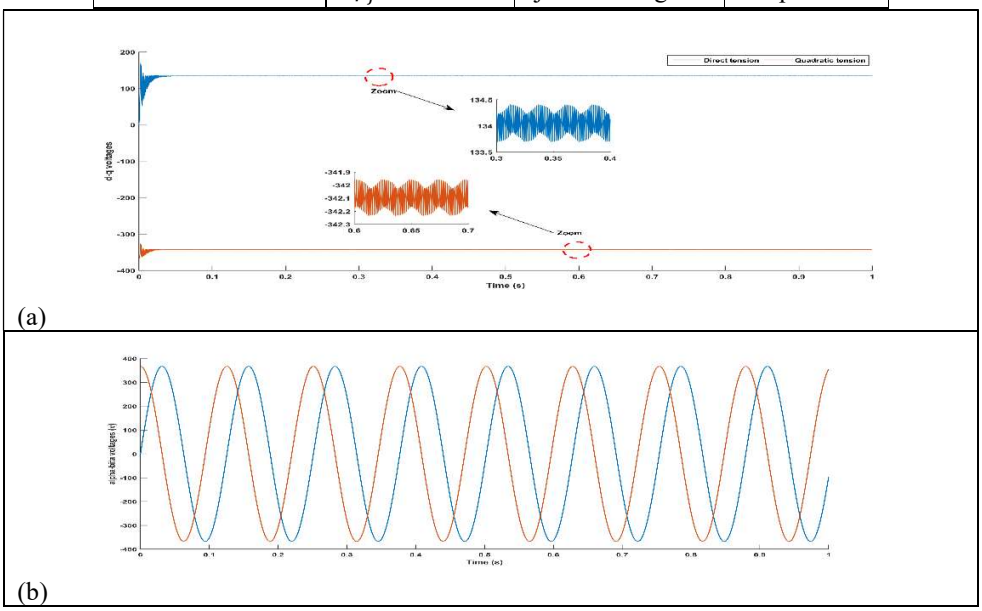

Figure II.19 : The voltages of the PMSM in the open loop; (a): d-q frame, (b): α-β frame

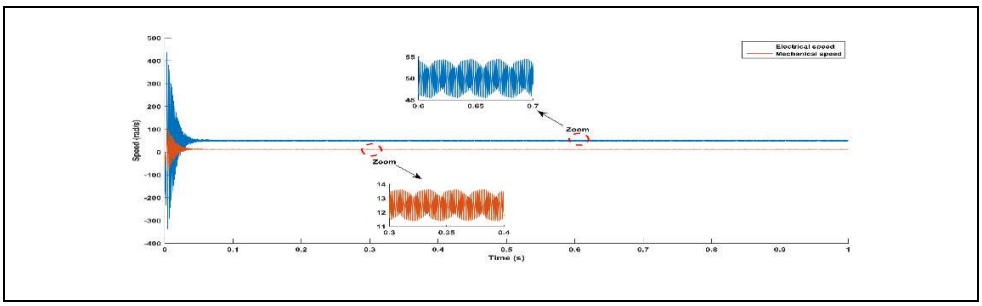

Figure II.20 : The Speeds of the PMSM in the open loop

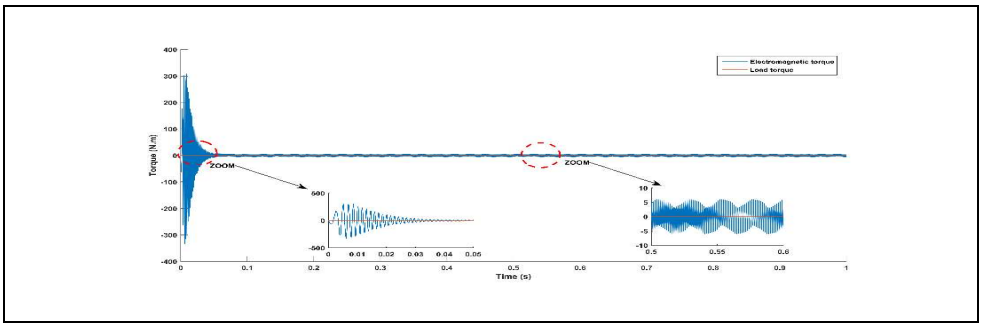

Figure II.21 : The Torques of the PMSM in the open loop

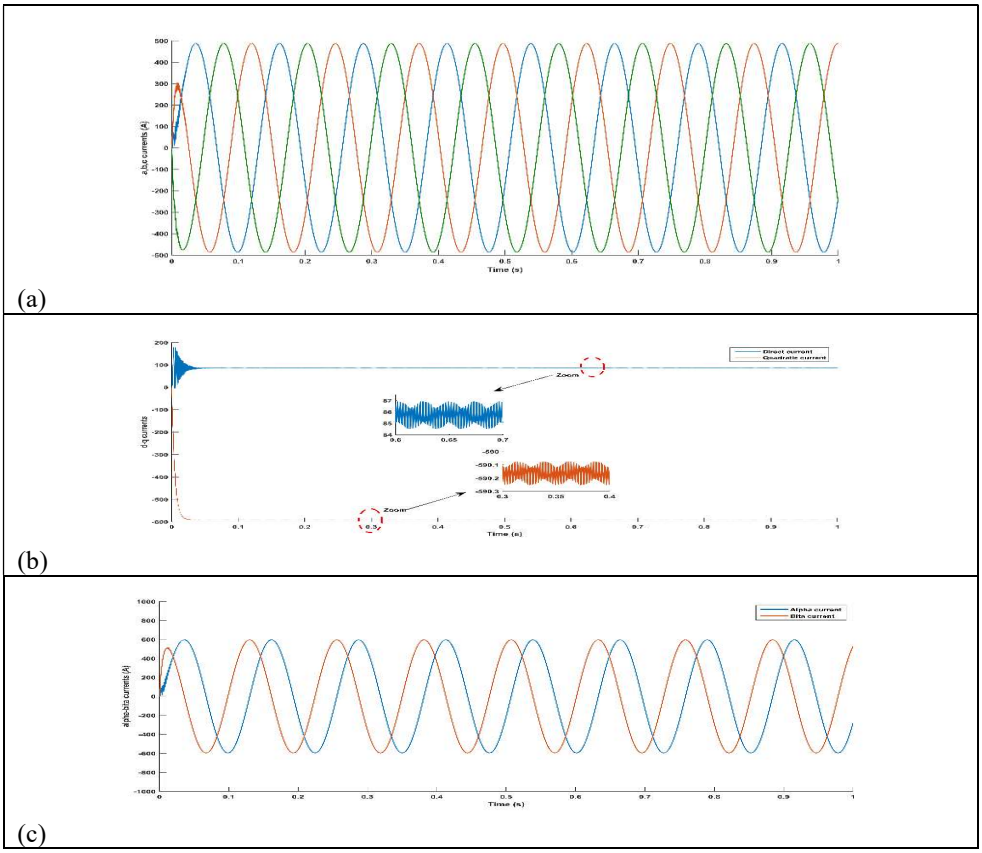

Figure II.22 : The currents of the PMSM in the open loop; (a): a,b,c frame, (b): d-q frame, α-β frame

II.8 Conclusion

This chapter presents the modeling of the Permanent Magnet Synchronous Motor (PMSM) and the inverter, along with a detailed exposition of the mathematical equations involved. Initially, traditional equations in the ABC frame reference for the machine are introduced, followed by the utilization of coordinate transformation techniques (Clark and Park) to transition to the α-β and d-q frame references. Additionally, various modeling approaches for the PMSM are explored, including the transfer function method, state-space method, and nonlinear method. The modeling of the three-phase, two-level voltage inverter is also addressed, alongside an in-depth explanation of its control methods based on Pulse Width Modulation (PWM). Finally, the validity of the PMSM model is verified using MATLAB Simulink."

CHAPITRE III

DESIGN OF THE PMSM DRIVE AND APPLICATION OF THE CONVENTIONAL CONTROLS TO THE PMSM

III.1 Introduction

Although PMSMs are widely used in many various areas such as electric vehicles, aerospace, numerical control systems, and wind power generation due to their high efficiency, high power factor, fast response, wide speed range, and good accuracy, they are a non-linear model, strongly coupled, and multivariable. Therefore, control techniques are applied to them in order to improve their performance as well as stabilize them. To create the right control for the machine, a thorough model analysis must be done before any controls are applied. Once the system model has been determined, the control design is regarded as a crucial phase that helps comprehend how the control can be used. Understanding the last one makes it easier to test the closed loop system-based control as a simulation and makes it more transparent. A motor typically receives electric power as input. The three electric variables are frequency, current, and tension. The motor's energy is provided by the grid, which controls its speed and torque. It needs to be fed the motor when we operate the inverter using his control. The function of the inverter is to convert the estimation signal into the reel signal. Mostly, the PMSM is modelled into two loops: the speed loop and the current loop. Furthermore, stability and controllability are important before applying the controls, where stability can be demonstrated using different methods such as Nyquist plots, Bode diagrams, pole-zero maps, etc. The controllability can be demonstrated using Kalman's theorem. PMSM control design methodologies can be broadly categorized into two types: vector control and scalar control. Although scalar control is simple to use and produces a response that is largely steady-state, it has slower dynamics. Therefore, the closed-loop vector control strategy is typically selected in order to realize a greater precision as well as good dynamic and steady-steady response. With both conventional and advanced techniques included, the vector control is the largest control group. Conventional techniques, such as field oriented control (FOC) and direct torque control (DTC). Nonlinear, optimal, adaptive, and intelligent techniques comprise the category of advanced techniques. The goal, characteristics, and control design of each technique vary; while some can be used directly to a nonlinear model, others require the use of a linearization or decoupling strategies. PMSM frequently employ nonlinear approaches, such as feedback linearization control (FBLC), sliding mode control (SMC), backstepping (BSC), and passivity-based control (PBC). Model predictive control (MPC), linear quadratic regulator control (LQR), and other methods are considered the best forms of control. In terms of adaptive control, direct, indirect, and matching commands are categorized using the Model Reference Adaptive Control (MRAC). Artificial neural networks (ANNC), genetic algorithms (GAC), fuzzy logic (FLC), and other intelligence techniques have been developed recently with the goal of enhancing data-based systems or the previously stated methodologies. In addition to studying control design and proving the controllability and stability of the PMSM system, applications of traditional vector control based on both FOC and DTC for the PMSM are also discussed in this chapter. Moreover, the PMSM based on the controls mentioned above has been validated using MATLAB Simulink.

III.2 Design of the PMSM drive

The control design is a crucial step following the identification of the system model. This stage plays a significant role in understanding how to implement control effectively. By grasping the fundamentals of control theory, the closed-loop system-based control becomes clearer and more easily validated through simulation. This process is exemplified in the context of the Permanent Magnet Synchronous Motor (PMSM) drive. Characterizing the machine using a d-q rotor reference frame results in considerably simpler equations for PMSM control design. This simplification expedites the numerical calculations necessary for computational simulations. Additionally, during steady-state operation, the generated variables remain constant, which further streamlines the control system's design and facilitates additional computations. The most prevalent and widely utilized model in the literature is the d-q frame-based model within the rotor reference frame. This model assumes a cage-free rotor, sinusoidal back-EMF, insignificant saturation, and negligible eddy current and hysteresis losses. Typically, the motor is powered by electric energy from the grid, characterized by three electrical variables: voltage, current, and frequency. The motor converts this electrical energy into mechanical energy, manifesting as speed and torque. When controlling the motor, it must be supplied with power through an inverter along with its control mechanism. The primary function of an inverter in the context of motor control is to convert DC (Direct Current) input into AC (Alternating Current) output, which is required for the operation of AC motors like the Permanent Magnet Synchronous Motor (PMSM). This transformation enables the motor to receive the appropriate electrical signals necessary for generating motion. Therefore, the inverter facilitates the conversion of input signals into real signals suitable for driving the motor.

III.2.1 Identification of the PMSM's loops

A nonlinearity feature for the electromagnetic torque, multi-state variable, and external disturbances created in the d-q axis, or what is called back EMF, along with hysteresis loss and eddy current, are what define the PMSM; magnetic circuit saturation is not taken into consideration. The PMSM closed loop can be split into two loops using these characteristics as well as the PMSM model that is described in the second chapter. Speed loop are the first one, and current loops are the second. Depending on the different methods for modeling the PMSM mentioned in the second chapter, decoupling, linearization, or nonlinear are strategies for applying the control techniques approaches for the PMSM. This means each control has characteristics that depend on one of these strategies. Through what was mentioned above, we'll explain the PMSM loops as follows [57]:

- **Speed loop of the PMSM:**

During the control technique application on the PMSM, the speed loop either take one or two state variables. If the one state variable, the speed loop will be single-input single-output (SISO). But if the two state variables, the speed loop become is single-input multi-output (SIMO), where the state variables rotor position and the speed. The SISO and SIMO also are called full state

model, this mean the output is designed by the state variables mentioned above. As for the input is designed by the electromagnetic torque. The speed is captured by a sensor; while the last one is dispensed during one of the observation technique application on the PMSM. In control systems, particularly when dealing with motor control, load torque can be considered an external disturbance to the system. Load torque refers to the torque opposing the motor's motion, typically arising from the load the motor is driving. The uncertainties in load torque can indeed stem from variations in the moment of inertia and friction constant of the rotor. Moment of inertia refers to the resistance of an object to changes in its rotational motion, and the friction constant relates to the frictional forces acting against the motion. Variations in these parameters can result in uncertainties in the load torque, impacting the motor's performance and necessitating appropriate control strategies to mitigate their effects. Figure. III.1 represents the speed loop design based PMSM drive.

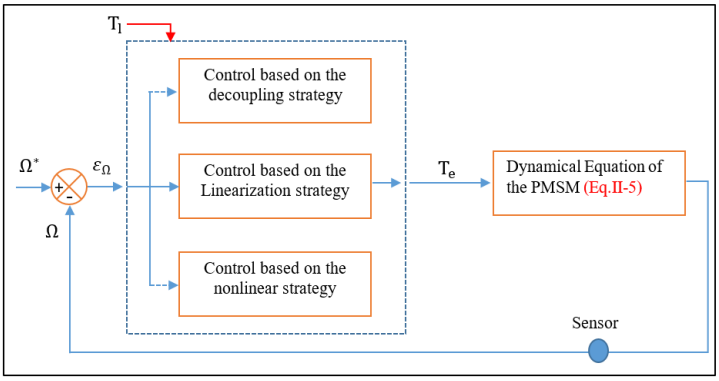

Figure III.1 Design of the speed loop of the PMSM control based on SISO

- **Current loop of the PMSM:**

Through the current loop, the law of control for the PMSM system can be designed. This loop is characterized by multi-input multi output (MIMO) as well as identified by full state model due to it has two state variables are the direct and quadratic currents. The outputs of this loop are the same of states variables and the inputs are the direct and quadratic voltages. Its disturbances are the back EMF and the uncertainties are the resistances and inductances of the direct and quadratic axes. In order to apply the control technique on the PMSM, one of the strategy mentioned in the speed loop section should be used. Figure. III.2 is represented more detailed about the current loop design for the PMSM.

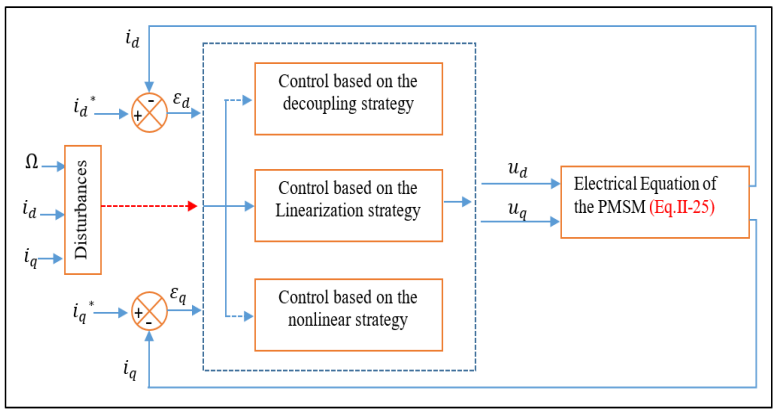

Figure III.2 Design of the current loop of the PMSM control based on MIMO

Where, ε_Ω, ε_d and ε_q are the speed, direct and quadratic errors respectively.

III.2.2 Classification of the PMSM control

The control design approaches for PMSMs can be broadly classified into scalar and vector control. Scalar control is easy to implement and provide a relatively steady-state response but it pose the problem of slower dynamics. Therefore, in order to realize a higher accuracy and good dynamic and steady-steady response, closed-loop vector control approach is usually preferred. The vector control is the largest control group, which includes the conventional and advanced techniques. The conventional techniques is dependent on PID or hysteresis regulators such as field oriented control (FOC) and direct torque control (DTC) respectively. The advanced techniques are divided into the nonlinear, optimal, adaptive and intelligent techniques. They are differ by purpose, characteristics and control design, where some technique can apply directly on the nonlinear model, other one need to the linearization or decoupling strategy. The nonlinear techniques are commonly used in the electric drive, from this type are sliding mode control (SMC), backstepping (BSC), Passivity-based control (PBC) and feedback linearization control (FBLC). While the optimal control are the model predictive control (MPC), Linear quadratic regulator control (LQR) and others. As the adaptive control like the model reference adaptive control (MRAC) which classified among direct, indirect and matching command. Recently, the different intelligences techniques like fuzzy logic (FLC), artificial neural network (ANNC), genetic algorithms (GAC) and others are built in order to improve the mentioned above techniques or improve the data-based system [91-93]. Figure. III.3 is summarized the control classifications for the PMSM drive.

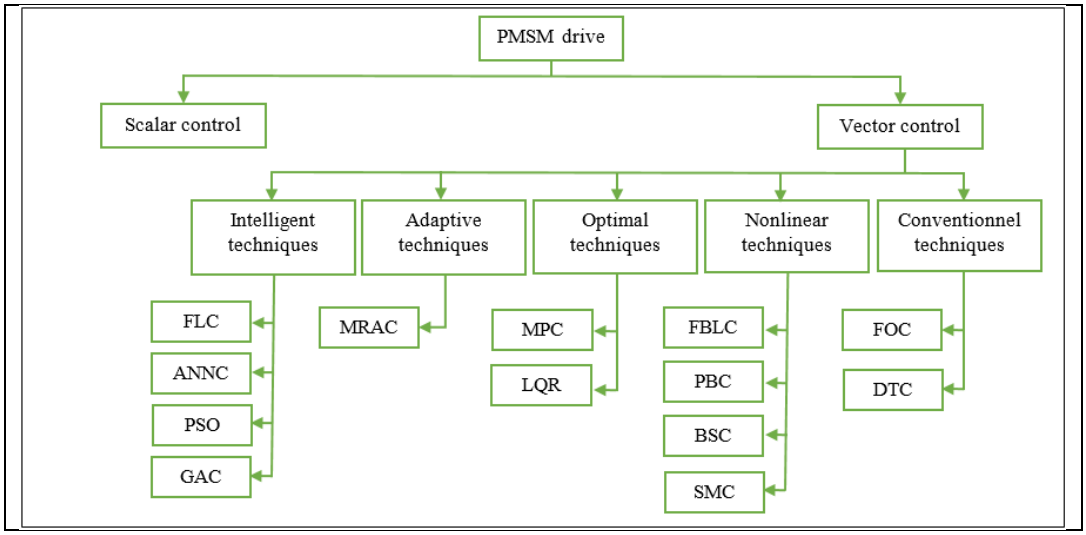

Figure III.3 Design of the PMSM control based on MIMO

III.3 Study the stability of the PMSM system

In order to investigate whether the PMSM plant is stable, a pole-zero map technique has been conducted using the MATLAB program. In this context, the speed, direct, and quadratic axes have been identified as separate subsystems, and stability has been demonstrated using the technique mentioned above, where Figure. III.4 shows that the poles are situated on the negative side of the map as well as that their absolute values are large.

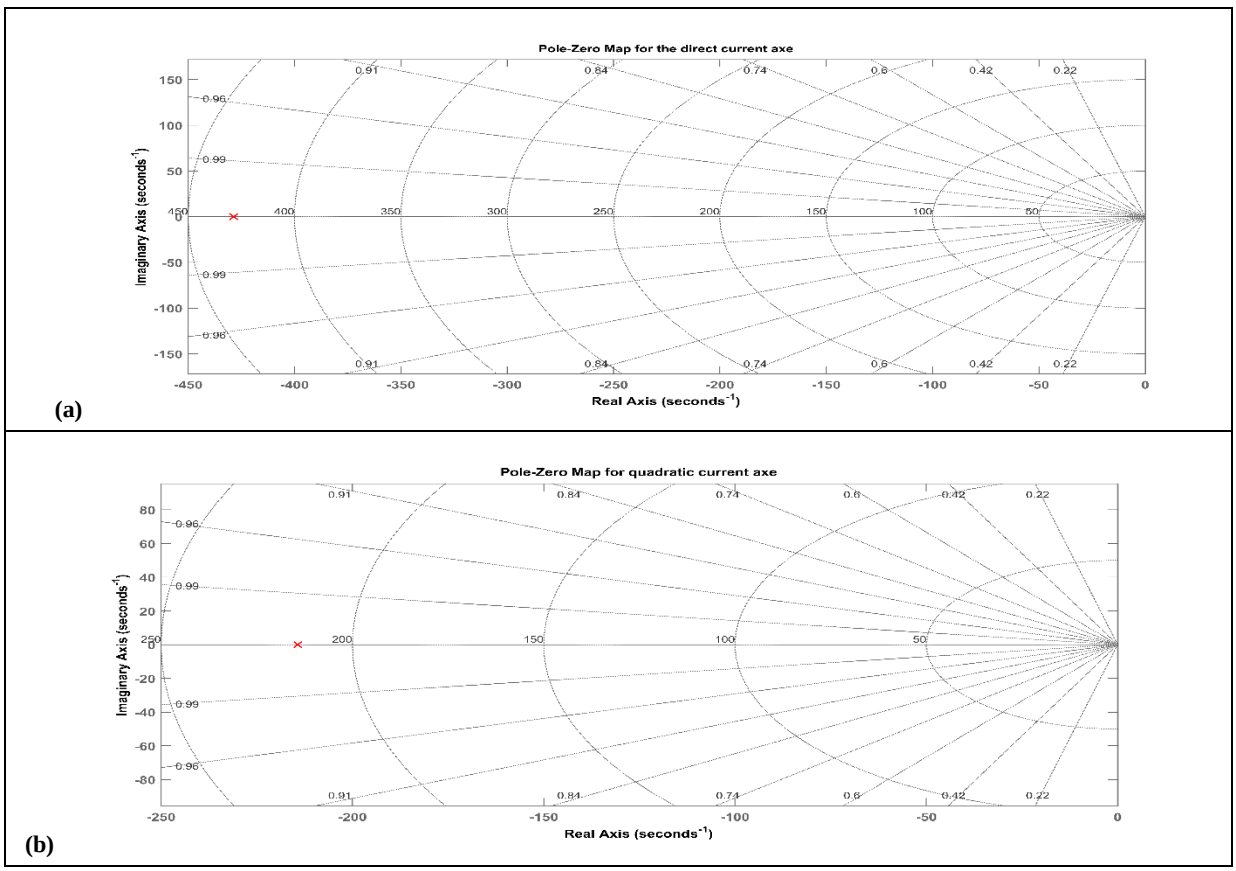

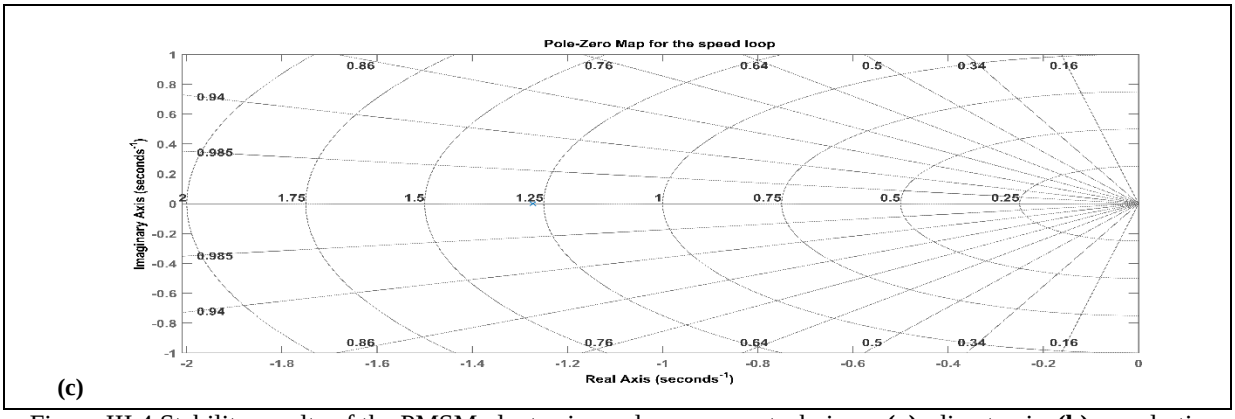

Figure III.4 Stability results of the PMSM plant using pole-zero map technique; **(a):** direct axis, **(b):** quadratic axis, **(c)** speed loop

Using the second method for PMSM modeling mentioned in equation (II.33), the code that was built to check out the stability of the machine loops is presented as follows:

```
%%%%%%% PMSM paramaters %%%%%%%%%%%%%%%%%%%%%
fs=1000;
ts=1/fs
r=0.6;
J=0.0011;
F=0.0014;
p=4;
Ld=1.4e-3;
Lq=2.8e-3;
flux=0.12;
%%%%%%% Direct axes subsystems %%%%%%%%%%%%%%
num1=[1];
den1=[Ld r];
H1= tf(num1,den1);
%%%%%%% Quadratic axes subsystems %%%%%%%%%%%
num2=[1];
den2=[Lq r];
H2= tf(num2,den2);
%%%%%%% Speed subsystems %%%%%%%%%%%%%%%%%%%%
num3=[1];
den3=[J F]
H3= tf(num3,den3);
%%%%%%%%%% Pole-zero map code %%%%%%%%%%%%%%%
pzmap(H1)
axis equal
sgrid
%%%%%%%%%%%%%%%%%%%%%%%%%%%%%%%%%%%%%%%%%%%%
```

III.4 Study the controllability of the PMSM system

Controllability analysis is indeed a crucial step before applying control techniques, especially in systems represented by state-space models like the Permanent Magnet Synchronous Motor (PMSM) system. In the context of state-space models, controllability refers to the ability to drive the system from any initial state to any desired state within a finite time using control inputs. Kalman's controllability theorem that described in the equation (III.1) provides a criterion for

assessing the controllability of a linear time-invariant system. It states that if the rank of the controllability matrix equals the order of the system, then the system is controllable. The controllability matrix is typically formed by the controllability matrix for a single-input system, extended to multi-input systems. Therefore, by checking whether the rank of the controllability matrix equals the order of the system (i.e., the number of states in the system), one can determine whether the state-space model-based system is controllable. If they are equal, it indicates that the system can be controlled effectively using appropriate control inputs [94].

$$P_c = [B \quad AB \cdots A^{n-1}B^n] \tag{III.1}$$

Depending on equation (II.31), it has been identified as having three variable states: speed, direct and quadratic current. Through this design, the system will be classified into the third-order. Consequently, the controllability matrix will become as follows:

$$P_c = [B \quad AB \quad A^2B] \tag{III.2}$$

$$P_c = \begin{bmatrix} \frac{1}{L_d} & 0 & 0 & -\frac{R_s}{{L_d}^2} & 0 & 0 & \frac{{R_s}^2}{{L_d}^3} & 0 & 0 \\ 0 & \frac{1}{L_q} & 0 & 0 & -\frac{R_s}{{L_q}^2} & 0 & 0 & \frac{{R_s}^2}{{L_q}^3} & 0 \\ 0 & 0 & \frac{p}{j} & 0 & 0 & -\frac{p.F}{j^2} & 0 & 0 & \frac{pF^2}{j^3} \end{bmatrix} \tag{III.3}$$

The rank of P_c {r (P_c) =3} is always three (3) which is the same as the system's order, so the PMSM system presented in equation (II-31) is always controllable.

III.5 Design of the conventional vector control based on FOC

The industry standard control technique that is most frequently employed is called field-oriented control, or FOC. Despite the progress made in theoretical modeling of induction motors, the earlier description of variable speed control for AC motors persisted until the late 1960s, when Blaschke and Hasse presented the notion of Field Oriented Control (FOC), a conventional vector control technique. Generally, the foundation of FOC is the conversion of three-phase quantities (represented by the abc reference frame) into a two-phase time invariant system (represented by the d-q reference frame). This process enables the separation of stator current into two components: the torque component (aligned with the quadrature axis coordinate) and the flux component (aligned with the d coordinate or direct axis coordinate). An AC machines that is controlled similarly to a DC motor is made possible by this decomposing stator current. Relatively, FOC ensures precise and effective motor control both in steady state and intermittent operation. Deeper penetration of AC drives into industrial applications was made possible by the introduction of FOC, advancements in semiconductor devices, and the development of strong and effective digital controllers. For the power range of a few hundred Watts to a few thousand Watts, variable speed operation. Originally designed to regulate induction machines, the FOC is currently the most widely used control method in PMSM drives. The FOC control structure consists of two control loops: the inner current control loop and the outer speed or position control loop. In FOC, the torque of the motor is regulated by changing the stator current vector. The

torque demand for the inner current control loop is provided by the outer control loop changing the speed, and the torque of the motor is managed by regulating the stator current vector. A PMSM's FOC depends on precise sensor-derived information about the reference rotor position or speed. It can be seen that once the rotor position is known, finding the torque becomes fairly easier, as explained and mentioned in the preceding set of equations as the torque expression depends on the synchronous axis currents, inductances, and permanent magnet flux linkage values. It follows that the torque control is enabled by appropriate current control through the use of a synchronous frame component. .Furthermore, the machine's dynamics become much simpler than in a fixed frame, where parameters change sinusoidal in response to rotor position. Additionally, since Park's transformation makes transposition to the frequency domain possible, this can be analyzed. In a synchronous reference frame, signals with rotating frequencies in a stationary reference frame can be moved to zero frequencies [95-97].

III.5.1 The overview objective of the FOC

By regulating the three-phase current, field-oriented control, or FOC, seeks to ensure that the rotor is perpendicular to the stator's magnetic field. Using three phases, this is accomplished by first measuring the rotor's position and then generating a three-phase current to create a field in the intended direction. In order to do this, the three phases are transformed into the d-q frame using Clarke and Park transforms, where d is orthogonal to q and contributes no torque, and q is the desired direction that delivers the largest torque contribution. This change of frame defines the sum of the three-phase magnetic field in the two dimensions d and q that spin with the rotor and is accomplished with the aid of the Clarke and Park transforms as well as the angle ϑ_{dq} (the direction of the permanent magnet). In this manner, the desired torque can be achieved by controlling the q-vector and setting the d-vector to zero. There is no force contribution from the d-vector since it induces a magnetic field in the same direction as the permanent magnetic field. The q-vector, in contrast, creates a magnetic field where the torque contribution is greatest and most beneficial. By using this technology, a magnetic flux that is constantly perfectly chasing the permanent magnets by 90 degrees controls the motor [98]

III.5.2 Speed loop of the PMSM based on the FOC

The FOC is considered one of the first traditional vector controllers that has been successfully applied to linear plants because it depends on the PI regulator. Because the torque expression is characterized as a nonlinear model, the physical explanation for the field-oriented control objective on the PMSM is to arrive at a model equivalent to that of a DC machine (a decoupled linear model). One such model consists of maintaining the component i_d equal to zero, as shown in Figure. III.5. Where K_f is a constant, p is the number of rotor permanent magnet pole pairs, and i_a and i_f are respectively the induced and the inductor current of the DC motor, respectively [92].

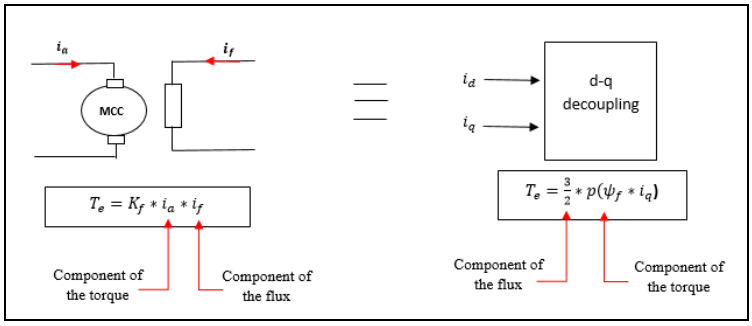

Figure III.5 Equivalence between decoupled DC motor and PMSMO

Following the torque expression's linearization in equation (II.26), the simplified dynamics are as follows:

$$T_e = (3.\frac{p}{2})\psi_f . i_q{}^* \tag{III.4}$$

Depending on the torque expression mentioned above, the dynamic equation of the PMSM presented in equation (II.5), become as follows:

$$j.\frac{d\Omega}{dt} = (3.\frac{p}{2})\psi_f . i_q{}^* - T_l - F\Omega \tag{III.5}$$

Using Laplace transfer:

$$\frac{\Omega(s)}{T_e(s)-T_l(s)} = \frac{1}{F+j.s} \tag{III.6}$$

According to equation (III.5) and equation (III.6) respectively, the speed loop could be described as follows:

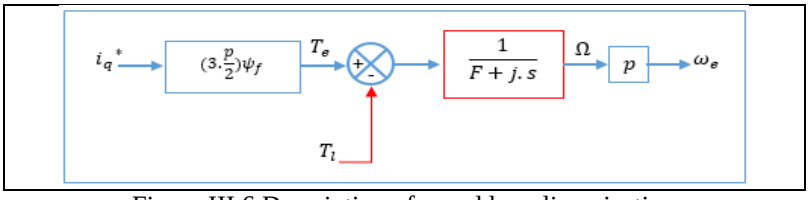

Figure III.6 Description of speed loop linearization

The speed's closed loop based on the PI regulator can be obtained as follows:

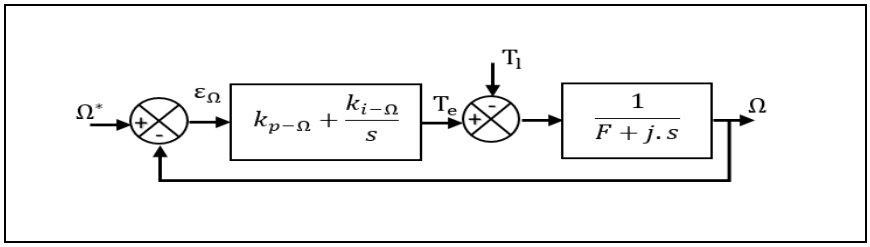

Figure III.7 Design of the closed loop speed regulation

Where the $k_{p\text{-}\Omega}$ and $k_{i\text{-}\Omega}$ are proportional and integral coefficients of the speed respectively.

In order to simplification, the transmittance of the PI regulator used can be expressed as follows:

$$k_{p-\Omega} + \frac{k_{i-\Omega}}{s} = \frac{k_{i-\Omega}}{s}(1+\tau s) \tag{III.7}$$

Where τ is the filter's time constant, and it is estimated to $\tau = \frac{k_{p-\Omega}}{k_{\mathrm{i}-\Omega}}$.

Additionally, as Figure. III.7 illustrates, a filter can be added to the speed control loop to reduce overshoot. This speed regulation loop's closed loop transfer function TFCL(s) was computed as follows:

$$\mathrm{TFCL(s)} = \frac{\Omega(s)}{\Omega(s)^*} = \frac{1+\tau s}{\frac{j}{k_{i-\Omega}}s^2+(\tau+k_{i-\Omega})s+k_{i-\Omega}} \tag{III.8}$$

Since the transfer function has second-order properties ($\tau = \frac{2\xi}{\omega_0}$), as can be seen, Equation (III.-9 provides the proportional ($k_{\mathrm{p}-\Omega}$) and integral ($k_{\mathrm{i}-\Omega}$) benefits.

$$\begin{cases} k_{\mathrm{i}-\Omega} = \frac{4.j}{\tau^2} \\ k_{\mathrm{p}-\Omega} = k_{\mathrm{i}-\Omega}.T_q \end{cases} \tag{III.9}$$

Where, ξ is the damping coefficient and ω_0 is the pulsating frequency in rad/s.

III.5.3 Current loop of the PMSM based on the FOC

In order to apply this control to the PMSM current loop, it should build a closed loop based on a PI regulator and use the decoupling and compensating techniques to detect the linear plant. In the event that the voltage supply decouples, terms of compensation must be established since the stator equations exhibit coupling between the quadratic and direct axes. The aforementioned axes are compensated in order to decouple, and the stator equations contain the following definitions of "disturbances," which are defined as currents from the opposite axis. These disturbances represent as the back EFM in equation (II.27) [57]. Depending on the decoupling method, equation (II.25) becomes as follows:

$$\begin{cases} v_d - E_d = R_s.i_d + L_d.\frac{di_d}{dt} \\ v_q - E_q = R_s.i_q + L_q.\frac{di_q}{dt} \end{cases} \tag{III.10}$$

Using Laplace transfer:

$$\begin{cases} \frac{i_d(s)}{v_d(s)-E_d(s)} = \frac{1}{R_s+L_d.s} \\ \frac{i_q(s)}{v_q(s)-E_q(s)} = \frac{1}{R_s+L_q.s} \end{cases} \tag{III.11}$$

According to equation (III.10) and equation (III.11) respectively, the coupling design could be described as follows:

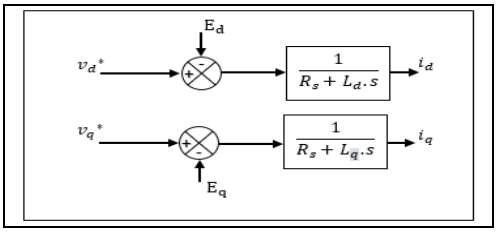

Figure III.8 Description of current loop coupling

In the closed loop, the disturbances of equation (II.25) replaced the cross-coupling between the currents of the two accesses. Based in this, the applied voltages, which are generally generated by the voltage source inverter "VSI", can be selected as follows:

$$\begin{cases} v_d^* = u_d + E_d \\ v_q^* = u_q + E_q \end{cases} \quad \text{(III.12)}$$

Where the u_d and u_q are linear model of PMSM "LPMSM", and designed as follow:

$$\begin{cases} u_d = R_s.i_d + L_d.\frac{di_d}{dt} \\ u_q = R_s.i_q + L_q.\frac{di_q}{dt} \end{cases} \quad \text{(III.13)}$$

Finally, PMSM can be obtained by FOC based PI regulator for the PMSM's current loop:

$$\begin{cases} u_d = k_{p-d}.\varepsilon_d + \frac{k_{i-d}}{S}.\varepsilon_d \\ u_q = k_{p-q}.\varepsilon_q + \frac{k_{i-q}}{S}.\varepsilon_q \end{cases} \quad \text{(III.14)}$$

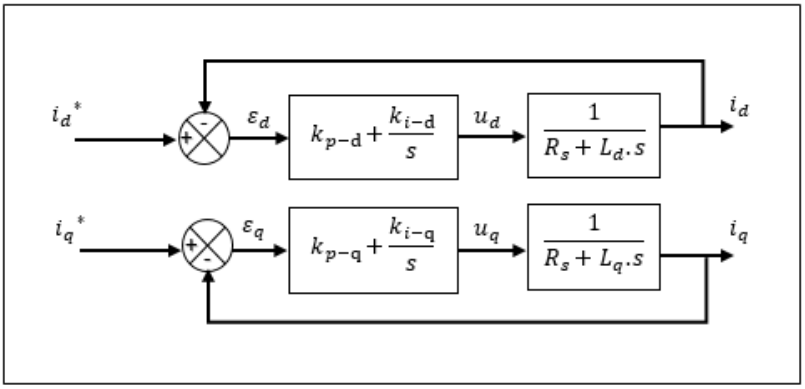

Figure III.9 Decoupling control based on the PI regulators

The PI gains can be computed as follows, depending on the closed loop and first-order stability conditions for the system:

$$[k_{p\_d} \quad k_{p-q} \quad k_{i-d} \quad k_{i-q}] = R_s.\left[1 \quad \frac{R_s}{L_d} \quad 1 \quad \frac{R_s}{L_q}\right] \quad \text{(III.15)}$$

Where the k_{p-d} and k_{p-q} are proportional coefficients of the direct and quadratic axis respectively, and the k_{i-d} and k_{i-q} are the integral coefficients of the direct and quadratic axis respectively.

Finally, the decoupling by compensation to the PMSM's current is designed as follows:

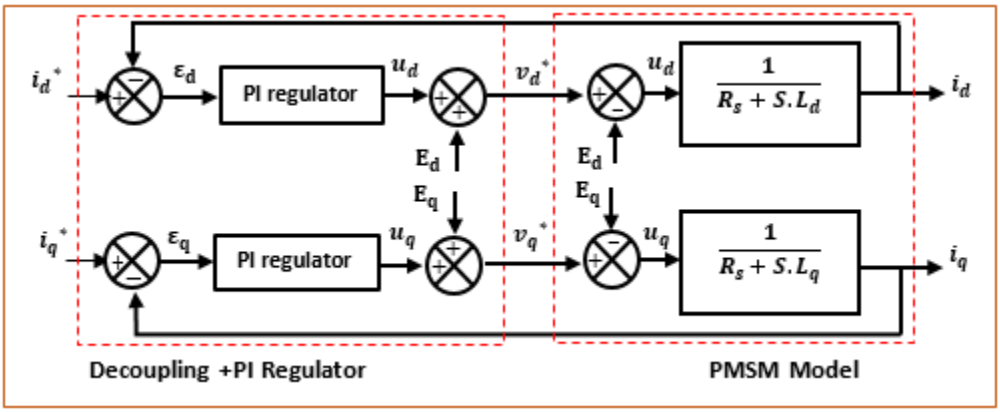

Figure III.10 PMSM Model based on FOC

III.5.4 Description of the overall structure (PMSM drive based on FOC)

The vector control based on the field-oriented control (FOC) for the three phases of the PMSM utilizing the frame (d-q) is depicted in Figure III.10, along with the PMSM model based on the transfer function method and the control based on the decoupling strategy. The speed regulator's output serves as the reference quadratic current $i_q{}^*$, while the reference direct current is fixed at $i_d{}^*$=0. They are compared separately with the actual PMSM currents i_d and i_q. The resulting errors between the reference and actuals currents mentioned above are modified by the classical PI regulator. A decoupling block generates the reference voltages $v_d{}^*$ and $v_q{}^*$. The reference quadratic current is limited to the maximum current. When the current regulation outputs i_d and i_q cross the mark (a, b, c), they act as voltage references (v_a, v_b, v_c) that controlled the PWM inverter.

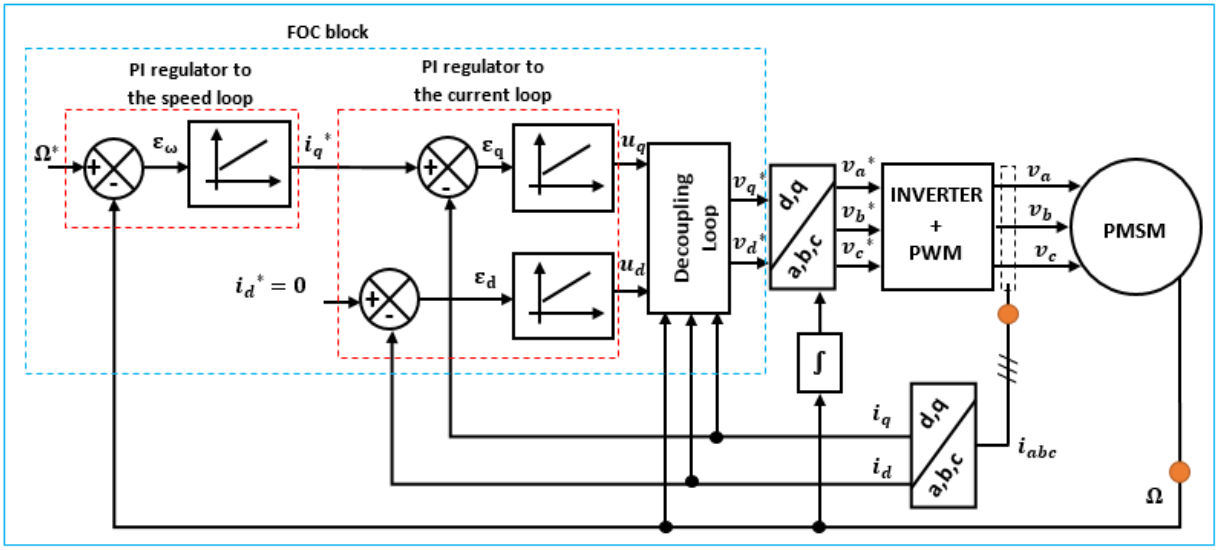

Figure III.11 Scheme of the general structure to the PMSM drive based on the FOC

III.6 Design of the conventional vector control based on the DTC

Early in the 1990s, scientists began looking into different methods of motor control that would be easier to apply and have quicker reaction times. In 1992, Takahashi and Noguchi, two European researchers, introduced the idea of Direct Torque Control (DTC) for induction motors. Due to the fact that the torque and flux were directly controlled without the need for a coordinate transformation, this represented a change from conventional vector control methods (FOC).The origins of DTC can be found in the late 20th century, when engineers and researchers started looking into different control schemes to enhance the efficiency of electric motor drives. The development of control techniques and the efforts of numerous researchers can be linked to the particular history of DTC. Depenbrock presented the first thorough work on DTC for induction motors in 1994. The fundamentals of DTC were presented in this study, with a focus on how it can deliver high-performance torque and flux control without requiring intricate mathematical calculations. Researchers and engineers concentrated on improving DTC algorithms and tackling issues like torque and flux ripple in the late 1990s and early 2000s. In the ensuing years, DTC kept developing and found use in a wider range of AC motors, including synchronous motors. In industrial applications where accurate control of motor torque and speed is crucial, direct torque control is now commonly used. It is now a common practice in variable frequency drives, or VFDs, and is essential to the effectiveness and functionality of electric motor systems. Research is still being done to improve DTC even further and modify it to fit new developments in electric drive technology [99,100, 106-108].

III.6.1 The overview objective of the DTC

Direct torque control of alternating current machines is based on the “direct” determination of the control sequence applied to the switches of a voltage inverter. This choice is generally based on the use of hysteresis regulators, whose function is to control the state of the system, namely the amplitude of the stator flux and the electromagnetic torque. This type of control is classified in the category of amplitude controls, as opposed to the more traditional duration control laws, which are based on an adjustment of the average value of the voltage vector by pulse width modulation (PWM). Originally, DTC commands were strongly based on the “physical sense” and on a relatively empirical approach to the variation of states (torque, flux) over a very short time interval (interval between two switchings). This reasoning has been clearly refined and is now based on increasingly solid mathematical foundations [101-103].

III.6.2 General characteristics of the DTC

Through the overview objectives of the DTC mentioned above, the general characteristics of the DTC can be classified as follow [104, 105]:

- Direct control of torque and flux, from the selection of the optimal switching vectors of the inverter;
- Indirect control of the currents and voltages of the machine stator;

- Obtaining stator fluxes and currents close to sinusoidal shapes;
- The existence of torque oscillations which depends, among other factors, on the bandwidth of the hysteresis regulators;
- The switching frequency of the inverter depends on the amplitude of the hysteresis bands.

III.6.3 Steps for utilizing DTC on the PMSM

Depending on the objective of the DTC, the PMSM drive should follow several interconnected steps in order to reach the control law based on the DTC. These steps can be summarized as follows:

- Description of the flux and torque controls;
- Identified the voltage vectors;
- Estimation of flux and couple;
- Design of the DTC adjustments;
- Elaboration of the switching table;

A. Description of the flux and torque controls

The machine's vector model highlights the dynamic torque control conditions of the PMSM system. We shall use the machine's vector expressions for this. We will then situate ourselves within the α-β frame of reference. Additionally, we will use the following notation to make expressing the quantities represented in the frame of reference simpler: $X_s = X_{\alpha\beta}$. Moreover, this step aims to describe the electromagnetic and flux control using the voltages of the PMSM, which are written as follows [106].

$$\bar{v}_s = R_s \bar{I}_s + \frac{d\bar{\varphi}_s}{dt} \quad \text{(III.16)}$$

- **Flux vector control**

Through equation (III.16), the expression of the flux become as follows :

$$\bar{\varphi}_s = \bar{\varphi}_{s0} + \int_0^t (\bar{v}_s - R_s \bar{I}_s) dt \quad \text{(III.17)}$$

Where: $\bar{\varphi}_{s0}$ is the flux vector at time t = 0.

The term $R_s \bar{I}_s$ will be regarded as negligible in this study when compared to the voltage vector $\bar{v}_s$, which is confirmed when the rotation speed is high enough. Using the preceding equation, we obtain:

$$\Delta\bar{\varphi}_s = T . \bar{v}_s \quad \text{(III.18)}$$

Figure. III.12 shows that the end of vector $\bar{\varphi}_s$ moves on a straight line whose direction is indicated by $\bar{v}_s$ across the time span [0, T].

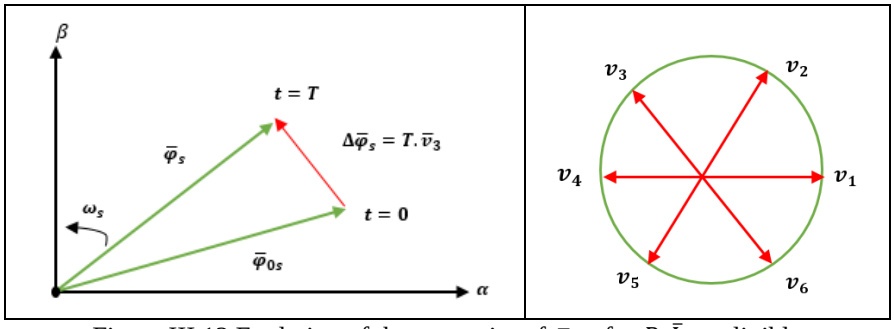

Figure III.12 Evolution of the extremity of $\bar{\varphi}_s$ s for $R_s\bar{I}_s$ negligible

To guide the endpoint of the $\bar{\varphi}_s$ vector along a desired trajectory, we carefully select a sequence of the $\bar{v}_s$ vector over successive time intervals of duration T. This ensures a nearly constant modulus of the flux ϕ_s. When the period T is significantly shorter than the rotation period of the flux T_s, achieving this goal merely requires guiding the endpoints of ϕ_s in an essentially circular trajectory. Due to the synchronous rotation of permanent magnets with the rotor, the stator flux undergoes variations even without a voltage vector. Hence, it's advisable to refrain from utilizing zero voltage vectors to regulate the stator flux of PMSMs. Essentially, there must be continuous movement between the stator and rotor fluxes. A three-phase voltage inverter generates the voltage vector $\bar{v}_s$. This vector, defined as the combination of simple voltages, is controlled by three Boolean values (S_j, where j=a, b, c) that theoretically represent the state of the inverter's switches.

$$\bar{v}_s = v_\alpha + jv_\beta = \sqrt{\frac{2}{3}}V_{dc}(S_a + S_b e^{j\frac{2\pi}{3}} + S_c e^{j\frac{4\pi}{3}}) \quad \text{(III.19)}$$

In Figure III.13, we illustrate the three potential orientations of the flux vector $\bar{\varphi}_s$. Thus, it is evident that the displacement of the flux's extremities and amplitude maintain their values when the applied voltage is perpendicular to the flux direction. Conversely, we observe a slowing (or acceleration) of the flux's end movement and a decrease (or increase) in its amplitude when $\bar{v}_s$ is offset from perpendicular to the flux vector.

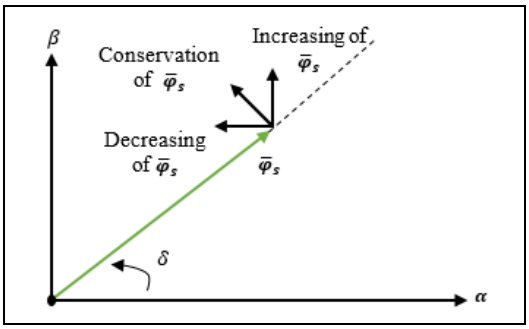

Figure III.13 Behavior of the flux for different voltage vectors

- **Electromagnetic torque control:**

The vector product of the stator and rotor flux vectors determines the electromagnetic torque in the following way [111]:

$$T_e = k\left(\bar{\varphi}_s \times \overline{\varphi'}_r\right) = k\|\bar{\varphi}_s\|.\left\|\overline{\varphi'}_r\right\|.\sin(\delta) \quad \text{(III.20)}$$

Where, $k = \frac{p}{L_q}$

With; $\bar{\varphi}_s$ is the stator flux vector; $\overline{\varphi'}_r$ is the rotor flux vector brought back to the stator and δ is the angle between the stator and rotor flux vectors.

Through the equation (III.16), the torque is determined by the relative positions and amplitudes of the two vectors, $\bar{\varphi}_s$ and $\overline{\varphi'}_r$. Achieving complete control over the flux $\bar{\varphi}_s$ (from $\bar{v}_s$) in both amplitude and position will allow us to decouple control over both the amplitude of $\bar{\varphi}_s$ and the electromagnetic torque T_e.

B. Identified the voltage vectors

The vector of the velocity ($\bar{v}_s$) can be chosen depending on the sector reference (S), the position of the flux ($\bar{\varphi}_s$), the direction of rotation of $\bar{\varphi}_s$ of the desired variation for the modulus of $\bar{\varphi}_s$, of the desired variation for the torque (T_e). The space development of the $\bar{\varphi}_s$in "sector (S)" is divided into six zones S_i, with i=[1..,6] as shown in the Figure. III.14. When the flux $\bar{\varphi}_s$ is in a zone S_i, control of the flux and torque can be achieved by selecting one of the following eight voltage vectors [112]:

- If $\bar{v}_i$ is selected then $\bar{\varphi}_s$ is increases and T_e is constant;
- If $\bar{v}_{i+1}$ is selected then $\bar{\varphi}_s$ and T_e are increase;
- If $\bar{v}_{i-1}$ is selected then $\bar{\varphi}_s$ is increases and T_e is decreases
- If $\bar{v}_{i+2}$ is selected then $\bar{\varphi}_s$ is decreases and T_e is increases
- If $\bar{v}_{i-2}$ is selected then $\bar{\varphi}_s$ and T_e are decreases
- If $\bar{v}_{i+3}$ is selected then $\bar{\varphi}_s$ is decreases and T_e is constant;
- If $\bar{v}_0$ and $\bar{v}_7$ are selected then the rotation of the flux ($\bar{\varphi}_s$) is stopped, resulting in a decrease in the torque while the modulus of flux($\bar{\varphi}_s$) remains unchanged.

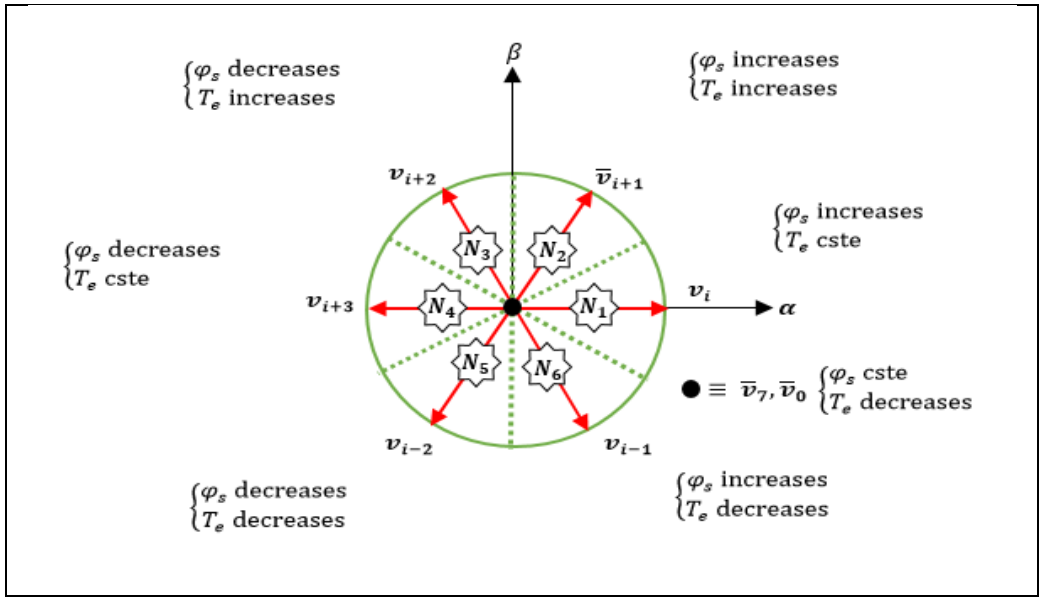

Figure III.14 Select the tension vector

Moreover, the level of efficiency of the applied voltage vectors also depends on the position of the flux vector in the S_i zone. In fact, the amplitude of the flux($\bar{\varphi}_s$) evolves slowly at the beginning of the zone because the vectors $\bar{v}_{i+1}$ and $\bar{v}_{i-2}$ are perpendicular to $\bar{\varphi}_s$, but at the end of the zone, the evolution is the opposite. At the beginning of the zone, the torque (T_e) evolves slowly and the amplitude of $\bar{\varphi}_s$ rapidly, corresponding to the vectors $\bar{v}_{i+2}$ and $\bar{v}_{i-1}$. At the conclusion of the zone, the opposite is true. The two vectors $\bar{v}_i$ and $\bar{v}_{i+3}$ are never employed, regardless of the direction in which the torque or flux in the S_i zone evolves. While it is true that these conditions exhibit the strongest "flux component," characterized by a rapid evolution of $\bar{\varphi}_s$, the torque is primarily impacted when $\bar{\varphi}_s$is positioned within a specific range, typically centered within the zone.

C. Estimation of flux and couple

The position of the vector $\bar{\varphi}_s$, along with the predicted torque and flux deviations from their reference values, are utilized to deduce the voltage vector at the output of the inverter. Consequently, both a torque estimator and a flux estimator in terms of both amplitude and position become essential. Moreover, the torque and flux amplitude serve as the control system's input instructions. The precision with which these parameters are estimated directly influences the effectiveness of the control system [107,111].

- **Estimation of the flux:**

Measurements of the PMSM's current and voltage values can be used to estimate the flux. From equation (III.16), we obtain the components (α, β) linked to vector of the flux $\bar{\varphi}_s$ [15,113]:

$$\begin{cases} \hat{\varphi}_\alpha = \int_0^t (\bar{v}_\alpha - R_s \bar{I}_\alpha) dt \\ \hat{\varphi}_\beta = \int_0^t (\bar{v}_\beta - R_s \bar{I}_\beta) dt \end{cases} \quad \text{(III.21)}$$

Where;

$$\bar{\varphi}_s = \hat{\varphi}_\alpha + j\hat{\varphi}_\beta \quad \text{(III.22)}$$

The voltages $\bar{v}_\alpha$ and $\bar{v}_\beta$ are determined from the commands (S_a, S_b, S_c) and the measurement of the voltage V_{dc} as follows:

$$\begin{cases} v_\alpha = \sqrt{\frac{2}{3}} V_{dc} \left(S_a - \frac{1}{2}(S_b + S_c) \right) \\ v_\beta = \frac{1}{\sqrt{2}} V_{dc} . (S_b - S_c) \end{cases} \quad \text{(III.23)}$$

Where;

$$\bar{v}_s = v_\alpha + j v_\beta \quad \text{(III.24)}$$

Likewise, the currents i_α and i_β are obtained from the measurement of the real currents i_a, i_b and i_c, where (i_a+ i_b+i_c =0) as follows:

$$\begin{cases} i_\alpha = \sqrt{\frac{2}{3}} i_a \\ i_\beta = \frac{1}{\sqrt{2}}(i_b - i_c) \end{cases} \quad \text{(III.25)}$$

Where;

$$\bar{\imath}_s = i_\alpha + j i_\beta \quad \text{(III.26)}$$

Depending on the expression of current and voltages mentioned previously, the amplitude of the flux is written as follows:

$$\hat{\varphi}_s = \sqrt{\hat{\varphi}_\alpha{}^2 + \hat{\varphi}_\beta{}^2} \quad \text{(III.27)}$$

The zone N_i in which the vector $\bar{\varphi}_s$: is located is determined from the components $\hat{\varphi}_\alpha$ and $\hat{\varphi}_\beta$. The angle δ between the reference frame (α, β) of the vector $\bar{\varphi}_s$ is equal to:

$$\delta = Arctg \frac{\hat{\varphi}_\beta}{\hat{\varphi}_\alpha} \quad \text{(III.28)}$$

- **Estimation of the electromagnetic torque:**

The electromagnetic torque can be estimated from the estimation of the flux and the measurement of the current using the expression of the torque as a function of the flux and the stator current given by the equation [112,113]:

$$\hat{T}_e = P(\hat{\varphi}_\alpha . i_\beta - \hat{\varphi}_\beta . i_\alpha) \quad \text{(III.29)}$$

D. Design of the DTC adjustments

In this section, the adjustments of the flux and electromagnetic component will be presented, as well as the applied two-level and three-level based hysteresis comparators, which will be explained as follows:

- **Adjustment of the flux component:**

The aim of this adjustment is to maintain the flux's amplitude within a band, thereby keeping the latter's end in a circular ring, as illustrated in Figure. III.15. The adjustment's output has to show which way the flux amplitude is evolving. This two-level hysteresis regulator for the flux component is ideal for good dynamic performance. The comparator's two thresholds are selected based on the amount of ripple that the flux can withstand. Next, we can write [106]:

$$\begin{cases} \text{If } \varepsilon_\varphi > \Delta\varphi_s & \text{then : } k_\varphi = 1 \\ \text{If } 0 \le \varepsilon_\varphi \le \Delta\varphi_s \quad \text{, and } \frac{d\varepsilon_\varphi}{dt} > 0 & \text{then : } k_\varphi = 0 \\ \text{If } -\Delta\varphi_s \le \varepsilon_\varphi \le 0 \quad \text{, and } \frac{d\varepsilon_\varphi}{dt} < 0 & \text{then : } k_\varphi = 1 \\ \text{If } \varepsilon_\varphi < -\Delta\varphi_s & \text{then : } k_\varphi = 0 \end{cases} \quad \text{(III.30)}$$

Where; ε_φ is the flux error. It is the value that expresses the difference between a reference and an estimate of the flux ($\varepsilon_\varphi = \varphi_s^* - \hat{\varphi}_s$), $\Delta\varphi_s$ is the hysteresis band limit of the flux, $k_\varphi = 0$: indicate that the flux must be reduced, and $k_\varphi = 1$: indicate that the flux must be increased

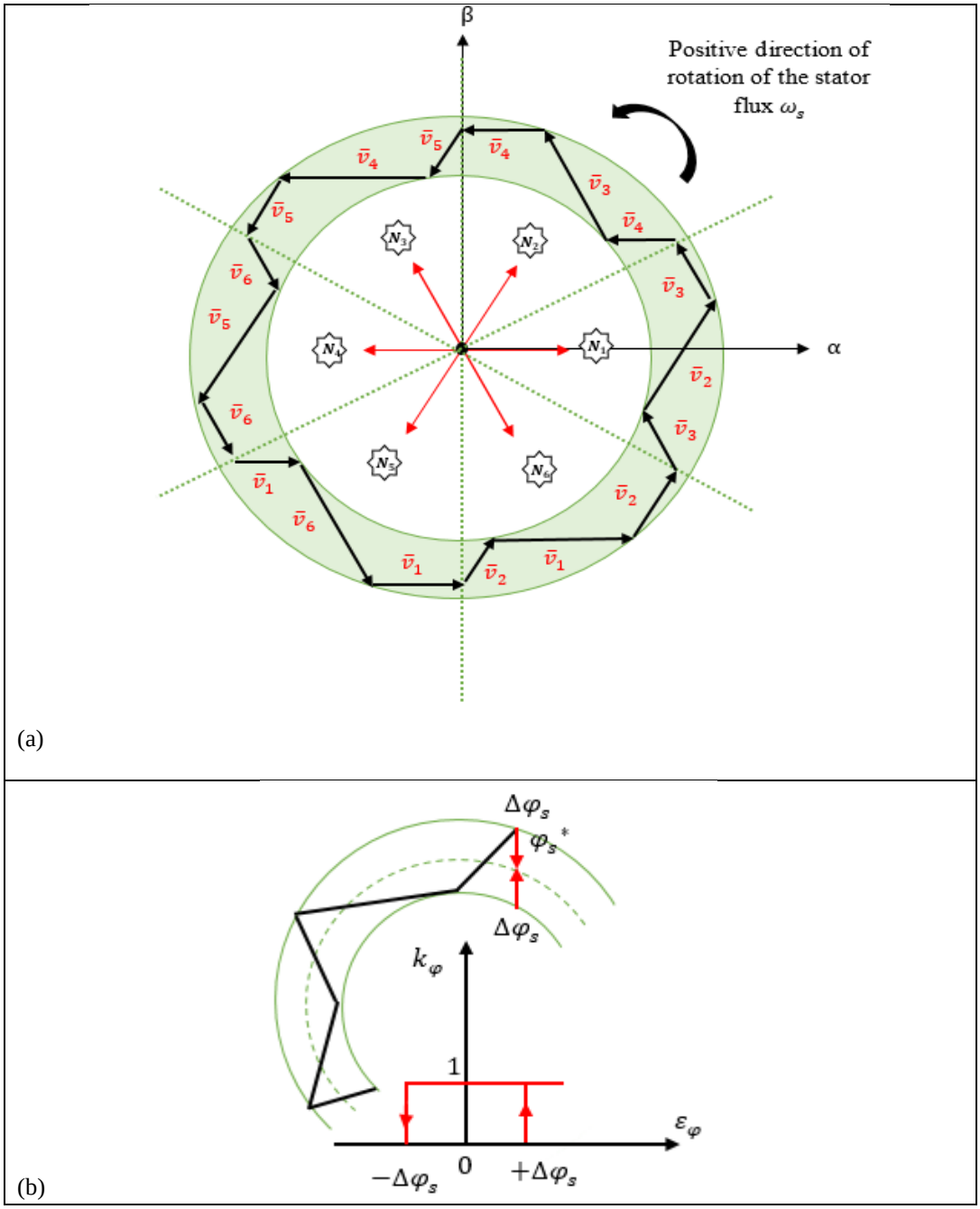

Figure III.15 Adjustment of the flux component**; (a):** Selection of $\bar{v}_i$ voltages to control the flux**; (b):** Two-level hysteresis comparator for flux control

- **Adjustment of the electromagnetic torque component:**

The function of the torque corrector is to maintain the torque within the limits [114]:

$$\left|T_e^* - \hat{T}_e\right| \leq \varepsilon_T \tag{III.31}$$

Where; T_e represents the torque set point.

One distinction with flux control, though, is that the torque can be either positive or negative based on the machine's rotational direction. There are two options to think about [112]:

❖ **Adjustment based on the two-level comparator:**

This adjustment is the same as the one that governs the $\bar{\varphi}_s$ amplitude. Only permits torque adjustment in a single rotational direction. Therefore, the only vectors that can be chosen to cause the flow $\bar{\varphi}_s$ to evolve are $\bar{v}_{i+1}$ and $\bar{v}_{i+2}$. As a result, only the zero vector option can result in a torque reduction. With this adjustment, should have to go through two machine operators in order to change the machine's direction of rotation. This adjustment is easier to use, though. Additionally, by accurately choosing the zero vectors in accordance with the zones N_i, can be observe that there is an inverter arm for each zone *i* that never switches. This allows us to lower the average switching frequency of the switches, which lowers switching losses at the inverter level.

❖ **Adjustment based on the three-level comparator:** It gives you the ability to adjustment the motor for either positive or negative torque in both rotational directions. The Boolean variable k_T, which represents the corrector's output, indicates whether the torque amplitude must be increased in absolute value {k_T= 1 for a positive set point and k_T =-1 for a negative set point} or must be reduced k_T =0 for.

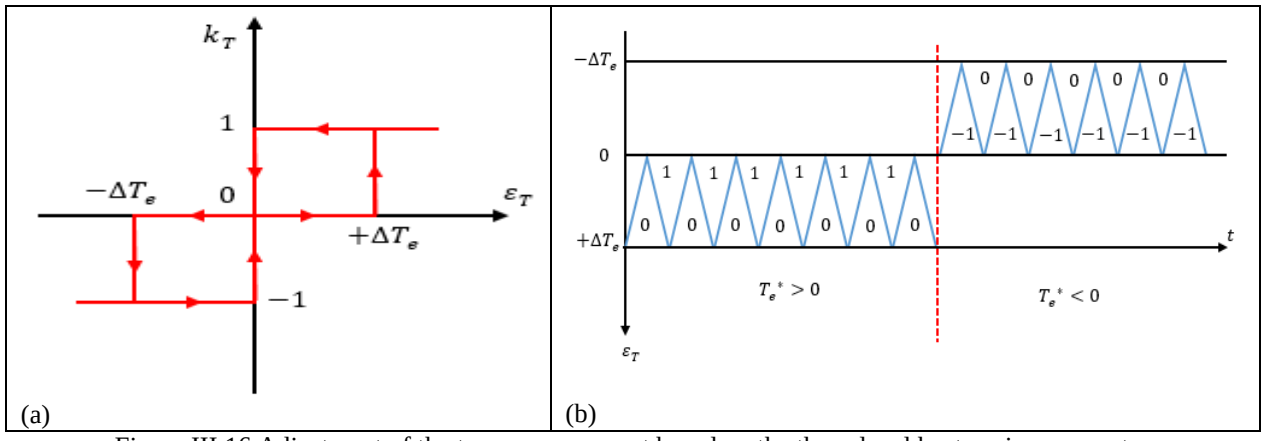

Figure III.16 Adjustment of the torque component based on the three-level hysteresis comparator

Without requiring structural modifications, the three-level adjustment enables operation in all four quadrants. Next, we could write:

$$\begin{cases} If\ \varepsilon_T > \Delta T_e & & \text{then}: k_T = 1 \\ \text{If } 0 \leq \varepsilon_T \leq \Delta T_e & ,and\ \frac{d\varepsilon_T}{dt} > 0 & \text{then}: k_T = 0 \\ \text{If } 0 \leq \varepsilon_T \leq \Delta T_e & ,and\ \frac{d\varepsilon_T}{dt} < 0 & \text{then}: k_T = 1 \\ \text{If } \varepsilon_T < -\Delta T_e & & \text{then}: k_T = -1 \\ \text{If } -\Delta T_e \leq \varepsilon_T < 0 & ,and\ \frac{d\varepsilon_T}{dt} > 0 & \text{then}: k_T = 0 \\ \text{If } -\Delta T_e \leq \varepsilon_T < 0 & ,and\ \frac{d\varepsilon_T}{dt} < 0 & \text{then}: k_T = -1 \end{cases} \tag{III.32}$$

Where; ε_T is the torque error. It is the value that expresses the difference between a reference and an estimate of the torque ($\varepsilon_T = T_e^* - \hat{T}_e$), ΔT_e is the hysteresis band limit of the flux, $k_\varphi = -1$: indicate that the flux must be reduced, $k_\varphi = 0$: to keep it constant within a $2\Delta T_e$ band around its reference, and $k_\varphi = 1$: indicate that the flux must be increased.

E. Elaboration of the switching table

The truth table has been elaborated based on the torque and flux errors, $\Delta\varphi_s$ and ΔT_e, and in accordance with the flux vector's position (N=1,...,6). According to Figure. III.17, the complex plan can be divided into six angular sectors. Within each sector, the control sequence of the inverter switches can be determined. This corresponds to the various states of the control quantities $\Delta\varphi_s$ and ΔT_e, based on the logic of flux and torque behaviour when a voltage vector is applied. The cumulative effect of all configurations on the flux and electromagnetic torque is summarized in Table. III.1 [115].

Table III.1. Switching table

	Increase(⇑)	Decrease (⇓)
Flux (φ_s)	$\bar{v}_i$, $\bar{v}_{i+1}$ and $\bar{v}_{i-1}$	$\bar{v}_{i+2}$, $\bar{v}_{i-2}$ and $\bar{v}_{i+3}$
Torque (T_e)	$\bar{v}_{i+1}$ and $\bar{v}_{i+2}$	$\bar{v}_{i-2}$ and $\bar{v}_{i-2}$

In order to identify the active voltage sequences to be applied to increase or decrease the stator flux amplitude and the electromagnetic torque depending on the sector, the table below has been built:

Table III.2. Table of the flux and torque control

	N=1	N=2	N=3	N=4	N=5	N=6
Flux (φ_s): (⇑)	v_6, v_1, v_2	v_1, v_2, v_3	v_2, v_3, v_4	v_3, v_4, v_5	v_4, v_5, v_6	v_5, v_6, v_7
Flux (φ_s): (⇓)	v_3, v_4, v_5	v_4, v_5, v_6	v_5, v_6, v_1	v_6, v_1, v_2	v_1, v_2, v_3	v_2, v_3, v_4
Torque (T_e): (⇑)	v_6, v_1	v_1, v_2	v_2, v_3	v_3, v_4	v_4, v_5	v_5, v_6
Torque (T_e): (⇓)	v_3, v_4	v_4, v_5	v_5, v_6	v_6, v_1	v_1, v_2	v_2, v_3

In the final DTC step, a single control table can be created by comparing the control tables of the electromagnetic torque and the flux amplitude. However, this single control table can be further broken down into two tables: one with active voltage vectors and the other with zero voltage vectors:

Table III.3. Extended DTC Switching Table

		Adjustment comparator types	Three–level			Three–level		
			Two-level			Two-level		
		Flux Boolean variable : k_φ	1			0		
		Torque Boolean variable: k_T	1	0	-1	1	0	-1
Sector Ni with respect to the angle δ	1	(330°, 30°)	v_2	v_7	v_6	v_3	v_0	v_5
	2	(30°, 90°)	v_3	v_0	v_1	v_4	v_7	v_6
	3	(90°, 150°)	v_4	v_7	v_2	v_5	v_0	v_1
	4	(150°, 210°)	v_5	v_0	v_3	v_6	v_7	v_2
	5	(210°, 270°)	v_6	v_7	v_4	v_1	v_0	v_3
	6	(270°, 330°)	v_1	v_0	v_5	v_2	v_7	v_4
$v_0 = [0,0,0];\ v_1 = [1,0,0], v_2 = [1,1,0], v_3 = [0,1,0], v_4 = [0,1,1], v_5 = [0,0,1], v_6 = [1,0,1], v_7 = [1,1,1]$								

III.6.4 Description of the overall structure (PMSM drive based on DTC)

In order to describe the overall structure of the PMSM drive using DTC, several steps are presented in this section:

- The three phases of the currents and voltages should be captured and transformed into the two phases frame (α-β);
- Through the (α-β) frame, the flux in this frame will be estimated using the voltage and current values as equation (III.21), where the sector block will need them in order to identify the flux position.
- Through the value of the flux in α-β frame, the flux amplitude will be computed; moreover, the torque will be estimated using the relationship among the flux and current in the α-β flux frame. The block of this step is called the estimation block.
- After the estimation step, the error of the torque and the flux will be computed through the difference between the reference and estimation signals of each one.
- Then, the error mentioned above will be adjusted through the flux and torque Boolean variables;
- Finally, depending on the flux and torque Boolean variables and flux position, the inverter signals will be generated through the switching table of the DTC, where the inverter is responsible for converting these signals into actual voltage values that feed the motor.

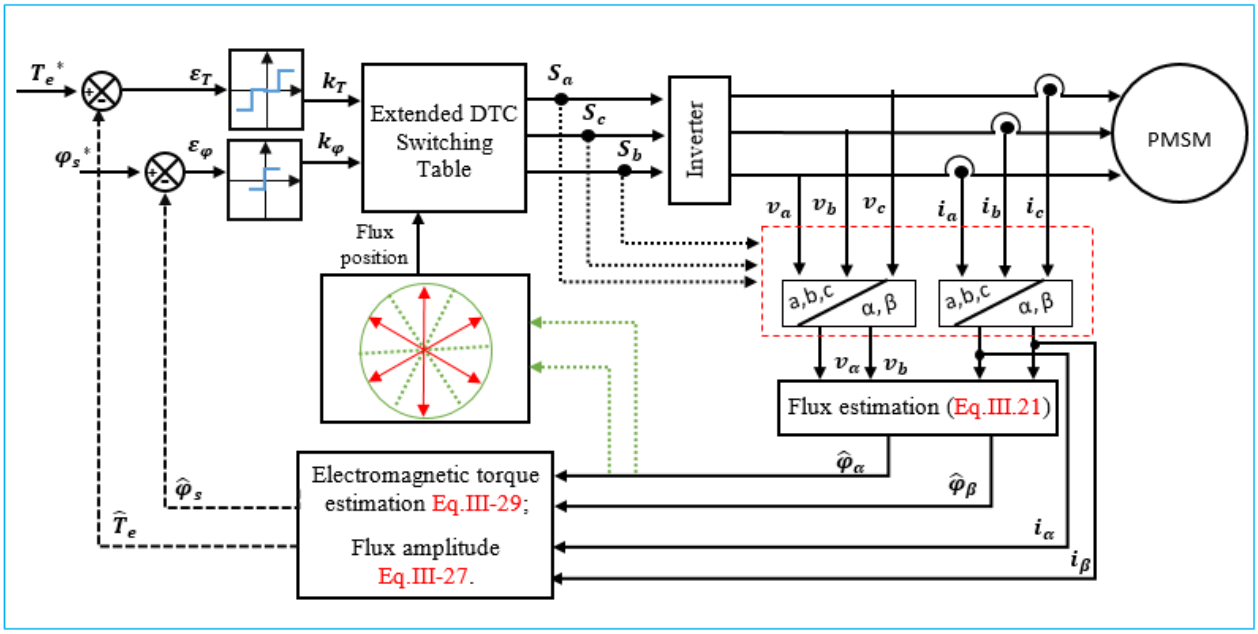

Figure III.17 Scheme of the general structure to the PMSM drive based on the DTC

III.7 Study comparative between the FOC and DTC

Conventional vector control based on the FOC and DTC are widely used control techniques in the PMSM drive. Although the DTC came after the FOC and the first is better than the second, each one has advantages, disadvantages, characteristics, technique, strategy, and goals.

Therefore, this section will combine everything mentioned above into a comparative study between them and will serve as a summary that brings together the two [105].

Table III.4. Study comparative between the control design of FOC and DTC

Comparison criteria	Filed Oriented Control	Direct Torque Control
Frame type used	d-q frame	α-β frame
Variable states	Speed and the currents	Torque, fluxes
Loops used	Speed and currents	Only the voltages
Methods applied	Decoupling	Direct control
Regulators used	PI	Hysteresis
Cost	Expansive to exist to the speed sensors and inverter control (PWM).	Less expensive due to offering sensorless control options as well as not-needed to the PWM.
The error nature	The difference of the reference and actual signals.	The difference of the reference and estimated signals.
Control design	• It involves coordinate transformations and may be perceived as more complex in theory; • It is often more straightforward to implement in practice.	• Conceptually simple and does not require coordinate transformations; • The implementation can be complex due to the use of hysteresis comparators.
Application	It is widely used in various applications, including industrial drives and high-performance electric vehicles, where precision and low torque ripple are essential.	It is often used in applications where simplicity, low speed and dynamic response are crucial, such as in certain types of electric vehicles.

Furthermore, the two controls can be compared through their performance characteristics, as follows:

Table III.5. Study comparative between the performance characteristics of the FOC and DTC

Comparison criteria	Filed Oriented Control	Direct Torque Control
Dynamic Performance	A good dynamic performance	It offers quick torque and flux response due to the direct nature of torque and flux control.
Torque Ripple	Lower torque ripple, contributing to smoother motor operation and reduced mechanical stress	A higher torque ripple, which can lead to acoustic noise and mechanical vibrations.
Steady-State Performance	It offers better steady-state performance	It can exhibit steady-state performance limitations, especially in terms of flux control precision
Robustness	More sensitive under the uncertainties and disturbances.	Less sensitive under the uncertainties and disturbances.

III.8 Simulation results with comparison study between FOC and DTC

After modelling and explaining the PMSM drive system using the FOC and DTC, respectively, this section provides the PMSM performance through the application of the FOC and DTC using MATLAB Simulink. The previous sections of this chapter detail how to arrive at the control law based on each control as well as how to calculate their control gains. Furthermore, several scenarios have been followed in order to determine the relative effectiveness of these controls. The first one, a fixed reference speed was given, which expresses the medium speed of the PMSM, while the load torque has been applied from 2 N.m. into 5 N.m. at 0.3 s. Through this scenario, Figure. III.18 demonstrates that the speed performance is close to the FOC and DTC in terms of stability and rise time (Tr). However, the other characteristics of performance are so

different, where the DTC excels over the FOC in terms of the undershoot during the load torque change at 0.3s as well as the speed chattering, while the steady-state error (SSE) for the FOC is better than the DTC. Regarding the electromagnetic torque performance of the PMSM, it is relatively similar between the two controls, where it suffers from big ripples; in addition, it appears to have overshoots during the change of the load torque. Moreover, the DTC causes an initial undershoot to it; this is proven by Figure. III.19. Because the approaches and steps of the two techniques differ from each other, as the FOC is dependent on the direct and quadratic reference frame (d-q) for calculating the control law, while the DTC is dependent on the α-β reference frame for calculating the control law, Figure. III.20 (a) and Figure. III.21 (a) explain the d-q currents for the FOC and the a-b current for the DTC, respectively. Furthermore, Figure. III.20 (b) and Figure. III.21 (b) present the current performance in the a, b, and c reference frames of the FOC and the DTC, respectively, where they also suffer from big ripples, or what is called the tolerance band. More details, accompanied by numerical estimates, are presented in Table. III.6.

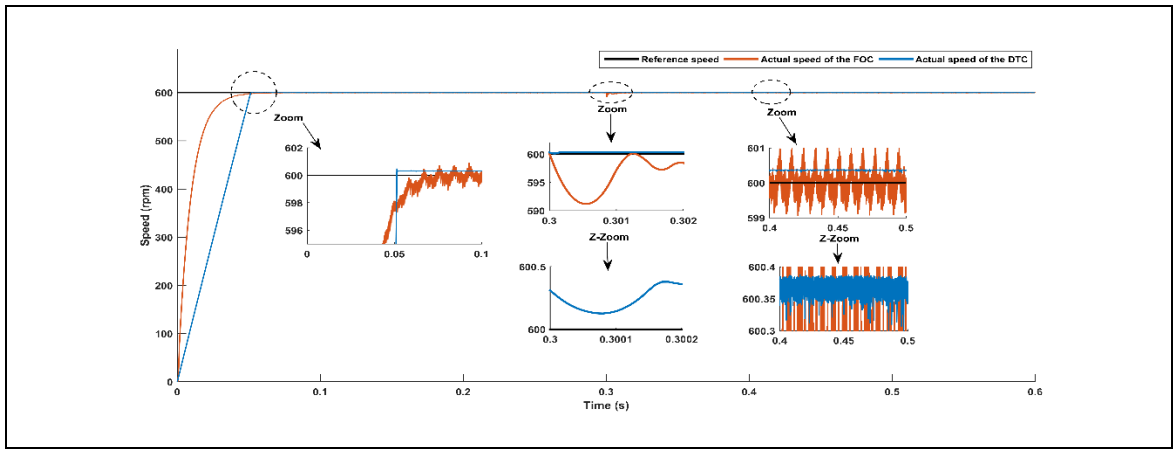

Figure III.18 The speed performance of the PMSM based on the FOC and the DTC under the first scenario

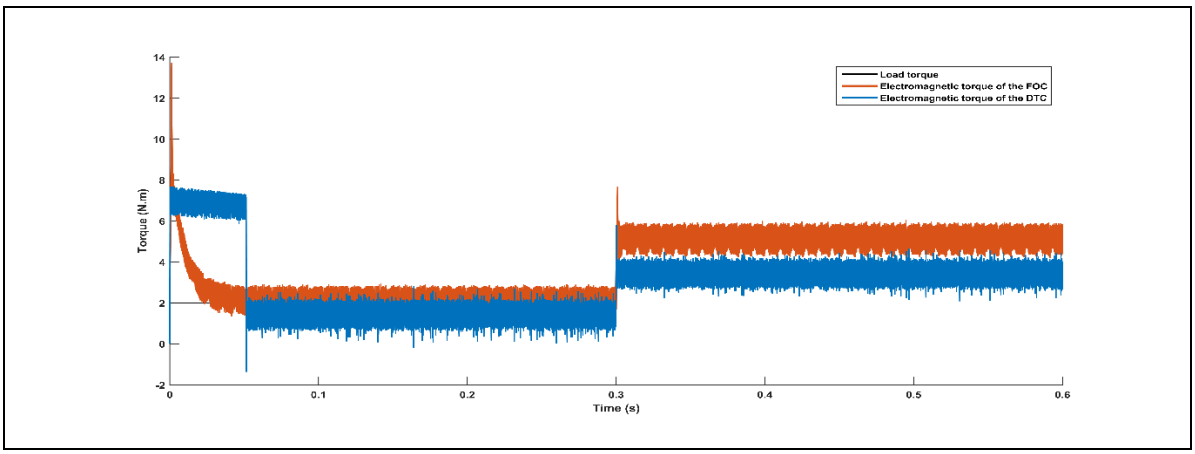

Figure III.19 The torque performance of the PMSM based on the FOC and the DTC under the first scenario

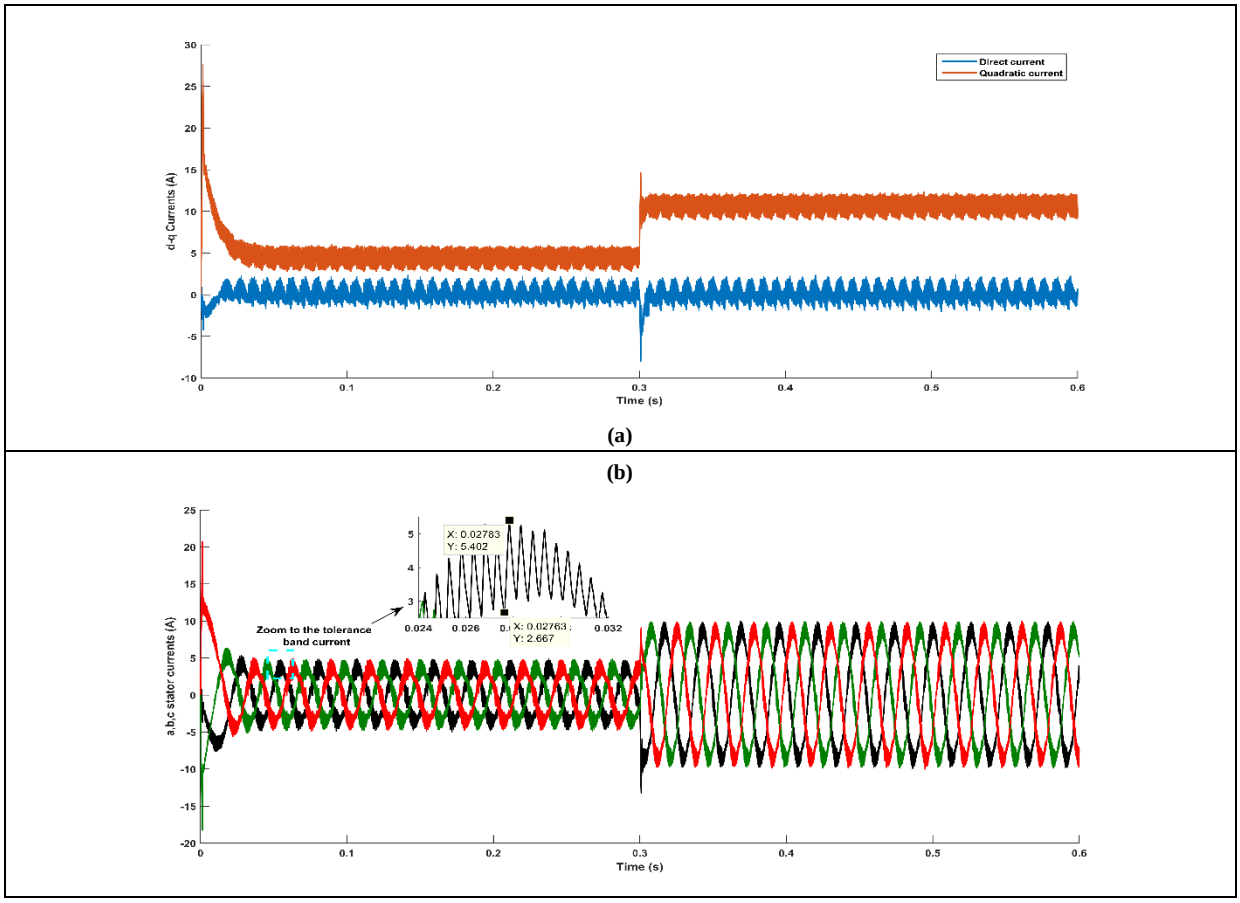

Figure III. 20 The currents performance of the PMSM based on the FOC under the first scenario; **(a)**: d-q currents, **(b)**: a,b,c currents

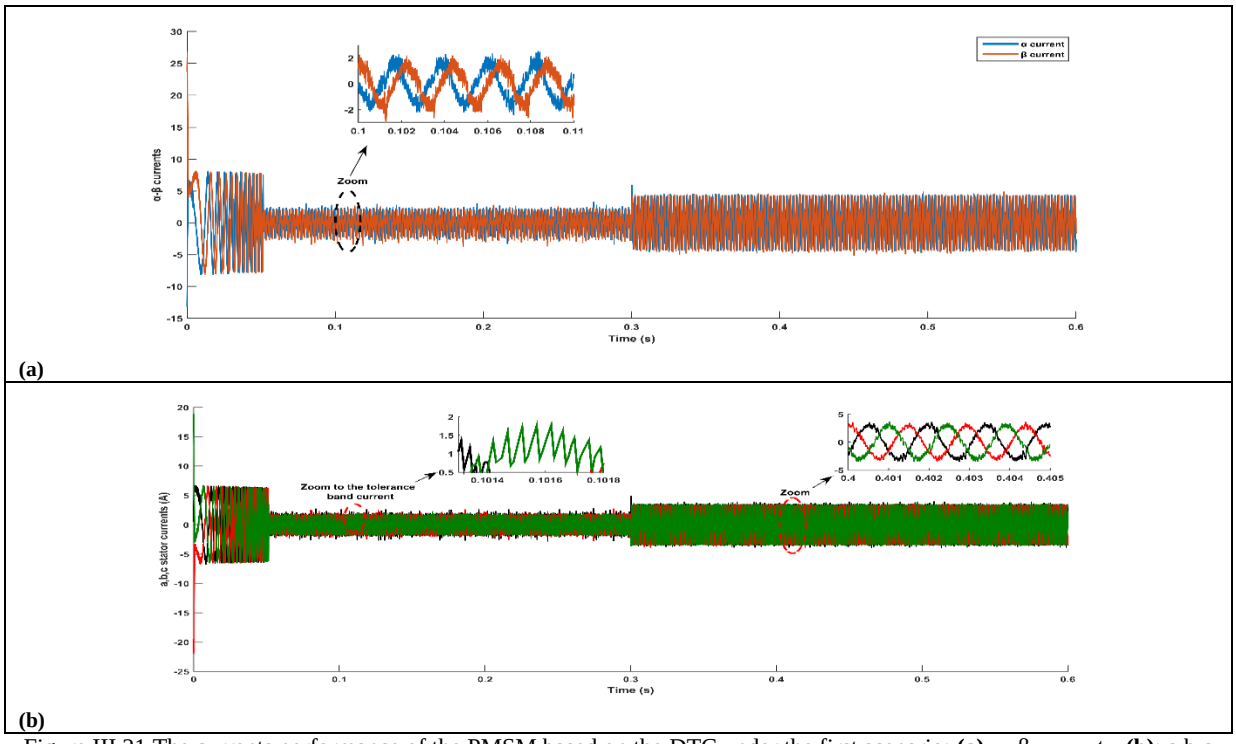

Figure III.21 The currents performance of the PMSM based on the DTC under the first scenario; **(a)**: α-β currents, **(b)**: a,b,c currents

In order to test the effectiveness of both controls, high-speed performance has been applied at 200 rpm, 600 rpm, and 1000 rpm as in Figure. III.22 in this scenario (second scenario). Through Figure. III.22 (b), Figure. III.22 (c), and Figure. III.22 (d), respectively, the effectiveness of the FOC deteriorates through chattering when the speed increases, especially when the speed reaches 1000 rpm, where the FOC is ineffective and loses control, as well as other performance characteristics such as the rise time and the steady-state error that are sensitive during each speed level change. While, the DTC is less sensitive than the FOC through chattering and steady-state errors, but it suffers from the appearance of little initial undershoots in the speed performance as well as its rise time increasing with each speed level. Furthermore, Figure. III.23 shows off the electromagnetic torque performance of the PMSM under this scenario when applying FOC and DTC, respectively, where the FOC effectivity is less than the DTC through the performance characteristics and robustness, too. In addition, the DTC suffers from steady-state errors, while the FOC suffers from increased torque ripple when changing the speed among its levels. This discussion also applies to the current performance of the d-q frame for the FOC (as shown in Figure. III.23(a)) and the a-b frame for the DTC (as shown in Figure. III.23(a)), respectively.

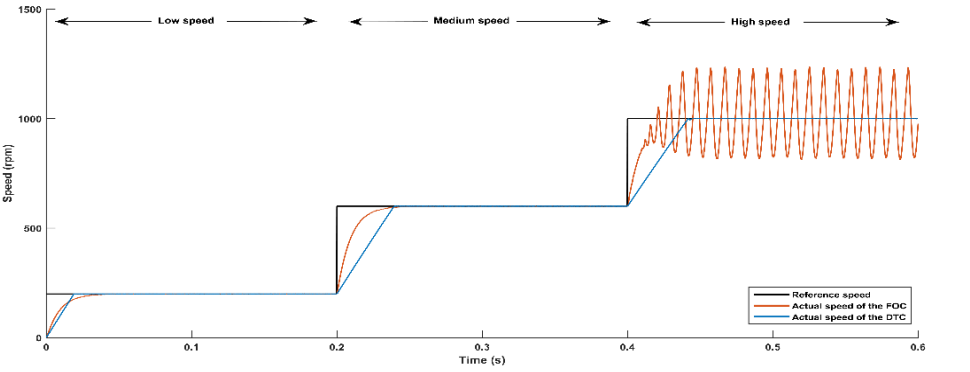

(a)

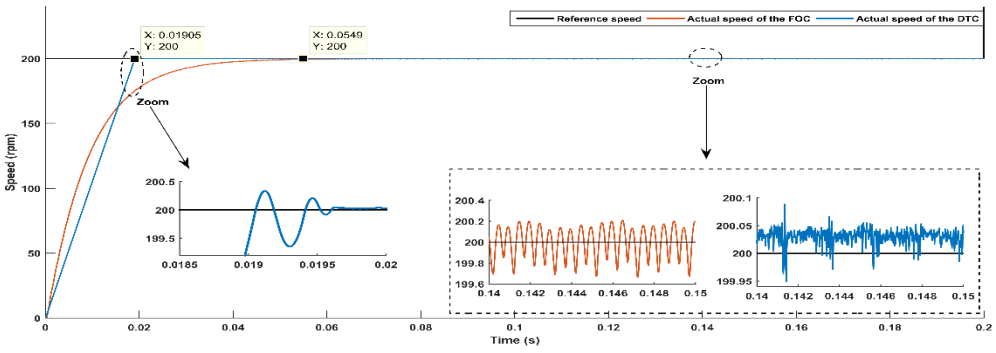

(b)

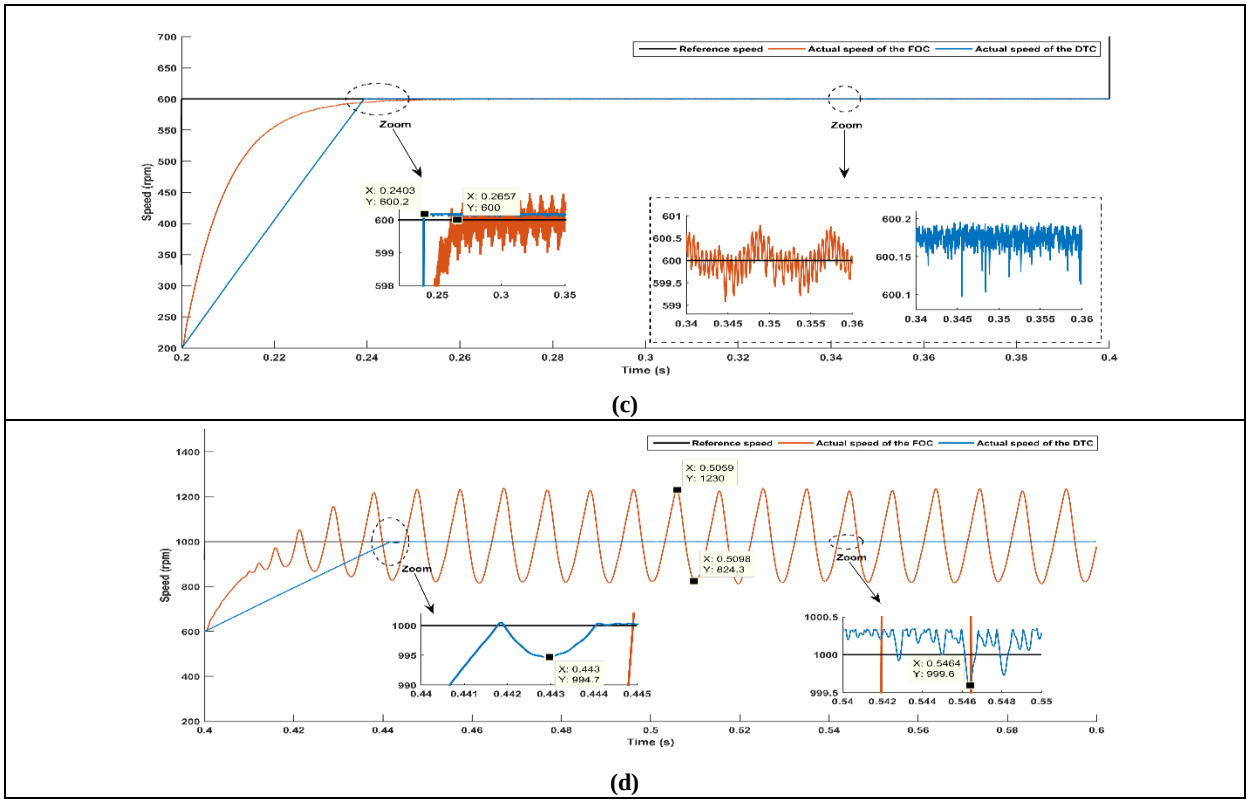

Figure III.22 The speed performance of the PMSM based on the FOC and the DTC under the second scenario

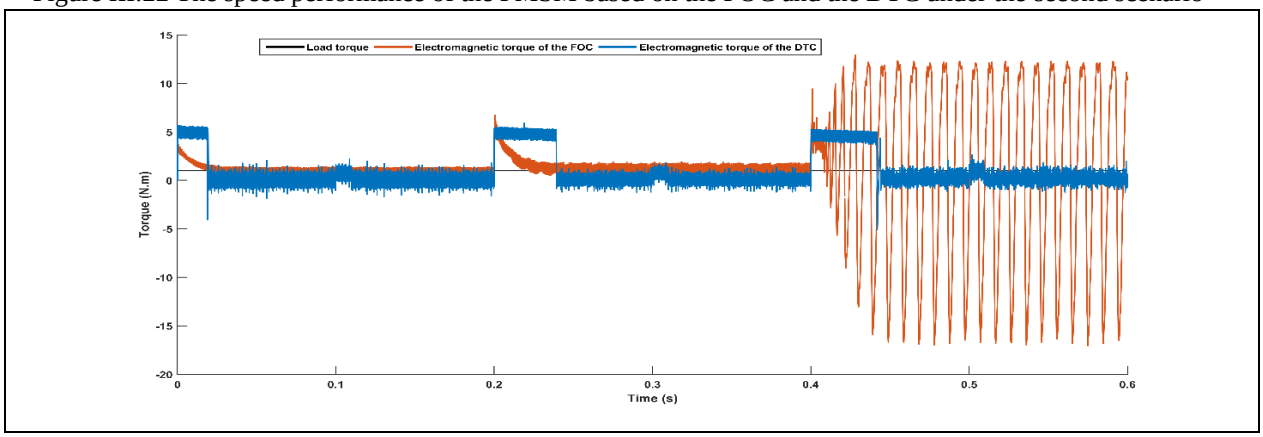

Figure III.23 The torque performance of the PMSM based on the FOC and the DTC under the second scenario

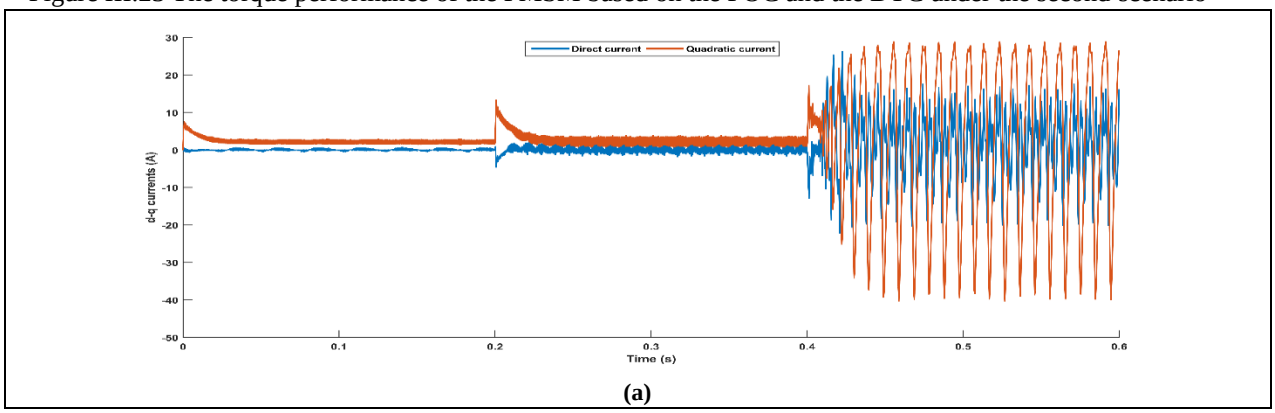

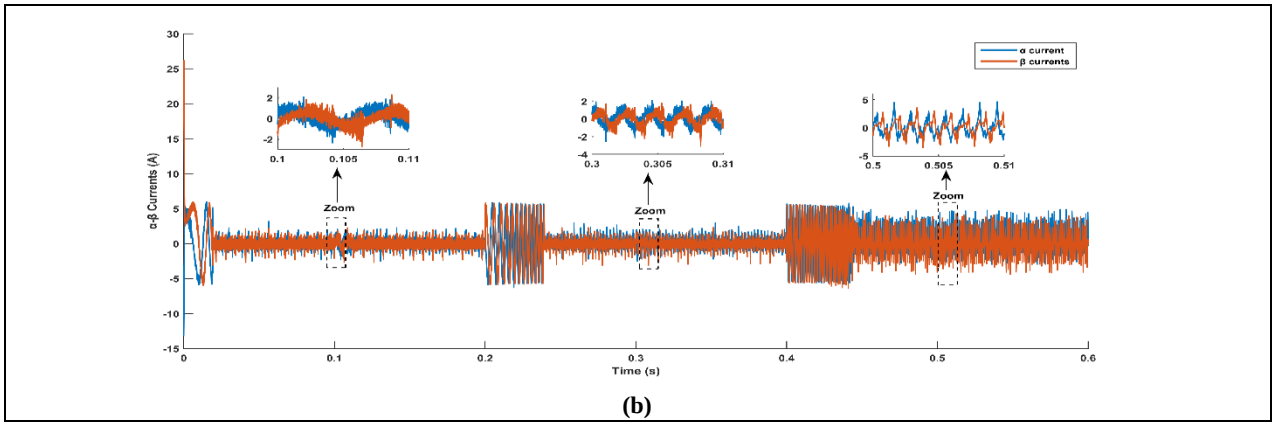

(b)

Figure III.24 The current performance of the PMSM under the second scenario; (a): d-q currents for the FOC, (b) α-β currents for the DTC

In the third scenario, the FOC and DTC have been studied for their robustness under uncertainties and disturbances. Depending on the scenario criteria, Figure. III.25 represents the speed performance under applying a load torque at different time zones estimated at 5 N.m. We observed that the FOC is better than the DTC through steady-state error, while the DTC is better than the FOC through rise time, less peaks (overshoots and undershoots), as well as less chattering. Furthermore, Figure. III.26 represents the speed performance under applying uncertainties, where the PMSM parameters have been changed between -50% and 50%, respectively. The FOC is little affected by the rise time; it is so affected by the other performance characteristics, such as the stead-state error and chattering. While the DTC is so affected by the rise time, it is better than the FOC in terms of the above-mentioned characteristics.

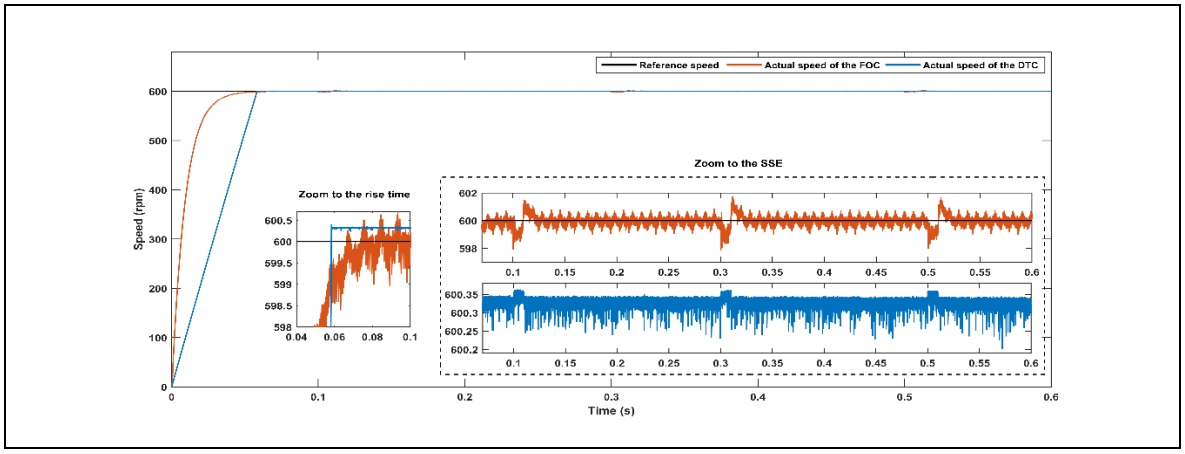

Figure III.25 The speed performance of the PMSM based on the FOC and the DTC under disturbances

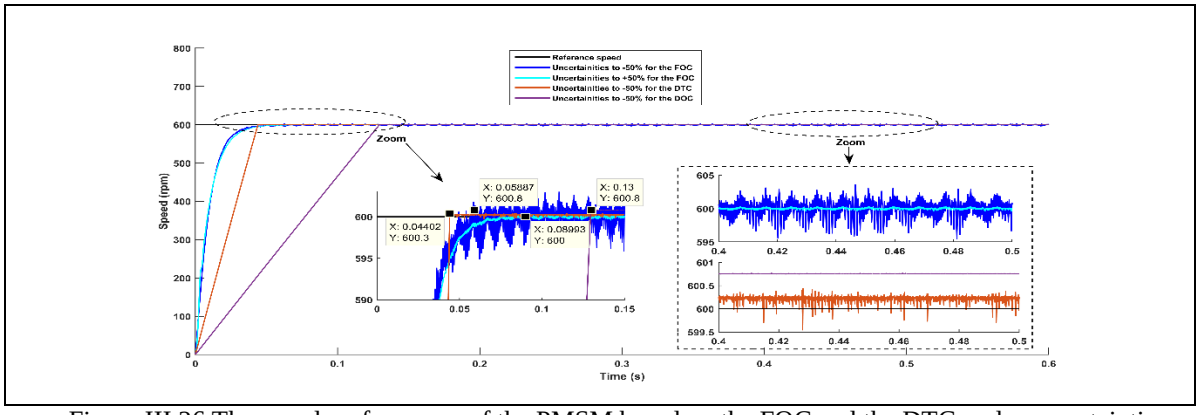

Figure III.26 The speed performance of the PMSM based on the FOC and the DTC under uncertainties

Table.III.6 has been detailed for the PMSM performance characteristics using the FOC and the DTC, respectively:

Table III.6. Numerical estimates of the PMSM performance under the FOC and the DTC

	FOC	DTC
Tr (ms)	65	40
SSE (%)	Almost 0	Almost 0.07
Speed chattering (rpm)	]-1;+1[	]-0.3;+0.38[
Speed undershoots (%)	1.33	0.03
Stability	Relative stability	Relative stability
Torque ripple (N.m)	]-1;+1[	]-1;+1[
Torque overshoots (N.m)	Almost +3	Almost +3
Initial torque undershoots (N.m)	0	Almost -3.5
Current tolerance band	]2.667; 5.402 [	]1; 2 [

III.9 Conclusion

This chapter has presented the design of the PMSM drive and the application of conventional controls to the PMSM, where the control design helped us to understand the PMSM as well as simplify its model. After that, a pole-zero map technique has been used in order to demonstrate the PMSM's stability, and the controllability has been demonstrated using Kalman's theorem, too. Next, the application of the FOC and the DTC on the PMSM model has been studied, where a comparative study was conducted between the two techniques through performance characteristics, robustness, as well as other criteria. Finally, the effectiveness of each control has been validated using MATLAB Simulink. In conclusion, the decision between DTC and FOC is based on the particular needs of the application, taking into account elements like torque ripple, dynamic response, simplicity, and sensor requirements. Every control approach has benefits and drawbacks, and the best one will rely on the motor control application's priorities.

CHAPITRE IV

DESIGN OF ADVANCED CONTROL BASED ON THE NONLINEAR TECHNIQUES APPROACHES FOR THE PMSM

IV.1 Introduction

Although field-oriented control (FOC) and direct torque control (DTC) are widely used for PMSM drives, they have some drawbacks. Whereas FOC requires precise knowledge of PMSM parameters, its performance is sensitive to external disturbances such as load torque changes and to variations in the machine parameters, such as inertia, resistance, and inductance. Changes in these parameters due to temperature variations or ageing can affect the control's accuracy. Therefore, FOC may struggle in applications where the PMSM is subject to significant disturbances or uncertainties. Achieving consistent performance across different operating conditions presents a notable challenge. One drawback of Direct Torque Control (DTC) is its tendency to produce torque ripple, attributed to its direct manipulation of torque and flux. Additionally, it often entails high switching frequencies and harmonics in motor currents, which elevate losses within the inverter and PMSM. This may require additional filtering or mitigation strategies to comply with efficiency and electromagnetic compatibility (EMC) standards. Furthermore, DTC is sensitive to variations in PMSM parameters, and inaccurate parameter values can degrade its performance. DTC algorithms involve complex calculations and decision-making processes. Due to the disadvantages of classical vector control mentioned above, nonlinear techniques are considered an alternative to those previously used because they have many advantages, such as developing the PMSM's performance under uncertainties, external disturbances, or even the high performance of the PMSM. In addition, the nonlinear control is suitable for the PMSM's saturation effects, where magnetic saturation in the iron core of the motor can cause nonlinearities in the relationship between the magnetic field and the current, the back-electromotive force (EMF) generated in the motor is nonlinear with respect to the rotor position, and interactions between different motor components can lead to nonlinear behavior. Furthermore, the superposition and homogeneity assumptions that define linear systems those in which there is a linear relationship between inputs and outputs do not apply to nonlinear systems. Developing control strategies capable of effectively stabilizing and governing these kinds of nonlinear systems is the aim of nonlinear control. When it comes to electrical machines, the nonlinear methodology is regarded as one of the most sophisticated and frequently utilized methods. Additionally, nonlinear control approaches address the problems caused by nonlinear dynamics and offer dependable and adaptable solutions for PMSM management. By applying these advanced control strategies, engineers may enhance the performance, efficiency, and reliability of PMSM-based systems in a range of applications covered in the first chapter. A variety of strategies are included in nonlinear control, such as back-stepping (BSC), sliding mode control (SMC), feedback linearization control (FBLC), and passivity-based control (PBC). Each technique has advantages and disadvantages, purpose, types, methods, goals, principals and stages. In this chapter, we'll study the detailed FBLC, BSC, and SMC as well as apply each one to the PMSM. Furthermore, we'll present a novel hybrid design based on the high-order super twisting algorithm "HO-STA" and terminal sliding mode control "T-SMC" for the PMSM's speed loop.

IV.2 Description on the nonlinear technique

The theory of nonlinear control systems and its applied studies have made significant advancements since the 1970s. A major factor in the field was the effective application of contemporary mathematical techniques like differential algebraic theory and modern differential geometry. Slotine, Khalil, Isidori, and others developed the state feedback approach for the input and output response of a nonlinear system, and they employed Lie algebra to accurately linearize it [116]. The area of control systems engineering known as "nonlinear control" deals with systems that behave nonlinearly. Nonlinear systems do not conform to the superposition and homogeneity assumptions that characterize linear systems, where the connection between inputs and outputs is linear. The goal of nonlinear control is to create control schemes that can successfully stabilize and govern these kinds of nonlinear systems. The nonlinear technique is considered one of the most advanced techniques as well as widely used when applied to electrical machines. Furthermore, the issues presented by nonlinear dynamics, parameter uncertainties, and external disturbances are addressed by the nonlinear control approaches, which provide flexible and reliable solutions for PMSM control [94].

IV.3 Design of the PMSM control based on the FBLC

In control systems engineering, the feedback linearization algorithm is a potent tool. It enables us to apply the methods created for linear systems to the construction of control strategies for nonlinear systems. Compared to the approximation linear method, this approach is entirely different. The distinction is that, as opposed to linearly approximating dynamic characteristics, feedback linearization is accomplished through strict state conversion and feedback [116].

IV.3.1 The principal of the FBLC

In control theory, feedback linearization is a control approach used to create controllers for dynamic systems that are not linear. The primary goal of feedback linearization is to modify the coordinates of a nonlinear system to make it linear. Finding an appropriate coordinate transformation to eliminate the nonlinearities in the system dynamics is usually the first step in the procedure. The system that results from applying the transformation can be shown as a linear system with observable and controlled states. Standard linear control methods can then be applied to this linearized system. In order to attain performance and stability in feedback linearization control, feedback is essential. In order to accomplish the intended control objectives, the control law is made to guarantee that the transformed (linearized) system responds in a desired manner [117, 118]. The nonlinear system is presented by equation (II.34). Figure. IV.1 illustrates this principle well. The linearization approach differs significantly from linearization around an operating point. Indeed, the linear model obtained with the latter is only valid in a neighborhood of the operating point, it is therefore an approximate model. On the other hand, the linear model given by the input-output linearization is valid throughout the state space. The linear compensator which then stabilizes the system is in principle more efficient [119].

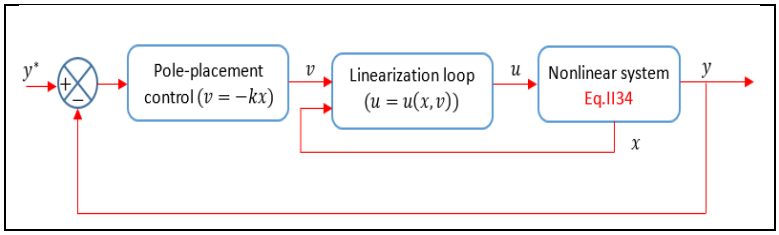

Figure IV.1 : Block diagram of input-output linearization

IV.3.2 General forms of FBL

The Feedback linearization control is categorized into two main types: input-state FBL and input-output FBL. The first on is assumed that all states ($x_1 \ldots x_N$) are available (either by direct measurement or calculation), and the goal is to cancel nonlinearity in "f "so that the state equation is in linear form. While the last one is similar except the goal is to design the controller to cancel nonlinearities in "g "so that the output equation is in linear form and explicitly tied to the input "*u*". Furthermore, the first one is more general and harder to find transformation for all states, while the second one is less general, easier to implement, focuses on linearizing the relation of input/output relation regardless of the other states and it requires to study the leftover dynamics to maintain the system stability [120].

IV.3.3 Necessary definitions In-Out FBLC

Before starting to explain the steps of the FBLC, some necessary definitions that must be known before applying this technique must be mentioned.

- **Relative degree (r):** is the number of times the output needs to differentiate to reach the input. Relative degree bounds: $1 \leq r \leq n$. If the system has relative degree r=n then the input-output FBL is equivalent to input-state FBL;
- **Leftover dynamic:** is considered the difference between the system order "n" and the system relative degree "r". It called 'zero dynamics' if the system output held at zero. It has three states as follows:
  - **a)** Internal dynamics: it is the leftover dynamics which doesn't appear in the input/output relation. It has the degree of n-r;
  - **b)** Zero dynamics: it is the internal dynamics if the output is keep continuously at zero;
  - **c)** Minimum phase system: it is defined as system with stable internal dynamics. for linear system if the system zeros are in open left half side of s plane, then it is minimum phase system If the zero dynamics of the system are (globally) asymptotically stable, the system is called minimum phase.
- **The gradient:** is defined of a scalar function h(x) with respect to the vector, by the line vector $\nabla h(x)_i$ follows:

$$\nabla h(x)_i = \left[\frac{\partial h}{\partial x_1} \quad \frac{\partial h}{\partial x_2} \quad \cdots \quad \frac{\partial h}{\partial x_{n-1}} \quad \frac{\partial h}{\partial x_n}\right] \tag{IV.1}$$

In a similar way, the gradient of a vector field $\emptyset(x)$ is defined by the Jacobean of $\emptyset$ "matrix of $(n\times n)$ elements" as follows:

$$(\nabla\emptyset(x))_{ij} = \begin{bmatrix} \nabla\emptyset_1(x) \\ \nabla\emptyset_2(x) \\ \vdots \\ \nabla\emptyset_n(x) \end{bmatrix} \begin{bmatrix} \frac{\partial\emptyset_1(x)}{\partial x_1} & \frac{\partial\emptyset_1(x)}{\partial x_2} & \cdots & \frac{\partial\emptyset_1(x)}{\partial x_{n-1}} & \frac{\partial\emptyset_1(x)}{\partial x_n} \\ \frac{\partial\emptyset_2(x)}{\partial x_1} & \frac{\partial\emptyset_2(x)}{\partial x_2} & \cdots & \frac{\partial\emptyset_2(x)}{\partial x_{n-1}} & \frac{\partial\emptyset_2(x)}{\partial x_n} \\ \vdots & \vdots & \vdots & \vdots & \vdots \\ \frac{\partial\emptyset_n(x)}{\partial x_1} & \frac{\partial\emptyset_n(x)}{\partial x_2} & \cdots & \frac{\partial\emptyset_n(x)}{\partial x_{n-1}} & \frac{\partial\emptyset_n(x)}{\partial x_n} \end{bmatrix} \quad \text{(IV.2)}$$

- **Diffeomorphism:** a function φ(x) is called a diffeomorphism if it is smooth (c^∞) and its inverse φ(x) $^{-1}$exists and it is smooth;
- **Lemma:** let φ(x) be a c^∞ function define in $\Omega \subset R^n$. If the Jacobean of φ(x) write x is non singular at some point $x_0 \subset \Omega$, then the function φ(x) is define as a diffeomorphism function in at least neighborhood of x_0.
- **Lie derivative:** the Lie derivative of a scalar function $h(x)$: $R^n \to R$ write a vector field f: $R^n \to R^n$ is given by:

$$L_f h = \nabla h.f = \frac{\partial h}{\partial x}.f = \left[\frac{\partial h}{\partial x_1} \quad \frac{\partial h}{\partial x_2} \quad \cdots \quad \frac{\partial h}{\partial x_n}\right].[f_1 \quad f_2 \quad \cdots \quad f_n]^T \quad \text{(IV.3)}$$

Where; $L_f h$: $R^n \to R$

For any order: $h = L_f\left(L_f^{i-1}h\right) = \nabla(L_f^{i-1}h)f$, Furthermore, if g is another vector field then the scalar function $L_g L_f h$ is given by: $L_g L_f h = \nabla(L_f h)g$.

IV.3.4 Steps of In-out FBLC design

In order to apply for the FBLC, you should follow these steps:

- Find relative degree of the system by computing $L_b {L_f}^i h(x)$ recursively until it becomes non-zero at $i = r - 1$;
- Compute $L_b {L_f}^i h(x) \quad \forall \quad 0 \le i \le n$;
- The matrix φ(x) as :

$$\varphi(x) = \begin{bmatrix} Z_1(x) \\ Z_2(x) \\ \vdots \\ Z_r(x) \\ Z_{r+1}(x) \\ \vdots \\ Z_n(x) \end{bmatrix} = \begin{bmatrix} \varphi_1(x) \\ \varphi_2(x) \\ \vdots \\ \varphi_r(x) \\ \varphi_{r+1}(x) \\ \vdots \\ \varphi_n(x) \end{bmatrix} = \begin{bmatrix} y(x) \\ \dot{y}(x) \\ \vdots \\ y^r(x) \\ ? \\ \vdots \\ ? \end{bmatrix} = \begin{bmatrix} h(x) \\ L_f h(x) \\ \vdots \\ {L_f}^r h(x) \\ ? \\ \vdots \\ ? \end{bmatrix} \quad \text{(IV.4)}$$

- Choose the leftover dynamic change of coordinates as:
  - ⇨ Jacobean of φ(x) in invertible;
  - ⇨ If 'normal form' is required, choose to achieve: $\frac{\partial \boldsymbol{\varphi}(\mathbf{x})_i}{\partial x} b = 0 \quad \forall \quad r+1 \le i \le n.$
- find the system dynamics after the change of coordinates (φ(x)):

$$\begin{cases} \dot{z}_1 = Z_2 \\ \dot{z}_2 = Z_3 \\ \quad \vdots \\ \dot{z}_{r-1} = Z_r \\ \dot{z}_r = a(z) + b(z)v \end{cases} \quad \text{(IV.5)}$$

- The control signal is give as: $v = -\frac{a(z)+u}{b(z)}$, where u gives the required performance;
- Check the stability of the zeros dynamics (the leftover dynamics while the output continuously equal to zero).

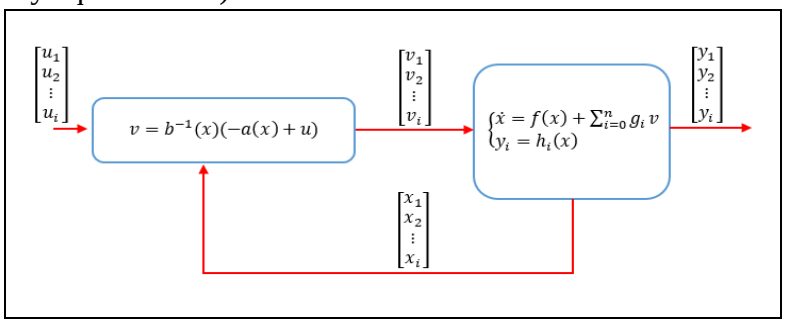

Figure IV.2 : Block diagram of linearization method

IV.3.5 Application the FBLC on the PMSM system

The objective from FBLC application on the PMSM system can be summarized into following points:

- Cancelling the PMSM nonlinearities and building a closed loop linear to the system;
- After applying the FBL design to the PMSM, the system's design will become simpler;
- The chosen linear control after the linearization method will contribute to stabilizing the system, giving the performance desired, and cancelling the igneous term.

Since the nonlinear model of the PMSM is explained in detail in the modelling section of the PMSM in the second chapter (equation (II.34), (II.35), and (II.36), the application of the in-out FBLC on the PMSM allows its model to be decoupled into two independent mono-variable linear subsystems, which amounts to separately controlling the direct current and the speed [121]. In this design approach, our aim is to maintain precise regulation of motor speed while consistently operating at maximum torque. This involves ensuring that the longitudinal component of the stator currents remains zero throughout operation. To achieve this objective, we employ input-output linearization of the model, which ensures full linearization between the outputs and the controls. Here, the outputs need to be the following:

$$\begin{cases} y_1 = i_d \\ y_2 = \Omega \end{cases} \quad \text{(IV.6)}$$

The trajectories that are imposed upon these two outputs must be followed. The strategy of runnling at maximum torque forces us to enforce $i_d{}^* = 0$, and the speed needs to adhere to its reference, which might be any path determined by Ω^*.

- **For the first output i_d :**

$$y_1 = i_d = h_1(x) \qquad , \nabla h_1(x) = [1\ 0\ 0] \tag{IV.7}$$

The derivative of the first output is calculated as follows:

$$\begin{aligned} \dot{y}_1 &= L_f h_1(x) + L_{g1} h_1(x).v_d + L_{g2} h_1(x).v_q \\ &= \frac{\partial h_1}{\partial x} f(x) + \frac{\partial h_1}{\partial x} g_1(x).v_d + \frac{\partial h_1}{\partial x} g_2(x).v_q \\ &= -\frac{R_s}{L_d} i_d + \frac{L_q}{L_d} p.\Omega.i_q + \frac{1}{L_d} v_d \end{aligned} \tag{IV.8}$$

Where, $g_1(x) = \left[\frac{1}{L_d} \quad 0 \quad 0\right]^T$ and $g_2(x) = \left[0 \quad \frac{1}{L_q} \quad 0\right]^T$

From equation (IV.8), we observe that the first input has appeared. This mean that the relative degree of this loop is $r_1 = 1$.

- **For the second output Ω:**

$$y_2 = \Omega = h_2(x) \qquad ; \nabla h_2(x) = [0\ 0\ 1] \tag{IV.9}$$

After the first derive to second output, we will reach as follows:

$$\begin{aligned} \dot{y}_2 &= L_f h_2(x) + L_{g1} h_2(x).v_d + L_{g2} h_2(x).v_q \\ &= \frac{\partial h_2}{\partial x} f(x) + \frac{\partial h_2}{\partial x} g_1(x).v_d + \frac{\partial h_2}{\partial x} g_2(x).v_q \\ &= \frac{3p}{2j}\left(\psi_f.i_q + \left(L_d - L_q\right) i_d i_q\right) - \frac{1}{j} T_l - \frac{F}{j}\Omega \end{aligned} \tag{IV.10}$$

Because the input has not appeared; therefore, the second derivative of the second output is calculated as follows:

$$\begin{aligned} \ddot{y}_2 &= L_f^2 h_2(x) + L_{g1}\left(L_f h_2(x)\right) v_d + L_{g2}\left(L_f h_1(x)\right) v_q \\ &= K_t\left(L_d - L_q\right).i_d.f_1(x) + K_t\left(\psi_f + \left(L_d - L_q\right) i_d\right).f_2(x) \\ &\quad - \left(\frac{1}{J}.T_l + \frac{F}{J}\right) f_3(x) + \frac{K_t}{L_q}\left(L_d - L_q\right) i_d.v_q + \frac{K_t}{L_q}\left(\psi_f + \left(L_d - L_q\right) i_d\right).v_d \end{aligned} \tag{IV.11}$$

Where $K_t = \frac{3.p}{2.j}$. $f_1, f_2(x)$ and $f_3(x)$ are given by equation (II.36).

We observe that the two inputs (v_d and v_q) appear in equation (IV.11); therefore, and the relative degree is $r_2 = 2$. The total relative degree is $r_1 + r_2 = 3$ and it is equal the system order. Therefore, we have performed an exact linearization. No internal dynamics need to be considered.

$$[\dot{y}_1 \ \ddot{y}_2]^T = a(x) + b(x).[v_d \quad v_q]^T \tag{IV.12}$$

Where:

$$\begin{cases} a(x) = \begin{bmatrix} L^1{}_f h_1(x) \\ L^2{}_f h_2(x) \end{bmatrix} = \begin{bmatrix} -\frac{R_s}{L_d} i_d + \frac{L_q}{L_d}.\Omega.i_d \\ K_t(L_d - L_q).i_d.f_1(x) + K_t(\psi_f + (L_d - L_q)i_d).f_2(x) - \left(\frac{1}{j}.T_l + \frac{F}{j}\right) f_3(x) \end{bmatrix} \\ b(x) = \begin{bmatrix} \frac{1}{Ld} & 0 \\ \frac{K_t}{L_q}(L_d - L_q)i_d & \frac{K_t}{L_q}(\psi_f + (L_d - L_q)i_d) \end{bmatrix} \end{cases} \quad \text{(IV.13)}$$

The b(x) matrix is smooth:

$$b^{-1}(x) = \begin{bmatrix} \frac{1}{Ld} & 0 \\ \frac{-(L_d - L_q)\, L_q.i_d}{\psi_f + (L_d - L_q)i_d} & \frac{L_q}{K_t(\psi_f + (L_d - L_q)i_d)} \end{bmatrix} \quad \text{(IV.14)}$$

After that, nonlinear terms will cancel as follows:

$$\begin{bmatrix} v_d \\ v_q \end{bmatrix} = b^{-1}(x)\left(\begin{bmatrix} u_1 \\ u_2 \end{bmatrix} - a(x)\right) \quad \text{(IV.15)}$$

By replacing equation (IV.15) in that given in equation (IV.12), we obtain a completely decoupled linear system of the form:

$$\begin{bmatrix} \dot{y}_1 \\ \ddot{y}_2 \end{bmatrix} = \begin{bmatrix} u_1 \\ u_2 \end{bmatrix} \quad \text{(IV.16)}$$

The new entries u_1 and u_2 must be designed to ensure that:

$$\begin{cases} \lim_{x\to\infty} y_1 = i_d^* \\ \lim_{x\to\infty} y_2 = \dot{\Omega}^* \end{cases} \quad \text{(IV.17)}$$

We start by putting up poles to do this. For a trajectory continuation problem in the general case, we have [121]:

$$\begin{bmatrix} u_1 \\ u_2 \end{bmatrix} = \begin{bmatrix} K_d.\varepsilon_d \\ \ddot{\Omega}^* + k_{\Omega 1}.\dot{\varepsilon}_\Omega + k_{\Omega 2}.\varepsilon_\Omega + k_{\Omega 3}\int_0^\infty \varepsilon_\Omega dt \end{bmatrix} \quad \text{(IV.18)}$$

Where

$$\begin{cases} \varepsilon_{d=} i_d^* - i_d \\ \varepsilon_{\Omega=} \Omega^* - \Omega \end{cases} \quad \text{(IV.19)}$$

Acknowledging the imposed trajectory as a step allows us to approach $\ddot{\Omega}^* = \dot{\Omega}^* = 0$, which in turn simplifies equation (IV.18) as follows:

$$\begin{bmatrix} u_1 \\ u_2 \end{bmatrix} = \begin{bmatrix} K_d.\varepsilon_d \\ -k_{\Omega 1}.\dot{\Omega} + k_{\Omega 2}.\varepsilon_\Omega + k_{\Omega 3}\int_0^\infty \varepsilon_\Omega dt \end{bmatrix} \quad \text{(IV.20)}$$

With $k_d, k_{\Omega 1}, k_{\Omega 2}$ and $k_{\Omega 3}$ are identified to the following values:

$$\begin{cases} k_d = 1000 \\ k_{\Omega 1} = 55000 \\ k_{\Omega 2} = 6000000 \\ k_{\Omega 3} = 80000 \end{cases} \quad \text{(IV.21)}$$

Figure. IV.3 shows the simulation of the PMSM control architecture based on FBLC:

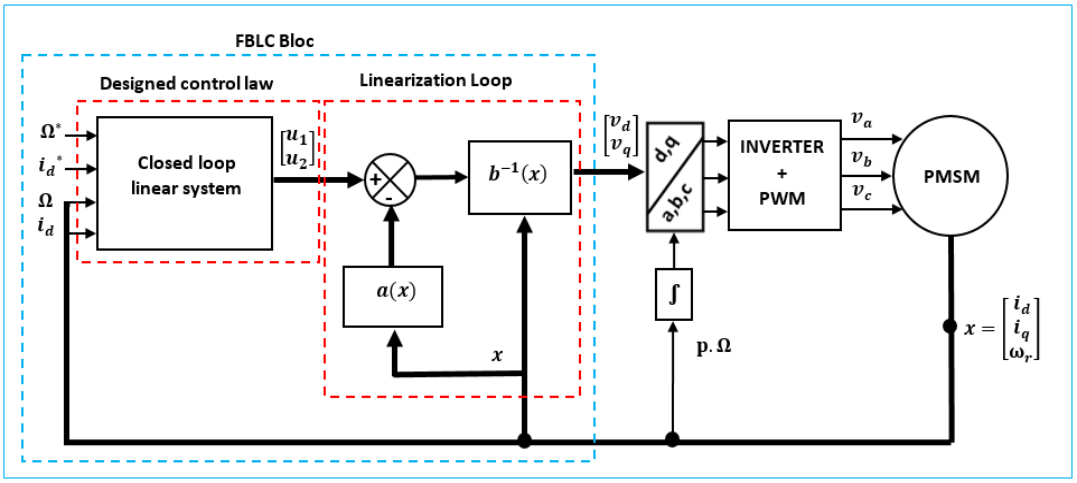

Figure IV.3: Block diagram of PMSM controlled by FBLC

IV.4 Design of the PMSM control based on the BSC

Backstepping or BSC is widely used in control theory and has been applied to various types of nonlinear systems, including mechanical systems, electrical systems, and more. It works especially well with systems that are challenging to regulate using conventional linear control techniques. Backstepping's main concept is to break down the control problem into a number of easier-to-manage sub problems, and then create a controller for each of these smaller issues. Ordinary differential equation (ODE) systems are frequently subjected to the backstepping control approach. The procedure entails iteratively creating a series of controllers, each of which handles a particular aspect of the dynamics of the system. A Lyapunov function is employed at each stage to show that the closed-loop system is stable. As more controllers are added, the Lyapunov function helps guarantee that the system as a whole stays stable.

IV.4.1 Definition of the BSC

Another well-liked nonlinear control method for examining system stabilization using the Lyapunov function candidate is backstepping control. It is a multi-step procedure where each stage creates a virtual control to guarantee that the system converges to its equilibrium state. It is a technique for designing controllers for nonlinear systems by breaking down the control problem into smaller, more tractable parts and designing controllers for each of these parts in a systematic and recursive manner. This approach is particularly useful for addressing complex and nonlinear dynamics in control systems. The concept of backstepping was created by Kanellakopoulos et al. (1991) and was influenced by the research of T. Sinias (1989), Kokotivic & Sussmann (1989), and Feurer & Morse (1978) [122,123].

IV.4.2 Principal of the BSC

Designing a controller for nonlinear systems can be done methodically with the help of BSC. Specifically, the goal is to compute a control law that ensures the derivative of a given (Lyapunov) function is always negative and is positive definite. By breaking up the system into a number of nested subsystems with descending order, the technique is implemented. The foundation of this control method is the development of an algorithm that, for a given subsystem, simultaneously designs the passive (virtual) control law, the adaption dynamics, and the Lyapunov function that ensures stability. Next, based on the system order, we compute a new virtual order and a second Lyapunov function for the second subsystem, and so on. Lastly, we derive the control expression that ensures the system's overall performance and stability. Similar to other control strategies examined, the backstepping technique's application is restricted to specific system types [122,124]. To be able to write the system in "strict feedback" form, we apply a change of variable, the system of equation (II.34) becomes:

$$\begin{cases} \dot{\varphi}_1 = \varphi_2 \\ \dot{\varphi}_2 = \varphi_3 \\ \quad \vdots \\ \dot{\varphi}_{i-1} = \varphi_1 \\ \quad \vdots \\ \dot{\varphi}_{n-1} = \varphi_n \\ \dot{\varphi}_n = f_n(\varphi_1, \varphi_2 \dots \varphi_n) + \mathrm{g}_n(\varphi_1, \varphi_2 \dots \varphi_n).u(\mathrm{t}) \\ y = \varphi_1 \end{cases} \tag{IV.22}$$

Where; φ is new state vector and it is identified as: $\varphi = [\varphi_1 \quad \varphi_2 \quad \dots \quad \varphi_n]^T$.

The aim of this variable modification is to identify, via the variable φ_2, a virtual control law for the system's first equation (IV.22). This control law is controlled by φ_3, and for the last equation, the control law u controls the entire system. The steps involved in this approach are outlined below.

- **1st step:** A specified trajectory must be able to be followed by the system. This is equivalent to creating a tracking controller. The following defines the error between output y and its reference y^*:

$$\varepsilon_1 = y^* - y = y^* - \varphi_1 \tag{IV.23}$$

The derivative of this error is:

$$\dot{\varepsilon}_1 = \dot{y}^* - \dot{\varphi}_1 = \dot{y}^* - \varphi_2 \tag{IV.24}$$

Then the first Lyapunov function will be chosen as follows:

$$V_1 = \frac{1}{2}{\varepsilon_1}^2 \tag{IV.25}$$

The derivative of this function is:

$$\dot{V}_1 = \varepsilon_1.\dot{\varepsilon}_1 = \varepsilon_1(\dot{y}^* - \dot{\varphi}_1) = \varepsilon_1(\dot{y}^* - \varphi_2) \tag{IV.26}$$

For the first variable to converge towards its reference, the derivative of the Lyapunov function must be negative, for this we choose:

$$\dot{y}^* - \varphi_2 = -k_1\varepsilon_1 \tag{IV.27}$$

With $k_1 > 0$

Through the relation of equation (IV.27), we can write as follows:

$$\varphi_2 = \dot{y}^* + k_1\varepsilon_1 \tag{IV.28}$$

The value that the state φ_2 must adopt for the Lyapunov function to remain stable is indicated by the previous equation. Nevertheless, direct action on the state φ_2 is not feasible. Therefore, to represent the desired (reference) value of the state, the notation ${\varphi_2}^*$ will be employed. The intended value that the state provides is indicated by:

$${\varphi_2}^* = \dot{y}^* + k_1\varepsilon_1 \tag{IV.29}$$

- **2nd step:** Since the state $\varphi 2$ cannot be directly altered, it is doubtful that it would follow its trajectory exactly. For this reason, an additional error term is included:

$$\varepsilon_2 = {\varphi_2}^* - \varphi_2 = \dot{y}^* + k_1\varepsilon_1 - \varphi_2 \tag{IV.30}$$

Its derivative is then:

$$\dot{\varepsilon}_2 = \ddot{y}^* + k_1\dot{\varepsilon}_1 - \dot{\varphi}_2 \tag{IV.31}$$

From equation (IV.24) and equation (IV.30):

$$\dot{\varepsilon}_1 = \dot{y}^* - \varphi_2 = \varepsilon_2 - k_1\varepsilon_1 \tag{IV.32}$$

Replacing equation (IV.31) in equation (IV.32):

$$\dot{\varepsilon}_2 = \ddot{y}^* + k_1(\varepsilon_2 - k_1\varepsilon_1) - \dot{\varphi}_2 \tag{IV.33}$$

This time, an additional term that accounts for any errors on the state φ_2 is added to the Lyapunov function. The following is the new candidate function:

$$V_2 = \frac{1}{2}({\varepsilon_1}^2 + {\varepsilon_2}^2) \tag{IV.34}$$

The derivative of this function is:

$$\begin{aligned} \dot{V}_2 &= \varepsilon_1.\dot{\varepsilon}_1 + \varepsilon_2.\dot{\varepsilon}_2 \\ &= \varepsilon_1(\varepsilon_2 - k_1\varepsilon_1) + \varepsilon_2(\ddot{y}^* + k_1(\varepsilon_2 - k_1\varepsilon_1) - \dot{\varphi}_2) \\ &= -k_1{\varepsilon_1}^2 + \varepsilon_2(\varepsilon_1 - \dot{\varphi}_2 + {\dot{\varphi}_2}^*) \end{aligned} \tag{IV.35}$$

In order to satisfy the Lyapunov criterion, the term enclosed in square brackets needs to equal $(-k_1\varepsilon_2)$, as this equation demonstrates:

$$\varepsilon_1\left(1 - {k_1}^2\right) + k_1\varepsilon_2 - \varphi_3 + \ddot{y}^* = -k_2\varepsilon_2 \tag{IV.36}$$

From where we can choose the second virtual order φ_3 as:

$$\varphi_3{}^* = \varepsilon_1\left(1 - k_1{}^2\right) + \varepsilon_2(k_1 + k_2) + \ddot{y}^* \quad \text{(IV.37)}$$

Where k_2 is a non-zero positive parameter in the same way as k_1, This would cause the Lyapunov function to take the following form:

$$\dot{V}_2 = -k_1\varepsilon_1{}^2 - k_2\varepsilon_2{}^2 \quad \text{(IV.38)}$$

In this sense, the function V_2 would fully satisfy the Lyapunov conditions. The error function then always converges towards zero since the selected control law guarantees that the function $\boldsymbol{V_2}$is always positive and its derivative $\dot{V}_2$ is always negative.

- **ith step:** for the step "i", it the same of the first step:

$$\varepsilon_i = \varphi_i{}^* - \varphi_i \quad \text{(IV.39)}$$

The lyapunov function is defined by:

$$V_i = \frac{1}{2}\sum_{j=1}^{i}\varepsilon_j^2 \quad \text{(IV.40)}$$

After that, we have:

$$\dot{\varepsilon}_{i-1} = \varepsilon_1 - k_{i-1}\varepsilon_{i-1} - \varepsilon_{i-2} \quad \text{(IV.41)}$$

$$\dot{V}_i = -\sum_{j=1}^{i-1} k_j\varepsilon_j^2 + \varepsilon_i(\varepsilon_{i-1} - \dot{\varphi}_i + \dot{\varphi}_i^*) \quad \text{(IV.42)}$$

The virtual control is therefore:

$$\varphi_{i+1}^* = k_i\varepsilon_i + k_{i-1}\varepsilon_{i-1} + \dot{\varphi}_i{}^* \quad \text{(IV.43)}$$

Where; $k_i, k_{i-1} > 0$

- **nth step :** the error in this step is defined by:

$$\varepsilon_n = \varphi_n^* - \varphi_n \quad \text{(IV.44)}$$

The lyapunov function of this step is defined by:

$$V_n = \frac{1}{2}\sum_{j=1}^{n}\varepsilon_j^2 \quad \text{(IV.45)}$$

Then, we have:

$$\dot{\varepsilon}_{n-1} = \varepsilon_n - k_{n-1}\varepsilon_{n-1} - \varepsilon_{n-2} \quad \text{(IV.46)}$$

$$\dot{V}_n = -\sum_{j=1}^{n-1} k_j\varepsilon_j^2 + \varepsilon_n(\varepsilon_{n-1} - \dot{\varphi}_n + \dot{\varphi}_n^*) \quad \text{(IV.47)}$$

The virtual control in this case represents the actual control u:

$$u = f_n(\varepsilon_{n-1}, \varepsilon_n, \dot{\varphi}_n^*) \quad \text{(IV.48)}$$

Finally, the control law based on the backstepping technique is designed as follows:

$$u = k_n\varepsilon_n + k_{n-1}\varepsilon_{n-1} + \dot{\varphi}_n^* \quad \text{(IV.49)}$$

Where, $k_n, k_{n-1}0$

Moreover, Figure. IV.4 is illustrated the backstepping control principle diagram:

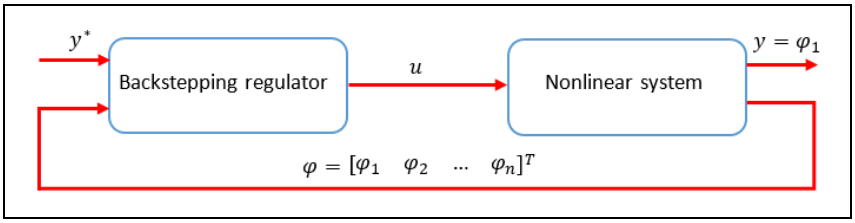

Figure IV.4 : Backstepping control principle diagram

IV.4.3 Design of the BSC on the PMSM model

Firstly, the model of PMSM is based on the nonlinear model given in equation (II.34), equation (II.35) and equation (II.36) respectively, where the variable states are direct and quadratic current and the speed. In order to apply the BSC, we should identified the dynamic errors as follows [121]:

$$\begin{cases} \varepsilon_\Omega = \Omega^* - \Omega \\ \varepsilon_\mathrm{d} = i^* - \mathrm{i}_d \\ \varepsilon_\mathrm{q} = \mathrm{i}_q{}^* - \mathrm{i}_q \end{cases} \tag{IV.50}$$

Two primary steps must be tracked in order to apply backstepping control to PMSM. These are as follows:

1st step : Initially, we will examine electromechanical decoupling and employ the candidate Lyapunov function (CLF) to guarantee the same reference by guaranteeing the direct current direction $\mathrm{I}_d{}^* = 0$). The definition of the CLF and its derivation is [121]:

$$\begin{cases} V_1 = \frac{1}{2}\varepsilon_\Omega^2 & (V_1 > 0) \\ \dot{V}_1 = \dot{\varepsilon}_\Omega \varepsilon_\Omega & (\dot{V}_1 < 0) \end{cases} \tag{IV.51}$$

By adopting this configuration, errors will be eradicated, and the system will attain stability. Consequently:

$$\begin{cases} \dot{\varepsilon}_\Omega = -k_\Omega \varepsilon_\Omega \\ \dot{V}_1 = -k_\Omega {\varepsilon_\Omega}^2 \end{cases} \tag{IV.52}$$

The tracking error of the angular speed in the closed-loop is displayed in following equation:

$$\dot{\varepsilon}_\Omega = \Omega^* - (3.\frac{p}{2.j})\psi_f . i_q{}^* + \frac{F}{j}.\Omega + \frac{1}{j}.T_l \tag{IV.53}$$

The quadratic current reference is provided as follows because the reference speed is a step function:

$$i_q{}^* = \frac{2}{3p\psi_f}(j.k_\Omega.\varepsilon_\Omega + F.\Omega + T_l) \tag{IV.54}$$

2nd step: The virtual control is created in the second stage by applying direct and quadratic current, and the real control voltage is then determined as follows:

$$\begin{cases} V_2 = \frac{1}{2}\varepsilon_{\Omega}^2 + \frac{1}{2}\varepsilon_{\mathrm{d}}^2 + \frac{1}{2}\varepsilon_{\mathrm{q}}^2 & (V_2 > 0) \\ \dot{V}_2 = \dot{\varepsilon}_{\Omega}\varepsilon_{\Omega} + \dot{\varepsilon}_{\mathrm{d}}\varepsilon_{\mathrm{d}} + \dot{\varepsilon}_{\mathrm{q}}\varepsilon_{\mathrm{q}} & (\dot{V}_2 < 0) \end{cases} \quad \text{(IV.55)}$$

For the stable system, we can write as:

$$\begin{cases} \dot{\varepsilon}_{\mathrm{d}} = {i_d}^* - i_d = \frac{R_s}{L_d}.i_d - \frac{L_q}{L_d}.p.\Omega.i_q - \frac{1}{L_d}.v_d = -k_{\mathrm{d}}.\varepsilon_{\mathrm{d}} \\ \dot{\varepsilon}_q = {i_q}^* - i_q = {i_q}^* + \frac{R_s}{L_q}.i_q + \frac{L_d}{L_q}.p.\Omega.i_d + \frac{\psi_f}{L_q}.p.\Omega - \frac{1}{L_q}.v_q = -k_{\mathrm{q}}.\varepsilon_{\mathrm{q}} \end{cases} \quad \text{(IV.56)}$$

Where ${i_q}^*$ is the derivate of the reference quadratic current that is represented in equation (IV.54)

Finally, the control law was obtained as follows:

$$\begin{cases} v_d = L_d.k_{\mathrm{d}}.\varepsilon_{\mathrm{d}} + R_s i_d - L_q.p.\Omega.i_q \\ v_q = L_q.k_{\mathrm{q}}.\varepsilon_{\mathrm{q}} + R_s I_q + L_d.p.\Omega.i_d + \psi_f.p.\Omega + L_q.{i_q}^* \end{cases} \quad \text{(IV.57)}$$

Where k_{d} , k_{q} *and* k_{Ω} are positive.

Figure. IV.5 shows the simulation of the PMSM control architecture based on BSC:

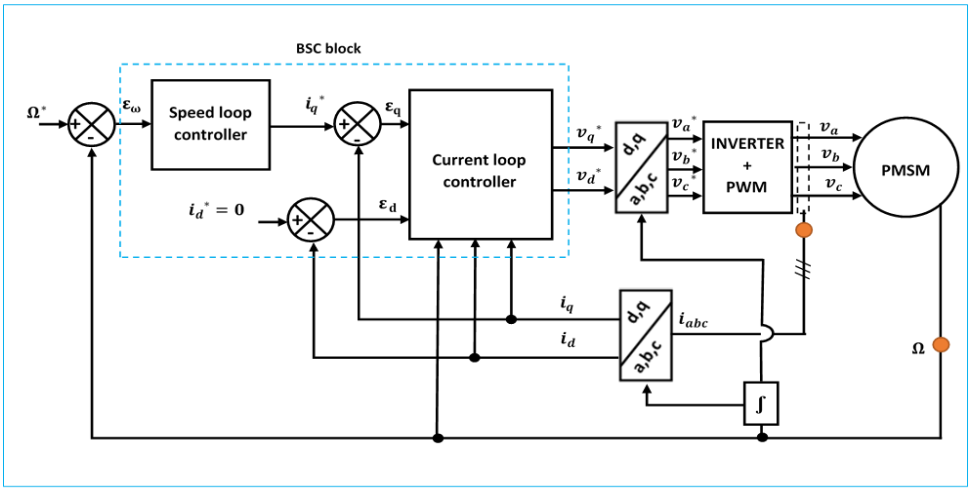

Figure IV.5 : Block diagram of BSC for the PMSM system

IV.4.4 Design of the IBSC on the PMSM model

Variations in PMSM parameters have an impact on how well the backstepping technique works. For this reason, improving this method through an integrated action is required to address this kind of issue. In essence, this means adding integrators to the PMSM model and continuing to use the traditional backstepping technique to this new model. The stabilization of the Lyapunov candidate will cause the integral action to be automatically transferred from the model to the control law [125, 126]. In order to apply the integral backstepping (IBSC), this section will present the essential steps to apply the integral backstepping technique, the dynamic errors of the speed and current loop for the IBSC design are designed as follows:

$$\begin{cases} e_\Omega = \varepsilon_\Omega + k_1 \int_0^t (\varepsilon_\Omega) dt \\ e_\mathrm{d} = \varepsilon_\mathrm{d} + k_2 \int_0^t (\varepsilon_\mathrm{d}) dt \\ e_\mathrm{q} = \varepsilon_\mathrm{q} + k_3 \int_0^t (\varepsilon_\mathrm{q}) dt \end{cases} \quad \text{(IV.58)}$$

Where $\varepsilon_\Omega, \varepsilon_\mathrm{d}\ and\ \varepsilon_\mathrm{q}$ are the dynamic errors to the BSC design (equation (IV.50))

- **1st step:** for the speed loop, we'll apply the same steps that the BSC based on the PMSM, the speed and equivalent currents in the d-q axis are taken as manipulating variables to make control action live. IBSC used to study the speed error in a static regime is based on the Lyapunov candidate as follows:

$$\begin{cases} V_\Omega = \frac{1}{2} e_\Omega^2 \\ \dot{V}_\Omega = \dot{e}_\Omega e_\Omega \end{cases} \quad \text{(IV.59)}$$

To ensure the system stability, the following conditions must be respected.

$$\begin{cases} V_\Omega > 0 \\ \dot{V}_\Omega < 0 \end{cases} \quad \text{(IV.60)}$$

Therefore, we have:

$$\begin{cases} \dot{e}_\Omega = -k_\Omega . e_\Omega \\ \dot{V}_\Omega = -k_\Omega . e_\Omega^2 < 0 \end{cases} \quad \text{(IV.61)}$$

Where $k_\omega\ and\ k_1$ are constant and positive.
From equation (IV.58) and equation (IV.60), we have:

$$\dot{e}_\Omega = -k_\Omega . e_\Omega = \dot{\Omega}^* - \dot{\Omega} + k_1 . (\Omega^* - \Omega) \quad \text{(IV.62)}$$

If the speed reference is in the form of a step function, the expression of the dynamic error derivative of the speed will be:

$$\dot{e}_\Omega = -\frac{3.p}{2.j}\left(L_d - L_q\right). i_d . i_q - \frac{3.p}{2.j} . \psi_f . i_q + \frac{1}{j} . T_l + \frac{F}{j}\Omega + k_1 \varepsilon_\Omega = -k_\Omega . e_\Omega \quad \text{(IV.63)}$$

This type of used control depends on the virtual variables which are the state variables: direct current and quadratic current. These virtual variables make it possible to give an estimated value of zero to the direct component of the current and to give the reference expressed by equation (IV.7) to the quadratic current. Hence, the direct and quadratic current references become as follows:

$$\begin{cases} {i_d}^* = 0 \\ {i_q}^* = \left(\frac{2.j}{3.p.\psi_f}\right) . (k_\Omega . e_\Omega + k_1 \varepsilon_\Omega + \frac{F}{J} . \Omega + \frac{1}{j} . T_l) \end{cases} \quad \text{(IV.64)}$$

- **2ndstep:** In the d-q axis, we study the stabilization of the dynamic errors of direct and quadratic currents to use the Lyapunov candidate.

$$\begin{cases} V_{dq} = \frac{1}{2} e_\Omega^2 + \frac{1}{2} e_\mathrm{d}^2 + \frac{1}{2} e_\mathrm{q}^2 & (V_{dq} > 0) \\ \dot{V}_{dq} = \dot{e}_\Omega e_\Omega + \dot{e}_\mathrm{d} e_\mathrm{d} + \dot{e}_\mathrm{q} e_\mathrm{q} & (\dot{V}_{dq} < 0) \end{cases} \quad \text{(IV.65)}$$

The Lyapunov candidate expression will become as follows:

$$\dot{V}_{dq} = -k_\Omega . e_\Omega^2 - k_d . e_d^2 - k_q . e_q^2$$
$$+e_\Omega \left(\frac{3.p}{2.j} \left(L_d - L_q \right) . \varepsilon_d . i_q + \frac{3.p}{2.j} . \psi_f . \varepsilon_q - \frac{1}{J} T_l - \frac{k_\Omega}{j} . e_\Omega \right)$$
$$+e_d \left(\frac{1}{L_d} \left(R_s . i_d - p . L_q . \Omega . i_q - v_d \right) + k_2 . \varepsilon_d + k_d . e_d \right)$$
$$+e_q \left(\frac{di_q^*}{dt} + \frac{1}{L_q} \left(R_s . i_q + p . L_d . \Omega . i_d + p . \psi_f . \Omega - v_q \right) + k_3 . \varepsilon_q + k_q . e_q \right) \quad \text{(IV.66)}$$

According to the stabilization law of this system, the differentiation of the new Lyapunov function must be negative. Thus, the laws of control of the v_d and v_q voltages will be given by following equation:

$$\begin{cases} v_d = R_s . i_d - p . L_q . \Omega . i_q + \frac{3.p.L_d}{2.j} \left(L_d - L_q \right) . \varepsilon_\Omega . i_q + L_d . k_2 . \varepsilon_d + L_d . k_d . e_d \\ v_q = \frac{di_q^*}{dt} + R_s . i_q + p . L_d . \Omega . i_d + p . \psi_f . \Omega + \frac{3.p.L_q}{2.j} . \psi_f . \varepsilon_\Omega + L_q . k_3 . \varepsilon_q + L_q . k_q . e_q \end{cases} \quad \text{(IV.67)}$$

Figure. IV.6 shows the simulation of the PMSM control architecture based on IBSC:

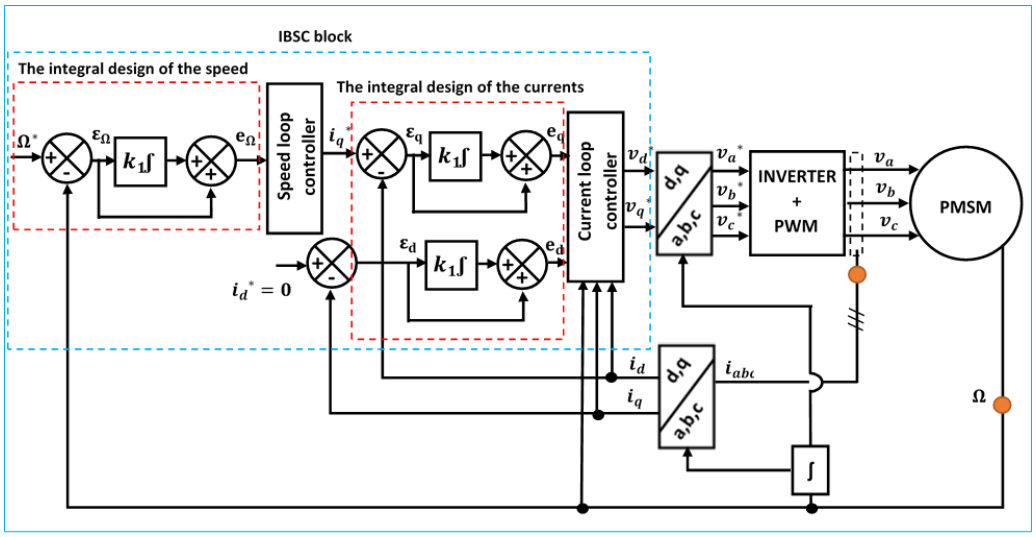

Figure IV.6 : Block diagram of IBSC for the PMSM system

IV.5 Design of the PMSM control based on SMC

The notion of sliding mode (SM) control was first presented in published works in the 1930s, and the first applications of SM control realization included ship-course control and DC generator control. Actually, Russian engineers were the ones who started the theory and application development of SM control, and in the 1950s, Russian literature reported on the theoretical framework that eventually made SM control applications widely available. Subsequently, the work was published in English-language manuscripts outside of Russia by Itkis (1976) and Utkin (1977). Since then, control theorists and working engineers all around the world have become quite interested in the SM control theory [127-129].

IV.5.1 Definition of the SMC

The SM control is a type of nonlinear control that was created mainly to govern systems with changeable structures. The goal is to force the dynamics of the system under control to follow precisely what is desired and predetermined. Technically, it consists of a time-varying state-feedback discontinuous control law that switches at a high frequency from one continuous structure to another according to the present position of the state variables in the state space. The primary benefit of a system possessing SM control characteristics is its assured stability and resilience against uncertainties and disturbances. Furthermore, compared to other nonlinear control systems, the SM control method is comparatively simple to apply since it offers a great degree of freedom in its design options. Because of these characteristics, SM control is widely used in industrial applications such as electrical drivers, renewable energy, automobile control, furnace control, etc. It is also highly suited for applications in nonlinear systems [127-131].

IV.5.2 Principal of the SMC

Providing a switching surface in accordance with the laws of existence, convergence, and stability is the primary function of sliding mode control. The state trajectory can reach the switching surface by making the necessary structural adjustments to the controlled system. A system whose structure varies while it is in operation is said to have a changeable structure. Such systems that are controlled by sliding mode typically operate in two ways: first by convergent towards the surface, and second by sliding along it. The phase trajectory, therefore, moves asymptotically towards the equilibrium point with a dynamic described by the sliding mode after reaching the switching surface in a finite amount of time (the non-sliding mode) from any initial state [130,132,133]. Reaching Mode (RM), Sliding Mode (SM), and steady-state mode (SS) are the three phases or modes that such a system often goes through in structure-variable control [134]. These modes are depicted in the phase plane in Figure. IV.7. The synthesis of sliding mode control systematically considers the issues of superior performance and stability in its methodology. Generally speaking, three actions need to be taken in order to implement this kind of control. [135,136]:

- Choice of the sliding surface;
- Determination of sliding conditions;
- Calculation of SMC law.

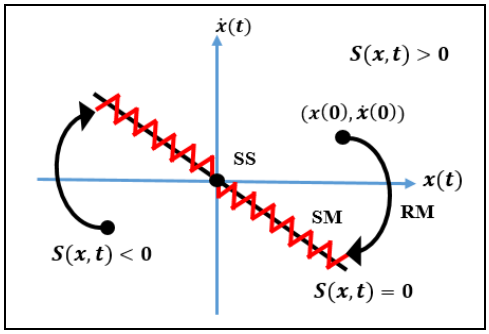

Figure IV.7 : System trajectory on the phase plane

A. Choice of the sliding surface

Depending on the application and the desired outcome, the surface chosen for sliding mode control takes into account not only the required number of these surfaces but also their shapes. These surfaces can be linear or non-linear expressions with constant or variable parameters, and their components can be represented by algebraic relationships between the system's state variables. A sliding mode controller's primary goal is to maintain the controlled system's states on a predetermined surface S(x), by directing them there. The intended nonlinear system is modelled in equation (II.34). Based on the J.J.Slotine proposition, the general formula for sliding surfaces is designed as follows [137-140]:

$$S(x,t) = \left(\frac{d}{dt} + \lambda\right)^{n-1} e(t) \tag{IV.68}$$

Where λ is a positive number chosen by the designer (scaling factor), $S(x,t)$ is the sliding surface, $e(t)$ is the tracking error between the reference and actual state variable and n is the system's order. The tracking error expression is obtained as follows:

$$e(\mathrm{x},t) = x^* - x \tag{IV.69}$$

Where, x^*, x are the reference and the actual of the state vectors, and they are identified as follows:

$$\begin{cases} x^* = [x^* \quad \dot{x}^* \quad \ddot{x}^* \quad ...]^T \\ x = [x \quad \dot{x} \quad ... \quad x^{n-1}]^T \end{cases} \tag{IV.70}$$

B. Determination of sliding conditions

The requirements that enable the various dynamics of the system to converge towards the sliding surface and stay there regardless of the disturbance are known as the conditions of existence and convergence. Two categories of conditions are presented here, namely[141]:

- **Direct approach:** The earliest method is this one, which is put forth and researched by Emilyanov [142] and Utkin [143]. In this condition, it is necessary to incorporate the values immediately preceding and following the commutation point for both S(x) and its derivative." It is provided as follows:

$$\dot{S}(x).S(x) < 0 \tag{IV.71}$$

- **Lyapunov approach:** In the Lyapunov approach, one selects a Lyapunov candidate function $V(x) > 0$ (a positive scalar function) for the system's state variables. The objective is to design a control law that ensures the function's derivative, $\dot{V}(x) < 0$ [144,145]. The candidate Lyapunov function is designed as follows:

$$V(x) = \frac{1}{2}S^2(x) \tag{IV.72}$$

By deriving the latter, we obtain:

$$\dot{V}(x) = \dot{S}(x).S(x) \tag{IV.73}$$

It is sufficient to guarantee that the derivative of the function V(x) is negative in order for it to decline. Thus, the requirement for convergence as stated by:

$$\dot{S}.S < 0 \tag{IV.74}$$

This condition is used to evaluate the robustness, stability, and control performance of nonlinear systems [100].

C. Calculation of control law

Firstly, the control law based on SMC consists of two components: the equivalent" $u_{eq}(t)$ "and the switching" $u_s(t)$". It is designed as follows:

$$u(t) = u_{eq}(t) + u_s(t) \tag{IV.75}$$

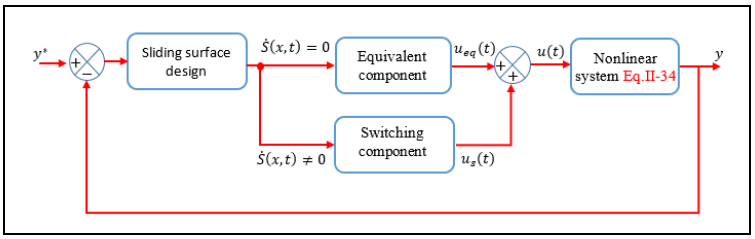

Figure IV.8 : Block diagram of SMC based nonlinear plant

In order to calculate the control law, the operation of SMC is often organized into two primary phases: a sliding phase and an approaching phase [129, 146]. To ensure that the system state stays on the sliding surface until the desired control performance is achieved, the first phase involves choosing an appropriate sliding manifold. Depending on the two conditions indicated in equation (IV.76), the equivalent component $u_{eq}(t)$ can be calculated to hold the system stationary on the sliding surface during this phase [57,142].

$$\begin{cases} s(x,t) = 0 \\ \dot{s}(x,t) = 0 \end{cases} \tag{IV.76}$$

The system is forced to reach the sliding surface in a finite period of time in the second phase, which makes the system state an invariant manifold. This allows for the creation of an appropriate control law, which is known as the switching or reaching component $u_s(t)$. Therefore, the suitable sliding conditions for this phase are as follows [94,142]:

$$\begin{cases} s(x,t) = 0 \\ \dot{s}(x,t) \neq 0 \end{cases} \tag{IV.77}$$

For the classical SMC design the switching component is given by the basic form which is that of a relay represented by the function "sign" abbreviated "sign" [141].

$$u_s(t) = K.sign(S(x)) \tag{IV.78}$$

The following figure represents the function of the discrete relay type control:

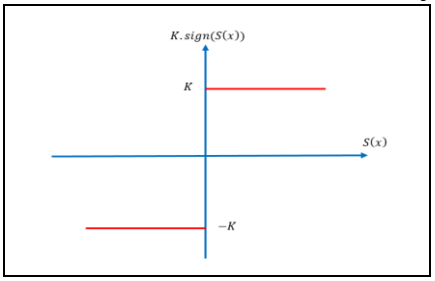

Figure IV.9 : Sign function (Relay type control)

IV.5.3 Stages of solving classical SMC problems

In reality, the sliding mode control is the feedback controller's structural changes that take place in accordance with predetermined rules when the system state moves across various state space regions. It gives the control systems a degree of adaptability to changes in internal parameters and outside disturbances, enabling the system to operate as intended. Nevertheless, chattering is present because of the discrete switch control and sliding mode control rule, this phenomenon is present in Figure. IV.7. Furthermore, the actual system is unable to achieve the optimum sliding mode control switching frequency of infinity. Furthermore, in real-world scenarios, the chattering phenomenon in sliding mode control might be caused by a switch with a time delay, discontinuous sampling, system inertia, or even an error in state measurement. The sliding mode control system can therefore be thought of as a high gain system with high frequency jitter, which could have disastrous effects for control systems. As a result, the chattering problem is now the largest barrier to sliding mode control technology development. Without interruption, the academics have persisted in lessening or stopping their chattering. Many researchers have worked quite hard in their various fields of study to decrease or eradicate chattering [116]. The enhanced SMC control structures that have been suggested to enhance the traditional SMC are depicted in the accompanying figure.

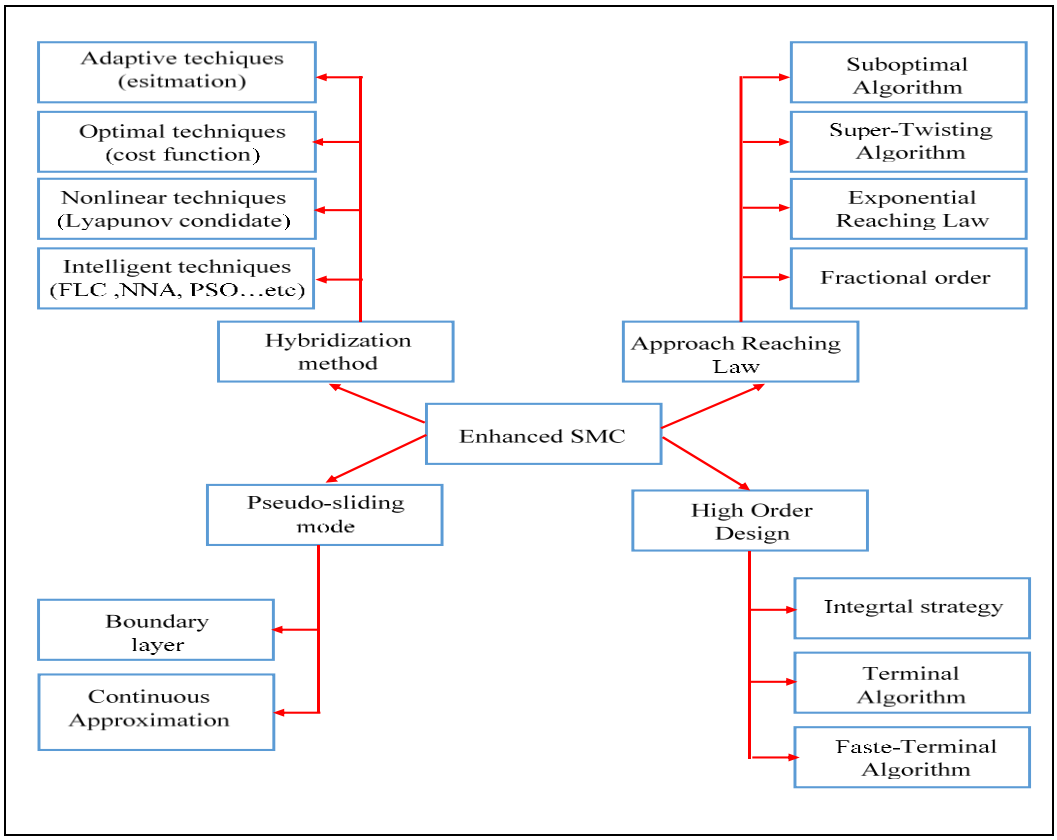

Figure IV.10 : Summary of SMC enhancement techniques

A. Pseudo-sliding mode

Improving the control law to lessen the effect of chattering is the initial idea in reducing chattering. The concepts of the "boundary layer" and the "pseudo-sliding mode" were first mentioned in literature [147]. To achieve sliding mode control, it used saturation function $sat(s,\delta)$rather than sign function $sgn(s)$.

$$sat(s,\delta)=\begin{cases} sgn(s) & if:\ |s|>\delta \\ s/\delta & if:\ |s|\le\delta \end{cases} \quad \delta>0 \tag{IV.79}$$

It employs switch sliding mode control when it is outside the boundary layer. If not, continuous state feedback control is used inside the boundary layer. It eliminates the chattering in this approach, but the finite time convergence is lost. The saturation function and sign function are shown in Figure. IV.11 [116].

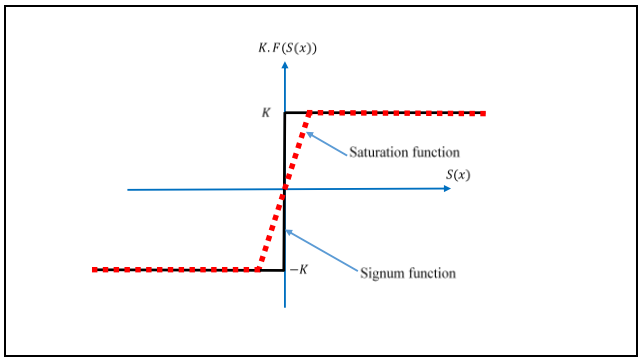

Figure IV.11 : Sign function sgn(s) and saturation function

Afterwards, a lot of academics begin researching the boundary layer and switch function. A few of them suggest serializing the unit vector.

$$u(s,\delta)=k\frac{s}{|s|+\delta} \tag{IV.80}$$

It is known as a signum-like function in some publications. In this case, choosing δ can ensure accuracy. In addition, power law interpolation exists.

$$u(s,\delta)=\begin{cases} ksgn(s) & if:\ |s|>\delta \\ \delta(\delta/|s|)^{(q-1)}sgn(s) & if:\ 0<|s|\le\delta \quad q\in[0,1) \\ 0 & if:\ s=0 \end{cases} \tag{IV.81}$$

In addition, the original switch function $sgn(s)$ has been replaced with arc tangent function $u(s,\delta)=k.\tan^{-1}(\frac{s}{\delta})$, hyperbolic curve $u(s,\delta)=\tanh(\frac{s}{\delta})$, and so on. Their goal is to lessen or get rid of the chatting. Figure. IV.12 displays the various approximations of the functions.

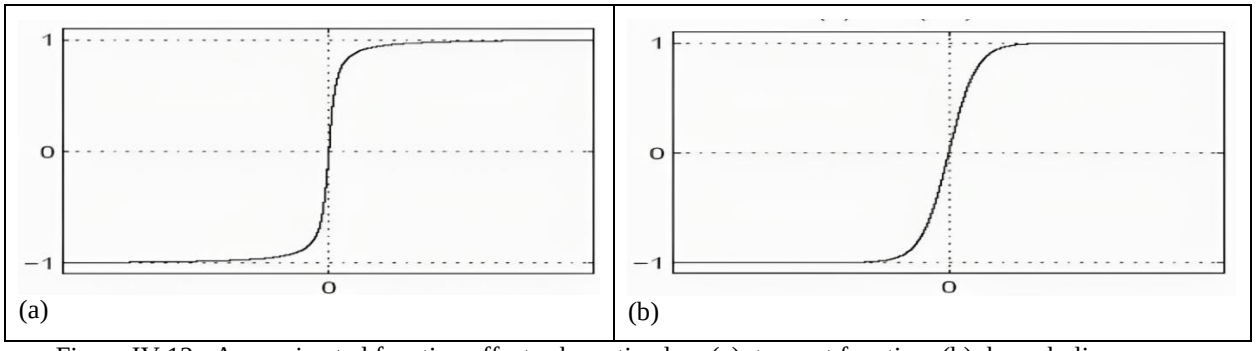

(a) (b)

Figure IV.12 : Approximated function effect schematic plan; (a): tangent function, (b): hyperbolic curve

The control effect will be better the smaller the boundary layer. However, this will also increase the control gain and improve chattering; conversely, chattering will decrease as the boundary layer increases. However, they will lessen the gain in control, making the effects of control worse. As a matter of fact, the approximate sliding mode control strikes a compromise between system robustness and performance [116].

B. Approach Reaching Law

Prof. Gao Weibing proposed approach law in 1989. Where, the reaching law method aims to eliminate the chattering caused by non-ideal reaching at the end of the reaching phase. In sliding mode control, reaching law is the differential equation that specifies the dynamics of a switching function. Moreover, it is used to study dynamic quality of arrival procession, when the system converges from the any initialization within limited time. According to the different system, we can design the various approach law, such as [116, 148,149]:

- **Uniform approach law (UAL):** $\dot{S} = -\epsilon.sgn(S)$, $\epsilon > 0$
- **Power approach law (PAL):** $\dot{S} = -k|S|^{\alpha}.sgn(S)$, $k > 0$, $0 < \alpha \leq 1$
- **Exponential approach law (ERL):** $\dot{S} = -\epsilon.sgn(S) - k.S$ $\epsilon > 0$, $k > 0$
- **Twisting Algorithm :** $\dot{S} = -r_1.sgn(S) - r_2.sgn(\dot{S})$ $r_1 > r_2 > 0$
- **Suboptimal Algorithm (SPA):** $\dot{S} = -r_1.sgn(S - S^*/2) + r_2.sgn(S^*)$ $r_1 > r_2 > 0$
- **Supper-twisting Algorithm (STA)** $\dot{S} = -\eta.|S|^{\rho}sign(S) - b\int sign(S)$ $\eta, b > 0$, $0 < \rho \leq 0.5$
- **General approach law:** $\dot{S} = -\epsilon.sgn(S) - f(S)$ $S.f(x) > 0$

Using the exponential approach law as an example, it is possible to lessen the high frequency chattering of the control signal while simultaneously ensuring the dynamic quality of the sliding mode arrival procession by adjusting the parameters k and ϵ. But chattering will occur if the ϵ is too high [116].

About the suboptimal algorithm, when $\dot{S}$ was equal to zero the last time, S^* is the value of S that was detected. S^* starts out with a value of 0. For this controller to be implemented on a computer, successive measurements of $\dot{S}$ or S are necessary. The detection $\dot{S}$=0 often happens when the sign of the difference between consecutive ΔS readings changes. Time-optimal control of a double integrator is the direct source of the suboptimal concept [150].

The super twisting algorithm has been proposed by Pr.Levant. The super twisting algorithm simultaneously stabilizes the sliding surface with its derivative at zero, where no noise input contributes to the design of the control law. In addition, it contributes to overcoming chattering problems, reaching speed, and anti-disturbance ability. The super twisting algorithms (STA) are

based on two important parts to construct the control law: the first part is related to time and is determined by its derivative. As for the second, it is determined by the function of the sliding variable [57,151].

C. High Order Design

Over the past ten years, a novel technique called high-order sliding mode control (HOSMC) has been put forth [151]. It is an advanced control methodology that extends the principles of traditional sliding mode control (SMC) to achieve improved performance, robustness, and tracking accuracy in dynamic systems. In HOSMC, the sliding surface is designed to have higher-order dynamics, allowing for the incorporation of additional derivatives of the system states. This enables a more sophisticated and precise representation of the system's behavior, particularly in the presence of uncertainties and disturbances. The HOSMC can be designed as multifilters, as shown in Figure. IV.13.

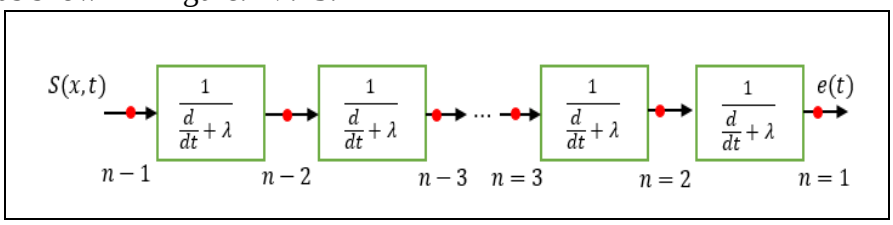

Figure IV.13 : Multifilters design to the HOSMC

The key advantage of HOSMC lies in its ability to address chattering, a phenomenon associated with traditional SMC, where the control signal exhibits high-frequency oscillations. By introducing higher-order terms in the sliding surface, HOSMC aims to reduce chattering and enhance the overall control quality. The methodology is particularly effective in systems with complex dynamics and nonlinearities, offering a robust solution for applications in aerospace, automotive, and other engineering domains.

- **Integral sliding mode control (I-SMC):** In traditional sliding mode control, the sliding phase is where the system becomes resilient against changes in parameters and outside disturbances. Until then, or in the reaching phase, the robustness cannot be assured. Utkin and Jingxin devised integral sliding mode control (ISMC) (equation (IV.82)) to solve this issue by doing away with the reaching phase, which enforces the sliding phase during the whole system response [152]. Additionally, in integral SMC, the order of motion equation is equal to the order of the original system rather than being lowered by the control input dimension. The continuous nominal control and discontinuous nominal control, which make up the control law, are in charge of maintaining the nominal system's operation in the absence of disturbances and rejecting disturbances, respectively. Therefore, system robustness may be ensured from the start with this kind of SMC. Furthermore, since the value is typically larger during the reaching phase, ISMC requires a smaller maximum control magnitude than conventional SMC [153, 154].

$$S(x,t) = e(t) - \int_0^t (a + bK).e(\tau)d\tau \qquad \text{(IV.82)}$$

- **Terminal sliding mode control (T-SMC):** For quick and finite-time state convergence during the sliding mode phase, terminal sliding mode (TSM) control uses terminal

sliding surfaces where fractional power is introduced. The rate of convergence will accelerate close to the equilibrium point, making this controller the preferable choice for high precision control. Due to the recursive structure of switching manifolds, the standard terminal SMC (equation (IV.83)) has a singularity problem that could arise if the beginning circumstances are not chosen properly [155,156,157]. The two-phase control approach, which induces the system state into a non-singular area before finite time convergence control, was used to overcome the singularity in TSM [158]. By alternating between TSM and linear hyperplane based sliding mode, non-singularity was guaranteed in [159]. Nevertheless, the singularity effect is not completely eliminated as the boundary approaches zero. Moreover, the benefit of TSM is lessened when the boundary is rather large [156].

$$S(x,t) = \dot{e}(t) + \beta . e(t)^{\frac{q}{p}} \tag{IV.83}$$

Where, $\beta > 0;\ p, q$ are positive odd integers, $p > q$

- **Non-singular terminal sliding mode controller (NT-SMC**): It was suggested that the traditional terminal sliding mode control's singularity issue be resolved entirely. Compared to traditional SMC, NTSM produces smaller tracking errors, improved anti-disturbance capabilities, faster settling times, and reduced chattering. According to SMC, controller enhancement still entails setting the switching gain at a greater value. Therefore, in order to enhance controller performance, significant chattering cannot be prevented because of discontinuity term. Providing good convergence has another disadvantage, particularly when the system state is out of equilibrium [160]. Furthermore, when NTSM's performance gets close to that of linear SMC, poor parameter selection may have an impact on the pace of convergence [161]. The surface design of the NT-SMC is identified as follows:

$$S(x,t) = \dot{e}(t) + \frac{1}{\beta} . e(t)^{\frac{p}{q}} \tag{IV.84}$$

Where, $\beta > 0;\ p, q$ are positive, $1 < \frac{p}{q} < 2$

- **Fast terminal sliding mode control (FS-SMC):** The non-singular fast terminal sliding mode (NFTSM) controller is an additional sort of terminal sliding mode controller that has been proposed in the literature. NFTSM has a quicker rate of state convergence while maintaining all of NTSM's benefits. In the vicinity of equilibrium, the linear sliding mode's convergence rate stays constant, whereas the NFTSM's convergence rate increases exponentially. In comparison to traditional SMC, NFTSM has demonstrated faster convergence, better robustness, higher precision, and less chattering in a variety of control applications [161,162].

$$S(x,t) = \dot{e}(t) + \alpha . e(t) + \beta . e(t)^{\frac{q}{p}} \tag{IV.84}$$

Where, $\alpha, \beta > 0;\ p, q$ are positive odd integers, $p > q$

D. Hybridization method

Recently, the hybridization method between vector control approaches has become widely common, where it is sufficient to overcome control problems in general by combining the advantages of two or three techniques and addressing the disadvantages of each technique through the other. This is what happens with sliding mode control in particular, where the problems that suffer from it have been solved using another vector control technique. Among these techniques, we briefly mention the following:

- **Nonlinear technique:** In this hybridization, the sliding mode control and backstepping control have been combined, where the main goal of this design is to reach robust control using the SMC's reaching law. At the same time, the sliding surface has been forced to stabilize towards its trajectory with less chattering using backstepping control through the Lyapunov candidate.
- **Adaptive technique:** There are two main principles of this design: the estimation of the SMC gains or the estimation of the sliding surface using model reference adaptive control, extended theories, or the matching command technique. The combination of Sliding Mode Control and Adaptive Control, known as Adaptive Sliding Mode Control (ASMC), leverages the robustness of sliding mode in handling uncertainties and the adaptability of online parameter adjustment. In ASMC, the sliding mode component ensures robustness against uncertainties, while the adaptive control component fine-tunes the control parameters to optimize performance and adapt to changing system conditions. This hybrid approach aims to provide the best of both worlds, achieving stability and robustness while allowing for dynamic adaptation.
- **Optimal technique:** Sliding Mode Optimal Control combines the robustness of Sliding Mode Control with the efficiency of Optimal Control. The sliding mode ensures robustness in the presence of uncertainties, while the optimal control component minimizes a performance criterion, aiming for optimal system behavior. Designing Sliding Mode Optimal Control requires careful consideration of the sliding surface, cost function, and tuning of parameters to achieve the desired balance between robustness and optimality. It often involves sophisticated mathematical techniques for optimal control problem formulations and solutions.
- **Intelligent Artificial technique:** The sliding mode theory, which has been researched for more than 50 years, is revolutionised by the integration of artificial intelligence (AI) into SMC. The technical overview of composite SMC and computational intelligence controllers was provided by Xinghuo and Kaynak [163], who highlighted the distinct benefits and drawbacks of incorporating different AI techniques into SMC, and by Kaynak et al. [164], who explored potential integration strategies. AI was added to sliding mode controllers for a variety of uses, including optimizing the controller's performance in conjunction with SMC, leveraging SMC's advantages to improve primary AI controllers, adjusting an SMC controller's parameters online or offline, estimating uncertainties, and removing chattering. Among intelligent Artificial technique, we mention the three most famous technologies as follows:
  - ✓ Fuzzy logic control (FLC)

- ✓ Neural Network Artificial control (NNAC)
- ✓ Fuzzy Neural Network control (FNNC)

The membership function must be both wide enough to reduce noise sensitivity and intense enough for precision when using fuzzy logic inference systems to generate a gain [165]. However, a composite fuzzy SMC was created, and its sliding mode characteristics can enhance the functionality of a traditional pure fuzzy controller. FLIS determined the control output based on three sliding conditions: approaching, sliding, and stable. It is possible to minimize the number of fuzzy rules since the sliding surface defines the input variable of the fuzzy inference rules [166]. In terms of removing overshoot, settling time, tracking accuracy, and steady-state error reduction, the suggested controller outperformed a pure fuzzy controller [167].

Fault tolerance, parallelism, and learning are features of neural networks [168]. Wavelets and neural networks are used to create Wavelet NN (WNN). It blends wavelet decomposition's identification capability with artificial neural networks' capacity for online learning [169]. Its great precision with smaller network sizes and rapid convergence are its standout features [170]. The uncertainty bound problem in SMC design was resolved by predicting uncertain system dynamics with a WNN bound observer. Strong speed control was made possible by this composite WNN-SMC controller for a variety of operating circumstances.

Neural networks and fuzzy logic are both universal approximators. Nevertheless, each of their unique qualities complements the other. Fuzzy logic-based controllers are enhanced by fuzzy neural network (FNN) in terms of their learning capabilities. As a result, it can handle ambiguous data using fuzzy reasoning and learn from processes using artificial neural networks. While the NFC is active during steady-state mode to provide a smooth, less chattering dynamic response, the SMC is engaged during transient mode to obtain a quick dynamic reaction. The goal is to combine the benefits of NFC and SMC while removing their respective drawbacks. Approximately 92% less chattering occurs in the suggested hybrid controller when compared to a traditional SMC. In contrast to a traditional SMC, the hybrid controller's speed response is faster by more than 7%. In comparison to a standard NFC, the hybrid controller is also less susceptible to changes in parameters and external load disturbances. In order to improve the performance of a sliding mode controller, the wavelet fuzzy neural network (WFNN) estimator estimates the unknown lumped uncertainty online by combining the theories of fuzzy and wavelet neural networks [162].

IV.5.4 Design of the SMC approaches for the PMSM model

In this section, we will study the design of the SMC based on some of the techniques mentioned above for the PMSM model, where we will use modelling of the machine equation (II.34) mentioned in the second chapter, and through this, the nonlinear strategy will be available in this study. Therefore, the speed and current loops have been identified, and the system will be designed as full-state variables. Through this design, the inputs will be reference quadratic current and direct-quadratic voltages, and the outputs will be the speed and direct-quadratic of

the actual currents. Firstly, we'll start with the classical SMC design on the PMSM model. Depending on the control design of the SMC mentioned mentioned in equation (IV.75), the SMC law "*u*(t)'' for the PMSM model is made of two components designed like the following:

- Equivalent component $u_{eq}(t) = [i_{q-eq} \quad V_{d-eq} \quad V_{q-eq}]^T$;
- Switching component $u_s(t) = [i_{q-s} \quad V_{d-s} \quad V_{q-s}]^T$.

The sliding surfaces of the speed and current loops are designed as follows:

$$\begin{bmatrix} S_\Omega \\ S_d \\ S_q \end{bmatrix} = \begin{bmatrix} \Omega^* - \Omega \\ i^* - i_d \\ {i_q}^* - i_q \end{bmatrix} \tag{IV.85}$$

The derivative of the sliding surfaces are calculated as follows:

$$\frac{d}{dt}\begin{bmatrix} S_\Omega \\ S_d \\ S_q \end{bmatrix} = \begin{bmatrix} \dot{\Omega}^* + \frac{F}{j}.\Omega - \frac{3.p}{2.j}.\psi_f.{i_{q-eq}}^* + \frac{1}{j}.T_l \\ \dot{i_d}^* + \frac{R_s}{L_d} i_d - \frac{L_q}{L_d} p.i_q.\Omega - \frac{1}{L_d} v_{d-eq} \\ \dot{i_q}^* + \frac{R_s}{L_q} i_q + \frac{L_d}{L_q} p.i_d.\Omega + p.\Omega \frac{\psi_f}{L_q} - \frac{1}{L_q} v_{q-eq} \end{bmatrix} \tag{IV.86}$$

Through the sliding conditions of the SMC design and equation (IV.76), respectively, the equivalent components of each PMSM's loops can be identified as the following vector:

$$\begin{bmatrix} {i_{q-eq}}^* \\ v_{d-eq} \\ v_{q-eq} \end{bmatrix} = \begin{bmatrix} \frac{2.j}{3.p.\psi_f}(\dot{\Omega}^* + \frac{F}{J}\Omega + \frac{1}{j}.T_l) \\ L_d.{\dot{i}_d}^* + R_s.i_d - L_q.p.i_q.\Omega \\ L_q.{\dot{i}_q}^* + R_s.i_q + L_d.p.i_d.\Omega + p.\Omega.\psi_f \end{bmatrix} \tag{IV.87}$$

In order to compute the reaching components (switching law), equations (IV.77) and (IV.78) are used. Therefore, the vector of the reaching components of the classical SMC can be designed as follows:

$$\begin{bmatrix} {i_{q-s}}^* \\ v_{d-s} \\ v_{q-s} \end{bmatrix} = \begin{bmatrix} K_\Omega.sign(S_\Omega) \\ K_d.sign(S_d) \\ K_q.sign(S_q) \end{bmatrix} \tag{IV.88}$$

Finally, the control law of the sliding mode for the PMSM system has been calculated as follows:

$$\begin{bmatrix} {i_{q-s}}^* \\ v_{d-s} \\ v_{q-s} \end{bmatrix} = \begin{bmatrix} {i_{q-eq}}^* + {i_{q-s}}^* \\ v_{d-eq} + v_{d-s} \\ v_{q-eq} + v_{q-s} \end{bmatrix} \tag{IV.89}$$

For the classical SMC solving to the pseudo-sliding mode, the equivalent component is the same of the classical SMC, but the contribution in the reaching component. If the boundary layer is applied, the reaching component becomes as follows:

$$\begin{bmatrix} {i_{q-s}}^* \\ v_{d-s} \\ v_{q-s} \end{bmatrix} = \begin{bmatrix} {K_\Omega}'.sat(S_\Omega) \\ {K_d}'.sat(S_d) \\ {K_q}'.sat(S_q) \end{bmatrix} \tag{IV.90}$$

While the continuous approximation is applied, the reaching component becomes as follows:

$$\begin{bmatrix} {i_{q-s}}^* \\ v_{d-s} \\ v_{q-s} \end{bmatrix} = \begin{bmatrix} {K_\Omega}''.\tanh(S_\Omega) \\ {K_\mathrm{d}}''.\tanh(S_\mathrm{d}) \\ {K_\mathrm{q}}''.\tanh(S_\mathrm{q}) \end{bmatrix} \quad \text{(IV.91)}$$

While the Approach Reaching Law is applied in order to solve the classical SMC, the reaching component approaches can be summarized in the following table:

Table IV.1. Design of the approach reaching law based SMC for the PMSM model

Approach Reaching Law	The reaching component vector for the PMSM model
Power approach law (PAL)	$\begin{bmatrix} {i_{q-s}}^* \\ v_{d-s} \\ v_{q-s} \end{bmatrix} = \begin{bmatrix} -k_\Omega \lvert S_\Omega \rvert^{\alpha_1}.sgn(S_\Omega) \\ -k_d \lvert S_\mathrm{d} \rvert^{\alpha_2}.sgn(S_\mathrm{d}) \\ -k_q \lvert S_\mathrm{q} \rvert^{\alpha_3}.sgn(S_\mathrm{q}) \end{bmatrix}$
Exponential approach law (ERL)	$\begin{bmatrix} {i_{q-s}}^* \\ v_{d-s} \\ v_{q-s} \end{bmatrix} = \begin{bmatrix} -\epsilon_1.sgn(S_\Omega) - k_1.S_\Omega \\ -\epsilon_2.sgn(S_\mathrm{d}) - k_2.S_\mathrm{d} \\ -\epsilon_3.sgn(S_\mathrm{q}) - k_3.S_\mathrm{q} \end{bmatrix}$
Twisting Algorithm	$\begin{bmatrix} {i_{q-s}}^* \\ v_{d-s} \\ v_{q-s} \end{bmatrix} = \begin{bmatrix} -r_{\Omega 1}.sgn(S_\Omega) - r_{\Omega 2}.sgn(\dot{S}_\Omega) \\ -r_{\mathrm{d}1}.sgn(S_\mathrm{d}) - r_{\mathrm{d}2}.sgn(\dot{S}_\mathrm{d}) \\ -r_{\mathrm{q}1}.sgn(S_\mathrm{q}) - r_{\mathrm{q}2}.sgn(\dot{S}_\mathrm{q}) \end{bmatrix}$
Suboptimal Algorithm (SPA)	$\begin{bmatrix} {i_{q-s}}^* \\ v_{d-s} \\ v_{q-s} \end{bmatrix} = \begin{bmatrix} -r_{\Omega 1}.sgn(S_\Omega - {S^*}_\Omega/2) + r_{\Omega 2}.sgn({S^*}_\Omega) \\ -r_{\mathrm{d}1}.sgn(S_\mathrm{d} - {S^*}_\mathrm{d}/2) + r_{\mathrm{d}2}.sgn({S^*}_\mathrm{d}) \\ -r_{\mathrm{q}1}.sgn(S_\mathrm{q} - {S^*}_\mathrm{q}/2) + r_{\mathrm{q}2}.sgn({S^*}_\mathrm{q}) \end{bmatrix}$
Supper-twisting Algorithm (STA)	$\begin{bmatrix} {i_{q-s}}^* \\ v_{d-s} \\ v_{q-s} \end{bmatrix} = \begin{bmatrix} -\eta_\Omega.\lvert S_\Omega \rvert^{\rho_\Omega} sign(S_\Omega) - b_\Omega \int sign(S_\Omega) \\ -\eta_\mathrm{d}.\lvert S_\mathrm{d} \rvert^{\rho_\mathrm{d}} sign(S_\mathrm{d}) - b_\mathrm{d} \int sign(S_\mathrm{d}) \\ -\eta_\mathrm{q}.\lvert S_\mathrm{q} \rvert^{\rho_\mathrm{q}} sign(S_\mathrm{q}) - b_\mathrm{q} \int sign(S_\mathrm{q}) \end{bmatrix}$

IV.5.5 Design of the hybrid technique between the T-SMC and STA for the PMSM speed loop

Even yet, HO-STA resolves the chattering issue in the CSMC and T-SMC solves the convergence problem. However, the identification of algorithm gain necessitates the satisfaction of the smooth and limited condition for the disturbance term, which is more challenging in scientific studies, making it challenging to guarantee system convergence. Furthermore, an excessively high profit value set in an attempt to guarantee system convergence might result in the dangerous occurrence of system jamming and collapse [171]. This control design suggests a hybrid control between T-SMC and STA in order to address the issues with C-SMC. The goal of the suggested control is to combine the benefits of both approaches and address issues in both T-SMC and STA. Furthermore, HO-STA based T-SMC may achieve tracking performance in a finite period of time in addition to reducing the chattering phenomena in the original TSMC architecture [172]. In order to show how applicable and efficient the HO-STA-based T-SMC schemes are, they will be used to manage a PMSM speed model. Based on this control design, five crucial procedures have been followed to calculate the control law, which are as follows:

- **Formulation to a high order of sliding surface based PMSM speed:**

As sliding surface selection has been extensively explored to address chattering and convergence of system states, it is the most crucial stage before applying surface conditions for sliding mode control. When using SMC, selecting a high-order surface is the best option. The PMSM speed system is constructed based on the high-order state model "HOSM" as follows [57]:

$$\begin{cases} x_1 = \theta_r \\ x_2 = \dot{\theta}_r = \Omega \\ x_3 = \ddot{\theta}_r = \dot{\Omega} \end{cases} \quad \text{(IV.92)}$$

And the HOSM based on tracking errors is designed like the following:

$$\begin{cases} \sigma_1 = \varepsilon_\theta = \theta_{r-ref} - \theta_r \\ \sigma_2 = \dot{\varepsilon}_\theta = \varepsilon_\Omega = \Omega_{ref} - \Omega \\ \sigma_3 = \ddot{\varepsilon}_\theta = \dot{\varepsilon}_\Omega \end{cases} \quad \text{(IV.93)}$$

In order to define the control law, the operation of classical SMC is often organized into two phases: a sliding phase and an approaching phase, as mentioned above. The following equation characterizes the PMSM speed system's equivalent and switching component laws:

$$[u_{eq}(t) \quad u_s(t)]^t = [\, i^*_{q-eq} \quad i^*_{q-s}]^t \quad \text{(IV.94)}$$

- **Calculating the equivalent law using T-SMC for the speed loop of the PMSM:**

Based on the sliding surface of T-SMC and state-model HOSM, the sliding surface is designed like the following [57,162]:

$$s_1 = \dot{\sigma_1} + \beta_2 . \sigma_1^{\frac{q_2}{p_2}} = \sigma_2 + \beta_2 \sigma_1^{\frac{q_2}{p_2}} \quad \text{(IV.95)}$$

The derivative of the sliding surface has been identified as follows:

$$s_2 = \dot{s}_1 = \dot{\sigma_2} + (\beta_2 \sigma_1^{\frac{q_2}{p_2}})' = \sigma_3 + \beta_2 \frac{q_2}{p_2} \sigma_2 \sigma_1^{(\frac{q_2}{p_2} - 1)} \quad \text{(IV.96)}$$

During the sliding phase, if $\boldsymbol{s_1(\sigma, t) = 0}$ and $\boldsymbol{s_2(\sigma, t) = 0}$, the equivalent component $\boldsymbol{u_{eq}(t)}$ is supposed to hold the system stationary on the sliding surface. Where, the input signal is the reference of quadratic current, and to depend on the vector control method, the equivalent law represents as follows:

$$\boldsymbol{T_e = j\dot{\Omega}^* + T_l + F.\Omega + j.\beta_2 . \frac{q_2}{p_2} \sigma_2 \sigma_1^{(\frac{q_2}{p_2} - 1)}} \quad \text{(IV.97)}$$

The reference quaratic current is identified as follows:

$$\boldsymbol{i_{q-eq}{}^* = \frac{2}{3p\psi_f} T_e} \quad \text{(IV.98)}$$

- **Calculating the switching law using HO-STA for the speed loop of the PMSM**

By exploiting the HO-STA-based T-SMC approach and replacing the signum function with a continuous approximation called hyperbolic tangent, the switching law of HO-STA is designed as follows:

$$\begin{cases} \boldsymbol{I^*_{q-s} = -\lambda_2 . |s_1|^{\rho_2} tgh(s_1) + w} \\ \boldsymbol{\dot{w} = -b_2 . tgh(s_1)} \end{cases} \quad \text{(IV.99)}$$

The general form for determining the value of $\boldsymbol{\rho_2}$ is as follows:

$$\boldsymbol{0 < \rho_2 \leq 0.5} \quad \text{(IV.100)}$$

But it often takes the value $\boldsymbol{\rho_2 = 0.5}$, in order to provide maximum control, high-order sliding mode control [160].

- **Calculating the control law:**

Finally, the law of control based on the HO-STA and the T-SMC is given as follows:

$$I_q^* = I_{q\_eq}^* + I_{q\_s}^* \tag{IV.101}$$

$$I_q^* = \frac{2}{3p\psi_f}\left(j\dot{\Omega}^* + T_l + F\Omega + j\beta_2\frac{q_2}{p_2}\sigma_2\sigma_1^{\left(\frac{q_2}{p_2}-1\right)}\right) - \lambda_2.|s_1|^{\rho_2}tgh(s_1) + w \tag{IV.102}$$

Where s_1 is a high order based terminal sliding surface and designed in equation (IV.95), w is an integral switching term of super-twisting algorithm and designed in equation (IV.9).

- **Proof stability:**

In order to demonstrate stabilization of the system during the application of the control law proposed in this paper, it must be using the Lyapunov function, which is selected as follows:

$$V = \frac{1}{2}{S_1}^2 \tag{IV.103}$$

The system is stable if the Lyapunov function is positive-definite and its derivative is negative. Depending on this method, its derivative can be written as follows:

$$\dot{V} = S_1.\dot{S}_1 = S_1.S_2 \tag{IV.104}$$

The first surface derivative gives the second surface derivative, from equation (IV.96) and equation (IV.104), we have:

$$S_1.S_2 = S_1.(\sigma_3 + \beta_2\frac{q_2}{p_2}\sigma_2\sigma_1^{\left(\frac{q_2}{p_2}-1\right)}) \tag{IV.105}$$

Substituting the value of the σ_3 represented by equation (IV.93), equation (IV.105) becomes as follows:

$$S_1.S_2 = S_1.(\dot{\Omega}_{ref} - \dot{\Omega} + \beta_2\frac{q_2}{p_2}\sigma_2\sigma_1^{\left(\frac{q_2}{p_2}-1\right)}) \tag{IV.106}$$

Depending on the expression of the dynamic equation to the PMSM represented in equation (II.26) :

$$S_1.S_2 = S_1.(\dot{\Omega}_{ref} - \frac{1}{J}(T_e - T_l - F.\Omega) + \beta_2\frac{q_2}{p_2}\sigma_2\sigma_1^{\left(\frac{q_2}{p_2}-1\right)}) \tag{IV.107}$$

Using equation (IV.97), equation (IV.98), equation (IV.101) and equation (IV.102), we can write equation (IV.108) as below:

$$S_1.S_2 = S_1.(-\frac{1}{J}.\left(\frac{3}{2}p.\psi_f\right).I_{q\_s}^*) \tag{IV.108}$$

Finally, the value of $I_{q\_s}^*$ must be positive definite. In order to achieve that, the gains of the HO-STA represented in equation (IV.99) must take a negative value.

"In order to ensure that the value of $I_{q\_s}^*$ is positive definite, the gains of the HO-STA outlined in equation (IV.99) need to be negative."

$$\begin{cases}\overline{\boldsymbol{\lambda_2}} = |-\boldsymbol{\lambda_2}| \\ \overline{\boldsymbol{b_2}} = |-\boldsymbol{b_2}|\end{cases} \tag{IV.109}$$

Figure. IV.14 shows the simulation of the PMSM control architecture based on SMC:

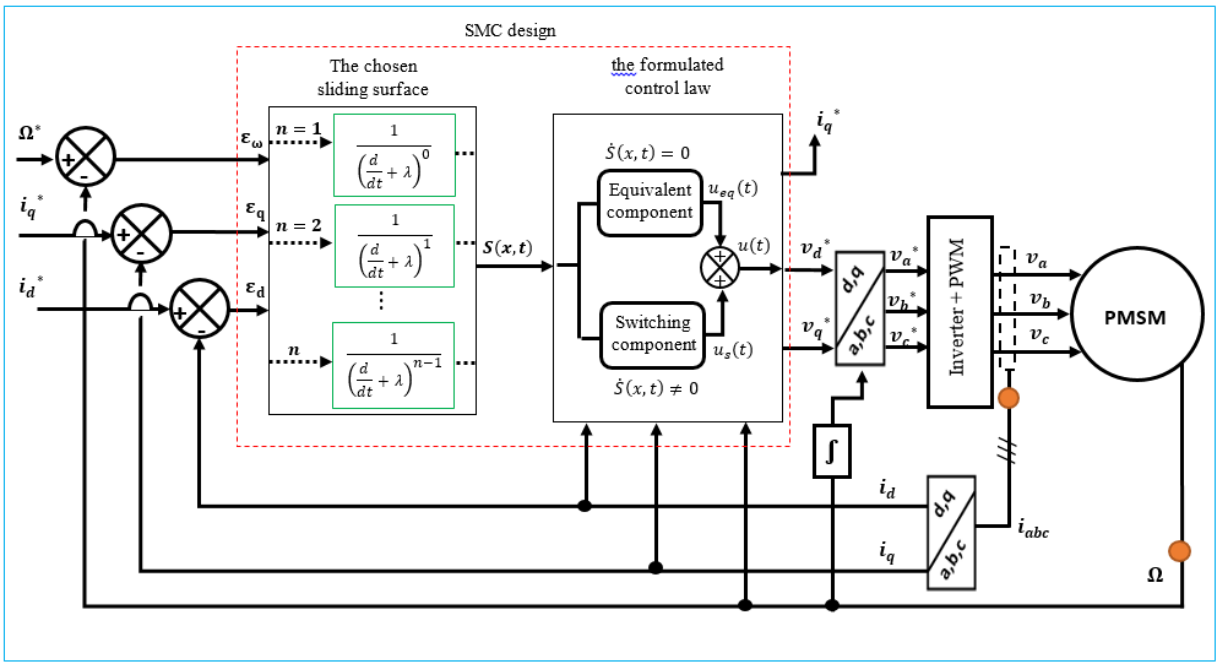

Figure IV.14 : Block diagram of SMC approaches for the PMSM system

IV.6 Simulation results and discussion

A simulation model was built in Matlab/Simulink, as shown in Figure. IV.14, to show the effectiveness of the HO-STA-based T-SMC for the PMSM under external disturbance, its robustness against uncertainties, as well as its durability under high performance speeds. Table II-3 lists the PMSM parameters that were used in the simulation. The most challenging conditions that the PMSM speed performance is experiencing are listed below in order to accomplish the aforementioned goal:

- Speed level varied to demonstrate the durability during the high performance;
- Parameters varied to demonstrate the robustness control.
- Load torque applied to demonstrate the effectiveness under external disturbance;

Furthermore, the HO-STA-based T-SMC, STA-SMC, T-SMC, ERL-SMC, AC-SMC, C-SMC, IBSC, BSC, and FBLC are compared and simulated to verify the efficiency and accuracy of the HO-STA-based T-SMC, where the first three mentioned controls are applied on the speed loop and the exponential reaching law based on the sliding mode control is applied on the current loop, while the other controls are applied on the speed and the current loop. Therefore, this comparison will be limited to PMSM speed performance only. In addition, it will be a comparative study regarding high-performance techniques (the first three controls mentioned above) under the third scenario. The control parameters designed in the simulation results are as follows, T-SMC parameters are $\beta_1 = 0.01, q_1 = 0.6, p_1 = 0.5, k_1 = 0.05, k_2 = 0.0001$, STA-SMC parameters are $\lambda_1 = 2, b_1 = 0.001, \rho_1 = 0.38$, HO-STA based T-SMC parameters $\beta_2 = 0.001, q_2 = 0.6, p_2 = 0.5, \overline{\lambda_2} = 1.9, \overline{b_2} = 0.1, \rho_2 = 0.5$. ERL-SMC parameters are $\epsilon_1 = 20, \epsilon_2 = 20, \epsilon_3 = 20, k_1 = 10, k_2 = 1, k_3 = 1$, AC-SMC parameters are $k_d'' = 30, k_q'' =$

30, $k_\Omega{}'' = 4$, C-SMC parameters are $k_d = 500$, $k_q = 500$, $k_\Omega = 4$, IBSC parameters are $k_d = 10^5$, $k_q = 16.10^5$, $k_\Omega = 100$, $k_1 = 0.1$, $k_2 = 0.1$, $k_3 = 0.1$ BSC parameters are $k_d = 100$, $k_q = 9.10^4$, $k_\Omega = 300$, FBLC parameters are mentioned in equation (IV.21).

Figure. IV.15(A) shows the PMSM adopts its high performance, where the speed level is varied between low, medium, and high speed. To study the performance changes that occur at the level of each speed. Figure. IV.15(B) and Table III-3 show the region (a) presented in Figure. IV.15(A), where it presents the speed performance of the PMSM during the start-up at low speed (200 rpm) with a comparative study among the techniques mentioned above, where the HO-STA-based T-SMC has the least rise time, approximately 4 ms, and the smallest steady-state error compared to the other controls. Figure. IV.15(C) and Table. IV.3 shows the region (b) presented in Figure. IV.15(A), which gives the second level of speed performance, which is characterized by the medium speed of the PMSM to 600 rpm. Despite this, the HO-STA-based T-SMC maintains its durability under the change of speed from low to medium in terms of the lowest percentage change for each lower settling time and the steady-state error compared to the eight controls. Figure. IV.15(D) and Table. IV.3 shows the region (c) presented in Figure. IV.15(A), where it shows a change in speed to the third level, which represents the highest speed of the performance at 1000 rpm. Even with this sudden variation in PMSM speed from medium speed to high speed, the HO-STA-based T-SMC maintains superior durability to the characteristics of the PMSM compared to the eight controls, too.

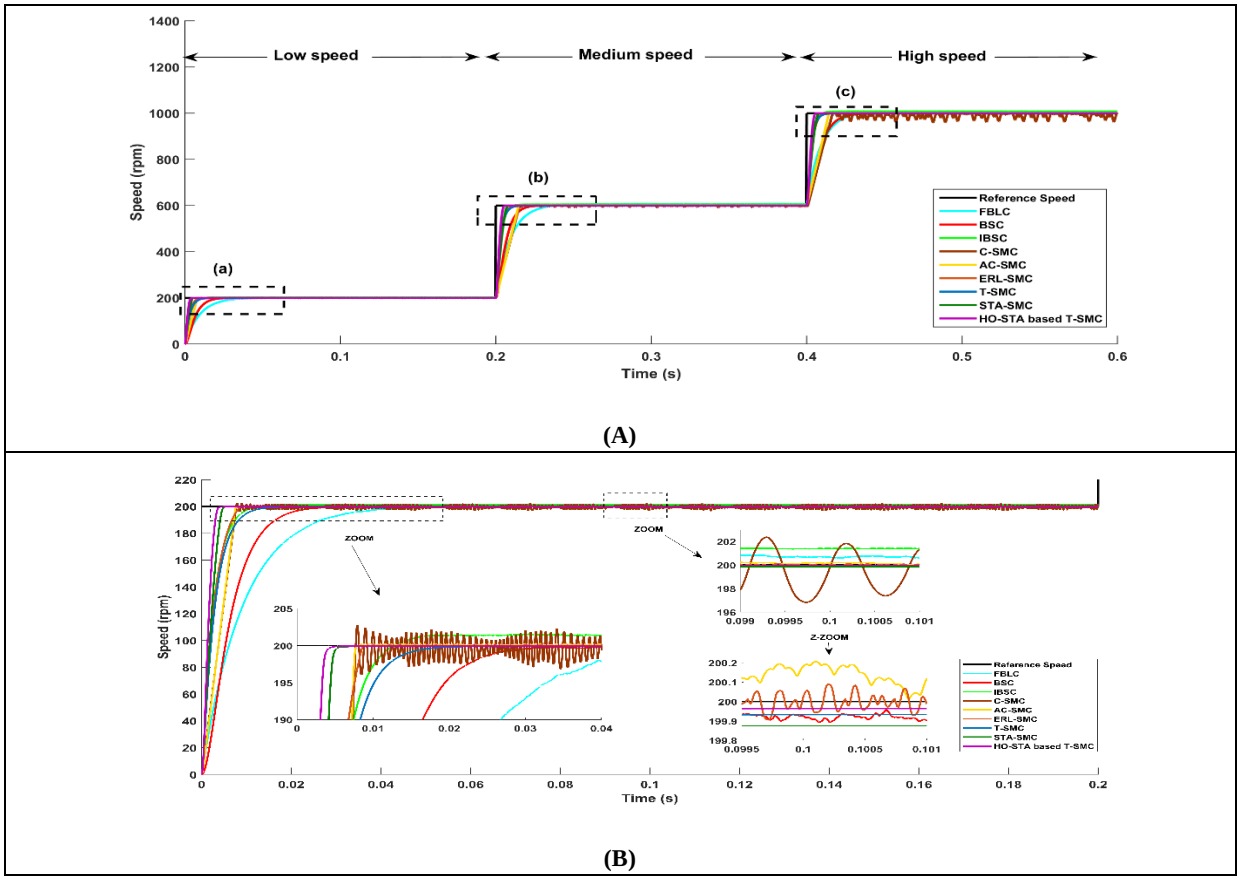

(A)

(B)

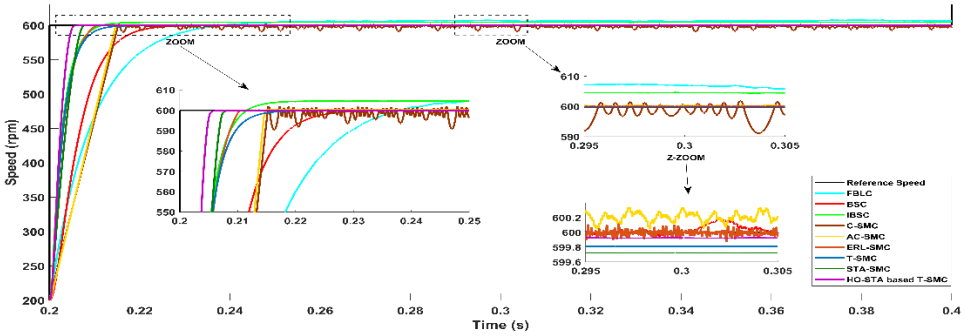

(C)

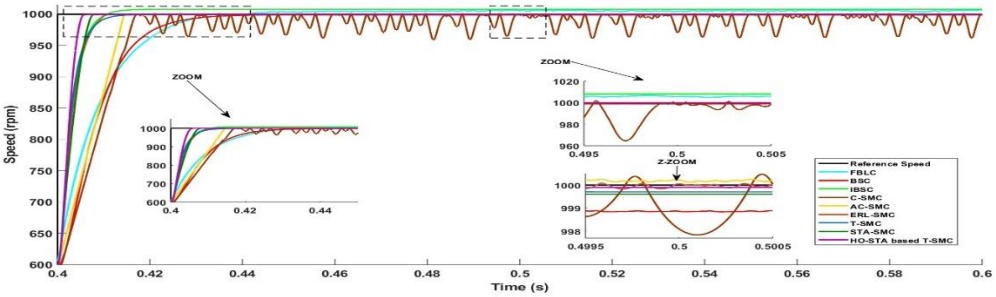

(D)

Figure IV.15 : Hiaqgh-performance of PMSM speed levels

Table IV.2. Performance characteristics of speed PMSM model under variation of speed level

Performance characteristics		HO-STA based T-SMC	STA-SMC	T-SMC	ERL-SMC	AC-SMC	C-SMC	IBSC	BSC	FBLC
Rise Time *(ms)*	Low speed	4	5	15	9	8	8	13	35	50
	Medium speed	5	7	18	12	22	22	17	50	70
	High speed	6	8	16	15	18	22	15	60	60
Steady-state error (%)	Low speed	0.015	0.06	0.03	0.08	0.1	0.5	0.25	0.5	0.5
	Medium speed	0.04	0.011	0.09	0.5	0.7	1.67	0.75	0.67	4
	High speed	0.01	0.04	0.03	0.15	0.4	5.8	1.5	0.11	1.4
Performance Stability		Extremely stable	Very stable	Very stable	Some stability	Oscillated	Very Oscillated	Little fluctuation	Quite fluctuations	Little fluctuation

In order to achieve the robustness of the HO-STA-based T-SMC control under the influence of uncertainties, the change of PMSM parameters, which are resistance, inductances (Ld and Lq), and inertia to increasing rates, was studied. Figure. IV.16 shows this scenario, where the PMSM parameters are changed among 0%, 50%, 100%, 150%, and 200% with a medium speed; moreover, the HO-STA-based T-SMC and the eight controls mentioned above are compared. To clarify the change in the performance of the PMSM characteristics in light of the change of parameters in the above-mentioned ratios, the region of the steady-state error and the rise time

of Figure. IV.15 are detailed from Figure. IV.16 (a) to Figure. IV.16 (I), respectively. Figure. IV.16 presents the rate uncertainty change in the rise time for each control, as the HO-STA-based T-SMC takes the lowest rate of uncertainty change, which is estimated to be 0.03 step among the percentage of parameter variation mentioned above. Furthermore, the rate of steady-state error change is presented to each control during the parameter variation of the aforementioned ratios; however, the HO-STA-based T-SMC is also characterized by the lowest rate of steady-state error change. With the rates of change presented by this scenario, therefore, the HO-STA-based T-SMC takes preference over the robustness of the control.

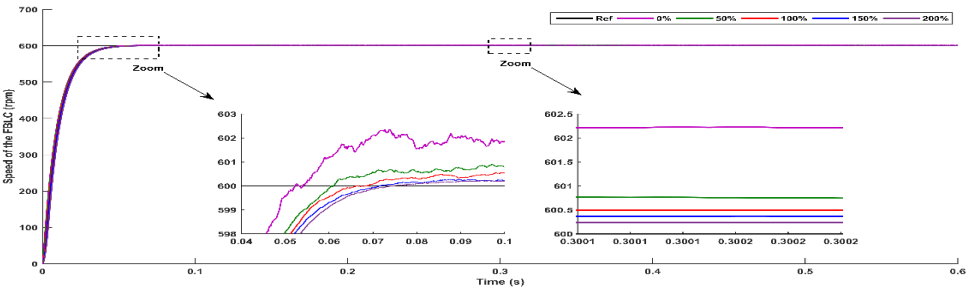

(A)

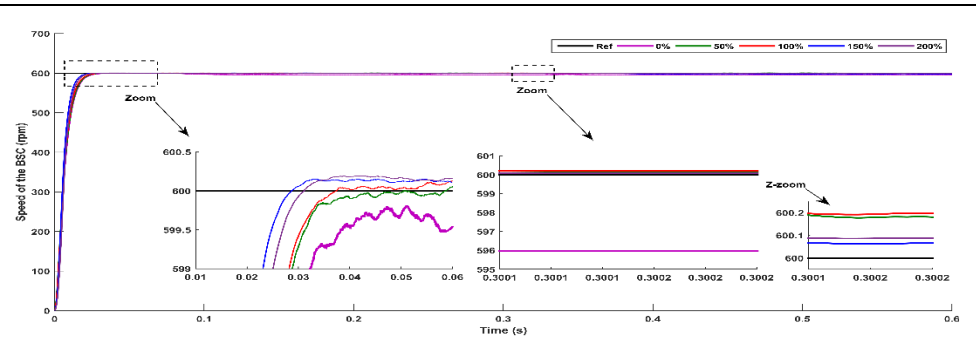

(B)

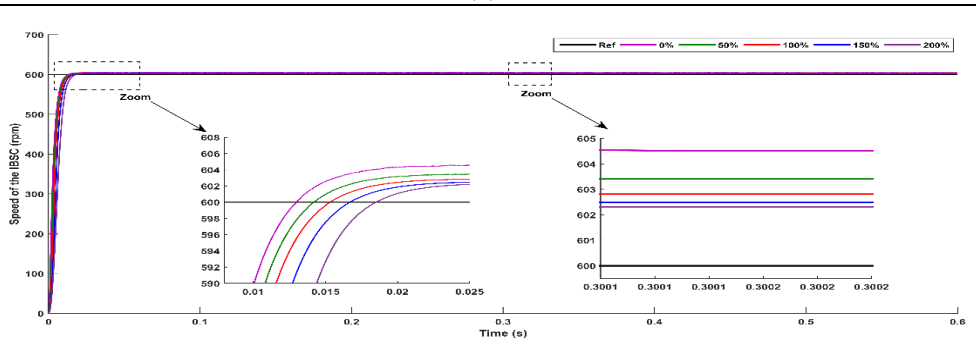

(C)

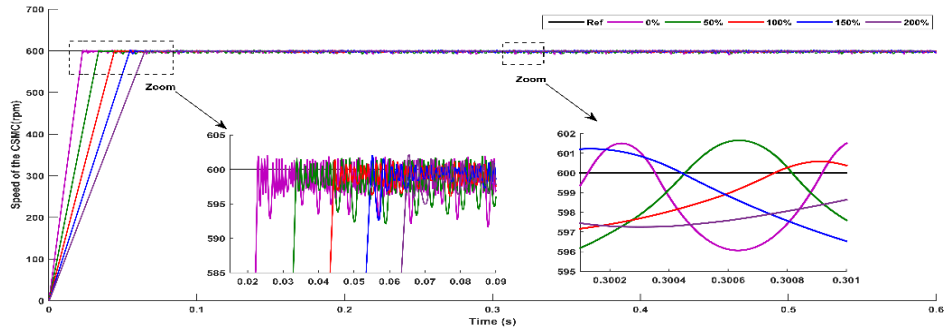
Ref
0%
50%
100%
150%
200%
Zoom
Zoom
Speed of the CSMC (rpm)
Time (s)

(D)

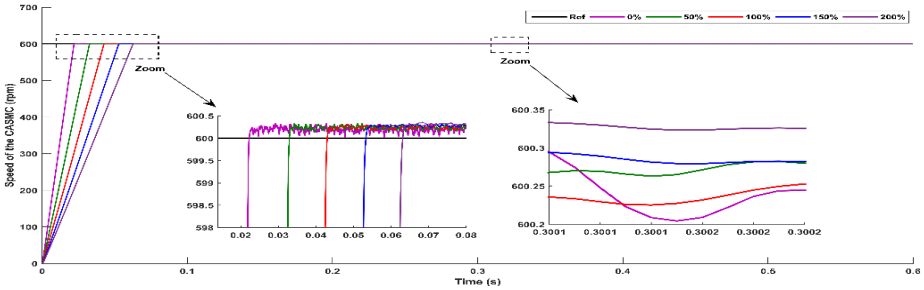
Ref
0%
50%
100%
150%
200%
Zoom
Zoom
Speed of the CASMC (rpm)
Time (s)

(E)

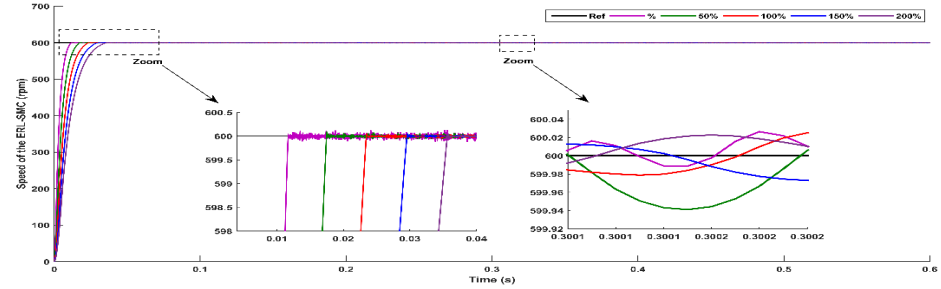
Ref
%
50%
100%
150%
200%
Zoom
Zoom
Speed of the ERL-SMC (rpm)
Time (s)

(F)

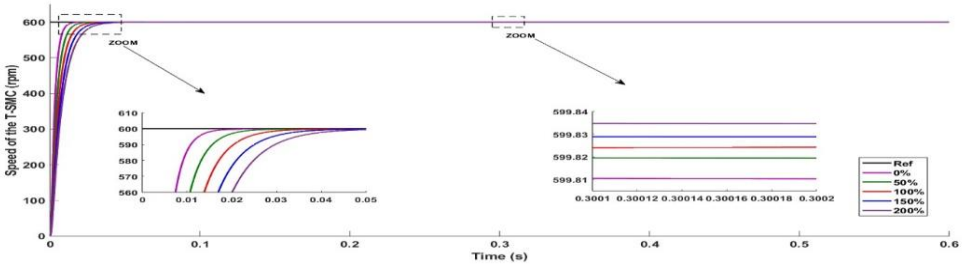
ZOOM
ZOOM
Speed of the T-SMC (rpm)
Time (s)
Ref
0%
50%
100%
150%
200%

(G)

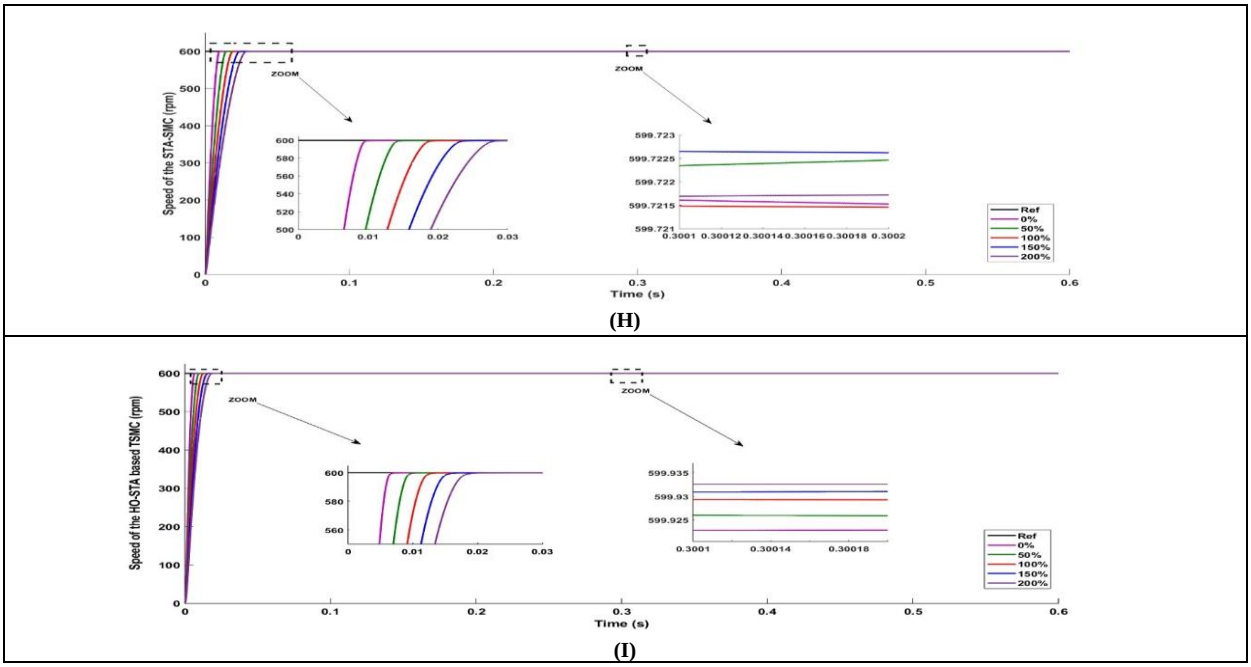

Figure IV.16 : Robustness scenario under the influence uncertainties for the PMSM speed

The most important problems that affect performance are external disturbances, which were addressed by the many conventional nonlinear controls: FBLC, BSC, IBSC, C-SMC, AC-SMC, and ERL-SMC, which were applied by a lot of research; however, there appear to be some overshoot or undershoot peaks on the level of the speed performance with a steady state error. To reduce these peaks and the steady state error, high-order controls were applied, such as the T-SMC, STA-SMC, and HO-STA-based T-SMC, which contributed significantly to improving the speed performance compared to the aforementioned controls. Therefore, a study compared to the three high-order controls has been conducted in this scenario. Therefore, Figure. IV.17(A) shows the effectiveness of three high-order controls under the effect of the external disturbance, where the latter was represented by an applied load torque at different times with a value of 1 Nm while keeping the medium speed (600 rpm). The regions (a), (b), and (c) of Figure. IV.17(A) are detailed in Figure. IV.17 (B), Figure. IV.17 (C), and Figure. IV.17 (D), respectively Figure. IV.17 (B) and Table. IV.5 present a comparative study with regard to the settling time among the three high-order contaminants mentioned above; through these results, the HO-STA-based T-SMC remains better compared to other controls in terms of settling time, which is estimated at 5 ms. Figure. IV.17 (C) and Table. IV.5 show the efficiency advantage of the the HO-STA-based T-SMC compared to two controls, where during load torque applied on the PMSM, the undershoot for the the HO-STA-based T-SMC is almost three times less compared to STA-SMC and six times less compared to T-SMC; moreover, its undershoot takes a period of 1 ms and represents the least estimated compared to the other controls mentioned above. Figure. IV.17 (D) and Table. IV.5 give a comparison of the steady-state error among each studied control; also, the HO-STA-based T-SMC contributed to reducing the steady-state error by three times compared to the STA-SMC and by four and a half times compared to the T-SMC, where its steady-state error is estimated to be 0.01%.

Table IV.3. Performance characteristics of speed model under PMSM's external disturbance

Performance characteristics	HO-STA based T-SMC	STA-SMC	T-SMC
Settling time (ms)	5	7	18
Steady-state error (%)	0.01	0.03	0.045
Undershoot (%)	0.15	0.4	1
Undershoot period (ms)	1	1.2	1.8

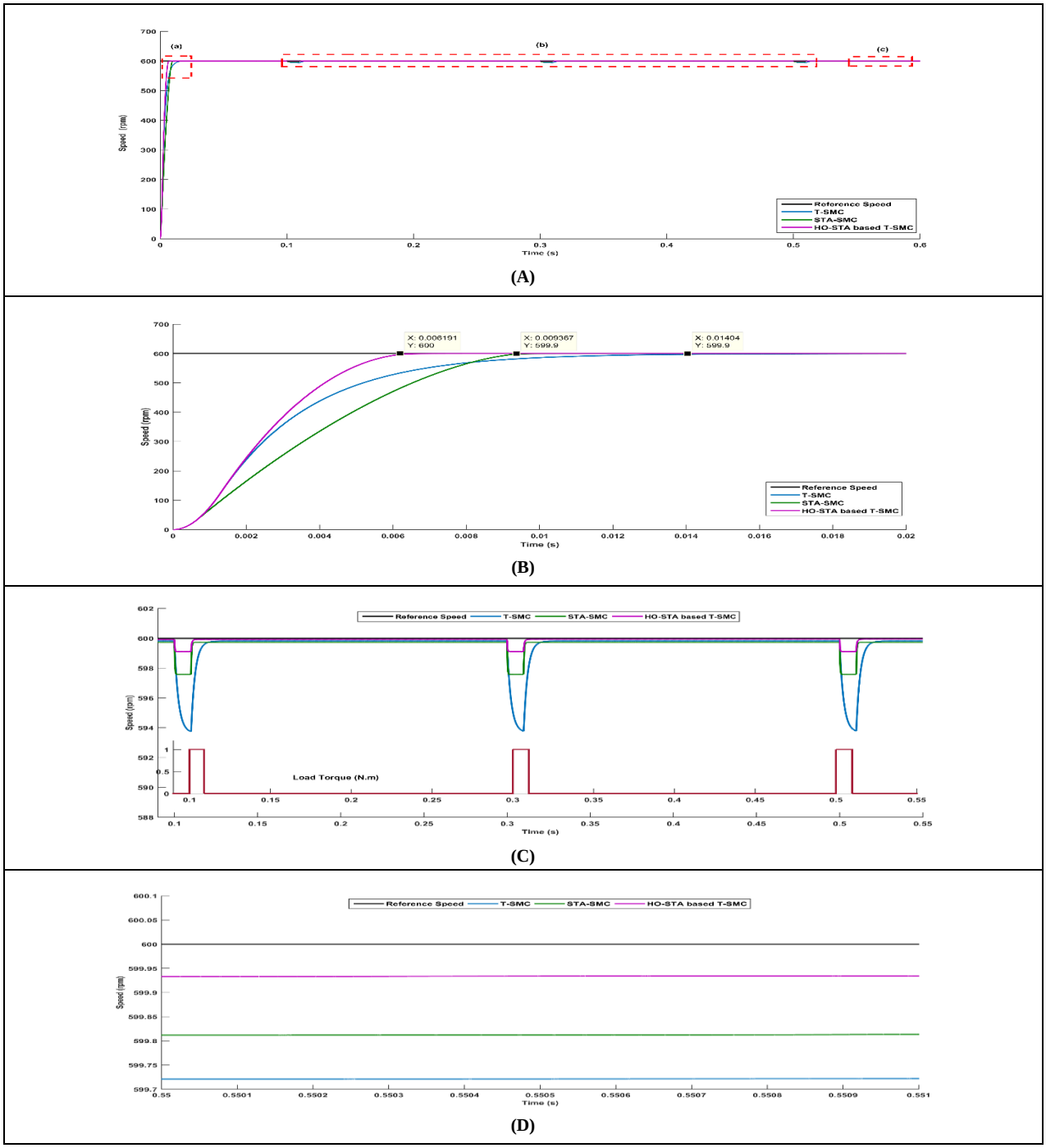

Figure IV.17 : High order controls effectiveness under external disturbance

Other scenarios have been studied in order to compute the current THD of each control. Where we applied the medium speed (600 rpm) and load torque to a 5 N.m. Through this scenario, the THD results have demonstrated that the HO-STA-based T-SMC had a good performance through the THD, which was estimated at 13.91%, while the STA-SMC, T-SMC, ERL-SMC, AC-SMC, IBSC, BSC, and FBLC got a bigger THD than the HO-STA-based T-SMC, where their THD was estimated at 33.78%, 32.85%, 32.52%, 28.75%, 25.17%, 19.14%, and 17.33%, respectively. In addition, the biggest THD was the C-SMC at 35.57 %. More detail is explained in Figure. IV.17.

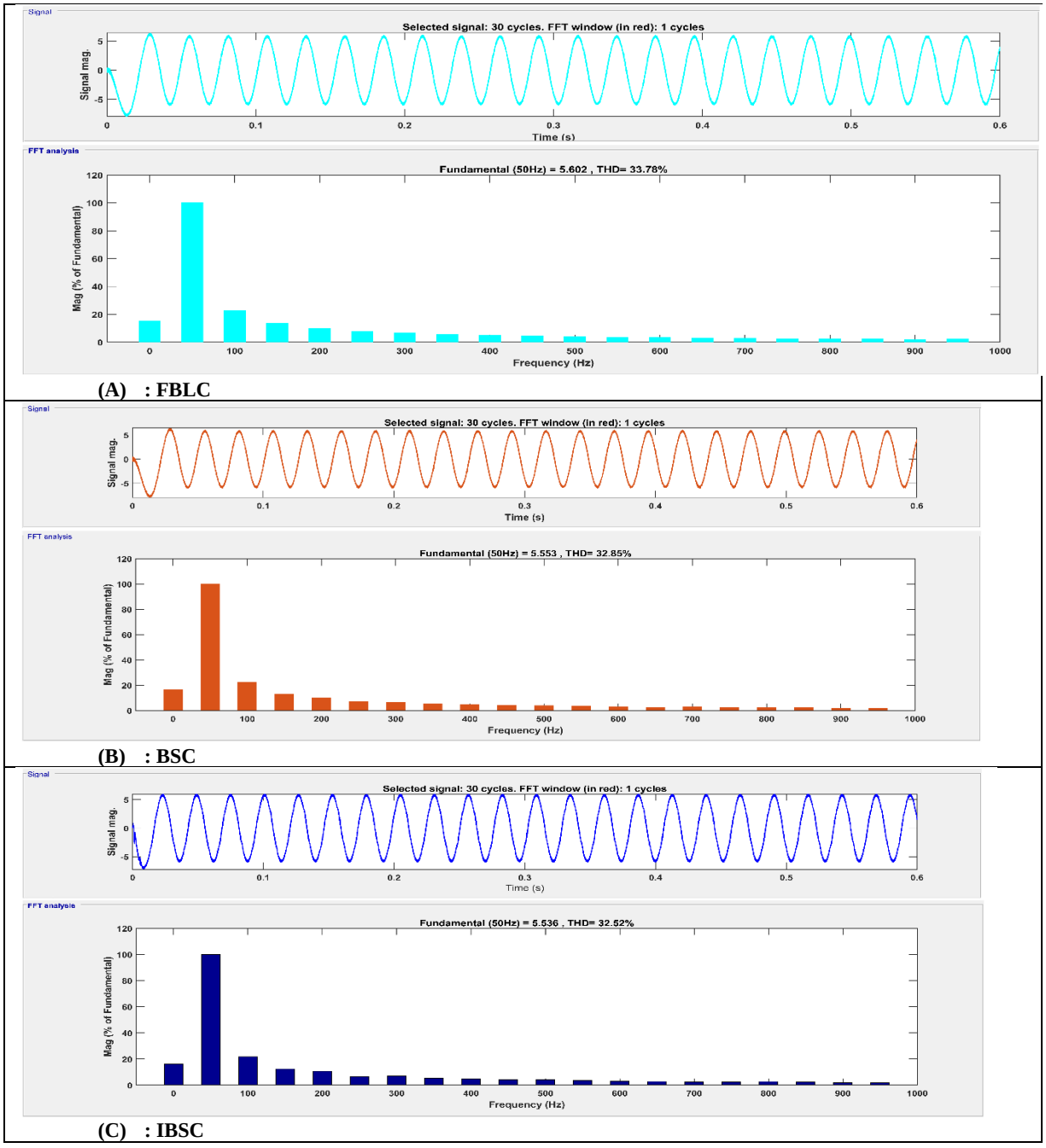

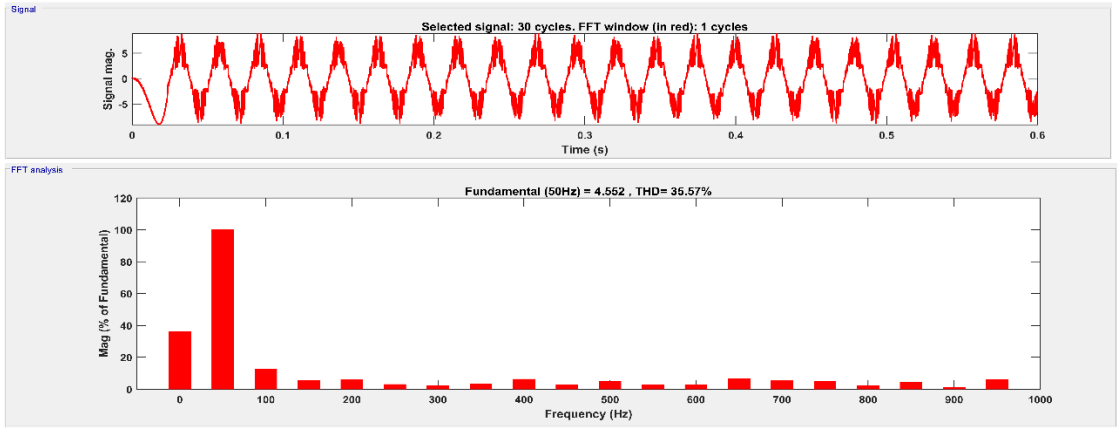

(D) C-SMC

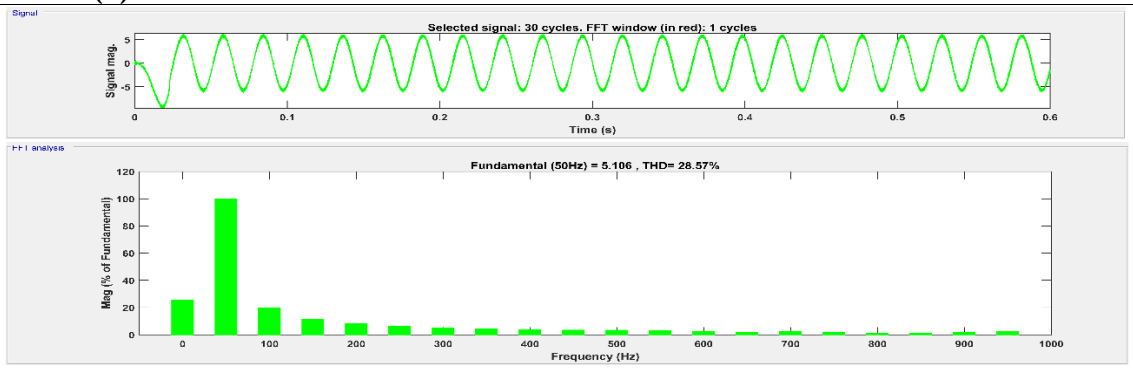

(E) AC-SMC

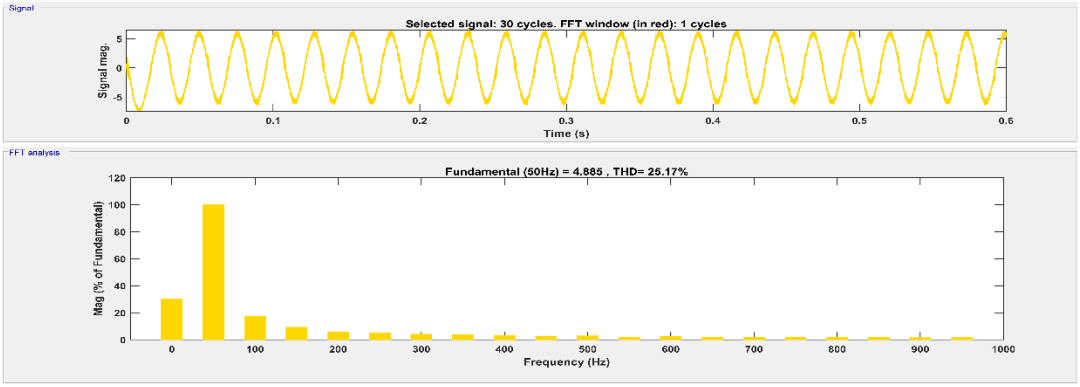

(F) ERL-SMC

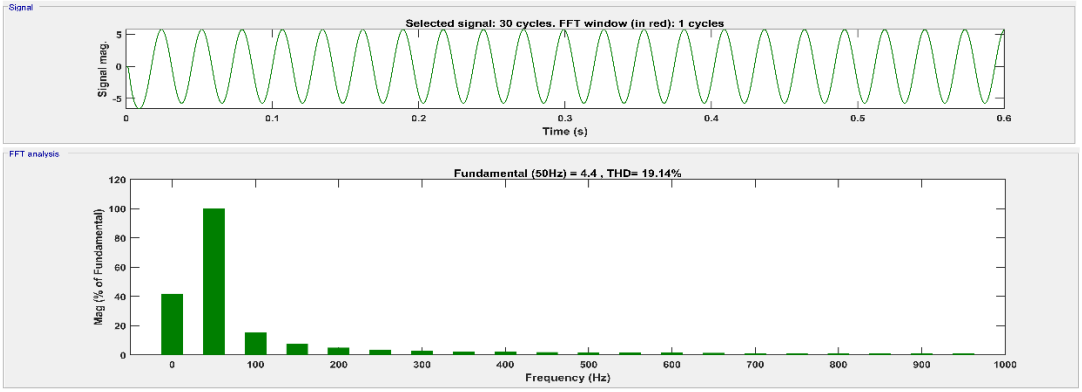

(G) T-SMC

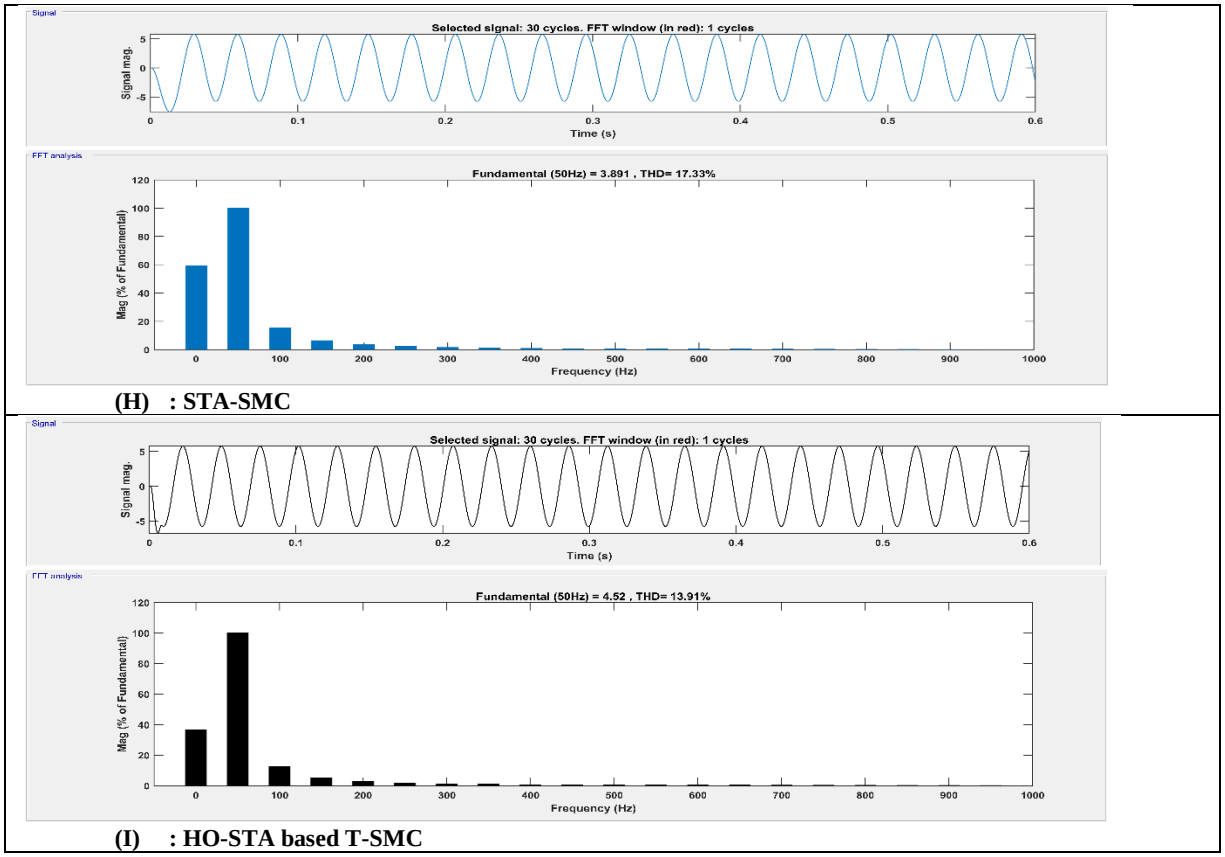

Figure IV.18 : THD of the PMSM drive based on the nonlinear approaches

IV.7 Conclusion

This chapter has studied the nonlinear techniques and approaches for the PMSM drive, where the explanations of the FBLC, BSC, and SMC have been presented. Each technique has been detailed through the definition, objective, control design, used methods, principals, features, and drawbacks. In addition, many algorithms, methods, and strategies have been studied for the SMC, such as the super-twisting algorithm "STA," high-order design "HO," terminal sliding mode control "SMC," approaches laws, and approximated continues for improving the classical SMC problems. Furthermore, the novel hybrid design between the HO-STA and T-SMC for the speed loop of the PMSM has been presented in this chapter. Moreover, each control mentioned above has been validated using MATLAB Simulink.

CHAPITRE V

DESIGN OF ADVANCED CONTROL BASED ON THE OPTIMAL TECHNIQUES APPROACHES FOR THE PMSM

V.1 Introduction

As technology develops, optimal control becomes more and more important in the creation of complex, high-performing systems in a variety of fields. Where, a strong foundation for creating control systems that function well, satisfy performance standards, and take limitations into account is provided by optimal control. Within the field of control theory, optimal control pertains to determining the most effective means of managing a dynamic system to attain a desired outcome while minimizing expenses or optimizing gains. It basically tackles the problem of making decisions over time to optimize a system's behavior while accounting for a variety of limitations and goals. Finding a control technique that moves the system from an initial state to a final state as efficiently as possible is the basic tenet of optimal control. This entails choosing a series of control inputs to be applied over time in order to minimize a given cost function, which measures the system's performance. In addition, numerous fields, such as aeronautical engineering, robotics, economics, finance, and chemical processes, employ the optimal control. It is applied in scenarios where optimizing a dynamic system's performance within bounds is necessary. To discover the best answer, the optimization process usually combines mathematical methods and computing algorithms. Depending on the particular situation at hand, several optimization criteria may be taken into account are dynamic, systems control inputs, cost function, constraints and feedback control. In this context, there are two primary subfields within optimum control: discrete-time optimal control (which deals with systems represented by difference equations) and continuous-time optimal control (which deals with systems defined by differential equations). These categories cover a wide range of strategies and tactics, such as numerical optimization techniques. Pontryagin's maximum principle, and dynamic programming. Engineers and researchers frequently modify their strategy in response to the particulars of the topic they are working on. Numerous optimization strategies can be employed to address optimal control problems, and the choice of strategy is often influenced by the specifics of the situation. Among the most important optimal techniques are techniques Linear Quadratic Regulator control (LQR) and model predictive control (MPC). In linear and multi-input multi-output (MIMO) systems, the linear quadratic regulator (LQR) is a suitable technique. With the use of both state and control input terms, this technique seeks to identify the best feedback control strategy that minimizes a quadratic cost function. The LQR technique makes the assumption that the performance requirements are quadratic and that the dynamics of the system can be adequately characterized by linear equations. The ideal state-feedback gain matrix is obtained by optimization by solving a matrix Riccati differential equation. Applications for LQR are found in many fields, including robotics, aerospace engineering, and process control. LQR offers a sophisticated method for attaining optimal control. LQR has remained prominent in the field of control theory because of its straightforward mathematical description and effective solutions. Although LQR is only applicable to linear systems, it is still a fundamental idea that has paved the way for more sophisticated control schemes, making it essential to the study and practice of optimal control. Model Predictive Control (MPC) is a versatile and powerful control strategy employed in

various fields to address complex dynamic systems. Unlike traditional control approaches, MPC operates by solving an online optimization problem at each time step to determine the optimal control input, considering a dynamic model of the system, prediction horizon, and specified performance criteria. This predictive nature allows MPC to systematically handle both linear and nonlinear systems, making it applicable to a wide range of real-world applications. The control algorithm utilizes a prediction model to forecast the future behavior of the system, incorporating constraints on states and inputs. MPC excels in situations where systems exhibit nonlinearity, uncertainty, and constraints, enabling its use in fields such as process control, automotive systems, robotics, and more. The adaptability and ability to consider constraints make MPC a preferred choice for applications where precise control, disturbance rejection, and responsiveness to changing conditions are crucial. The continual development of MPC techniques and their successful implementation underscore MPC's significance in modern control theory and its ongoing impact on advancing control strategies in dynamic and uncertain environments. In this chapter, both techniques are applied for the PMSM current loop, while the speed loop has been applied using the sliding mode technique. Furthermore, we have improved the conventional LQR using a novel design based on steady state as new state variables (SS-LQR). The effectiveness of each technique has been validated using MATLAB Simulink.

V.2 Description of the optimal techniques

Optimal control is a branch of control theory that deals with finding the best possible control strategy for a dynamic system, subject to certain criteria or objectives. Finding control signals that will enable a process (plant) to meet certain physical restrictions and simultaneously extremize (maximize or minimize) a selected performance criterion (performance index or cost function) is the primary goal of optimum control. The plant P will be driven from its starting state to its end state with certain constraints on controls and states while simultaneously extremizing the provided performance index J, as shown in Figure. V.1 by the optimal control u*(t) (* denotes optimal condition). The optimal control is configured through the following criteria [173]:

- **Dynamic Systems:** Optimal control is commonly utilized in dynamic systems that undergo continuous evolution. The relationships between the system's state variables and control inputs can be represented using differential or difference equations, which can be used to explain these systems.
- **Control Inputs:** The parameters or variables that can be changed to affect how the system behaves are known as control inputs. To accomplish a particular goal, the optimum control issue entails determining the time-dependent values of various inputs.
- **Cost Function:** A mathematical formula known as the cost function is used to quantify the system's behaviour or performance. It is the standard that should be maximized or minimized. The precise objectives of the control problem determine which cost function should be used, and factors like energy usage, system stability, or other performance indicators may be taken into account.

- **Constraints:** The state variables and control inputs of the system are constrained in many real-world applications. These limitations could be related to operations, safety regulations, or physical limitations. Optimal control techniques must take these limitations into consideration.
- **Feedback Control:** Feedback mechanisms, in which control inputs are modified in real-time in response to the system's present state, are frequently used in optimal control solutions. The controller can adjust to changes in the system or outside disturbances thanks to this feedback.

The following are a few popular categories of optimization methods used in optimum control:

- **Dynamic Programming:** It is a technique for resolving complicated issues by dividing them into more manageable, overlapping sub-problems. Discrete-time, finite-horizon optimal control issues are frequently solved with it.
- **Pontryagin's Minimum Principle:** This concept, which bears the name of the Russian mathematician Lev Pontryagin, lays forth the prerequisites for optimality in optimal control problems. It is very helpful for a variety of applications and challenges involving continuous dynamics.
- **Linear Quadratic Regulator (LQR):** LQR is a type of optimal control technique used for linear systems with quadratic cost functions. It is well-suited for problems with continuous dynamics and is computationally efficient.
- **Model Predictive Control (MPC):** MPC is an advanced control strategy that involves solving an optimization problem at each time step based on a model of the system. It is widely used in process control, robotics, and automotive control systems.
- **Gradient-Based Optimization:** To optimize continuous functions, techniques like gradient descent and its variations, such the conjugate gradient method, are used. These are frequently applied to optimum control issues in continuous time.
- **Genetic Algorithms:** A class of evolutionary algorithms called genetic algorithms is motivated by natural selection. They can be used to discrete and continuous variables and are utilized in optimization problems.
- **Simulated Annealing:** A probabilistic optimization technique called "simulated annealing" was motivated by the metallurgical annealing procedure. It is very helpful in locating global optima in high-dimensional, intricate settings.
- **Interior-Point Methods:** An algorithmic class known as interior-point methods is applied to the solution of both linear and nonlinear optimization problems including equality and inequality constraints. They are frequently used in optimization with constraints.
- **Sequential Quadratic Programming (SQP):** SQP is an iterative optimization method that solves a set of quadratic sub-problems one after the other. It is frequently applied to the resolution of constrained, nonlinear optimization issues.

- **Particle Swarm Optimization (PSO):** PSO is an algorithm for population-based optimization that draws inspiration from fish and bird social behavior. It is frequently used to solve issues with continuous optimization.
- **Finite Element Method (FEM):** FEM is a numerical method for solving partial differential equations that is frequently used in engineering. It can be used to solve complex dynamics and constraint optimal control problems.
- **Mixed-Integer Linear Programming (MILP):** When some decision variables must accept integer values, MILP is employed. It is frequently used in discrete decision variable optimizations issues.

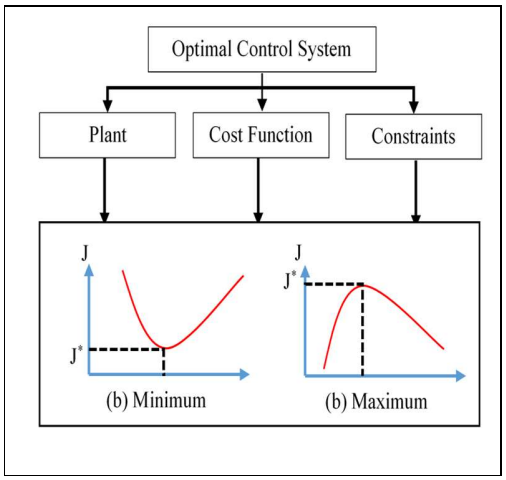

Figure V.1 Optimal Control Problem

V.3 Design of the LQR controller for the PMSM

In vector control theory, the linear quadratic regulator (LQR) strategy is a popular approach for resolving optimum control problems involving linear dynamic systems and quadratic performance requirements. It offers a refined and effective way to create control plans that maintain system stability while reducing overall costs. For linear systems with quadratic performance criteria, the LQR technique provides a mathematically beautiful solution. It is a reliable and effective method of achieving optimal control. Its continued importance in contemporary control theory is demonstrated by its broad usage and success in a variety of practical applications.

V.3.1 Definition of the LQR

LQR is indeed a well-established technique in control theory used for designing optimal feedback controllers for linear dynamic systems. It aims to minimize a quadratic cost function, typically representing a combination of control effort and system performance criteria. LQR provides feedback gains that stabilize the closed-loop system while optimizing a defined performance measure. It is widely applied across various fields due to its effectiveness and versatility in achieving stable and high-performance control designs for linear systems.

V.3.2 Principal of the LQR

The primary goal of LQR is to design control strategies that optimize system performance by minimizing a quadratic cost function while ensuring stability. Finding the best control input to minimize the total of the quadratic penalties related to the system's state and control input is the aim of the LQR problem, which frames the control task as a mathematical optimizations issue. The trade-off between minimizing control effort and attaining desirable system behavior is elegantly captured by this quadratic cost function. The calculus of variations and the concepts of dynamic programming are used to derive the LQR solution. The expression of the control law as a linear feedback function of the system's state provides the crucial insight. The corresponding algebraic Riccati equation is solved to compute the consequent state feedback gains, yielding a computationally efficient analytical solution. Because LQR is especially appealing for systems with linear dynamics, it can be used to a wide range of technical fields, such as robotics, process control, and aerospace. Its success in real-time applications can be attributed to its simplicity and computational efficiency. Desirable characteristics of LQR also include guaranteed stability and optimality under particular circumstances. For MIMO systems, the LQR control is necessary. It uses feedback control to calculate the matrix corrector (k) and regulate the input. Its job is to reduce the cost function, which has two major components. Performance stability determined by the Q matrix makes up the first section. Energy minimization based on the R matrix, the cost function provided in equation (V.1) [94,174,175], makes up the second section.

$$J = \int_0^\infty ((x^T . Q . x) + (u^T . R . u))dt \tag{V.1}$$

Where R and Q are both positive definite matrix.

The feedback control law that minimizes the value of the quadratic cost function is presented as follows:

$$u(t) = -k . x(t) = (-R^{-1} . B . P) . x(t) \tag{V.2}$$

Where P is positive definite matrix. Its solution given in the Algebra Riccati Equation (ARE) as follows:

$$\mathrm{A^T . P + P . A - P . B . R^{-1} . B^T . P + Q = 0} \tag{V.3}$$

The statement suggests that LQR control design is applied within the framework of a state-space model, with equation II.30 representing the dynamics of the system, and the LQR technique used to calculate feedback gains for optimal control:

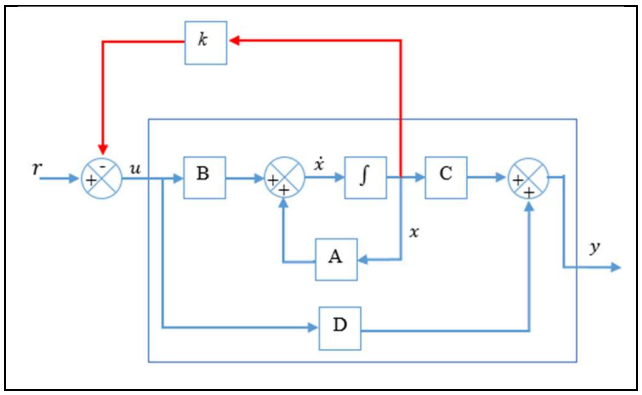

Figure V.2 LQR controller for SSM based system

V.3.3 Implementing LQR Control for PPMSM system

This study employs one of the best control strategies that have been suggested over the previous few decades in order to control the PMSM based on the virtual inputs received through the use of the nonlinear techniques approach (BSC, SMC, hybrid control) given in the previous chapter. Using a generated quadratic cost function and the system's linear state equation, this technique known as linear quadratic regulator (LQR) control uses an optimal control strategy to ensure dynamic system control. The LQR technique is a representative technique in modern control theory since it is robust against uncertainties and distractors for dynamic systems and has a high efficiency that leads to optimal system performance. Furthermore, the development of many methods with closed-loop features relies heavily on the LQR. Since the LQR technique has specific traits, it can be considered a feasible choice to combine the improvement of performance characteristics with the control of systems under uncertainties and disturbances [175,176,177]. The second chapter's "SSM" state space method (equation (II.30) should be used to construct the system in order to apply the LQR control. In this context, two designs have been applied based on the LQR techniques for the current loop of the PMSM.

- **Design of the current loop based on the 2nd order using the LQR:**

In this design, the PMSM's current loop model is built through the sum of both the linear model and the disturbances. For that, decoupling compensation is applied in order to apply the closed loop based on the novel control design. The disturbances have been presented in equation (II.27), and the linear model of the system is based on two state variables: direct and quadratic current. Therefore, the system model is designed as below:

$$\begin{cases} \frac{d}{dt}x_{dq}(t) = A.x_{dq}(t) + Bu_{dq}(t) \\ y_{dq}(t) = C.x_{dq}(t) + D.u_{dq}(t) \end{cases} \quad (V.4)$$

Based on equation (V.4), the internal model of the PMSM becomes as follows:

$$\begin{cases} \frac{d}{dt}[i_d \quad i_q]^T = \begin{bmatrix} -R_s/L_d & 0 \\ 0 & -R_s/L_q \end{bmatrix}.[i_d \quad i_q]^T + \begin{bmatrix} 1/L_d & 0 \\ 0 & 1/L_q \end{bmatrix}.[u_d \quad u_q]^T \\ [y_1 \quad y_2]^T = \begin{bmatrix} 1 & 0 \\ 0 & 1 \end{bmatrix}.[i_d \quad i_q]^T \end{cases} \quad \text{(V.5)}$$

In order to apply the LQR control, we should identified state variable vector $x_{dq}(t)$, input vector $u_{dq}(t)$, and the state matrix "A", input matrix "B". Therefore, they have designed as follows:

$$\begin{cases} A = \begin{bmatrix} -\mathrm{R_s/L_d} & 0 \\ 0 & -\mathrm{R_s/L_q} \end{bmatrix} \\ \mathrm{B} = \begin{bmatrix} 1/\mathrm{L_d} & 0 \\ 0 & 1/\mathrm{L_q} \end{bmatrix} \\ x_{dq}(t) = [i_d \quad i_q]^T \\ u_{dq}(t) = [u_d \quad u_q]^T \end{cases} \quad \text{(V.6)}$$

Through this identification, cost function (equation (V.1) based on the current loop model (equation (V.4) becames as follows:

$$J = \int_0^\infty (([i_d \quad i_q].Q.\begin{bmatrix} i_d \\ i_q \end{bmatrix}) + ([u_d \quad u_q].R.\begin{bmatrix} u_d \\ u_q \end{bmatrix}))dt \quad \text{(V.7)}$$

Where R and Q are both positive definite matrix (matrix (2×2)).

The feedback control law based on this control design become as follows:

$$u(t) = -k.\begin{bmatrix} i_d \\ i_q \end{bmatrix} = (-R^{-1}.B.P).\begin{bmatrix} i_d \\ i_q \end{bmatrix} \quad \text{(V.8)}$$

Where P is defined in the equation (V.3)

- **Design of the current loop based on the 4th order using the LQR:**

With this design, we will introduce a new variable state known as steady-state error as variable state (SS-LQR), which will enhance the internal linear model's performance features. Through the following formula defines the new state space model:

$$\begin{cases} \dot{x}_{dq}(t) = A.x_{dq}(t) + B.u_{dq}(t) \\ y_{dq} = C.x_{dq}(t) \\ \dot{\varepsilon}_{dq}(t) = r_{dq}(t) - C.x_{dq}(t) \end{cases} \quad \text{(V.9)}$$

Where: $r_{dq}(t) = [\mathrm{i_d}^* \quad \mathrm{i_q}^*]^\mathrm{T}$ and $\varepsilon_{dq}(\mathrm{t}) = [\varepsilon_d \quad \varepsilon_q]^\mathrm{T}$

Figure. V.3 illustrates the block schematic of this design:

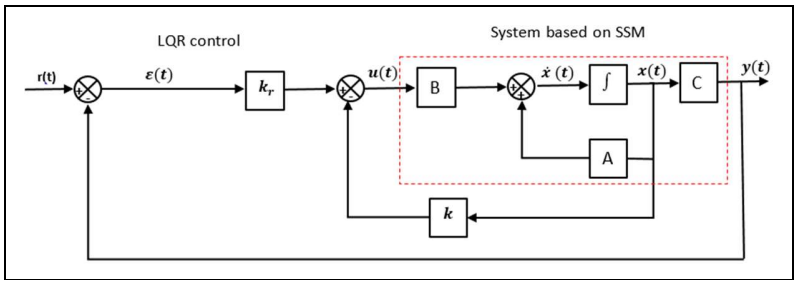

Figure V.3 : SS-LQR controller for SSM based system

The law of feedback control in this design provides as follows:

$$u_{dq}(t) = -k.x_{dq}(t) + k_r.\varepsilon_{dq}(t) \tag{V.10}$$

The new state space model provides in equation (V.11):

$$[\dot{x}_{dq}(t) \quad \dot{\varepsilon}_{dq}(t)]^T = \begin{bmatrix} A & 0 \\ -C & 0 \end{bmatrix}.[x_{dq}(t) \quad \varepsilon_{dq}(t)]^T + \begin{bmatrix} B \\ 0 \end{bmatrix}.[u_d \quad u_q]^T + \begin{bmatrix} 0 \\ I \end{bmatrix}.[{i_d}^* \quad {i_q}^*]^T \tag{V.11}$$

Where, I is identity matrix

The objective of redesigning the internal linear model based on the state feedback law is to eliminate steady-state errors and achieve asymptotic stability in system tracking. This entails ensuring that $x_{dq}(\infty)$, $\varepsilon_{dq}(\infty)$, and $u_{dq}(\infty)$converge to constant values. Additionally, the steady-state solution of equation (V.9) is represented by equation (V.12) below:

$$[\dot{x}_{dq}(\infty) \quad \dot{\varepsilon}_{dq}(\infty)]^T = \begin{bmatrix} A & 0 \\ -C & 0 \end{bmatrix}.[x_{dq}(\infty) \quad \varepsilon_{dq}(\infty)]^T + \begin{bmatrix} B \\ 0 \end{bmatrix}.[u_d(\infty) \quad u_q(\infty)]^T + \begin{bmatrix} 0 \\ I \end{bmatrix}.[{i_d}^*(\infty) \quad {i_q}^*(\infty)]^T \tag{V.12}$$

The reference vector represents the step vector, it is considered constant within each step. Which means that:

$$\begin{bmatrix} 0 \\ I \end{bmatrix}.[{i_d}^*(\infty) \quad {i_q}^*(\infty)]^T = \begin{bmatrix} 0 \\ I \end{bmatrix}.[{i_d}^*(t) \quad {i_q}^*(t)]^T = constant \quad \text{For } t > 0 \tag{V.13}$$

After that, the error dynamics are subtracted between values (t) and values (∞):

$$\begin{bmatrix} \dot{x}_{dq}(t) - \dot{x}_{dq}(\infty) \\ \dot{\varepsilon}_{dq}(t) - \dot{\varepsilon}_{dq}(\infty) \end{bmatrix} = \begin{bmatrix} A & 0 \\ -C & 0 \end{bmatrix}.\begin{bmatrix} (x_{dq}(t) - x_{dq}(\infty)) \\ \varepsilon_{dq}(t) - \varepsilon_{dq}(\infty) \end{bmatrix} + \begin{bmatrix} B \\ 0 \end{bmatrix}.\begin{bmatrix} (u_d(t) - u_d(\infty)) \\ (u_q(t) - u_q(\infty)) \end{bmatrix} \tag{V.14}$$

We put:

$$\begin{cases} \bar{x}_{dq}(t) = x_{dq}(t) - x_{dq}(\infty) \\ \bar{\varepsilon}_{dq}(t) = \varepsilon_{dq}(t) - \varepsilon_{dq}(\infty) \\ \bar{u}_{dq}(t) = u_{dq}(t) - u_{dq}(\infty) \end{cases} \tag{V.15}$$

To track a constant reference:

$$\begin{cases} y_{dq} = C.x_{dq}(\infty) + D.u_{dq}(\infty) \to r(t) \\ \dot{x}_{dq}(\mathrm{t}) = A.x_{dq}(\infty) + B.u_{dq}(\infty) \to 0 \end{cases} \tag{V.16}$$

From equation (V.15) and equation (V.16), we have:

$$\left[\dot{\bar{x}}_{dq}(\mathrm{t}) \quad \dot{\bar{\varepsilon}}_{dq}(\mathrm{t})\right]^{\mathrm{T}} = \begin{bmatrix} \mathrm{A} & 0 \\ -\mathrm{C} & 0 \end{bmatrix} . \left[\bar{x}_{dq}(t) \quad \bar{\varepsilon}_{dq}(\mathrm{t})\right]^{\mathrm{T}} + \begin{bmatrix} \mathrm{B} \\ 0 \end{bmatrix} . \left[\bar{u}_{dq}(t)\right]^{\mathrm{T}} \tag{V.17}$$

After that, the error vector is represented in equation equation (V.18):

$$e(t) = [\bar{x}(t) \quad \bar{\varepsilon}(\mathrm{t})]^{\mathrm{T}} \tag{V.18}$$

From the equation (V.17) and equation (V.18), the error dynamic is represented as follows:

$$\dot{e}_{dq}(t) = \bar{A} . e_{dq}(t) + \bar{B} . \bar{u}_{dq}(t) \tag{V.19}$$

Where:

$\bar{A} = \begin{bmatrix} \mathrm{A} & 0 \\ -\mathrm{C} & 0 \end{bmatrix}$, and $\bar{B} = \begin{bmatrix} \mathrm{B} \\ 0 \end{bmatrix}$

It is evident that the control law of the dynamic error represented in equation (V.19*)* can be described as:

$$\bar{u}_{dq} = -\bar{K} . e_{dq}(t) \tag{V.20}$$

Where $\bar{K} = [\bar{k} \quad -\bar{k}_r]$

However, from equation (V.19*)* and equation (V.20) the closed loop dynamic error is designed as follows:

$$\dot{e}(t) = (\bar{A} - \bar{B}\bar{K}) . e(t) \tag{V.21}$$

The direct and quadratic currents are decoupled from each other in equation (V.5) and equation (V.11); for this reason, equation (V.4) clarifies this decoupling based on optimal LQR control, whereby the linear state feedback law is designed as follows:

$$[u_d \quad u_q]^T = -[\bar{k} \quad -\bar{k}_r] . [i_d \quad i_q \quad \bar{\varepsilon}_d \quad \bar{\varepsilon}_q]^T \tag{V.22}$$

Where:

$$[\bar{k} \quad -\bar{k}_r] = \bar{R}^{-1} . \bar{B} . \bar{P} \tag{V.23}$$

Where $\bar{P}$ is a positive definite matrix. Its solution is given in the Algebra Riccati Equation (ARE) which represents the equation (V.3) with the new condition of steady state error. The current loop of the PMSM drive based on the SSE-LQR is designed as follows:

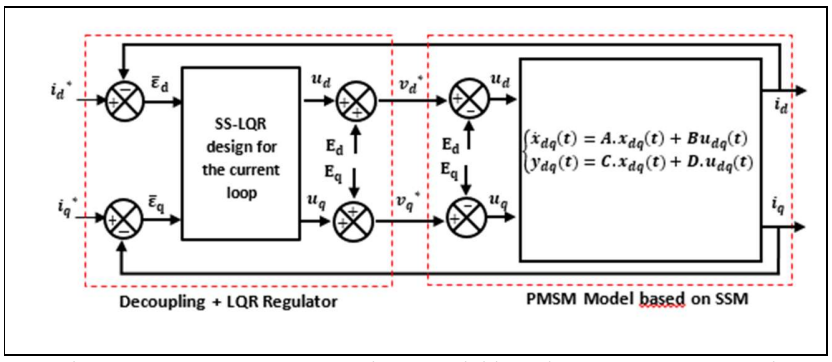

Figure V.4 : PMSM's current loop model based on SSE-LQR control

Figure. V.5 shows the simulation of the PMSM control architecture based on SSE-LQR:

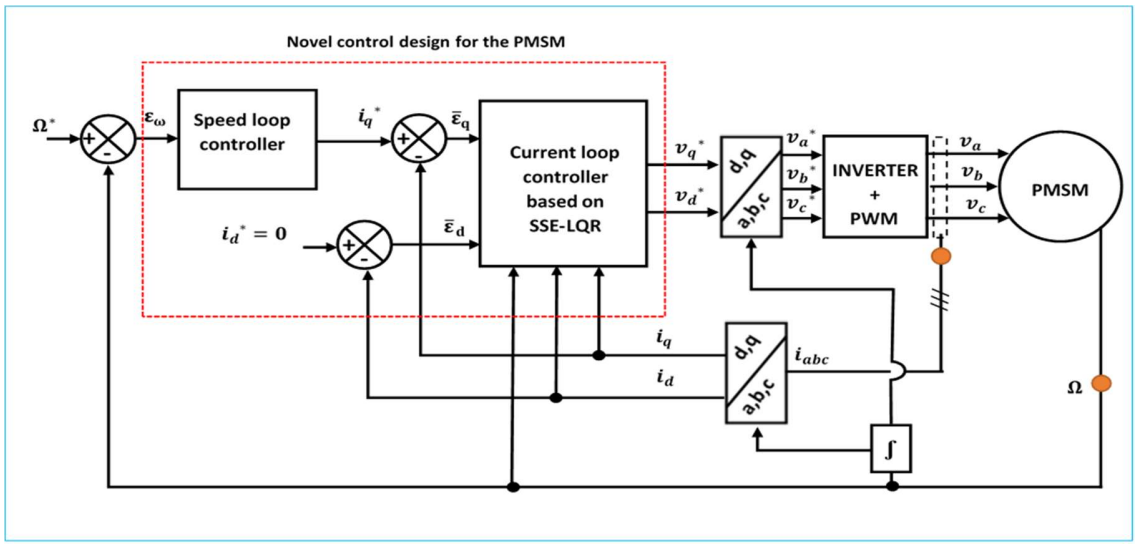

Figure V.5 The novel control design based on the SSE-LQR for the PMSM drive

V.4 Design of the MPC controller for the PMSM

MPC is one of the advanced control methods that is, more sophisticated than conventional PID control that has been effectively applied in industrial settings [178-180]. While MPC originated as an application of optimum control theory in the 1960s, industrial interest in these concepts dates back to the late 1970s [181]. Since then, the chemical process industry has effectively used MPC since time constants there are long enough to complete all necessary computations. The 1980s saw the introduction of MPC concepts into power electronics, with a focus on high-power systems with low switching frequencies [182]. At that time, the control algorithm's lengthy calculation time prevented the usage of higher switching frequencies. Nonetheless, within the last years, interest in the use of MPC in power electronics has grown significantly due to the advancement of quick and potent microprocessors. Rather than focusing on a single control approach, MPC provides a broad family of controllers [178]. There are numerous significant benefits to this control [184]:

- Concepts are very intuitive and easy to understand;
- It can be applied to a great variety of systems;
- The multivariable case can be easily considered;
- Dead times can be compensated;
- Easy inclusion of nonlinearities in the model;
- Simple treatment of constraints;
- The resulting controller is easy to implement;
- This methodology is suitable for the inclusion of modifications and extensions depending on specific applications.

V.4.1 Definition of the MPC

Predictive control is a model-based control strategy that utilizes a dynamic mathematical model of the system being controlled to predict future system behavior. It optimizes the control inputs over a specified time horizon, considering system dynamics, constraints, and desired objectives. The controller continually updates its predictions and optimization calculations in real-time, adapting to changes and disturbances to achieve optimal performance. Predictive control is widely used in complex systems where precise and adaptive control is required, such as in industrial processes, robotics, and energy systems.

V.4.2 Principal of the MPC

Common characteristics of this type of controller include choosing the best actuations by minimizing a cost function and using a system model to predict how the variables will behave in the future up to a predetermined time horizon. A summary of the MPC operating principle can be seen in Figure. V.6. Using the system model and the information (measurements) available up to time k, the future values of the system's states are projected until a predetermined horizon in time k + N. By minimizing the cost function, the sequence of optimal actuations is determined, and the first element of this series is applied. Every sampling instant, this entire procedure is repeated while taking the most recent measured data into account. The prediction model is a discrete-time model, which has the following state space expression [183,184]:

$$\begin{cases} x(k+1) = A.x(k) + Bu(k) \\ y(k) = C.x(k) + D.u(k) \end{cases} \quad \text{(V.24)}$$

It is necessary to define a cost function that reflects the desired system behavior. Future states, actuations, and references are taken into account by this function:

$$J = f(x(k), u(k), \dots\dots, u(k+N)) \quad \text{(V.25)}$$

The goal of the MPC optimization problem is to minimize the cost function J over a predetermined time horizon (N), taking into account the constraints and system model. A series of N optimum actuations is the outcome. Only the initial element in the sequence will be applied by the controller.

$$u(k) = [1\ 0 \dots 0]\, arg\, min_u J \quad \text{(V.26)}$$

Where the new measured data is used to solve the optimization issue once more at each sampling instant, producing a fresh set of ideal actuations every time. A tactic known as a receding horizon is this [184].

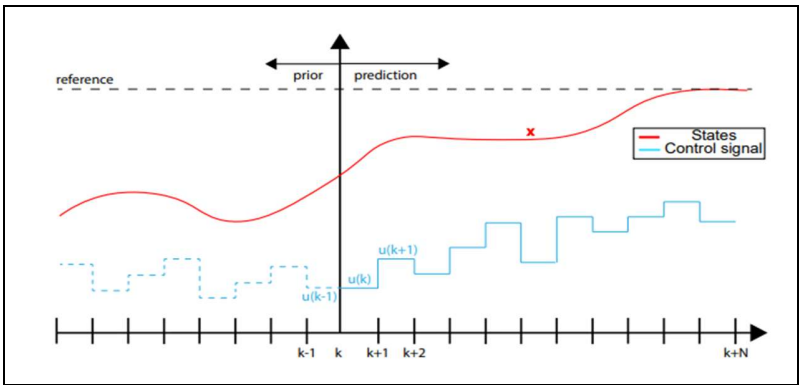

Figure V.6 : MPC principle of working

V.4.3 Application the MPC control on the PMSM system

The two primary categories of MPC methods are finite-control-set model predictive control (FCS-MPC) and continuous control set MPC (CCS-MPC). The benefits of CCS-MPC are its constant switching frequency and ease of incorporating nonlinearities and limitations [185]. However, utilizing a straightforward hardware platform, the entire control system cannot be implemented online. By using the restricted number of switching states in the FCS-MPC, the issue of computational optimization time is reduced. As a result, the FCS-MPC is easily implementable with basic hardware [186-188]. In order to obtain an optimized behavior of the system, the FCS-MPC offer high performance, fast response times, and the capacity to manage various variables and restrictions [189-192]. Despite its strength, the FCS-MPC has many limitations that make using it in drive systems extremely difficult [193]. A high steady state ripple is produced by the FCS-MPC when only one voltage vector (VV) is applied during a single control period [194-196]. Using a high sampling frequency is the way to have a high steady state control performance in FCS-MPC. But this approach requires expensive FPGA (Field Programmable Gates Array) or digital signal processor (DSP) hardware, as well as a significant computing load [197]. As a result, it is essential and desirable to enhance the steady state performance of the FCS-MPC algorithm without increasing the sample frequency. Ultimately, FCSMPC accounts for the converter's discrete nature. Because of this, FCS-MPC just uses the converter's actual states rather than the complete converter control area Figure. II.8 and Figure. II.17. The cost function may select the same discrete real state as the ideal state multiple times for this reason, which suggests that the FCS-MPC has a non-constant switching frequency [198,199]. In this section, the conventional FCS-MPC is presented as follows:

- **Traditional Finite-Control-Set Model Predictive Control (FCS-MPC):**

The permanent magnet synchronous motor in this project is connected to a widely used three-phase source inverter, as seen in Figure. II.8. There are eight distinct switching vectors in this inverter, which results in the production of eight voltage vectors, $u_0 - u_7$. Two zero vectors and six nonzero vectors are present. The amplitude of the active voltage vectors in the stationary reference frame αβ is displayed in Figure. II.8 and Table. V.1. A discrete time model is needed to forecast the currents at a future sample period in order to develop the conventional FCS-MPC. Hence, the

forward Euler method is applied to the time continuous model (1) with a sampling time period T_s [in s]. For small $T_s << 1$, the following holds $x(k)= x(kT_s) \approx x(t)$ and $\frac{d}{dt}x(t) = \frac{x(k+1)-x(k)}{T_s}$for all $t \in [kT_s, (k+1)T_s]$ and $k \in \mathbb{N} \cup \{o\}$. Therefore, the following expression can be used to describe the discrete time of the PMSM in the rotating (d-q) reference frame [200,201]:

$$\begin{cases} i_d(k+1) = \left(1 - \frac{R_s T_s}{L_d}\right) i_d(k) + T_s \omega_e(k) i_q(k) + \frac{T_s}{L_d} u_d(k) \\ i_q(k+1) = \left(1 - \frac{R_s T_s}{L_q}\right) i_q(k) - T_s \omega_e(k) i_d(k) + \frac{T_s}{L_q} u_q(k) - \frac{\psi_p T_s}{L_q} \omega_e(k) \end{cases} \quad \text{(V.27)}$$

The PMSM's stator voltage, v_{dq}, can be expressed as a function of the inverter's switching vector, $S_{abc}[k] \in \{0,1\}^3$. [183]:

$$v_{dq}(k) = T_p(\theta_e)^{-1}.T_C.\frac{1}{3}v_{dc}[k].v_{abc} \quad \text{(V.28)}$$

Where;

$$\begin{cases} T_p(\theta_e)^{-1} = \underline{T}_{dqo \to \alpha\beta o} \\ T_C = \underline{T}_{\alpha\beta o \to abc} \\ v_{abc} = \begin{bmatrix} 2 & -1 & -1 \\ -1 & 2 & -1 \\ -1 & -1 & 2 \end{bmatrix}.S_{abc}[k] \end{cases} \quad \text{(V.29)}$$

where, $\underline{T}_{dqo \to \alpha\beta o}$ and $\underline{T}_{\alpha\beta o \to abc}$ are inverse Park and Clarke transformations that mentioned in equation (II.13) and equation (II.22), respectively. v_{dc} is the DC-Bus voltage [in V] and v_{abc} is the stator voltage in the *abc* frame [in V]. $\theta_e = p\int \Omega$ is the electrical rotor position of the PMSM [in rad]. $S_{abc} = [S_a \quad S_b \quad S_c]^T$represent the switching states of each leg of the voltage source inverter as shown in Table 1[200].

Table V.1. Different switching modes and corresponding voltage vector of the voltage source converter

Conducting Modes	**Switching States**			**Output Voltage**	
	Sa	*Sb*	*Sc*	*Uα*	*Uβ*
U_0	0	0	0	0	0
U_1	1	0	0	$\frac{2V_{dc}}{3}$	0
U_2	1	1	0	$\frac{V_{dc}}{3}$	$\frac{\sqrt{3}V_{dc}}{3}$
U_3	0	1	0	$-\frac{V_{dc}}{3}$	$\frac{\sqrt{3}V_{dc}}{3}$
U_4	0	1	1	$\frac{2V_{dc}}{3}$	0
U_5	0	0	1	$-\frac{V_{dc}}{3}$	$-\frac{\sqrt{3}V_{dc}}{3}$
U_6	1	0	1	$\frac{V_{dc}}{3}$	$-\frac{\sqrt{3}V_{dc}}{3}$
U_7	1	1	1	0	0

The control scheme of the conventional finite-set MPC is depicted in Figure. V.7. The discrete-time predictive model predicts seven vectors in accordance with (equation (V.27). Next, over

the course of the sampling period, the seven predicted vectors are assessed to determine which states minimize the cost function and produce the lowest absolute error between the reference and predictive currents ($i_d[\mathrm{k}+1], i_q[\mathrm{k}+1]$) [197]. The definition of the cost function formula is:

$$g = \left|{i_d}^*[k+1] - i_d[k+1]_{u_{0,\dots 7}}\right| + \left|{i_q}^*[k+1] - i_q[k+1]_{u_{0,\dots 7}}\right|$$

$$+ \begin{cases} 0 \;\; if \;\; \sqrt{i_d[k+1]^2 + i_q[k+1]^2} \le i_{max} \\ \infty \;\; if \;\; \sqrt{i_d[k+1]^2 + i_q[k+1]^2} > i_{max} \end{cases} \qquad \text{(V.30)}$$

Where, the first part indicates the reduction of the reactive power, the second part is for the tracking of the torque producing current, and the last part is for the maximum allowable stator current of the PMSM. i_{max} is the maximum current allowed for the direct and quadrature axis d and q, respectively. ${i_d}^*[k+1]$ and ${i_q}^*[k+1]$ are the future reference currents predicted from the previous sampling instants $[k]$,$[k-1]$, and $[k-2]$ using Lagrange extrapolation as [183]. The decrease of reactive power is indicated in the first part, the tracking of the torque-producing current is indicated in the second part, and the maximum permissible stator current of the PMSM is indicated in the final part. The maximum current permitted for the quadrature axis (q) and the direct axis (d) is denoted by i_{max}. The future reference currents (${i_d}^*[k+1]$ and ${i_q}^*[k+1]$), are estimated using Lagrange extrapolation as [183] from the prior sampling instants $[k]$ ($[k-1]$, and $[k-2]$):

$${i_{dq}}^*[k+1] = 3{i_{dq}}^*[k] - 3{i_{dq}}^*[k-1] + {i_{dq}}^*[k-2] \qquad \text{(V.31)}$$

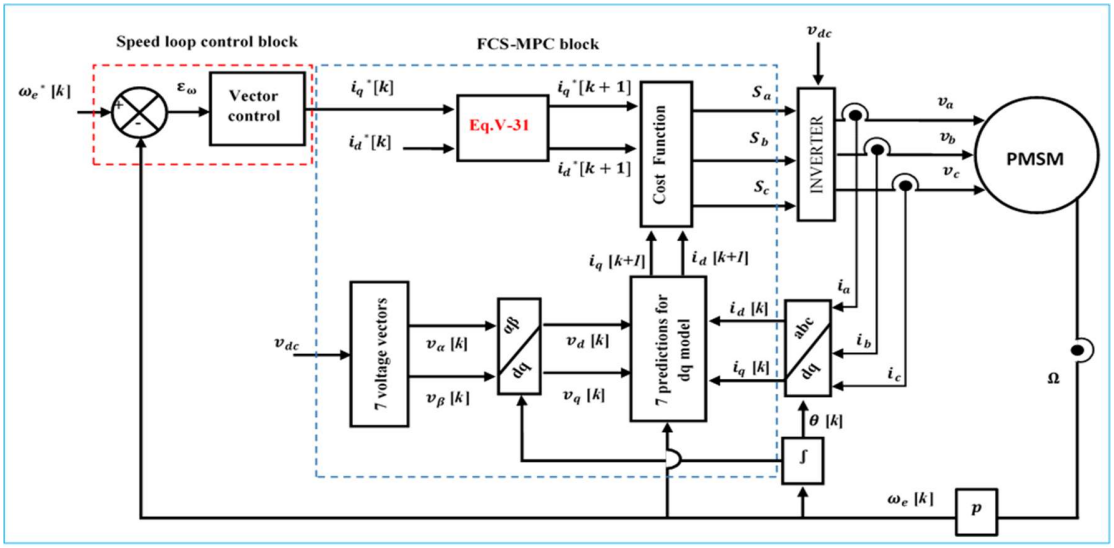

Figure V.7 : Conventional FCS-MPC (finite-control-set model predictive control) for a PMSM drive system

V.5 Simulation results and discussion

In order to demonstrate the effectiveness of the optimal controls studied in this chapter for the PMSM (SSE-LQR and FCS-MPC), a simulation model was built in Matlab/Simulink through

Figures. V.5 and V.7 for the SSE-LQR and FCS-MPC, respectively. Where the mentioned control is applied on the current loop of the PMSM, while the ERL-SMC is applied on the speed loop of the machine. Due to the fact that the quadratic current is linear with the electromagnetic torque, the reference quadratic current becomes the input to the speed loop, and the speed is the output of the speed loop. In other hand, the current loop has been designed to be MIMO, Where the inputs are the direct and quadratic voltages and the outputs are the direct and quadratic currents. To validate the optimal controls (SSE-LQR and FCS-MPC), some scenarios are presented to prove its effectiveness. The selection of these design parameters was based on a thorough analysis of PMSM performance using several criteria: stability, performance characteristics, robustness, cost function, and energy minimization. The PMSM parameters that were applied in this chapter are mentioned in Table. II.3. In the first scenario, the PMSM is operated in a stable state, where the speed is stabilized at the medium level (600 rpm) as well as applying a load torque estimated at 5 N.m. Through this scenario, speed, torque, and the direct and quadratic currents performances are all shown. In addition, the comparison study between the classical design of the PMSM drive based on the ERL-SMC and the novel design of the PMSM drive based on the hybrid control that was studied in this chapter (mentioned above). Through Figure. III.8(a), the speed performance demonstrates that the novel design-based on the SSE-LQR outperforms the FCS-MPC and the classical design-based on the ERL-SMC from the rise time (Tr) and the steady state error (SSE), where the rise time to the SSE-LQR is estimated to be 4 ms and the FCS-MPC is estimated to be 6 ms, while the ERL-SMC is estimated to be 12 ms. The steady-state error for the SSE-LQR is estimated at 0.006% and the FCS-MPC is estimated at 0.0078%, while the steady-state error for the ERL-SMC is estimated at 0.05%. %. Moreover, the novel design based on the SSE-LQR is stabilized without chattering, while the FCS-MPC and the ERL-SMC suffer from chattering, where the FCS-MPC's chattering is (+0.055 and -0.035) and the ERL-SMC's chattering is (+0.15 and -0.85).

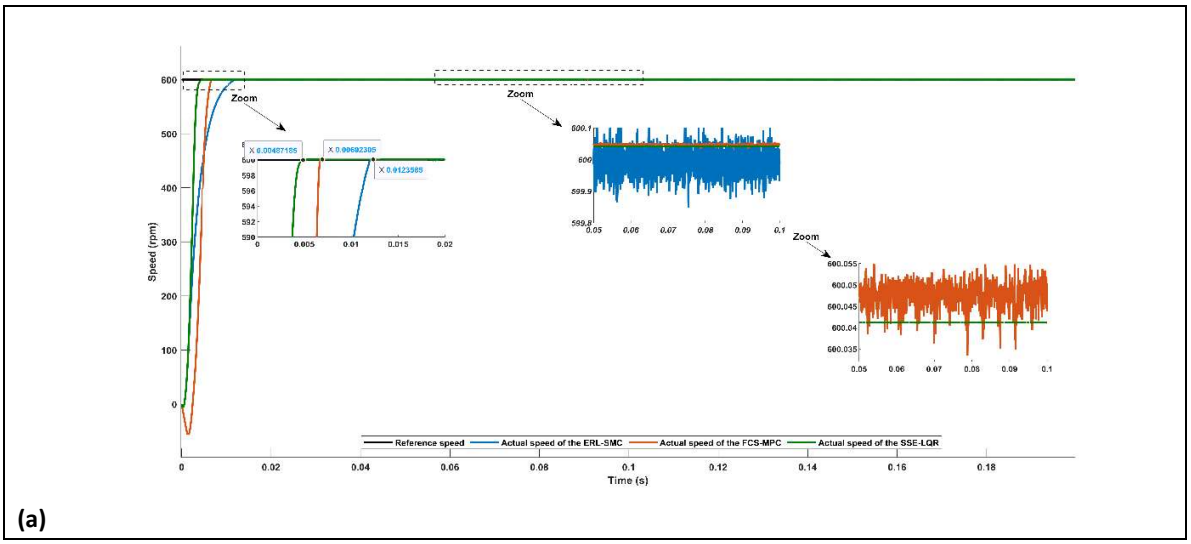

(a)

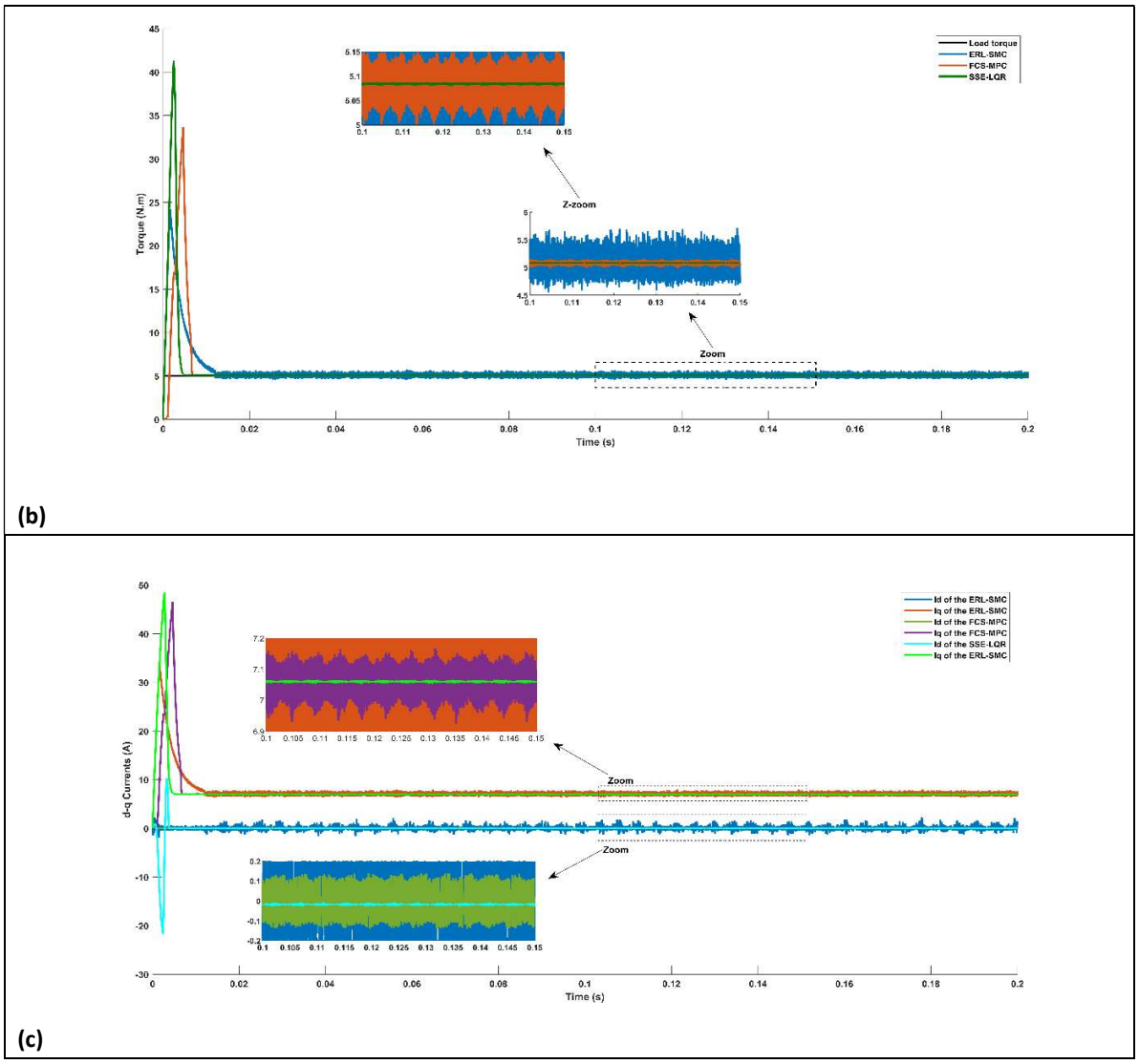

Figure V.8 : First scenario of the simulation (a) Speed (b) Electromagnetic torque (c) d-q currents

Regarding the electromagnetic torque performance of Figure. IV.8 (b), the novel design based on the SSE-LQR and FCS-MPC contributes to minimizing the torque ripple compared to the classic design based on the ERL-SMC, which suffers from a big torque ripple. Where the torque ripple of the novel design of the SSE-LQR is estimated between +0.1 and -0.1, the FCS-MPC's torque ripple is estimated between +0.15 and -0.15. While the ERL-SMC's torque ripple is estimated to be between +0.55 and -0.5. Furthermore, Figure. IV.8 (b) demonstrates the effectiveness of the novel design based on the optimal control for the direct and quadratic current performances. The tolerance band in the SSE-LQR is considered smaller than the FCS-MPC and ERL-SMC. The tolerance band of the direct current for the SSE-LQR is estimated between 0 and -0.01, for the FCS-MPC's it is estimated between +0.15 and -0.15, and for the ERL-SMC it is estimated between +0.5 and -0.5. In addition, these estimates also apply to the quadratic current. Moreover, the optimal control (SSE-LQR and FCS-MPC) has a big effect on the THD

criteria compared the nonlinear control (ERL-SMC). Where this criteria for the three controls has been computed, it was found that the estimates were judged as follows: SSE-LQR's THD is 1.58%, and FCS-MPC's THD is 3.83%. This is confirmed by Figure. V.9.

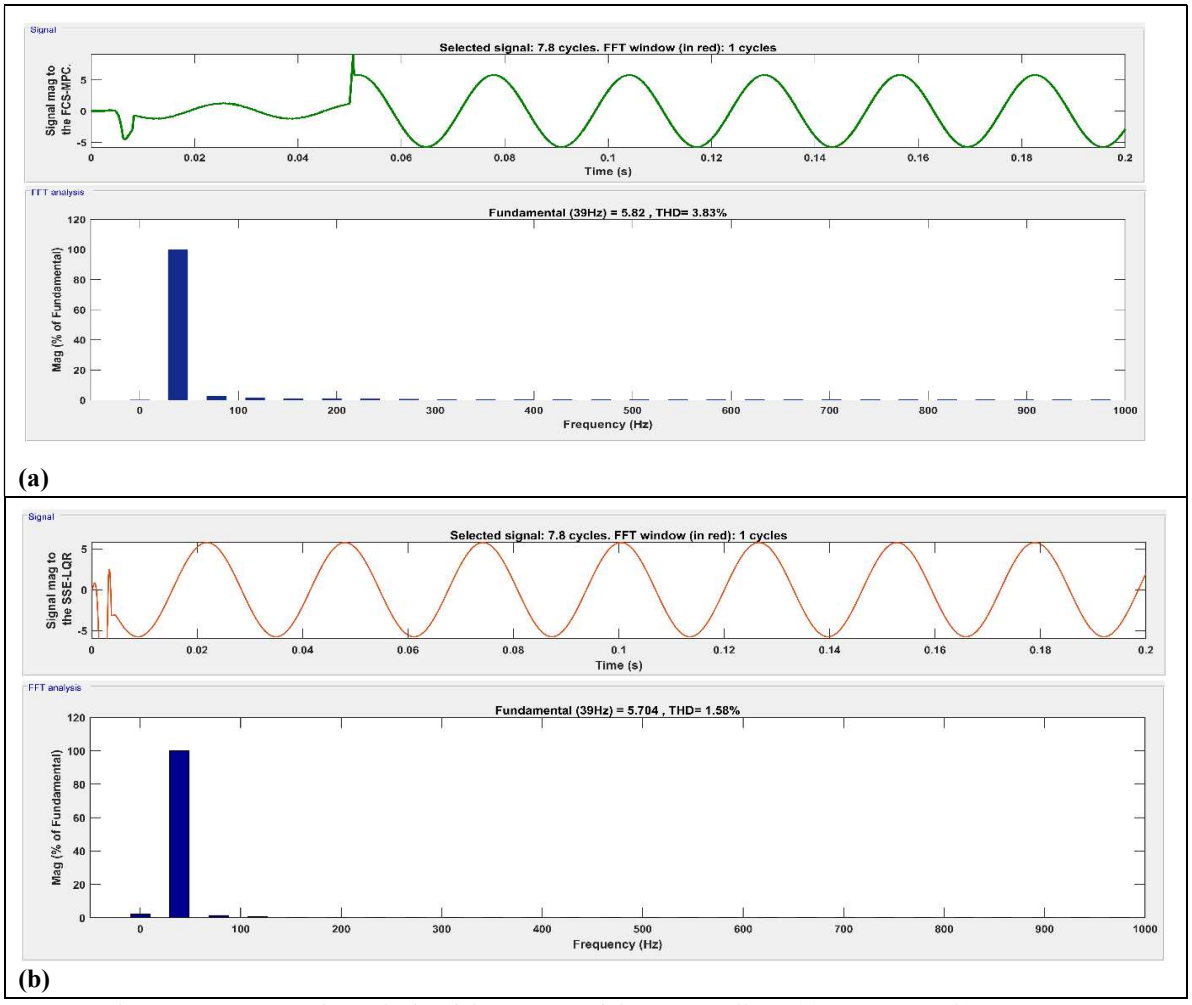

Figure V.9 : Harmonic analysis of the current of three controllers: (a) FCS-MPC (b) SSE-LQR

The second scenario has been presented in order to prove the robustness of the optimal controls (SSE-LQR and FCS-MPC) under an external disturbance. Therefore, a load torque with different values (1 N.m., 2 N.m., 5 N.m., and 3 N.m.) has been applied in different time instances, as seen in Figure. V.10 (b). Under this scenario, the speed performance is better when applying the novel control design based on the SSE-LQR and FCS-MPC compared to the classical control design based on the ERA-SMC, where the rise time stays the same as in the first scenario for each control while overshoots and undershoots appear in the speed performance during the load torque value change. The overshoots/undershoots rate reached on the SSE-LQR at 0.3%, which is smaller than the FCS-MPC at small percentages. While they take larger values when applying control, the ERL-SMC compared to the two controls mentioned above is estimated at 0.56%, this is demonstrated in Figure. V.10 (a). Regarding the electromagnetic torque performance that is represented in Figure. V.10 (a), the SSE-LQR is

better than the FCS-MPC, where the two are better than the ERL-SMC in very significant ways through the littler steady-state error and the littler chattering. Furthermore, the SSE-LQR is characterized by good performance through stability, which contributes to protecting the PMSM's operation from external disturbances as well as reducing power losses. In addition, it is seen in Figure. IV-10(c) that the SSE-LQR has good durability in the case of direct and quadratic currents, which give good-quality electrical power, less noise, less losses, and better stability under any external disturbances than the FCS-MPC and ERL-SMC, respectively.

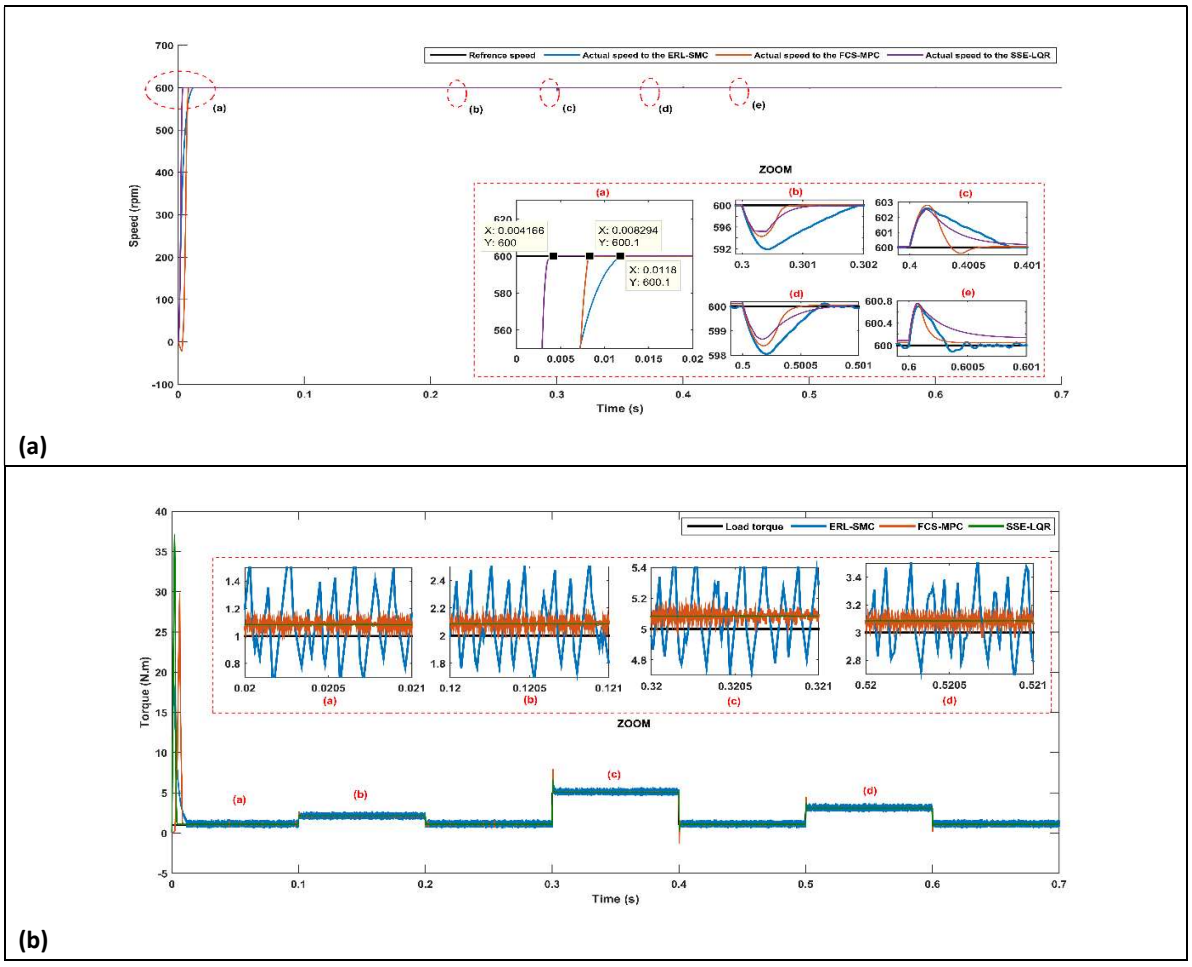

(a)

(b)

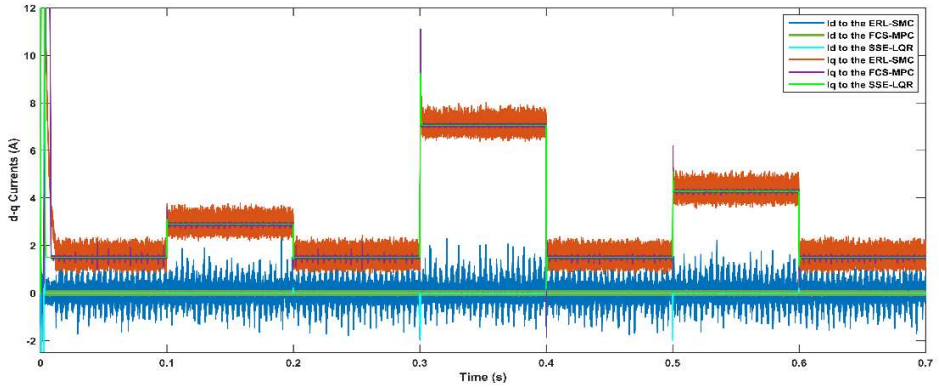

(c)

Figure V.10 : Second scenario of the simulation (a) Speed (b) Electromagnetic torque (c) d-q currents

About the three phases current performance has been designed to be better when applying the SSE-LQR, where this control contributes to minimizing the current oscillations as well as stabilizing the current performance in the same tolerance band during load torque changes, like what is presented in Figure. V.11(c). For the FCS-SMC, the current performance is affected little when the load torque is changed, while the FCS-MPC is given the worst performance for the three-phase current compared to the two controls mentioned above, where there is a bigger tolerance band as well as less stabilization during the changing of the load torque compared to the SSE-LQR and FCS-MPC. More detailed information about the current performance of the three controls is presented in Figure.V.10.

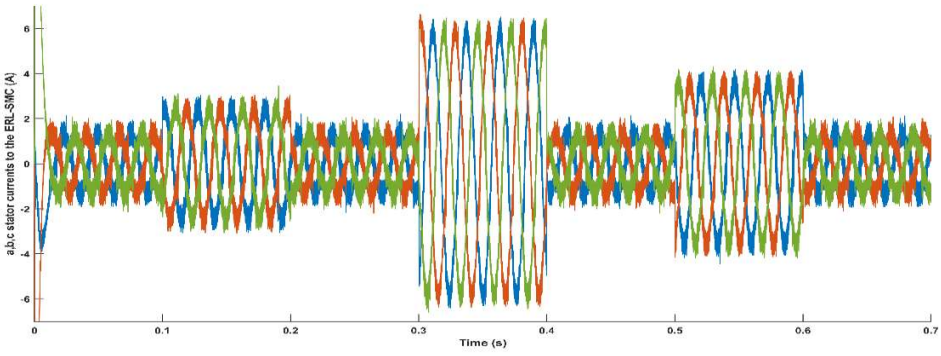

(a)

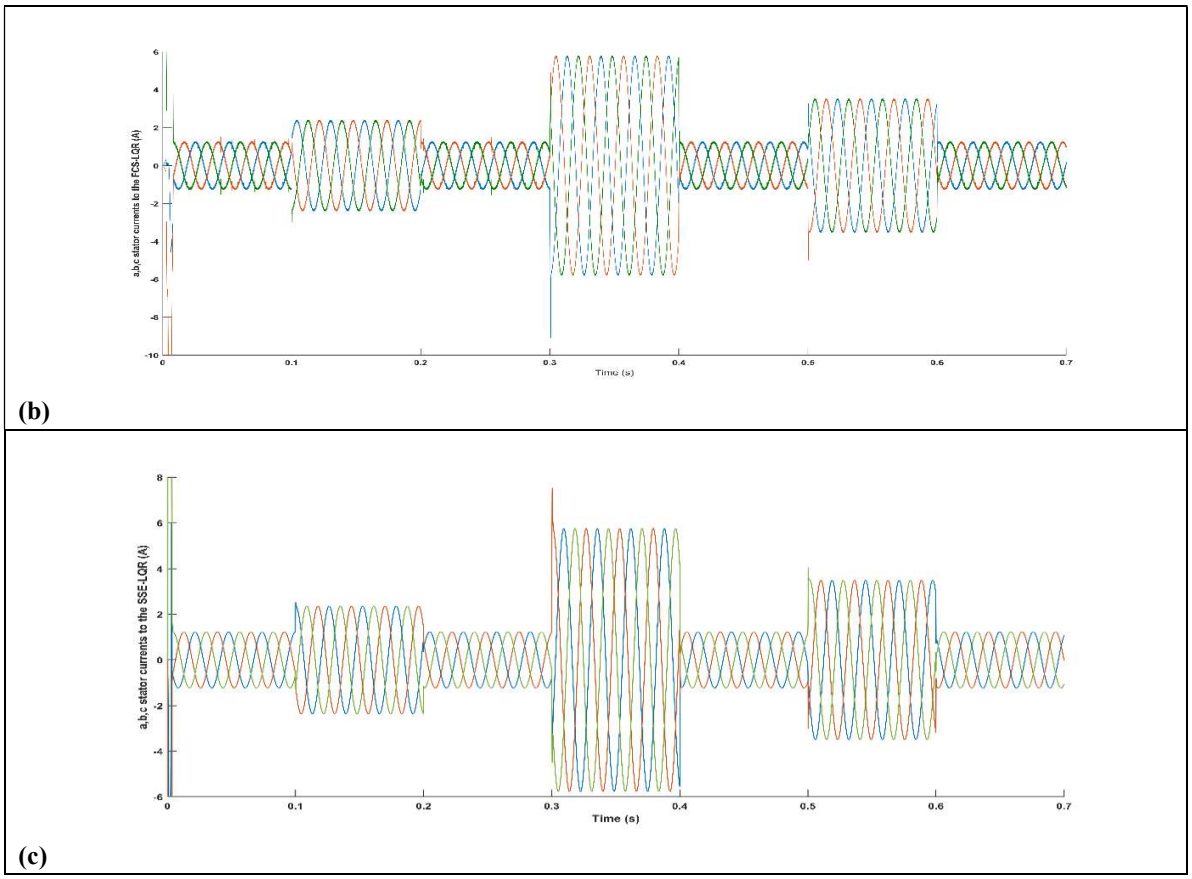

Figure V.11 : The three phases current of three controllers for the second scenario: (a) ERL-SMC (b) FCS-MPC (c) SSE-LQR

Just like what happened in the scenarios of the previous chapters, the robustness scenario for the novel design control based on the SSE-LQR and FCS-MPC is studied in this section, too. The change of PMSM parameters, which are resistance, direct-quadratic inductances, and inertia, to increasing rates was studied. Figure. V.12 shows this scenario; they are changed to 0%, 50%, 100%, 150%, and 200% with a medium speed (600rpm). The results shown in Figure. IV.12 showed that both techniques (SSE-LQR and FCS-MPC) were close after the robustness test. Figure. IV.12 (a) and Figure. IV.12 (b), respectively, demonstrate that the SSE-LQR is better than the FCS-MPC through the rise time. However, the FCS-MPC is better than the SSE-LQR through the uncertainty rate (UR) for the change in rise time between percentages of the PMSM parameters' changes mentioned above, where the UR of the FCS-MPC is estimated to be 0.004096s, while the SSE-LQR's UR is estimated to be 0.0049095s. In addition, the uncertainties between 0% and 200% are better for the FCS-MPC compared to the SSE-LQR, which are estimated to be 0.016384s and 0.019638s, respectively. On the other hand, the steady-state error is very small for both controls, with minor differences between them. The FCS-MPC is better than the SSE-LQR, where the percentage of the steady-state error between the reference speed and the 200% uncertainties for both is estimated at 0.025% and 0.05%, respectively, as well as between the reference speed and the 0% uncertainties, estimated at 0.008%, while the

percentage between the 0% and 200% uncertainties for both is estimated at 0.017% and 0.041%. However, the SSE-LQR is better than the FCS-MPC through the stability of the steady-state error, whereas the FCS-MPC suffers from the chattering to the speed performance, especially during the uncertainties phenomenon.

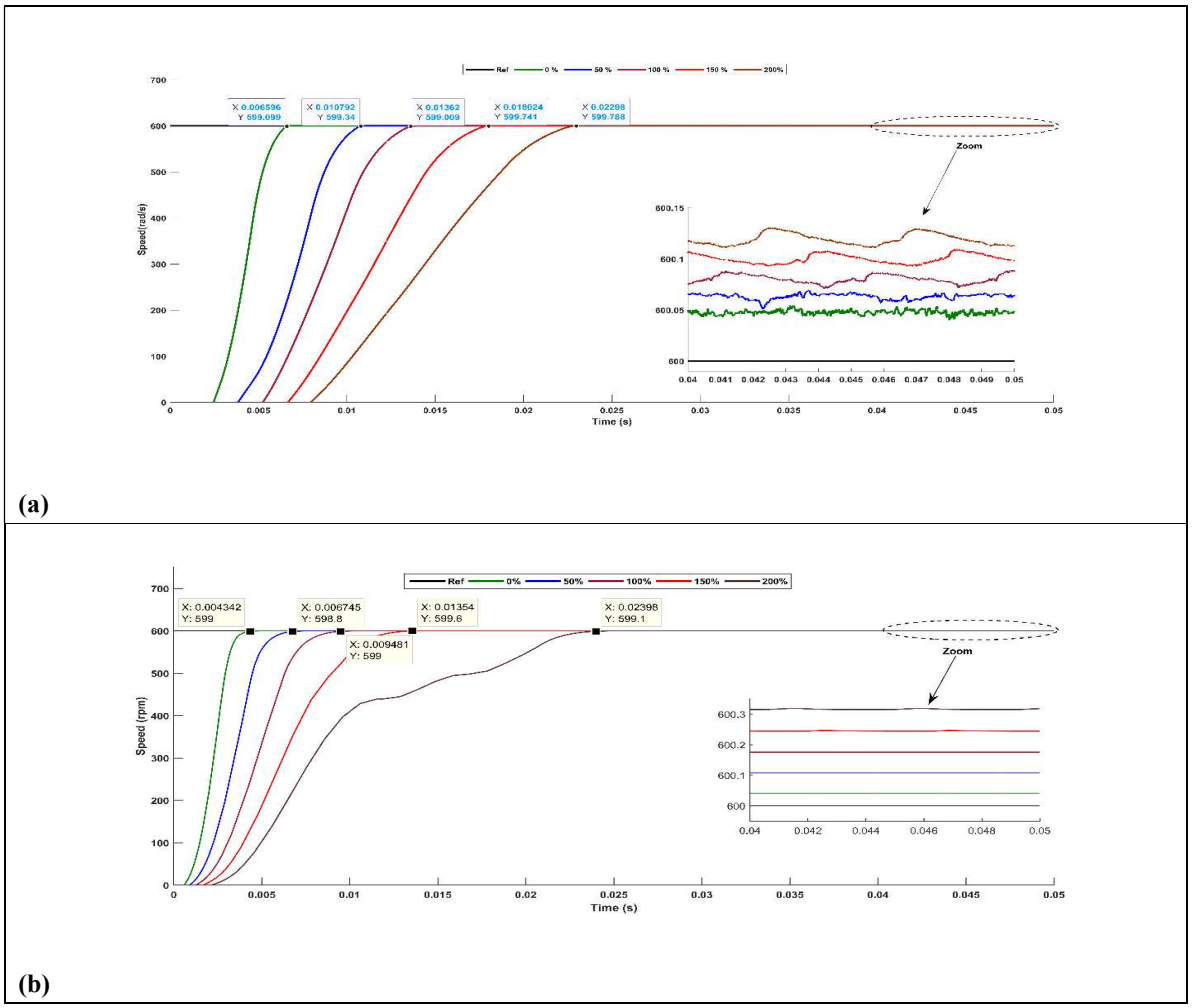

Figure V.12 : The novel control design based PMSM drive under the uncertainties; (a) FCS-MPC (b) SSE-LQR

The last scenario is testing the novel control design based on the SSE-LQR and FCS-MPC for the speed performance of the PMSM at high levels of speed. Furthermore, the two control designs mentioned above are compared to the classical control design based on the ERL-SMC. This scenario is considered one of the hardest due to the fact that the PMSM is operated with completely different speed ranges; each range represents an operation state, and between each state and another is a large rotation value. Under this scenario, the studied controls have been tested for their durability. Therefore, Figure. V.12 shows the PMSM adopts its high performance, where the speed level is varied between low (50 rpm), medium (375 rpm), and high speed (1000 rpm). We will also delve into the performance characteristics and phenomena that will hinder the PMSM's performance, and we will discover the flexibility of the control in responding to the change in speed level from one case to another.

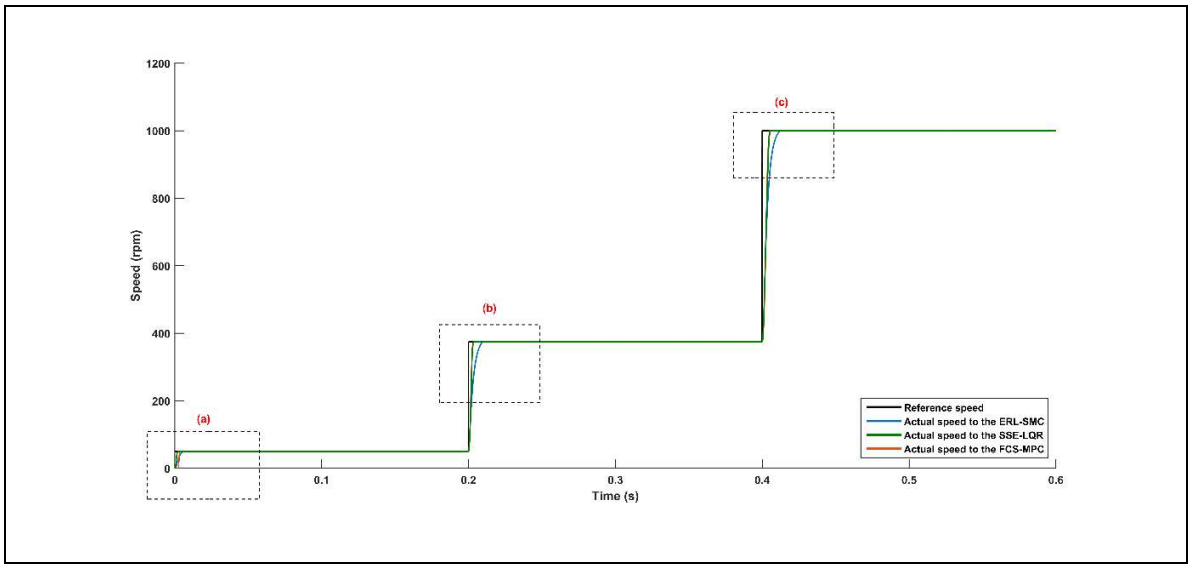

Figure V.13 High-performance PMSM speed levels

In order to determine which technique is better, we will comment on each speed level separately. Therefore, Figure. V.14 shows the region (a) presented in Figure. IV.13, where it presents the speed performance of the PMSM at low speed (50 rpm) with a comparative study among the techniques mentioned above. Depending on Figure. V.14 and Table.V.2, the novel control design based on the optimal controls mentioned above is better compared to the classical control design based on ERL-SMC from all the characteristics of performance and durability, where the SSE-LQR takes the littlest rise time, which is estimated at 2.4 ms, while the FCS-MPC has the smallest steady-state error, estimated at 0.02%. However, the SSE-LQR contributes to the best performance stability compared to the two controls mentioned above.

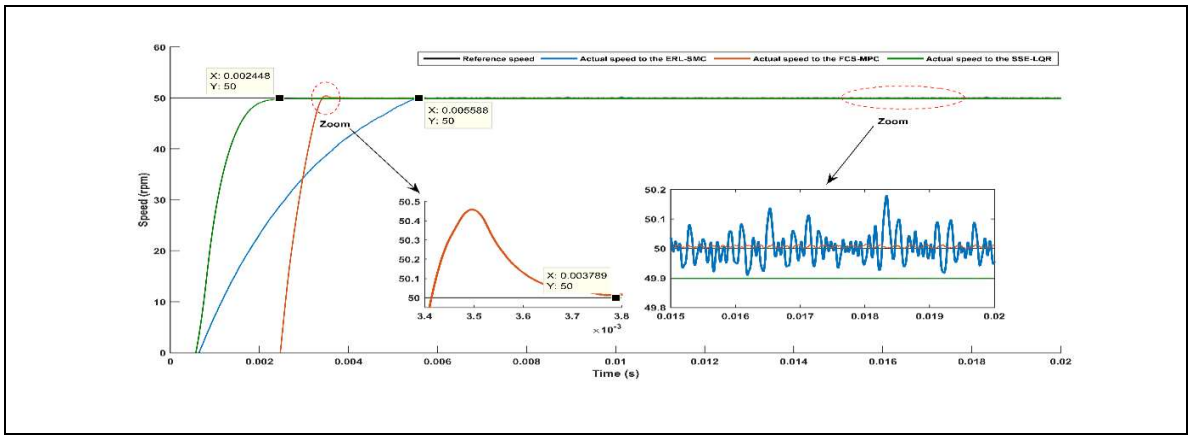

Figure V.14 : Enlargement of the performance characteristics of low speed (region (a) of Figure V.13)

The second level is to start up the meduim speed as well as express the PMSM speed, moving from the slow operation to the medium operation. Figure.V.15 and Table. IV.2 show the region (b) presented in Figure. V.13, which gives the second level of speed performance, which is characterised by the medium speed of the PMSM to 375 rpm. In this level, the novel design based on SSE-LQR takes the lead from speed performance characteristics compared to the other

controls, where the rise time of the speed during application is estimated to be 3ms, the steady state error is estimated to be 0.003%, and the stability performance is optimal during application of the SSE-LQR control. Through these results, the SSE-LQR is extremely suitable for the medium speed, especially when changing the speed from the low speed into the medium speed.

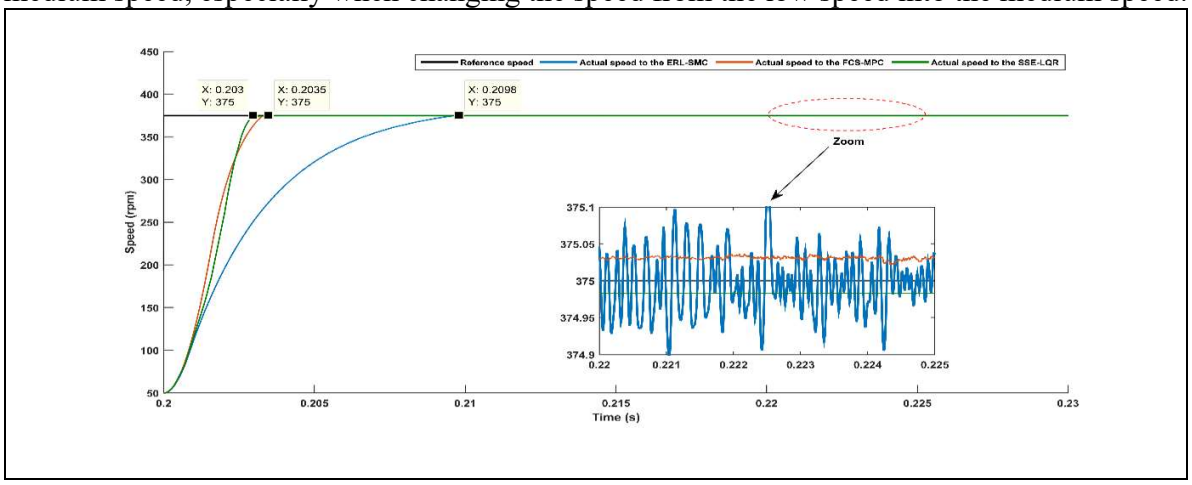

Figure V.15 : Enlargement of the performance characteristics of medium speed (region (b) of Figure V.13)

Figure. V.16 and Table. IV.2 show the region (c) presented in Figure. V.13, where it shows a change in speed to the third level, which represents the highest speed of the performance at 1000 rpm. Even with this sudden variation in PMSM speed from medium speed to high speed, the novel control design based on the SSE-LQR and FCS-MPC maintains superior durability to the characteristics of the PMSM compared to the classical control design based on the ERL-SMC. In a deep study of estimates of performance characteristics based on Figure. V.13, Figure. II.14, Figure II.15, Figure. II.16, and Table. III.2, the average rise time of each of the SSE-LQR, FCS-MPC, and ERL-SMC is estimated at 3.7 ms, 4 ms, and 9.2 ms, respectively. The average uncertainties of the speed performance of each control are estimated at 1.6 ms, 0.8 ms, and 3.3 ms. Therefore, the LQR-SSE is better than the others in most speed performance characteristics except for average uncertainties, where the FCS-MPC is suitable for speed performance.

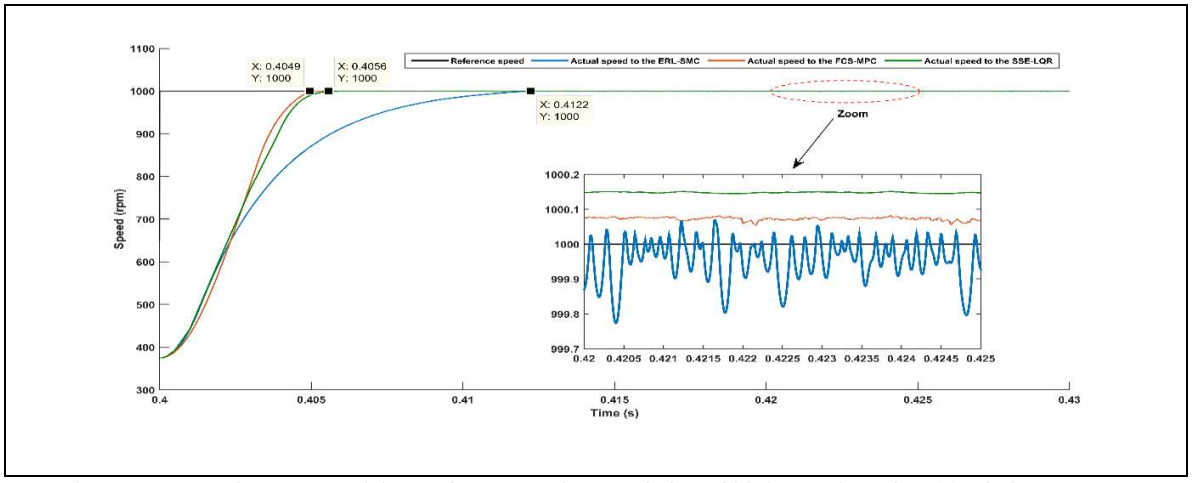

Figure V.16 : Enlargement of the performance characteristics of high speed (region (c) of Figure V.13)

Table V.2. Performance characteristics of speed PMSM model under variation of speed level

Performance characteristics		SSE-LQR	FCS-MPC	ERL-SMC
Rise Time *(ms)*	Low speed	2.448	3.789	5.588
	Medium speed	3	3.5	9.8
	High speed	5.6	4.9	12.2
Steady-state error (%)	Low speed	0.2	0.04	0.4
	Medium speed	.0003	0.01	0.03
	High speed	0.01	0.008	0.02
Performance Stability		Extremely stable	medium stable	Little stability

V.6 Conclusion

In the realm of Permanent Magnet Synchronous Motors (PMSM), the application of optimal control techniques plays a pivotal role in enhancing performance, efficiency, and reliability. The choice of optimal control methods, such as Model Predictive Control (MPC) or Linear Quadratic Regulator (LQR), depends on the specific requirements and characteristics of the PMSM system. Linear Quadratic Regulator control, tailored for linear systems, may find application in scenarios where the PMSM dynamics can be accurately modeled using linear equations. The elegance and simplicity of LQR make it a viable choice for certain PMSM configurations, especially when the system behavior closely aligns with linear assumptions. On the other hand, Model Predictive Control proves to be a compelling choice for PMSM applications due to its ability to systematically handle complex, nonlinear dynamics and constraints. By leveraging predictive models of the motor behavior, MPC allows for precise tracking of desired trajectories, efficient energy utilization, and effective management of system constraints. This makes MPC particularly suitable for applications where rapid response, disturbance rejection, and adaptability to varying operating conditions are essential, such as in electric vehicles, robotics, and industrial automation. MPC and LQR are presented in this chapter to address the PMSM current loop, where the sliding mode approach is used to address the speed loop. Additionally, we have enhanced the traditional finite-control-set model predictive control by employing multiple vectors (MV-FCS-MPC) and improved the conventional LQR by means of a novel design based on steady state as new state variables (SS-LQR). The ease of implementation, strong performance, and optimal characteristics offered by both techniques are the main reasons behind their application to the motor current loop. Moreover, the simulation results using MATLAB Simulink demonstrated that both techniques contributed to better performance characteristics, and they excelled at the robustness feature under the disturbances and uncertainties, as well as giving a high performance during the speed variation among different levels.

General Conclusion

In this comprehensive exploration of Permanent Magnet Synchronous Motor (PMSM) control, we embarked on a journey from understanding the fundamental principles to applying state-of-the-art techniques, striving to optimize the performance of PMSMs in various applications. The thesis delved into the realms of Field-Oriented Control (FOC) and Direct Torque Control (DTC), and extended to the realms of nonlinear and optimal control. The application of both FOC and DTC allowed for a thorough examination of the strengths and weaknesses inherent in these traditional control methods. Insights gained from these investigations formed the basis for pushing the boundaries towards more advanced techniques. The incorporation of nonlinear control techniques (FBLC, BSC and SMC) addressed challenges related to the inherently nonlinear nature of PMSMs. By leveraging advanced techniques, we achieved a more robust control strategy capable of handling complex motor behaviors and mitigating issues such as torque ripple. The exploration of optimal control strategies (MPC and LQR) aimed at maximizing efficiency and minimizing energy losses. This segment highlighted the significance of optimizing control parameters for improved overall system performance, emphasizing the crucial role of energy efficiency in contemporary PMSM applications. This not only contributed to cost-effectiveness but also demonstrated the adaptability of advanced control techniques in real-world scenarios. Through what was explained above, this thesis has two contributions for the PMSM, which can be summarized as follows:

1. The first contribution is a novel hybrid controller that was applied to a permanent magnet synchronous motor PMSM between the super-twisting algorithm based on high-order design (HO-STA) and terminal sliding mode control (T-SMC). On the other hand, it combines the benefits of both the super twisting algorithm (STA) and terminal sliding mode control while also taking into consideration their shortcomings. This proposed hybrid technique helps to gain robust control under variation between slow, medium, and high speed levels, regardless of what load torque is applied or whatever PMSM parameters change. It also offers optimum performance characteristics like a smaller settling time and steady state error. Moreover, it provides exceptional characteristics like fast finite-time convergence, stabilization of the performance, and its reaching law developer based on a new design, which contributes to reducing the chattering problems afflicted by C-SMC.
2. The development of the two most reliable vector optimal control strategies for the PMSM's current loop constituted the second contribution. The utilization of effective control approaches is crucial for improving performance, efficiency, and reliability in the domain of permanent magnet synchronous motors. The particular needs and features of the PMSM system determine which appropriate control strategies, such as linear quadratic regulators (LQR) or model predictive control (MPC), to use. Linear quadratic regulator control is intended for linear systems and may be useful in applications where PMSM dynamics can be accurately represented using linear equations. Because of its elegance and simplicity, LQR is a good choice for some PMSM designs, especially if the system behavior is expected to be linear. However, model predictive control seems to be a desirable solution

for PMSM applications due to its ability to carefully handle complex, nonlinear dynamics and limitations. By using predictive models of motor behavior, MPC allows for precise tracking of intended trajectories, economical energy consumption, and effective management of system constraints. As a result, MPC is particularly well suited for applications where quick response, resilience to disturbances, and adaptability to changing operating conditions are essential, such as industrial automation, robotics, and electric vehicles. The PMSM current loop is handled by MPC and LQR, while the speed loop is addressed by the sliding mode approach (ERL-SMC). Furthermore, we have employed conventional model predictive control based on the finite control set (FCS-MPC) and enhanced the standard LQR utilizing a novel design based on steady state as new state variables (SS-LQR). Their perfect features, robust performance, and ease of implementation are the main reasons to apply both techniques to the motor current loop.

All of the established objectives have been successfully met; this can be determined by contrasting the work presented in this thesis with the research goals stated in the introduction. This thesis serves as a testament to the continuous pursuit of excellence in PMSM control, showcasing the transformative power of advanced techniques in shaping the future of electric motor applications. As we conclude this thesis, it becomes evident that the journey into PMSM control is a dynamic and evolving field. The exploration of advanced techniques has not only provided solutions to existing challenges but has also raised new questions and possibilities.

Aspirations and Future Directions:

Owing to practical limitations with regard to the thesis organization, time, and resources, this study examined a number of areas of PMSM control employing innovative control design, most likely the most significant ones. It would be prudent, therefore, to verify this identity through experimental findings. All of this gives a lot of scope for the new research that can be done. Future research could delve deeper into the integration of emerging technologies such as machine learning and artificial intelligence for adaptive control, paving the way for intelligent and self-learning PMSM systems. Moreover, this research has far-reaching implications for the advancement of PMSM control strategies. The successful application of advanced techniques not only optimized motor performance but also laid the groundwork for future innovations in electric propulsion systems, renewable energy applications, and industrial automation. The following aspirations are some potential goals in the future:

1. Studying the novel control design that was applied in this thesis for the electrical vehicle;
2. Applying the studied controls to the wind energy system;
3. Design of the multi-PMSM for aeronautics;
4. Improving the photovoltaic pumping system using the PMSM based on the novel control design that was applied in this thesis.

BIBLIOGRAPHY

[1] Chau K, Li W, Lee C. Challenges and opportunities of electric machines for renewable energy (Invited Paper). Progress in Electromagnetics Research, B. 2012;42:45-74. DOI: 10.2528/PIERB1205200.

[2] Mecrow, B. C. and Jack, A. G. (2008) Efficiency trends in electric machines and drives. Energy Policy, 36, 4336–4341.

[3] Balashanmugham, A., & Maheswaran, M. (2019). Permanent-magnet synchronous machine drives. In Applied Electromechanical Devices and Machines for Electric Mobility Solutions. IntechOpen

[4] H. A-R,A.R,J.G. (2012).” HIGH PERFORMANCE CONTROL OF AC DRIVES WITH MATLAB/SIMULINK MODELS “India.

[5] Bimbra PS. Electric Machinery. 7th ed. Delhi, India: Khanna Publishers; 2011. p. 1060. ISBN: 978-8174091734.

[6] A. KADDOURI," Étude d'une commande non-linéaire adaptative d'une machine synchrone à aimants permanents", Thèse de doctorat Philosophie, Université LAVAL QUÉBEC Canada, 2000.

[7] Bernard, N. "Machine synchrone : de la boucle ouverte a l’autopilotage". Ecole Normale Supérieure de Cachan Campus de Ker Lann – 35170 BRUZ, Revue 3EI, n° 30, septembre 2002.

[8] G. Brando, L. Piegari and I. Spina, "Simplified Optimum Control Method for Mono-inverter Dual Parallel PMSM Drive," in IEEE Transactions on Industrial Electronics, vol. PP, no. 99, pp. 1-1.

[9] J.R. Hendershot. Brushless DC Motor Phase, Pole and Slot Configurations. Magna Physics Corporation, pages 1–8. URL http://www.jimhendershot.com/Jim_Hendershot/Articles_files/ brushlessdcmotorphasepoleslotconfigurations.pdf. Online; Accessed 22-January-2015.

[10] Liu, T. (2017). Control strategy for a mono-inverter multi-PMSM system-Stability and efficiency (Doctoral dissertation).

[11] Yongjae Lee and J. I. Ha, "Minimization of stator currents for mono inverter dual parallel PMSM drive system," 2014 International Power Electronics Conference (IPEC-Hiroshima 2014 - ECCE ASIA), Hiroshima, 2014, pp. 3140- 3144.

[12] Y. Lee and J. I. Ha, "Control Method for Mono Inverter Dual Parallel Surface-Mounted Permanent-Magnet Synchronous Machine Drive System," in IEEE Transactions on Industrial Electronics, vol. 62, no. 10, pp. 6096-6107, Oct. 2015.

[13] Önnheim, P., & Isaksson, H. (2015). High Precision Positioning and Very Low Velocity Control of a Permanent Magnet Synchronous Motor.

[14] B.Boukais, « Contribution a la modélisation des systèmes couples machines convertisseurs : application aux machines a aimants permanents (bdcm-pmsm) », Thèse de doctorat, UMMTO, 2012.

[15] K. Li, F. C. Chou and J. Y. Yen, "Real-Time, Energy-Efficient Traction Allocation Strategy for the Compound Electric Propulsion System," in IEEE/ASME Transactions on Mechatronics, vol. 22, no. 3, pp.

[16] T. M. Jahns, "Torque Production in Permanent-Magnet Synchronous Motor Drives with Rectangular Current Excitation," in IEEE Transactions on Industry Applications, vol. IA-20, no. 4, pp. 803-813, July 1984

[17] A. Akrad, M. Hilairet and D. Diallo, "Design of a Fault-Tolerant Controller Based on Observers for a PMSM Drive," in IEEE Transactions on Industrial Electronics, vol. 58, no. 4, pp. 1416-1427, April 2011.

[18] G.LACOMBE," Définition et Réalisation d’une Nouvelle Génération de Logiciels pour la Conception des Moteurs Futurs ", Thèse de doctorat, Institut National Polytechnique de Grenoble, 2007.

[19] Krishnamurthy P. Khorrami, F and H. Melkote. Modelling and Adaptive Nonlinear Control of Electric Motors. Springer, 2003. ISBN 3-540-00936-1.

[20] R.Lateb, « Modélisation des machines asynchrones et synchrones a aimants avec prise en compte des harmoniques d'espace et de temps : application à la propulsion marine par POD», Thèse de doctorat,Institut National Polytechnique de Lorraine, Nancy, France, 2006.

[21] G.Lacroux, '' Les aimants permanents '', Edition technique et documentation, 1989.

[22] D.C Hanselman. Brushless Permanent-Magnet Motor Design. R. R. Donnelley & Sons Compamy, 1994. ISBN 0-07-026025-7.

[23] Parviainen, A. (2005). Design of axial-flux permanent-magnet low-speed machines and performance comparison between radial-flux and axial-flux machines. Phd thesis, Lappeenranta University of Technology,Finland.

[24] ABB, 2004. Product Catalogue: DriveIT Permanent Magnet Motors

[25] Salminen, P., 2004. Fractional Slot Permanent Magnet Synchronous Motors For Low Speed Applications. Dissertation. Lappeenranta University of Technology, Finland, p. 150.

[26] Magnussen, F., Sadarangani, C., 2003a. Winding Factors and Joule Losses of Permanent Magnet Machines with Concentrated Windings. In Proceedings of IEEE Electric Machines and Drives Conference, IEMDC'03, Vol. 1, pp. 333-339.

[27] A.J. Mitcham, J.J. Cullen, « Motors and Drives for Surface Ship Propulsion- Comparison of Technologies », Electric propulsion the effective solution, 5-6 Octobre 1995, pp 4.1- 4.10.

[28] S. M. Husband, A. G. Hodge, « The Rolls-Royce Transverse Flux Motor Development », Electric Machines and Drives Conference, 2003. IEMDC'03. IEEE International, Publication Date: 1-4 June 2003, Volume: 3, pp 1435- 1440 vol.3.

[29] P. Lettelier, "Electrical Propulsion Motors", Electric Propulsion; The Effective Solution, IMarest Conference Proceedings, 5-6 October 1995. pp. 7.1-7.8.

[30] A.J. Mitcham, « Transverse Flux Motors for Electric Propulsion of Ships», IEE Colloquium on New Topologies for Permanent Magnet Machines (Digest N° 1997/090), Date: 18 Jun 1997, London, UK, pp 3/1- 3/6.

[31] R. Michaux, P.Letellier, « Les Machines Discoïdes à Champ Axial dans les Systèmes de Propulsion Électriques », REE N°3/1997, pp 37-42.

[32] A. Parvianen, J. Pyhönen, M. Niemelä, « Axial Flux Interior Permanent Magnet Synchronous Motor with Sinusoïdal Shaped Magnets », ISEF 2001, Cracovie, Pologne septembre 20-22, 6 pages.

[33] M. Olszewski, « Fractional-Slot Surface Mounted PM Motors with Concentrated Windings for HEV Traction Drives », Oak Ridge National Laboratory, report ONRL/TM-2005, pp 1-30.

[34] Heikkilä, T., 2002. Permanent Magnet Synchronous Motor for Industrial Inverter Applications – Analysis and Design. Dissertation. Lappeenranta University of Technology, Finland, p. 109.

[35] Wildi, T., & Sybille, G. (2005). Électrotechnique, 4 eme édition, de boeck.

[36] F. Caricchi, F. Crescimbini, E. Santini, Basic Principle and Design Criteria of Axial-Flux PM Machines Having Counterrotating Rotors, IEEE Transactions on Industry Applications, Vol. 31, pp. 1062-1068, 1995.

[37] F. Profumo, Z. Zhang, A. Tenconi, Axial Flux Machines Drives: A New Viable Solution for Electric Cars, IEEE Transactions on Industrial Electronics, Vol. 44, pp. 39-45, 1997.

[38] J.F. Gieras, M. Wing, Permanent Magnet Motor Technology- Design and Applications, New York: Marcel Dekker Inc, 1997, pp. 242-277.

[39] Z. Zhang, F. Profumo, A. Tenconi, Design of an Axial Flux Interior PM Synchronous Motor with a Wide Speed Range, Proceedings of International Conference on Electrical Machines, Vol. III, pp. 273-278, 1996

[40] Qu, R., Aydin, M., Lipo, T.A., 2003. Performance Comparison of Dual-Rotor Radial-Flux and AxialFlux Permanent-Magnet BLDC Machines. In Proceedings of IEEE Electric Machines and Drives Conference, IEMDC'03, Madison, United States, 1-4 June 2003, Vol. 3, pp. 1948- 1954.

[41] Magnussen, F., Thelin, P., Sadarangani, C., 2003b. Design of Compact Permanent Magnet Machines for a Novel HEV Propulsion System. In Proceedings of the 20th International Electric Vehicle Symposium

(EVS) and Exposition, on CD-ROM.

[42] Mendoza, C. E. A. (2022). Control strategies for permanent magnet synchronous machines without mechanical sensors by sliding modes (Doctoral dissertation, École centrale de Nantes; Universidad autónoma de Nuevo León).

[43] S. Singh and A. Tiwari, « Various techniques of sensorless speed control of pmsm: a review », in 2017 Second International Conference on Electrical, Computer and Communication Technologies (ICECCT), IEEE, 2017, pp. 1–6.

[44] Jawad Ahmed FAROOQ : Etude du problème inverse en électromagnétiques en vue de la localisation des défauts de désaimantation dans les actionneurs à aimant permanents. Thèse de doctorat, Université BELFORT-MONTBELIARD ,5 décembre 2008.

[45] Campbell, P., 1974. Principles of a Permanent-Magnet Axial-Field D.C. Machine. Proceedings of the IEE, Vol. 121, No. 12, pp. 1489-1494.

[46] Kurronen, P., 2003. Torque Vibration Model of Axial-Flux Surface-Mounted Permanent Magnet Synchronous Machine. Dissertation. Lappeenranta University of Technology, Finland, p. 123.

[47] Huang, S., Aydin, M., Lipo, T.A., 2001. TORUS Concept Machines: Pre-Prototyping Design Assessment for Two Major Topologies. In Proceedings of IEEE Industry Applications Conference, ThirtySixth IAS Annual Meeting. Vol. 3, p. 1619-1625.

[48] Aydin, M., Huang, S., Lipo, T.A., 2001. Design and 3D Electromagnetic Field Analysis of Non-slotted and Slotted TORUS Type Axial-flux Surface-mounted Permanent Magnet Disc Machines. In Proceedings of IEEE Electric Machines and Drives Conference, IEMDC'01, pp. 645-651.

[49] Parviainen, A., Pyrhönen, J., Niemelä, M., 2002a. Axial-flux Permanent Magnet Synchronous Motor With Sinusoidally Shaped Magnets. Studies in Applied Electromagnetics and Mechanics, Vol. 22, pp. 271- 276. Amsterdam, The Netherlands: IOS Press.

[50] Profumo, F., Tenconi, A., Zhang, Z., Cavagnino, A., 1998. Novel Axial-flux Interior PM Synchronous Motor Realized with Powdered Soft Magnetic Materials. Industry Applications Conference, 1998. In Proceedings of IEEE Industry Applications Conference, Thirty- Third IAS Annual Meeting. Vol. 1, p.152- 158.

[51] Sahin, F., 2001. Design and Development of a High-Speed Axial Flux Permanent-Magnet Machine, Dissertation. Eindhoven University of Technology, The Netherlands, p. 228.

[52] Spooner, E., Chalmers, B.J., 1988. Toroidally-wound, slotless, axial-flux permanent magnet, Brushless-DC motor. In Pr oceedings of International Conference on Electrical Machines, ICEM'88, Pisa, Italy, 1988. pp. 81-86.

[53] Braid, J., van Zyl, A., Landy, C., 2003. Unbalanced Load Sharing in a Prototype Multistage Axial-Flux Permanent Magnet Synchronous Machine. In Proceedings of IEEE Electric Machines and Drives Conference, IEMDC'03, Madison, United States, 1-4 June 2003, Vol. 3, pp. 1935-1940.

[54] El-Hasan, T.S., Luk, P.C.K., Bhinder, F.S., Ebaid, M.S., 2000. Modular Design of High-Speed PermanentMagnet Axial-Flux Generators. IEEE Transactions on Magnetics, Vol. 36, No. 5, pp. 3358-3561.

[55] Carrichi, F., Crescimbini, F., Honorati, O., 1998. Low-Cost Compact Permanent Magnet Machine for Adjustable-Speed Pump Application. IEEE Transactions on Industry Applications, Vol. 34, No. 1, pp. 109- 116

[56] El-Shahat, A. (2018). Introductory Chapter: Electric Machines for Smart Grids and Electric Vehicles Applications. IntechOpen. doi: 10.5772/intechopen.80659.

[57] Karboua, D., Toual, B., Kouzou, A., Douara, B. O., Mebkhouta, T., Bendenidina, A. N. "High-order Suppertwisting Based Terminal Sliding Mode Control Applied on Three Phases Permanent Synchronous Machine", Periodica Polytechnica Electrical Engineering and Computer Science, 67(1), pp. 40–50, 2023. https://doi.org/10.3311/PPee.21026.

[58] Makrygiorgou, J.J.; Alexandridis, A.T. Power Electronic Control Design for Stable EV Motor and Battery Operation during a Route. Energies 2019, 12, 1990. [CrossRef].

[59] Pamuła, T.; Pamuła, W. Estimation of the Energy Consumption of Battery Electric Buses for Public Transport Networks Using Real-World Data and Deep Learning. Energies 2020, 13, 2340. [CrossRef].

[60] Andwari, A.M.; Pesiridis, A.; Rajoo, S.; Martinez-Botas, R.; Esfahanian, V. A Review of Battery Electric

Vehicle Technology and Readiness Levels. Renew. Sustain. Energy Rev. 2017, 78, 414–430. [CrossRef].

[61] Pellegrino, G.; Vagati, A.; Boazzo, B.; Guglielmi, P. Comparison of Induction and PM Synchronous Motor Drives for EV Application Including Design Examples. IEEE Trans. Ind. Appl. 2012, 48, 2322–2332. [CrossRef].

[62] Mokrani, Z.; Rekioua, D.; Mebarki, N.; Rekioua, T.; Bacha, S. Proposed energy management strategy in electric vehicle for recovering power excess produced by fuel cells. Int. J. Hydrog. Energy 2017, 42, 19556– 19575. [CrossRef].

[63] Kakouche, K.; Oubelaid, A.; Mezani, S.; Rekioua, D.; Rekioua, T. Different Control Techniques of Permanent Magnet Synchronous Motor with Fuzzy Logic for Electric Vehicles: Analysis, Modelling, and Comparison. Energies 2023, 16, 3116. https://doi.org/10.3390/en16073116.

[64] Shanker, T., & Singh, R. K. (2012, March). Wind energy conversion system: A review. In 2012 Students Conference on Engineering and Systems (pp. 1-6). IEEE.

[65] http://www.fnh.org/francais/doc/en_ligne/energie/dossier_intro.htm (Energies Renouvelables 2001).

[66] Zhao, Y.; Wei, C.; Zhang, Z.; Qiao, W. A review on position/speed sensorless control for permanent magnet synchronous machine-based wind energy conversion systems. IEEE J. Emerg. Sel. Top. Power Electron. 2013, 1, 203–216. 10.

[67] Mourabit, Y.E.; Derouich, A.; Allouhi, A.; Ghzizal, A.E.; Ouanjli, N.E.; Zamzoumyes, O. Sustainable production of wind energy in the main Morocco's sites using permanent magnet synchronous generators. Int. Trans. Electr. Energy Syst. 2020, 30, e12390. https://doi.org/10.1002/2050-7038.12390.

[68] Bossoufi, B.; Karim, M.; Lagrioui, A. Contribution à la commande de la Machine Synchrone à Aimant Permanent, Utilisation des Solutions Numériques FPGA; Presses Académiques Francophones (PAF): Allemagne, 2015; p. 184.

[69] Bossoufi, B. Contrôle des Machines Electriques et Convertisseurs de Puissance; Editions Universitaires Européennes: Allemagne, 2020

[70] Bekiroglu, E.; Yazar, M.D. MPPT Control of Grid Connected DFIG at Variable Wind Speed. Energies 2022, 15, 3146. https://doi.org/10.3390/en15093146.

[71] Kifel D, Urbanek S, Ponick B. Design study on additive manufacturing technologies in permanent magnet synchronous machines for electric aircraft. In: 2021 IEEE Workshop on Electrical Machines Design, Control and Diagnosis (WEMDCD). IEEE; 2021. p. 325–330.

[72] Giangrande P, Madonna V, Sala G, Kladas A, Gerada C, Galea M. Design and testing of PMSM for aerospace EMA applications. In: IECON 2018-44th Annual Conference of the IEEE Industrial Electronics Society. IEEE; 2018. p. 2038–2043.

[73] Setlak L, Ruda E. Review, Analysis and Simulation of Advanced Technology Solutions of Selected Components in Power Electronics Systems (PES) of More Electric Aircraft. In: 17th International Conference on Electrical Power and Energy Systems (ICEPES 2015), Spain. vol. 9; 2015

[74] Barzkar A, Ghassemi M. Electric power systems in more and all electric aircraft: A review. IEEE Access. 2020; 8:169314–169332. https://doi.org/10.1109/ACCESS.2020.3024168.

[75] Zhao T, Wu S, Cui S. Multiphase PMSM with asymmetric windings for more electric aircraft. IEEE Transactions on Transportation Electrification. 2020; 6(4):1592–1602. https://doi.org/10.1109/TTE. 2020.2997609

[76] Mendoza, C. E. A. (2022). Control strategies for permanent magnet synchronous machines without mechanical sensors by sliding modes (Doctoral dissertation, École centrale de Nantes; Universidad autónoma de Nuevo León).

[77] Jacob, J. High-speed control issues and advanced self-commissioning techniques for Permanent Magnet Synchronous Motors (Doctoral dissertation, Free University of Bozen-Bolzano).

[78] Chattopadhyay, S., Mitra, M., Sengupta, S., Chattopadhyay, S., Mitra, M., & Sengupta, S. (2011). *Electric power quality* (pp. 5-12). Springer Netherlands.

[79] Fitzgerald and Kingsley's Electric Machinery. McGraw-Hill Education, 2013.

[80] F. Zhao, L. U. O. Wen, G. A. O. Fengyang, and Y. U. Jiale , "Improved control strategy for PMSM based on fuzzy sliding mode ① control and sliding-mode observer." Journal of Measurement Science and Instrumentation, 2021,12(4):433-441.

[81] ABDESSAMED, R. (2011). Modélisation et simulation des machines électrique. livre en électrotechnique, Ellipses Edition Marketing S, A, 2011, Paris.

[82] P. Pillay and R. Krishnan, "Modeling of permanent magnet motor drives", IEEE Transactions on Industrial Electronics, vol. 35, no. 4, pp. 537-541, November 1988.

[83] T. Boileau, N. Leboeuf, B. Nahid-Mobarakeh and F. Meibody-Tabar, "Online identification of PMSM parameters: parameter identifiability and estimator comparative study", IEEE Transactions on Industry Applications, vol. 47, no. 4, pp. 1944-1957, July/August 2011.

[84] H. Chaoui and P. Sicard, "Adaptive fuzzy logic control of permanent magnet synchronous machines with nonlinear friction", IEEE Transactions on Industrial Electronics, vol. 59, no. 2, pp. 123-1133, February 2012.

[85] P. Pillay and R. Krishnan, "Modeling, simulation, and analysis of permanent-magnet motor drives. I. the permanent-magnet synchronous motor drive," IEEE Transactions on Industry Applications, vol. 25, no. 2, pp. 265-273, March/April 1989.

[86] H. Liu and S. Li, "Speed control for PMSM servo system using predictive functional control and extended state observer", IEEE Transactions on Industrial Electronics, vol. 59, no. 2, pp. 1171-1183, February 2012.

[87] A. A. Hassan and M. Azzam, "Robust control of a speed sensorless permanent magnet synchronous motor drive", 5th International Conference on Technology and Automation, Thessaloniki, Greece, 15-16 October 2005.

[88] S. Po-Ngam and S. Sangwongwanich, "Stability and dynamic performance improvement of adaptive full-order observers for sensorless PMSM drive", IEEE Transactions on Power Electronics, vol. 27, no. 2, pp. 588-600, February 2012.

[89] C. Xia, Y. Yan, P. Song and T. Shi, "Voltage disturbance rejection for matrix converterbased PMSM drive system using internal model control", IEEE Transactions on Industrial Electronics, vol. 59, no. 1, pp. 361-372, January 2012.

[90] W. Kaewjinda and M. Konghirun, "Vector control drive of permanent magnet synchronous motor using resolver sensor", ECTI Transactions on Electrical Engineering, Electronics and Comunications, vol. 5, no. 1, February 2007.

[91] Khalil HK. Nonlinear control. New York, NY: Pearson, 2015.

[92] Karboua D, Belgacem T, Khan ZH, et al. Robust performance comparison of PMSM for flight control applications in more electric aircraft. PLoS One 2023; 18: e0283541.

[93] Abu-Rub H, Iqbal A, Guzinski J. High Performance Control of AC Drives with Matlab/Simulink. John Wiley & Sons; 2021.

[94] Karboua D, Belgacem T, Khan ZH, Labiod C, Ibraheem IK. Toward an optimal twisting-sliding mode control of a three-phase PMSM for electric vehicles. *Advances in Mechanical Engineering*. 2023;15(9). doi:10.1177/16878132231198664

[95] F. Blaschke, "Das Prinzip der Feldorientierung, die Grundlage für die Transvektor- Regelung von Drehfeldmaschinen (The Principle of Field Orientation – the Basis for the Transvector Control of Three-Phase Machines)," Siemens Zeitschrift, 1971.

[96] K. Hasse, "Zur Dynamik Drehzahlgeregelter Antriebe Mit Stromrichter gespeisten Asynchron Kuzschlublaufermaschinen (On the Dynamics of Speed Control of a Static AC Drive with a Squirrel Cage Induction Machine)," Techn. Hochschule Darmstadt, 1969.

[97] Kumar, P. (2020). *Permanent magnet synchronous motor control for efficient motor drives* (Doctoral dissertation, Free University of Bozen-Bolzano).

[98] Faisal Amin, Erwan Sulaiman, and Hassan Soomro. Field oriented control principles for synchronous motor. International Journal of Mechanical Engineering and Robotics Research, 8:284–288, 01 2019. doi: 10.18178/ijmerr. 8.2.284-288.

[99] I. TAKAHASHI, T. NOGUCHI, "A new quick response and high efficiency control strategy of an induction motor", IEEE Trans. Ind. Appl, Vol. IA-22, pp. 820–827, 1986.

[100] I. TAKAHASHI, Y. OHMORI, "High-Performance Direct Torque Control of An Induction Motor", Industry Applications, IEEE Transactions on, Vol. 25, Issue: 2, pp. 257-264, Mar/Apr 1989.

[101] M. DEPENBROAK, "Direct Self-Control (DSC) of Inverter-Fed Induction Machine", IEEE Trans. on Power Electronics, Vol. 3, N°. 4. Oct, pp. 420-429, 1988.

[102] Trounce, J. C., Round, S., & Duke, R. (2001). Evaluation of direct torque control using space vector modulation for electric vehicle applications.

[103] Lachtar Salah, " Commande à Structure Variable d'un Moteur Synchrone à Aimant Permanent (MSAP)", mémoire de Magister, Université de Annaba 2006.

[104] Faiz, J., Sharifian, M. B. B., Keyhani, A., & Proca, A. B. (2003). Sensorless direct torque control of induction motors used in electric vehicle. *IEEE Transactions on Energy conversion*, *18*(1), 1-10.

[105] R. Toufouti," Contribution à la commande directe du couple de la machine asynchrone", Thèse de doctorat, Université de Constantine, 2008.

[106] Casadei, D., Profumo, F., Serra, G., & Tani, A. (2002). FOC and DTC: two viable schemes for induction motors torque control. *IEEE transactions on Power Electronics*, *17*(5), 779-787.

[107] Akkouchi Kamel, "Commande directe du couple (DTC) d'une machine asynchrone ", Mémoire de Magister, Université Badji Mokhtar d'Annaba, 2007.

[108] M. Kadjoudj, C. Ghennai, C. Bouchareb, and N. Golea, "Variable Band Hysteresis Controller for Direct Torque Control of PMSM Drive", In Proceedings of MS'02 conference, Girona, Spain 2002

[109] P. A. Arias, "Improvements in Direct Torque Control of Induction Motors", Thèse de Doctorat, Université de Catalunya, Espagne, 2000.

[110] Z. Rabah," Contrôle Direct du Couple d'une Machine Asynchrone Alimentée par des Onduleurs Multi-niveaux", Thèse de doctorat de l'ENP El-Harrach, 2007.

[111] M. Staebler, "TMS320F240 DSP solution for obtaining resolver angular position and speed", Texas Instruments, Application report, Feb. 2000.

[112] MESLOUB. H, " Commande DTC Prédictive D'une Machine Synchrone à Aimants Permanents", Thèse de Doctorat, Université Mohamed Khider – Biskra, 2016.

[113] Benaissa Malika, " Minimisation des pulsations du couple dans une commande directe du couple (DTC) d'une machine asynchrone ", Mémoire de Magister, Université de Batna, 2008.

[114] Merzoug Med Salah," Etude comparative des performances d'un DTC et d'un FOC d'une Machine synchrone à aimants permanents (MSAP)", Mémoire pour Obtenir le diplôme de Magister en Électrotechnique.

[115] Mohammed Ilyes Hemmami, " Commande sans capteur de vitesse d'un moteur synchrone à aimants permanents (MSAP) par l'utilisation de la commande directe du couple et d'un observateur de vitesse à mode glissant ", Mémoire de Magister en Electrotechnique, Université Mohamed Khider de Biskra, 2015.

[116] Yi-Geng Huangfu. Research of Nonlinear System High Order Sliding Mode Control and its Applications for PMSM. Chemical and Process Engineering. Northwestern Polytechnical University (Chine), 2010. English. ffNNT : 2010BELF0130ff. fftel-00608229f

[117] Xiao-Jing S. Design and simulation of PMSM feedback linearization control system. TELKOMNIKA: Indonesian Journal of Electrical Engineering. 2013; 11(3):1245–1250. https://doi.org/10.11591/telkomnika.v11i3.2192

[118] Zhou K, Ai M, Sun D, Jin N, Wu X. Field weakening operation control strategies of PMSM based on feedback linearization. Energies. 2019; 12(23):4526. https://doi.org/10.3390/en12234526

[119] M. Zerikat, M. Bendjebbar and N. Benouzza, "Dynamic Fuzzy-Neural Network Controller for induction motor drive", IEEE Transactions on Engineering,Computing and Technology, World Enformatika Society, Vol. 12, No10, pp.278-283, December.2005.

[120] Mellodge, P. (2015). *A practical approach to dynamical systems for engineers*. Woodhead Publishing.

[121] Karboua D, Belgacem T, Khan ZH, Kellal C (2023) Robust performance comparison of PMSM for flight control applications in more electric aircraft. PLoS ONE 18(7): e0283541. https://doi.org/10.1371/journal.pone.0283541.

[122] A. R. Benaskeur, "Aspects de l'application du backstepping adaptatif à la commande décentralisée des systèmes non linéaires", Thèse de Doctorat, Université Laval, Québec, 2000

[123] Lin CH. Permanent-magnet synchronous motor drive system using backstepping control with three adaptive rules and revised recurring sieved pollaczek polynomials neural network with reformed grey

wolf optimization and recouped controller. Energies. 2020; 13(22):5870. https://doi.org/10.3390/en13225870

[124] Belabbes, B., Fellah, M. K., Lousdad, A., Meroufel, A., & Massoum, A. (2006). Speed control by backstepping with nonlinear observer of a permanent magnet synchronous motor. *Acta Electrotechnica et Informatica No*, *6*(1), 4.

[125] FAROOQ Jawad Ahmed, Study of the inverse problem in electromagnetism for the localization of demagnetization faults in permanent magnet actuators, PhD thesis, University of Technology of Belfort, MONTBELIARD, France. Year 2008

[126] Eddie Smigiel and Guy Sturtzer, Modeling and control of three-phase motors, edition: Ellipses, Collection: Technosup, Year 2000

[127] V. Utkin, J. Guldner, and J. X. Shi , Sliding Mode Control in Electromechanical Systems. London, U.K.: Taylor and Francis, 1999.

[128] V. Utkin, Sliding Modes in Control Optimization. Berlin: SpringerVerlag, 1992

[129] C. Edwards and S. K. Spurgeron, Sliding Mode Control: Theory and Applications. London, U.K.: Taylor and Francis, 1998.

[130] W. Perruquetti and J. P. Barbot, Sliding Mode Control in Engineering. New York: Marcel Dekker, 2002

[131] J. J. E. Slotine and W. Li, Chapter 7: Sliding control, in Applied Nonlinear Control. Englewood Cliffs, NJ: Prentice-Hall, Inc., 1991

[132] Salam Eddine REZGUI, "Techniques de commande avancées de la machine asynchrone : étude comparative et application", Thèse Doctorat en sciences, Université de Frères Mentouri Constantine, 08 Juin 2015.

[133] Ayman HUSSAIN, "Contribution à la commande adaptative robuste par modes glissants", Thèse Doctorat Université de Reims champagne, 2009.

[134] W. GAO, Y. WANG, A. HOMAIFA, "Discrete-Time Variable Structure Control Systems", IEEE Trans. on Ind. Elec, Vol. 42, N°. 2, Aprl, pp. 117-122, 1995.

[135] Lilia SIDHOM, "Sur les différentiateurs en temps réel: algorithmes et applications", Thèse Doctorat, Institut National des Sciences Appliquées (INSA) de Lyon, France 29/09/2011.

[136] Abdelmadjid BOUMEDEIENE, "Recherche et développement de nouvelles approches de commandes d'une machine synchrone autopilotée alimentée en tension" Thèse Doctorat, ENP Alger, 2007.

[137] Mourad LOUCIF, "Synthèse de lois de commande non-linéaires pour le contrôle d'une machine asynchrone à double alimentation dédiée à un système aérogénérateur", Thèse Doctorat 3ème Cycle Génie Electrique, Université Aboubakr Belkaïd – Tlemcen, 12 May 2016

[138] J. J. E. SLOTINE, Weiping. LI, "Applied nonlinear control", Prentice Hall, ISBN 0-13-040890-5, 1991.

[139] V. UTKIN, "Sliding mode control design principles and applications to electric drives", IEEE Transactions on Industrial Electronics, 1993

[140] K. KOUZI, "Commande vectorielle d'un moteur à induction sans capteur vitesse par un réglage PI-Flou à gains flou adaptés associé à un observateur d'état par mode de glissement", Mémoire présentée pour l'obtention du diplôme de Magister, Université de Biskra, 2002

[141] Perruquetti, W., & Barbot, J. P. (Eds.). (2002). Sliding mode control in engineering (Vol. 11). New York: Marcel Dekker.

[142] Benamor, A. (2019). *Contribution à la Modélisation, à la Commande et au Contrôle des Systèmes de Production de l'Energie Électrique Renouvelable* (Doctoral dissertation, Université Mohamed Khider-Biskra).

[143] J. TSINIAS. Sufficient, LYAPUNOV, "Conditions for stabilization. Mathematical Control Signal Systems", Mathematics of Control, Signals, and Systems, Vol. 2, Issue 4, pp. 343-357, December 1989.

[144] Abdelhalim BORNI, "Etude et optimisation d'un multi système hybride de conversion d'énergie électrique", Thèse Doctorat en sciences en électrotechnique, Modélisation des machines électriques, Université Constantine 1, 12 Mars 2015.

[145] U. BENZ, "Réglage par Mode de Glissement Hybride, Applique au Réglage de Position de Systèmes Electromécaniques", Thèse Doctorat, Ecole Polytechnique Fédérale de Lausanne 1992

[146] Utkin, V., Guldner, J., & Shi, J. "Sliding mode control in electromechanical systems", CRC press, 2017.

[147] J.J. Slotine and S.S. Sastry. Tracking control of non-linear system using sliding surfaces with application to robot manipulators[J]. International Journal of Control, Vol. 38(2), 465-492, 1983

[148] Gao, W.; Hung, J.C. Variable structure control of nonlinear systems: A new approach. IEEE Trans. Ind. Electron. 1993, 40, 45–55. [CrossRef]

[149] Gao Weibing, "Variable structure control theory and design method." Science Press, 1996

[150] Shtessel, Y., Edwards, C., Fridman, L., & Levant, A. (2014). *Sliding mode control and observation* (Vol. 10). New York: Springer New York.

[151] Levant, A. "Sliding order and sliding accuracy in sliding mode control", International journal of control, 58(6), 1247-1263, 1993. https://doi.org/10.1080/00207179308923053

[152] Utkin, V.; Jingxin, S. Integral sliding mode in systems operating under uncertainty conditions. In Proceedings of the 35th IEEE Conference on Decision and Control, Kobe, Japan, 11–13 December 1996; pp. 4591–4596.

[153] Liang, Y.W.; Ting, L.W.; Lin, L.G. Study of Reliable Control Via an Integral-Type Sliding Mode Control Scheme. IEEE Trans. Ind. Electron. 2012, 59, 3062–3068. [CrossRef]

[154] Castanos, F.; Fridman, L. Analysis and design of integral sliding manifolds for systems with unmatched perturbations. IEEE Trans. Autom. Control 2006, 51, 853–858. [CrossRef]

[155] Shihua, L.; Mingming, Z.; Xinghuo, Y. Design and Implementation of Terminal Sliding Mode Control Method for PMSM Speed Regulation System. IEEE Trans. Ind. Inform. 2013, 9, 1879–1891. [CrossRef]

[156] Feng, Y.; Yu, X.; Man, Z. Non-singular terminal sliding mode control of rigid manipulators. Automatica 2002, 38, 2159–2167. [CrossRef]

[157] Liu, J.; Wang, X. Advanced Sliding Mode Control for Mechanical Systems: Design, Analysis and MATLAB Simulation; Springer: Berlin/Heidelberg, Germany, 2012.

[158] Wu, Y.; Yu, X.; Man, Z. Terminal sliding mode control design for uncertain dynamic systems. Syst. Control Lett. 1998, 34, 281–287. [CrossRef]

[159] Man, Z.; Xing Huo, Y. Terminal sliding mode control of MIMO linear systems. IEEE Trans. Circuits Syst. I Fundam. Theory Appl. 1997, 44, 1065–1070. [CrossRef]

[160] Elmas, C.; Ustun, O. A hybrid controller for the speed control of a permanent magnet synchronous motor drive. Control Eng. Pract. 2008, 16, 260–270. [CrossRef]

[161] Xinghuo, Y.; Man, Z. Fast terminal sliding-mode control design for nonlinear dynamical systems. IEEE Trans. Circuits Syst. I Fundam. Theory Appl. 2002, 49, 261–264. [CrossRef]

[162] Mohd Zaihidee, F., Mekhilef, S., & Mubin, M. (2019). Robust speed control of PMSM using sliding mode control (SMC)—A review. *Energies*, *12*(9), 1669.

[163] Xinghuo, Y.; Kaynak, O. Sliding-Mode Control With Soft Computing: A Survey. IEEE Trans. Ind. Electron. 2009, 56, 3275–3285. [CrossRef]

[164] Kaynak, O.; Erbatur, K.; Ertugnrl, M. The fusion of computationally intelligent methodologies and sliding-mode control-a survey. IEEE Trans. Ind. Electron. 2001, 48, 4–17. [CrossRef]

[165] Lee, C.C. Fuzzy logic in control systems: Fuzzy logic controller. I. IEEE Trans. Syst. ManCybern. 1990, 20, 404–418. [CrossRef]

[166] Guo, Y.; Long, H. Self organizing fuzzy sliding mode controller for the position control of a permanent magnet synchronous motor drive. AIN Shams Eng. J. 2011, 2, 109–118. [CrossRef]

[167] Kuo, C.-F.; Hsu, C.-H.; Tsai, C.-C. Control of a permanent magnet synchronous motor with a fuzzy sliding-mode controller. Int. J. Adv. Manuf. Technol. 2007, 32, 757–763. [CrossRef]

[168] Faa-Jeng, L.; Po-Hung, S. Robust Fuzzy Neural Network Sliding-Mode Control for Two-Axis Motion Control System. IEEE Trans. Ind. Electron. 2006, 53, 1209–1225. [CrossRef]

[169] El-Sousy, F.F.M. Robust wavelet-neural-network sliding-mode control system for permanent magnet synchronous motor drive. IET Electr. Power Appl. 2011, 5, 113–132. [CrossRef]

[170] Pan, H.; Xia, L.Z. Efficient Object Recognition Using Boundary Representation and Wavelet Neural Network. IEEE Trans. Neural Netw. 2008, 19, 2132–2149. [CrossRef]

[171] Wang, Y., Feng, Y., Zhang, X., Liang, J. "A new reaching law for antidisturbance sliding-mode control of PMSM speed regulation system", IEEE Transactions on Power Electronics, 35(4), pp. 4117–4126, 2020. https://doi.org/10.1109/TPEL.2019.2933613

[172] Ouchen, S., Benbouzid, M., Blaabjerg, F., Betka, A., Steinhart, H. "Direct power control of shunt active power filter using space vector modulation based on supertwisting sliding mode control", IEEE Journal of Emerging and Selected Topics in Power Electronics, 9(3), pp. 3243–3253, 2021. https://doi.org/10.1109/JESTPE.2020.3007900

[173] Desineni Subbaram Naidu , "Optimal Control Systems" , Idaho State University CRC Press, Inc., 2003

[174] M. A. M. Cheema and J. E. Fletcher, "Optimal, Combined Speed and Direct Thrust Force Control of a Linear Permanent Magnet Synchronous Motors," Power Syst., vol. 31, no. 3, pp. 135–153, 2020, doi: 10.1007/978-3-030-40325-6_5.

[175] Mebkhouta, T., Golea, A., Boumaraf, R., Benchouia, T. M., & Karboua, D. (2024). A High Robust Optimal Nonlinear Control with MPPT Speed for Wind Energy Conversion System (WECS) Based on Doubly Fed Induction Generator (DFIG). *Periodica Polytechnica Electrical Engineering and Computer Science*, *68*(1), 1-11.

[176] Ha, V. T., & Giang, P. T. (2023). A study on PMSM drive systems fed by multi-level inverter using linear quadratic regulator control for electric vehicle applications. TELKOMNIKA (Telecommunication Computing Electronics and Control), 21(4), 917-925.

[177] M. A. M. J. E. D. M. F. Cheema, "A Linear Quadratic Regulator-Based Optimal Direct Thrust Force Control of Linear Permanent-Magnet Synchronous Motor," IEEE Transactions on Industrial Electronics, vol. 63, no. 5, pp. 2722-2733, 2016.

[178] E. F. Camacho and C. Bordons, Model Predictive Control Springer Verlag, 1999.

[179] J. M. Maciejowski, Predictive Control with Constraints. Englewood Cliffs, NJ: Prentice Hall, 2002.

[180] G. C. Goodwin, M. M. Seron, and J. A. D. Dona, Constrained Control and Estimation – An Optimization Perspective. Springer Verlag, 2005.

[181] C. E. Garcia, D. M. Prett, and M. Morari, "Model predictive control: theory and practice – a survey," Automatica, vol. 25, no. 3, pp. 335–348, May 1989.

[182] J. Holtz and S. Stadtfeld, "A predictive controller for the stator current vector of AC machines fed from a switched voltage source," in International Power Electronics Conference, IPEC, Tokyo, pp. 1665–1675, 1983.

[183] Rodriguez, J., & Cortes, P. (2012). *Predictive control of power converters and electrical drives*. John Wiley & Sons.

[184] Joel A E Andersson, Joris Gillis, Greg Horn, James B Rawlings, and Moritz Diehl. CasADi – A software framework for nonlinear optimization and optimal control. Mathematical Programming Computation, In Press, 2018.

[185] Hackl, C.M. Mpc with analytical solution and integral error feedback for lti mimo systems and its application to current control of grid-connected power converters with lcl-filter In Proceedings of the 2015 IEEE International Symposium on Predictive Control of Electrical Drives and Power Electronics (PRECEDE), Valparaiso, Chile, 5–6 October 2015; pp. 61–66.

[186] Rodriguez, J.; Kazmierkowski, M.P.; Espinoza, J.R.; Zanchetta, P.; Abu-Rub, H.; Young, H.A.; Rojas, C.A. State of the art of finite control set model predictive control in power electronics. IEEE Trans. Ind. 2012, 9, 1003–1016.

[187] Garcia, C.; Rodriguez, J.; Odhano, S.; Zanchetta, P.; Davari, S.A. Modulated model predictive speed control for pmsm drives. In Proceedings of the 2018 IEEE International Conference on Electrical Systems for Aircraft, Railway, Ship Propulsion and Road Vehicles & International Transportation Electrification Conference (ESARS-ITEC), Nottingham, UK, 7–9 November 2018; pp. 1–6.

[188] B.Q. Van Ngo, P. Rodriguez-Ayerbe, Olaru, S.; Model predictive control with two-step horizon for three-level neutral-point clamped inverter. In Proceedings of the 20th International Conference on Process Control (PC), Štrbské Pleso, Slovak Republic, 9–12 June 2015; pp. 215–220.

[189] Vázquez Pérez, S.; Rodríguez, J.; Rivera, M.; García Franquelo, L.; Norambuena, M. Model predictive control for power converters and drives: Advances and trends. IEEE Trans. Ind. 2017, 64, 935–947.

[190] Zhang, Y.; Xie, W.; Li, Z.; Zhang, Y. Low-complexity model predictive power control: Double-vector-based approach. IEEE Trans. Ind. 2014, 61, 5871–5880.

[191] Riar, B.S.; Scoltock, J.; Madawala, U.K. Model predictive direct slope control for power converters.

IEEE Trans. Power Electron. 2017, 32, 2278–2289.

[192] Zhang, Y.; Yang, H. Two-vector-based model predictive torque control without weighting factors for induction motor drives. IEEE Trans. Power Electron. 2016, 31, 1381–1390.

[193] Sheng, L.; Li, D.; Ji, Y. Two-vector fcs-mpc for permanent-magnet synchronous motors based on duty ratio optimization. Math. Probl. Eng. 2018, 2018, 9061979.

[194] Zhang, Y.; Gao, S.; Xu, W. An improved model predictive current control of permanent magnet synchronous motor drives. In Proceedings of the 2016 IEEE Applied Power Electronics Conference and Exposition (APEC), Long Beach, Canada, 20–24 March 2016; pp. 2868–2874.

[195] J. Rodríguez, Kennel, R.M.; Espinoza, J.R.; Trincado, M.; Silva, C.A.; Rojas, C.A. High-performance control strategies for electrical drives: An experimental assessment. IEEE Trans. Ind. Electron. 2012, 59, 812–820.

[196] Abdelrahem, M.; Hackl, C.M.; Kennel, R.; Rodriguez, J. Efficient direct-model predictive control with discrete-time integral action for pmsgs. IEEE Trans. Energy Convers. 2018, 34, 1063–1072.

[197] Zhang, Y.; Xu, D.; Liu, J.; Gao, S.; Xu, W. Performance improvement of model-predictive current control of permanent magnet synchronous motor drives. IEEE Trans. Ind. Appl. 2017, 53, 3683–3695.

[198] Vazquez, S.; Leon, J.I.; Franquelo, L.; Carrasco, J.; Martinez, O.; Rodriguez, J.; Cortes, P.; Kouro, S. Model predictive control with constant switching frequency using a discrete space vector modulation with virtual state vectors. In Proceedings of the 2009 IEEE International Conference on Industrial Technology, Churchill, Victoria, Australia, 10–13 February 2009; pp. 1–6.

[199] Bouguenna, I.F.; Tahour, A.; Kennel, R.; Abdelrahem, M. Multiple-Vector Model Predictive Control with Fuzzy Logic for PMSM Electric Drive Systems. Energies 2021, 14, 1727. https://doi.org/10.3390/en14061727

[200] Gao, X.; Abdelrahem, M.; Hackl, C.M.; Zhang, Z.; Kennel, R. Direct predictive speed control with a sliding manifold term for pmsm drives. IEEE J. Emerg. Sel. Top. Power Electron. 2019, 8, 1258–1267.

[201] Abdelrahem, M.; Hackl, C.; Kennel, R.; Rodriguez, J. Sensorless predictive speed control of permanent-magnet synchronous generators in wind turbine applications In Proceedings of the PCIM Europe 2019, International Exhibition and Conference for Power Electronics, Intelligent Motion, Renewable Energy and Energy Management, VDE, Nuremberg, Germany, 7–9 May 2019; pp. 1–8.